Université de Montréal

Association des composés quinonoïdes : conception de nouveaux solides cristallins pour l'électronique organique

par Sophie Langis-Barsetti

Département de Chimie
Faculté des arts et des sciences

Thèse présentée à la Faculté des études supérieures et postdoctorales
en vue de l'obtention du grade de *Philosophiae Doctor* (Ph.D.)
en chimie

Janvier 2019

Résumé

En chimie supramoléculaire, le tout est plus grand que la somme de ses parties : les caractéristiques d'un matériau ne sont pas toujours définies par les attributs de molécules isolées et émergent parfois seulement de leur collectivité. Les propriétés dépendent alors de l'organisation moléculaire et l'impossibilité de la prévoir est un obstacle majeur à notre habileté à concevoir des matériaux ayant des caractéristiques prédéfinies. Bien que différentes méthodes permettent de moduler l'organisation, leur portée est généralement limitée et les fragments employés sont souvent étrangers aux propriétés ultimement visées. Ainsi, les organisations favorables sont parfois atteintes aux dépens des propriétés moléculaires. Par conséquent, nous avons choisi d'étudier l'association moléculaire dans des familles de composés pertinentes en électronique organique et de nous pencher sur les façons dont les fragments moléculaires déterminant les propriétés intrinsèques attrayantes peuvent aussi être utilisés pour diriger l'association moléculaire. Nous avons aussi choisi de nous limiter à des composés structurellement apparentés et nous nous sommes concentrés sur des composés de forme quinonoïde qui combinent trois caractéristiques essentielles : (1) La présence d'un système-π étendu; (2) la capacité de s'engager dans diverses interactions intermoléculaires; et (3) un caractère électrodéficitaire favorisant des phénomènes de transfert de charge ou la participation à des réactions rédox.

Une première partie de la thèse se concentre sur l'association des thiadiazoles aromatiques. Ces unités sont communes à plusieurs matériaux optoélectroniques et se sont révélées particulièrement efficaces lorsqu'intégrées aux cellules solaires organiques. Afin d'approfondir la pertinence de notre étude à cette technologie, nous avons aussi étudié la formation de co-cristaux entre des dérivés de thiadiazoles et des fullerènes, une autre classe de matériaux couramment intégrée à ce type de dispositif. Cette section est suivie d'un chapitre qui détaille une partie des efforts synthétiques déployés dans la préparation des thiadiazoles. La seconde partie de la thèse se tourne vers des dérivés de triptycène portant des unités quinone et hydroquinone et sur les façons dont leur association et leurs propriétés rédox peuvent être utilisées de concert à l'état solide.

Mots-clés : chimie supramoléculaire, association moléculaire, composé quinonoïde, thiadiazole, triptycène, quinone, hydroquinone, cristallographie

Abstract

In supramolecular chemistry, the whole is greater than the sum of its parts: a material's characteristics are not always defined by the attributes of isolated molecules and may only emerge from their collectivity. Properties then depend on molecular organization. The difficulty of predicting it from molecular identity alone prevents the design of materials with predefined properties. Few methods allow modulation of organization, and the necessary molecular fragments are often not relevant to the targeted properties. Therefore, useful organizations are often reached at the expense of molecular properties. For those reasons, we have chosen to examine molecular association in families of molecules relevant to organic electronic and to study how the molecular fragments defining the attractive properties can also be exploited to direct molecular association. We have chosen to focus on structurally related compounds that combine three essential characteristics: (1) the presence of an extended π system; (2) the ability to engage in various intermolecular interactions, and (3) an electron-poor nature that promotes either charge transfer or redox reactions.

The first part of the thesis details the association of a series of aromatic thiadiazoles. These units are widely used in many optoelectronic materials and are particularly valuable as components of the active layers of organic solar cells. To ensure that our structural analyses are relevant to studies in which the typical components of molecular thin-film devices must be properly organized, we have also examined co-crystallizations of thiadiazole derivatives with the fullerenes C_{60} and C_{70}, which define a class of compounds widely used as electron acceptors in solar cells. This section is followed by a chapter describing problems in synthesis encountered during the preparation of the thiadiazoles and our efforts to overcome them. The second part of the thesis turns to derivatives of triptycenes containing quinone and hydroquinone units and on how their association and their redox properties can be used in concert in the solid state.

Keywords : supramolecular chemistry, molecular association, quinonoid compound, thiadiazole, triptycene, quinone, hydroquinone, crystallography

Table des matières

Liste des tableaux

Chapitre 2. Organisation moléculaire de 2,1,3-benzothiadiazoles à l'état solide.

Chapitre 3. Synthèse de sels de naphtalènetétramine

Chapitre 4. Les dérivés quinonoïdes du triptycène : des solides cristallins et perméables pouvant participer à des réactions redox

Liste des figures

Chapitre 1. Introduction

Chapitre 2. Organisation moléculaire de 2,1,3-benzothiadiazoles à l'état solide.

Chapitre 3. Synthèse de sels de naphtalènetétramine

Chapitre 4. Les dérivés quinonoïdes du triptycène : des solides cristallins et perméables pouvant participer à des réactions redox

Chapitre 5. Perspectives

Liste des abréviations

°C	Degré Celsius
Å	Ångström
A. U.	Unité arbitraire
Ac	Acétyle
ADN	Acide désoxyribonucléique
Anal.	Analyse
APCI	Ionisation chimique à pression atmosphérique
APPI	Photoionisation à pression atmosphérique
ASAP	Sonde d'analyse de solide à pression atmosphérique
ATR	Réflectance totale atténuée
calcd	Calculé
Cbz	Carboxybenzyle
cm	Centimètre
CSD	*Cambridge Structural Database*
CV	Voltampérométrie cyclique
D	Debye
DAT	2,4-Diamino-1,3,5-triazine
DDQ	2,3-Dichloro-5,6-dicyano-1,4-benzoquinone
dec.	Décomposition
DMF	*N*,*N*-Diméthylformamide
DMSO	Diméthylsulfoxyde
$E_{1/2}$	Potentiel de demi-vague
Eq.	Équivalent
ESI	Ionisation par électronébuliseur
F_c	Ferrocène
F_c^+	Ferrocénium
FTIR	Spectroscopie infrarouge à transformée de Fourier
g	Gramme
h	Heure
HOMO	Orbitale occupée de plus haute énergie
HRMS	Spectrométrie de masse à haute résolution
hν	Irradiation lumineuse
Hz	Hertz
I	Intensité
J	Constante de couplage
K	Degré Kelvin
kcal	Kilocalorie

LUMO	Orbitale vide de plus basse énergie
M	Molaire
m/e	Rapport masse/charge
m/z	Rapport masse/charge
Me	Méthyle
mg	Milligramme
MHz	Mégahertz
ml	Millilitre
mM	Millimolaire
mm	Millimètre
mmol	Millimole
mol	Mole
mp	Point de fusion
mV	Millivolt
nm	Nanomètre
NMP	*N*-Méthyl-2-pyrrolidone
NMR	Résonance magnétique nucléaire
obs	Observé
ORTEP	*Oak Ridge Thermal Ellipsoid Program*
Ph	Phényle
ppm	Partie par million
R_1	Facteur d'accord
ωR_2	Facteur d'accord pondéré
SWV	Voltammétrie à ondes carrées
TBAP	Tétrabutylammonium hexafluorophosphate
TFA	Acide trifluoroacétique
THF	Tétrahydrofurane
TIPS	Triisopropylsilyle
TOF	Temps de vol
Ts	4-Toluènesulfonyle
UV	Ultraviolet
V	Volt
Vis	Visible
Z	Nombre d'unités formulaires par maille
δ	Déplacement chimique
ΔG	Variation d'énergie libre
ε	Coefficient d'absorption molaire
λ	Longueur d'onde
μ	Coefficient d'absorption
ρ	Densité
Σ	Sommation

Remerciements

Cette thèse n'aurait pu être réalisée sans l'appui et la contribution de plusieurs personnes que je tiens à remercier :

D'abord, j'aimerais remercier mon directeur de recherche de m'avoir accordé sa confiance et de m'avoir permis de travailler avec autonomie tout au long de mon doctorat. Ses standards élevés, son sens aigu du détail ainsi que ses connaissances encyclopédiques ont sans aucun doute fait de moi une meilleure chercheure, une meilleure chimiste et une meilleure rédactrice.

Il est plus facile de traverser un projet de l'envergure d'un doctorat en étant entouré d'une équipe dans laquelle règnent l'entraide et le plaisir. J'aimerais ainsi remercier tous les membres du groupe Wuest que j'ai eu la chance de côtoyer : Alice, Tina, Sébastien, Nino, Alexandre, Fatima, Norbert, William, Jean-Christophe, Minh, Daniel, Pierre-Louis, Olivier, Virginie, ainsi que les membres de Solaris : Dominic et Frank. J'aimerais particulièrement souligner la générosité de Daniel Beaudoin qui m'a encadrée au début de mes études graduées.

L'entraide a dépassé les limites du groupe et je suis aussi redevable aux membres des autres unités de recherches du département de chimie, notamment aux membres du groupe Martel, du groupe Skene et du groupe Winnick. Je suis particulièrement reconnaissante aux membres du groupe Hanan pour leur générosité dans le partage de leur équipement et surtout de leur expertise.

J'aimerais aussi remercier le personnel des différents services associés au département de chimie, notamment les services de spectrométrie de masse, de résonnance magnétique nucléaire et d'analyse élémentaire, ainsi que le personnel du secrétariat et des laboratoires

d’enseignement pour leur contribution à un environnement de recherche et d’apprentissage de haute qualité.

Je suis énormément redevable au service de cristallographie aux rayons X et à Thierry Maris, sans qui la majeure partie de cette thèse n’aurait pu avoir lieu. Mon travail a nécessité l’apport constant de son expertise, et je suis reconnaissante d’avoir eu la chance de travailler avec une personne si patiente, généreuse et avenante.

J’aimerais finalement remercier mes parents, ma famille et mes amis de m’avoir soutenue tout au long de ce projet. Mon doctorat aurait été particulièrement plus difficile sans l’amour et le soutien quotidien de mon amoureux, Jean-Sébastien, merci infiniment.

Notes

Les résultats acquis grâce à la diffraction des rayons X ont été obtenus en collaboration avec Thierry Maris qui a réalisé les mesures cristallographies effectuées sur des monocristaux et des poudres microcristallines.

Les publications présentées dans la thèse ont été rédigées en collaboration avec mon directeur de recherche, James D. Wuest, et Thierry Maris. Afin de présenter le contenu des articles sous une forme qui se rapproche de celle de leur publication, la numération des composés, des figures, des schémas, des tableaux et des références est indépendante d'un chapitre à l'autre. Le style des graphiques a cependant été uniformisé.

À travers la thèse, la couleur des atomes dans les représentations des structures cristallographiques est standardisée selon le modèle suivant : les atomes de carbone sont représentés en gris, les atomes d'hydrogène en blanc, les atomes d'oxygène en rouge, les atomes d'azote en bleu et les atomes de soufre en jaune. Les interactions intermoléculaires sont représentées par des lignes pointillées.

Chapitre 1.

Introduction

Chapitre 1. Introduction

Le lien covalent est au cœur de la chimie organique. À partir du 19^{e} siècle, les chimistes organiciens ont déployé des efforts titanesques afin d'établir ce qui allait devenir les lignes directrices de la synthèse moderne en explorant comment les liens covalents pouvaient être formés et rompus. Notre compréhension des liaisons chimiques nous permet désormais aussi de manipuler des systèmes plus délicats et de nous aventurer au-delà des molécules, vers ce que plusieurs ont nommé la synthèse non covalente.[1, 2]

1.1 La chimie supramoléculaire

La chimie supramoléculaire est la chimie du lien intermoléculaire.[3] Elle se préoccupe de l'association des molécules plutôt que de leur construction. Plusieurs chimistes ont cependant assimilé l'édification supramoléculaire à la synthèse organique. Notamment, Whitesides parlait de synthèse covalente et de synthèse non-covalente[1] et le Nobel Jean-Marie Lehn affirmait que les supermolécules sont aux molécules et au lien intermoléculaire ce que les molécules sont aux atomes et au lien covalent.[3] Le désir de vouloir construire des entités supramoléculaires de façon analogue à la synthèse classique est ancré dans le fait que les caractéristiques d'un composé ne sont pas complètement encapsulées dans les molécules individuelles, mais peuvent aussi être le résultat de leur association. Il est ainsi nécessaire de pouvoir contrôler cette association pour pouvoir accéder à ces propriétés.

Les chimistes familiarisés avec les systèmes biologiques ont reconnu depuis longtemps l'importance des interactions intermoléculaires qui sont au cœur d'une multitude de processus biochimiques. L'exemple le plus connu est sans aucun doute l'aptitude des brins d'ADN à s'associer deux à deux grâce à un réseau de ponts hydrogène entre les bases azotées qui confère à l'assemblage final sa célèbre forme hélicoïdale (Figure 1a). L'influence des interactions non covalentes s'étend outre les systèmes biologiques et elles sont susceptibles d'être déterminantes aux propriétés dans toutes les sphères de la chimie. Par exemple, les

fibres de Kevlar, utilisées notamment dans la fabrication des vestes pare-balles, doivent leur résistance aux interactions entre les chaînes de polymère associées à la fois par des ponts hydrogène et l'empilement des segments aromatiques.

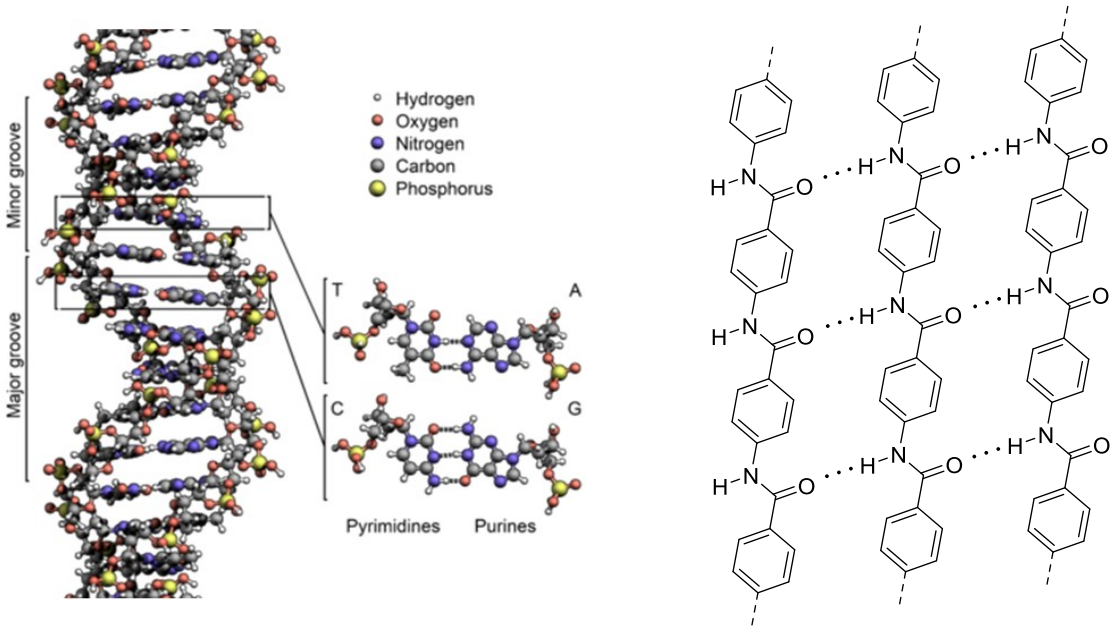

a **b**

Figure 1. Exemples d'assemblages supramoléculaires. a) Représentation de la structure d'un double brin d'ADN. La structure hélicoïdale est le résultat de l'association de brins individuels par l'entremise d'un réseau de ponts hydrogène entre les bases azotées empilées. b) Représentation de la structure du Kevlar. La résistance du matériau provient des interactions non covalentes interchaînes, plus particulièrement de ponts hydrogène entre les fonctions amides et de l'empilement π des portions aromatiques.

1.1.1 Les interactions intermoléculaires

Les interactions non covalentes susceptibles de régir l'association supramoléculaire dans les composés organiques varient en origine et en force. Elles peuvent correspondre à 85 kcal

mol^{-1} pour les interactions ioniques et à une fraction de kcal mol^{-1} dans le cas des forces de van der Waals alors que la force d'un lien covalent simple varie normalement entre 35 et 100 kcal mol^{-1}. Les principales forces supramoléculaires sont décrites ci-dessous et les plages d'énergies qui leur sont associées sont résumées à la Figure 2.[4]

- Les interactions ioniques et dipolaires sont des forces électrostatiques entre charges ou dipôles permanents et varient de 45 à 85 kcal mol^{-1} dans le cas des interactions entre ions, de 12 à 50 kcal mol^{-1} pour les interactions ion-dipôle et entre 1 et 12 kcal mol^{-1} pour les interactions entre dipôles.
- Les ponts hydrogène forment une catégorie particulière d'interactions dipôle-dipôle entre un donneur et un accepteur de proton. Il s'agit sans aucun doute des liens non covalents les plus importants, car ils sont à la fois forts et directionnels. Bien qu'ils peuvent atteindre jusqu'à 30 kcal mol^{-1}, ils restent généralement inférieurs à 15 kcal mol^{-1}.
- Les liaisons π se manifestent dans les composés aromatiques entre des anneaux parallèles ou perpendiculaires et peuvent atteindre 12 kcal mol^{-1}. Dans les deux cas, le lien est le résultat d'interactions entre le centre et le pourtour des cycles aromatiques, respectivement riche et pauvre en électrons.
- Les liens de van der Waals résultent des fluctuations de la distribution électronique entre des molécules adjacentes et restent généralement inférieurs à 2 kcal mol^{-1}.

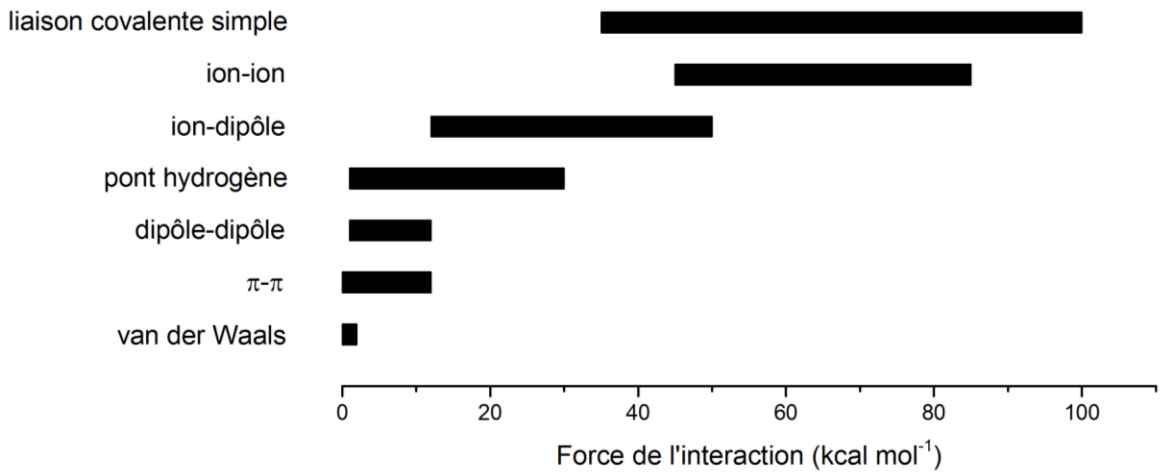

Figure 2. Plages d'énergie associées à quelques interactions supramoléculaires.

1.2 Le cristal, la supermolécule par excellence

Constitués de milliard de molécules assemblées par l'intermédiaire de lien non covalent, les cristaux ont été décrits comme étant les supermolécules par excellence.[5] Ils se sont révélés particulièrement importants dans l'histoire de la chimie, car leur réseau périodique offre l'avantage de pouvoir être visualisé précisément par l'entremise de la cristallographie aux rayons X.[6]

La découverte par von Laue en 1912 que l'exposition d'un cristal aux rayons X produit un patron de diffraction a originellement permis de confirmer que les cristaux sont constitués de particules ordonnées (Figure 3a-b).[7] Cette découverte a ensuite été exploitée par William Lawrence Bragg et son père William Henry Bragg, qui ont montré que la position relative des atomes dans le cristal peut être déterminée par l'analyse du patron de diffraction.[8-10] Ces connaissances ont lancé les débuts de la cristallographie et la détermination des premières structures a permis d'établir ou de confirmer plusieurs modèles théoriques sur les liaisons chimiques en fournissant des informations importantes sur les longueurs et les angles de liaison ainsi que sur la géométrie et la conformation des molécules. Par exemple, l'analyse de

la structure du diamant[11, 12] en 1913 a validé la géométrie tétraédrique du carbone et l'analyse de la structure de l'hexaméthylbenzène[13] en 1928 a montré que les anneaux aromatiques sont plats et que les liaisons entre carbone sont identiques, ce qui allait alors à l'encontre du modèle prépondérant de Kékulé. William Lawrence Bragg a éventuellement décrit l'impact de sa propre invention en 1937 en disant: «*The history of X-ray diffraction ranks as one of the epoch-making discoveries in the history of science*».[14]

Bien que l'impact initial de la diffraction aux rayons X ait d'abord surtout concerné l'identité moléculaire, la cristallographie permet aussi de sonder les propriétés supramoléculaires des molécules. Ce sont par exemple des images de diffraction aux rayons X qui ont permis à Watson et Crick de finaliser leur modèle de la structure de l'ADN en 1953 (Figure 3c)[15-17] et à Pauling et Corey d'établir les structures secondaires des chaînes polypeptidiques quelques années plus tôt.[18]

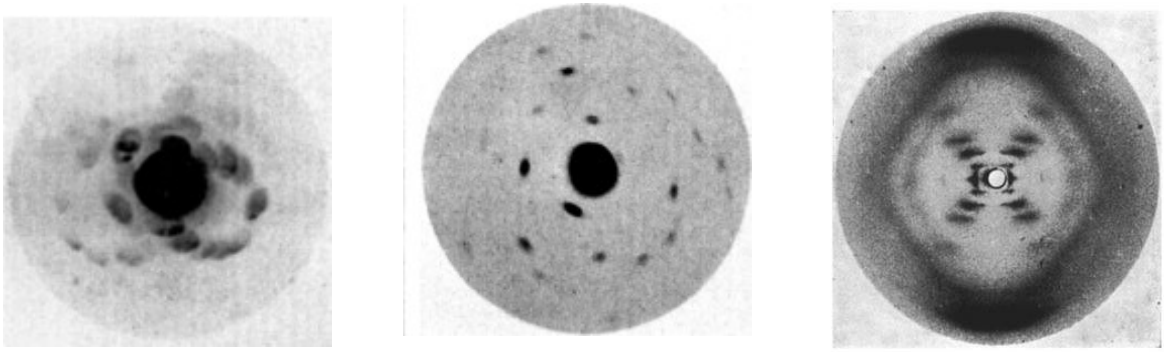

a **b** **c**

Figure 3. Premiers pas de la cristallographie aux rayons X. (a) Tout premier patron de diffraction obtenu par von Laue résultant de l'exposition de cristaux de sulfate de cuivre (II) aux rayons X. (b) Patron de diffraction obtenu après avoir optimisé la taille des fentes.[7] (c) La célèbre *Photo 51 :* patron de diffraction de cristaux d'ADN tel qu'obtenu par Gosling et Franklin.[16, 17]

Alors que la détermination d'une structure cristalline a été pendant longtemps un travail susceptible de s'échelonner sur plusieurs mois, les progrès technologiques permettent aujourd'hui de passer de cristal à structure en quelques heures. Dans les années soixante, face à la multiplication des structures cristallines publiées, le groupe d'Olga Kennard à l'Université de Cambridge a entrepris l'enregistrement systématique des études portant sur les petites molécules. Cette collection, la *Cambridge Structural Database* (CSD), compte aujourd'hui près d'un million d'entrées différentes et est un outil indispensable à l'exploration des structures moléculaires et supramoléculaires.[19]

1.2.1 La cristallisation

Les mécanismes exacts de la cristallisation demeurent généralement méconnus. Le modèle classique, élaboré au 19^{e} siècle, stipule que la cristallisation débute par la formation spontanée d'agrégats organisés qui deviennent des sites de nucléation auxquels s'additionnent une à une de nouvelles molécules jusqu'à l'édification d'un cristal.[20, 21] Cependant, les études modernes suggèrent que la réalité est plus complexe et que la croissance d'un cristal peut s'opérer d'une multitude de façons. On a par exemple observé le réarrangement de domaines amorphes en phases cristallines et le fusionnement de nanocristaux.[22-26] Bien que certaines facettes du processus soient bien approximées par les modèles actuels, la compréhension superficielle des différents stades de cristallisation nuit à notre capacité à en prédire le résultat.

Globalement, la cristallisation est un processus thermodynamiquement irréversible qui débute dans une solution hypersaturée dans laquelle la perte d'entropie associée à la formation d'un solide organisé est compensée par le gain d'enthalpie provenant de la formation des interactions intermoléculaires attractives. La cristallisation permet d'assembler des objets nanométriques en un réseau tridimensionnel périodique dont la taille est généralement de l'ordre du micromètre ou du millimètre. Le processus d'association de chacune de ces millions de molécules doit donc nécessairement être réversible afin de permettre au système de se corriger et d'empêcher l'apparition de diversité en convergeant vers un puits thermodynamique local. Ainsi, grâce à ce processus d'autoassemblage, l'association mène à

la formation d'une seule organisation, bien qu'elle soit régie par des éléments de reconnaissance chimique et géométrique souvent isotropiques et faibles. Le résultat est extrêmement précis. On a par exemple calculé plus 100 structures cristallines possibles pour l'acide acétique dans une marge de 1,2 kcal mol^{-1} alors qu'un seul polymorphe a été obtenu expérimentalement.[27]

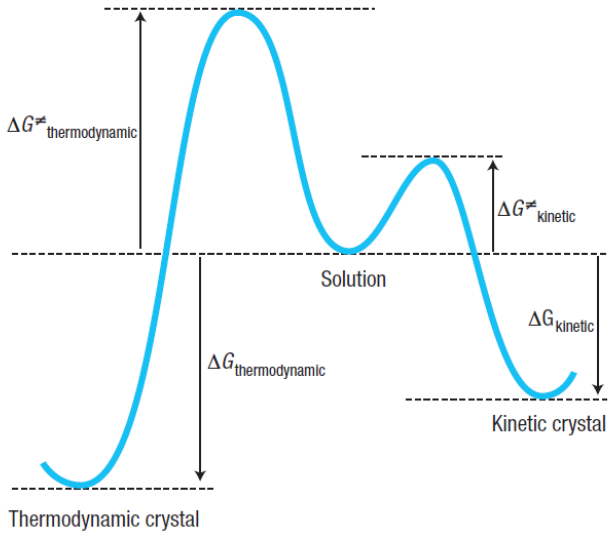

Figure 4. Diagramme de Curtin-Hammett associé au processus de cristallisation. La distribution des produits de cristallisation reflète la stabilité des intermédiaires qui mènent à ces organisations.[28]

Si l'on étend l'analogie qu'a faite Lehn entre les supermolécules et les molécules, la construction de ces supermolécules − la cristallisation − peut être assimilée à une réaction chimique. À l'instar de celle-ci, le produit thermodynamique est seulement obtenu si le chemin réactionnel qui y aboutit est accessible (Figure 4). Des arrangements moins stables peuvent être isolés s'ils se propagent plus facilement. On obtient alors le produit cinétique de la cristallisation. Par exemple, en phase liquide, les molécules d'acide acétique sont

principalement associées sous forme de dimères, mais seul le catémère cristallise, car l'association des dimères n'est pas favorable.[29, 30]

L'organisation cristalline est un compromis délicat entre une multitude d'interactions de force et d'orientation différentes et les mécanismes de son édification demeurent souvent nébuleux. Il est ainsi généralement impossible de prédire la structure cristalline à partir de l'identité moléculaire. Il est de surcroit impossible de prédire d'autres caractéristiques de l'organisation tels l'incorporation de solvant, l'interpénétration, la conformation ou le polymorphisme. Puisque les propriétés d'un composé dépendent en partie des arrangements moléculaires, notre piètre habileté à prédire ces arrangements entrave notre capacité à concevoir des matériaux aux propriétés prédéfinies.

1.2.2 Le polymorphisme

L'une des conséquences associées à la complexité des mécanismes de cristallisation et à la fragilité des interactions en jeu est que plusieurs composés peuvent être isolés dans plus d'une forme cristalline. On considère ces différentes organisations comme des polymorphes lorsque la composition des cristaux est identique et des pseudo-polymorphes lorsque les structures varient par la quantité ou la nature du solvant incorporé.[31-35] L'écart énergétique entre les polymorphes d'un même composé est généralement faible, moins de 1 kcal mol^{-1}. Pour les molécules flexibles, qui sont susceptibles de cristalliser dans différentes conformations, l'écart peut se creuser légèrement, mais demeure inférieur à 3 kcal mol^{-1} dans la majorité des cas.

La fréquence du polymorphisme est difficile à évaluer et varie beaucoup en fonction de l'échantillon considéré.[32,35] Dans l'ensemble des composés organiques répertoriés dans la CSD, environ 2% sont polymorphiques. Ce chiffre sous-estime cependant l'incidence du phénomène puisque la majorité des molécules ne sont pas sondées pour le polymorphisme et ne sont cristallisées qu'une seule fois, souvent afin de confirmer la structure moléculaire. Si

l'on considère plutôt uniquement les structures qui ont été redéterminées au moins une fois, la proportion des systèmes polymorphiques grimpe à 37%. Cette valeur est plus proche de celles que l'on retrouve dans les groupes de molécules pour lesquels les conditions de cristallisation ont été explorées extensivement, souvent par l'industrie pharmaceutique, qui se situent généralement entre 50 et 60%. La majorité des composés polymorphiques ne présente que deux organisations cristallines différentes et plus de trois polymorphes sont connus pour seulement une vingtaine de composés.[34]

Ces analyses montrent que le polymorphisme est un phénomène commun, mais aussi qu'il demeure imprévisible. En effet, il reste impossible de corréler l'incidence du polymorphisme à la structure moléculaire. Ni la flexibilité, l'aptitude à former des ponts hydrogène ou la taille, tous des facteurs préalablement évoqués pour rationaliser l'apparition du phénomène, ne semblent favoriser la multiplication des arrangements supramoléculaires.

1.2.3 La co-cristallisation

La portée du terme co-cristal est encore le sujet de débat. Les définitions les plus larges évoquent tout cristal formé de plus d'un type de molécules alors que d'autres spécifient que ces molécules doivent se trouver à l'état solide à température ambiante ce qui exclut les hydrates, les solvates et certains composés d'inclusions du domaine.[36-39] Dans le cadre de la chimie supramoléculaire, les co-cristaux sont généralement considérés comme le résultat de complémentarité entre deux ou plusieurs entités et la co-cristallisation a lieu lorsque les interactions entre ces entités sont plus favorables que les interactions entre les molécules de la même espèce. Par exemple, le premier cas de co-cristallisation relevé dans la littérature remonte à 1844 alors que Wöhler a noté que les cristaux de la substance appelée quinhydrone sont composés à parts égales de 1,4-benzoquinone et de 1,4-hydroquinone. Les études cristallographiques modernes ont montré que la reconnaissance moléculaire a lieu via une série de ponts hydrogène et d'interactions π où s'alternent les molécules riches et pauvres en électrons (Figure 5).[40-42]

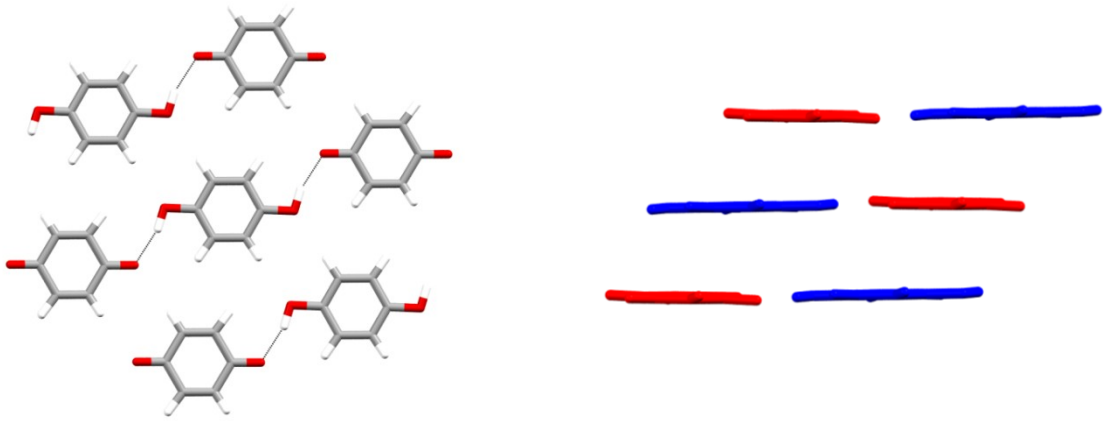

a **b**

Figure 5. Représentations de la structure cristallographique de la quinhydrone.[41] (a) Les molécules de 1,4-benzoquinone et de 1,4-hydroquinone sont associées grâce à des ponts hydrogène (b) Empilement π donnant lieu aux interactions de transfert de charge présentes dans la structure. Les molécules de 1,4-benzoquinone sont représentées en bleue et celles de 1,4-hydroquinone en rouge.

L'étude des co-cristaux s'est particulièrement développée en chimie pharmaceutique, car l'association d'une molécule active à une autre espèce peut affecter la stabilité, la solubilité, le taux de dissolution et la disponibilité biologique du composé thérapeutique sans affecter ses propriétés physiologiques.[43] En chimie des matériaux, où les propriétés sont évaluées à l'état solide et dépendent de l'arrangement des molécules dans l'espace, la formation d'un co-cristal peut produire un matériau dont les caractéristiques sont différentes de celles de ses constituants.

1.3 L'ingénierie cristalline

Bien que la première utilisation de l'expression *ingénierie cristalline* remonte à Pepinsky en 1955,[44] elle fut principalement popularisée par Schmidt lors de ses travaux sur la photo-dimérisation à l'état solide.[45] Ces recherches montraient que la stéréochimie des photo-

dimères peut être expliquée grâce au principe topochimique (Figure 6). Cette observation était à l'origine de la nécessité de développer l'ingénierie cristalline afin de pouvoir contrôler la position des molécules dans leurs cristaux et ainsi contrôler leur réactivité. L'ingénierie cristalline a donc d'abord été introduite en tant qu'outil de la synthèse organique.

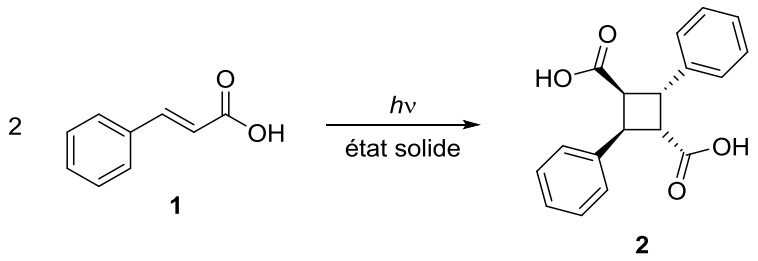

a

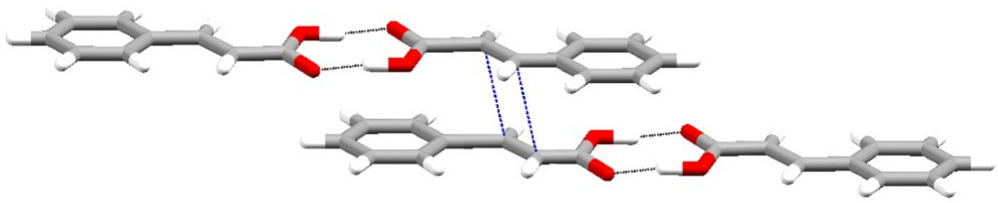

b

Figure 6. (a) Photo-dimérisation de l'acide *trans*-cinnamique à l'état cristallin. (b) La stéréochimie du dimère est dictée par la position relative des molécules d'acide *trans*-cinnamique dans le cristal. Les liaisons hydrogène sont représentées par des lignes pointillées noires et les sites de réactions par des lignes pointillées bleue.[46]

Aujourd'hui, l'ingénierie cristalline est généralement décrite par la définition qu'en a fait Desiraju, soit la compréhension des interactions intermoléculaires dans le contexte de l'empilement cristallin et l'utilisation de ces notions dans la conception de nouveaux solides possédant des caractéristiques physiques et chimiques prédéfinies.[2,47] Il ne s'agit pas du premier ou du seul modèle visant à expliquer et à prédire l'organisation cristalline. Par exemple, Kitaigorodskii proposait une approche géométrique qui stipulait que les interactions

intermoléculaires étant généralement faibles et peu directionnelles, les systèmes les plus denses et faisant le meilleur usage de l'espace sont favorisés.[48] Etter proposait plutôt une hiérarchie de ponts hydrogène dont la formation doit être priorisée dans un certain ordre afin de comprendre et prédire l'association moléculaire.[49] L'ingénierie cristalline n'est pas nécessairement incompatible avec ces modèles, mais se présente plutôt comme une méthode empirique se basant sur l'analyse de multiples structures cristallines dans le but d'en dégager les motifs d'associations récurrents. L'organisation est ensuite simplifiée en la réduisant à ces patrons d'interactions dont la formation semble diriger l'association. Ces motifs supramoléculaires, que l'on nomme synthons, peuvent être des éléments de reconnaissance géométrique et chimique et leur présence dans une multitude de structures montre que leur formation est favorisée thermodynamiquement et cinétiquement. L'ingénierie cristalline est donc une méthode probabiliste qui contourne les zones méconnues des mécanismes de cristallisation en se basant sur des résultats expérimentaux et en extrayant des tendances.

Par exemple, la Figure 7 montre l'organisation cristalline d'une série de molécules dont l'association est gouvernée par les doubles ponts hydrogène formés entre des paires d'acides carboxyliques.[2] La formation récurrente de ce motif suggère qu'il est susceptible de diriger l'association d'autres molécules possédant cette fonctionnalité. Ainsi, de la même façon que la planification d'une synthèse organique est basée sur la connaissance des différentes réactions chimiques connues grâce à l'exploration performée pendant des dizaines d'années sur la réactivité des différentes familles de molécules, la planification de l'organisation supramoléculaire peut être basée sur l'extrapolation des tendances observées dans les structures cristallines. Dans l'analogie de Lehn, l'ingénierie cristalline correspond à la rétrosynthèse.

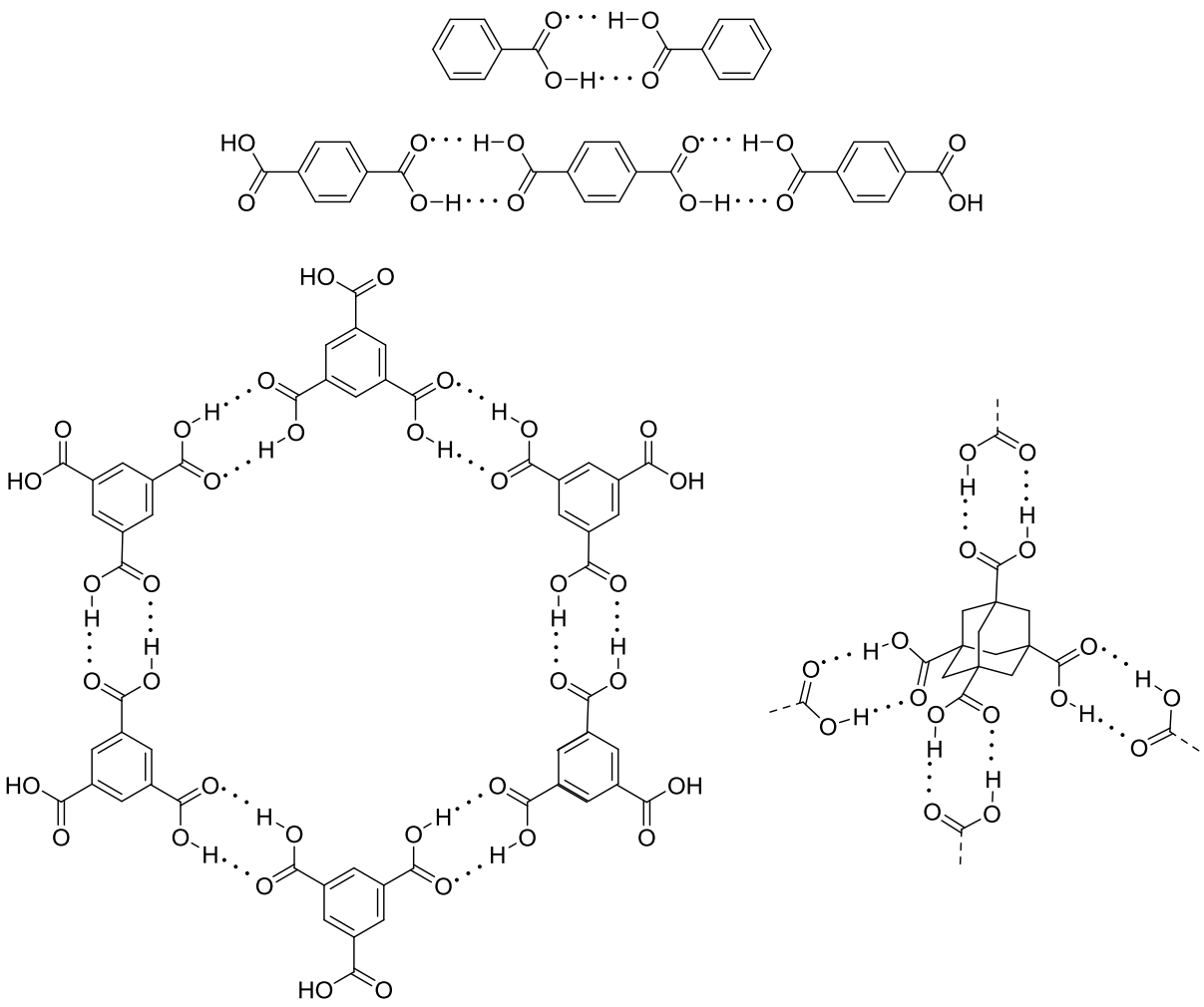

Figure 7. Schématisation de l'organisation cristalline d'une série de molécules possédant des groupes carboxyles. En ingénierie cristalline, la récurrence d'un patron d'interactions suggère qu'il dirige l'association et qu'il est susceptible de la gouverner aussi dans des composés similaires.

1.3.1 Les synthons

Les synthons ont d'abord été introduits en chimie organique par Corey en 1967 qui les définissait comme des fragments moléculaires pouvant être assemblés lors d'une étape synthétique.[50] Bien que le terme sous cette forme soit maintenant désuet après être

progressivement devenu synonyme d'intermédiaire synthétique, la définition originale est le fondement des synthons supramoléculaires. Ces derniers sont définis comme les motifs d'association qui expriment les éléments fondamentaux d'une structure cristalline en termes de reconnaissance moléculaire.[2] Les synthons ne correspondent pas à des interactions spécifiques, mais bien à des fragments moléculaires et leur association supramoléculaire. Plusieurs exemples de synthons sont présentés à la Figure 8.

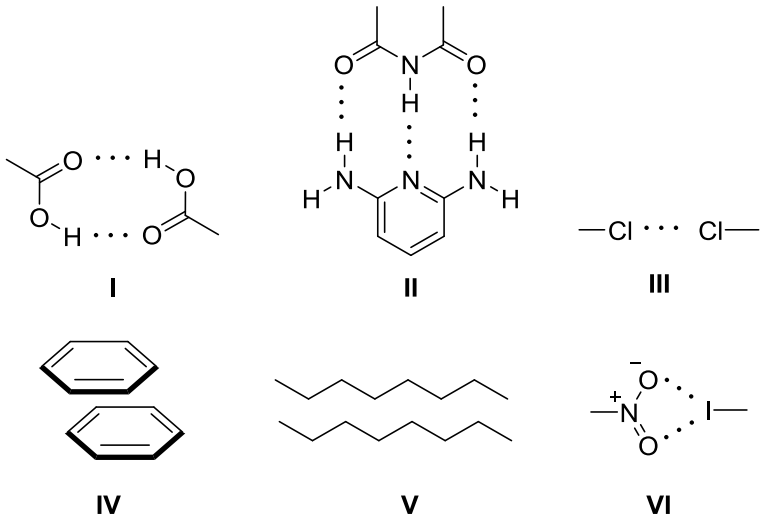

Figure 8. Exemples de synthons supramoléculaires.

Les synthons les plus utiles à l'ingénierie cristalline sont ceux qui se manifestent dans une grande gamme de structures, car ils permettent d'établir des tendances et ainsi de faire des prédictions (Figure 7). Ils sont généralement basés sur des interactions fortes qui leur permettent de dominer l'association supramoléculaire en présence d'une variété d'autres synthons de façon à ce que ces derniers n'interfèrent pas avec l'association du synthon principal. Cependant, un cristal demeure un compromis et des interactions faibles peuvent parfois perturber la formation d'un synthon fort. Par exemple, l'association des acides phenylpropioliques n'est généralement pas régie par le synthon **I** malgré la présence de l'acide carboxylique, car la formation de liens C-H···O entre le carbonyle et un hydrogène aromatique pousse les molécules à adopter un arrangement de ponts hydrogène différent (Figure 9).[51-53]

Ainsi, bien que l'ingénierie cristalline soit un bon outil de rationalisation des structures cristallines, son utilisation à des fins de prédiction nécessite des synthons particulièrement robustes.

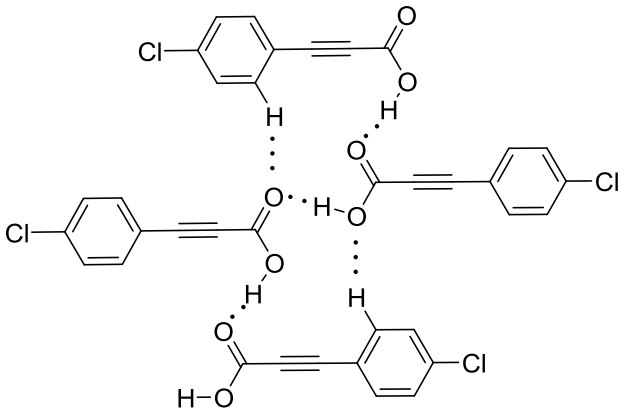

Figure 9. Schématisation de l'organisation cristalline de l'acide 4-chlorophénylpropiolique. La formation d'un lien C-H···O entre l'arène et le carbonyle conduit à l'adoption d'un patron de ponts hydrogène différent de celui normalement formé par les acides carboxyliques.

1.3.2 La tectonique moléculaire

Ultimement, l'approche des synthons peut être utilisée pour concevoir des molécules dont l'association cristalline est prévisible.[54, 55] On nomme ces molécules tectons, du mot grec *tekton* qui signifie bâtisseur.[56] Ces molécules sont conçues de façon à ce que leurs interactions soient dominées par des forces à la fois fortes et directionnelles, qui mènent ainsi à la formation d'organisations prédéterminées.

La stratégie la plus fréquemment employée consiste à greffer des fragments moléculaires s'associant par de multiples ponts hydrogène à des noyaux d'hydrocarbures. Les interactions provenant du squelette étant négligeables par rapport au synthon de ponts hydrogène, on peut alors compter uniquement sur ces derniers pour prédire l'association. Par exemple, les groupes diaminotriazine (DAT) s'assemblent préférablement dans le synthons

VII (Figure 10).[57-61] Lorsqu'ils sont liés à des squelettes aromatiques comme dans le composé **3**, les groupes DAT peuvent être considérés seuls afin de prédire l'association moléculaire. La Figure 10 permet de comparer l'organisation prévue à celle obtenue pour ce système et souligne la capacité des diaminotriazines à générer des organisations prévisibles.

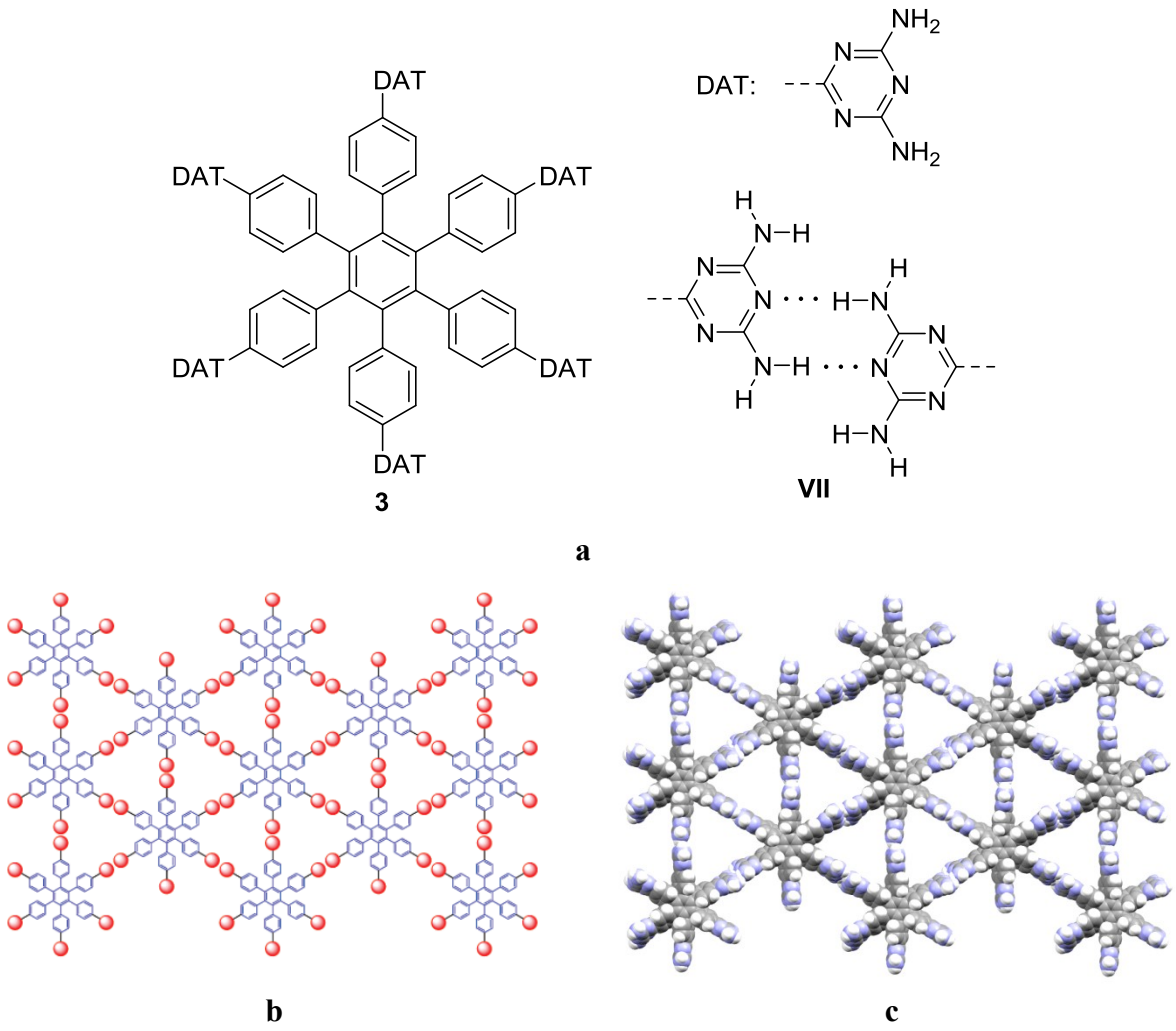

Figure 10. Utilisation de la tectonique moléculaire pour générer des organisations prédéfinies. (a) Structure du synthon associé aux groupements diaminotriazine (DAT) et structure d'un tecton basé sur ces fonctionnalités. (b) Organisation cristalline prévue pour le composé **3**. (c) Organisation cristalline obtenue. [57]

La tectonique moléculaire permet ainsi de concevoir des solides qui possèdent des propriétés ciblées et s'est montrée particulièrement efficace dans l'élaboration de matériaux cristallins poreux analogues aux zéolites. Par exemple, les groupements DAT attachés à un squelette spirobifluorène (**4**) ont permis de générer un cristal dont 75% du volume est accessible au solvant (Figure 11a). Différentes organisations peuvent être obtenues en variant les synthons de ponts hydrogène et la géométrie du squelette auquel ils sont attachés. Pour former des réseaux poreux, on privilégie des charpentes rigides, développées dans les trois dimensions, dont la forme défavorise un empilement compact des molécules. En plus des dérivés de spirobifluorène, l'utilisation des dérivés de triptycène (**5**) est aussi répandue, car ses trois panneaux aromatiques ancrés dans un noyau bicyclique permettent à la fois d'orienter les synthons dans des directions prévisibles et nuisent à l'émergence d'organisations compactes. Notamment, le réseau moléculaire le moins dense rapporté à ce jour est formé d'un dérivé de triptycène portant des fonctions urée (**6**). Les molécules y sont assemblées dans des canaux hexagonaux par de doubles ponts hydrogène (Figure 11b). La tendance des dérivés de triptycène à former des solides assemblés inefficacement en fait aussi de bons candidats pour les études de co-cristallisation.

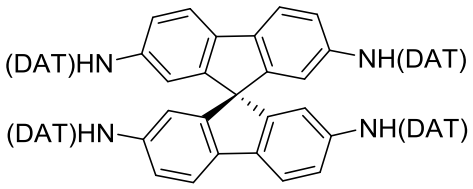

4

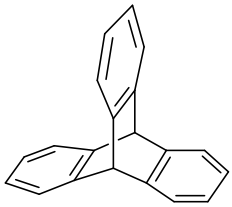

5

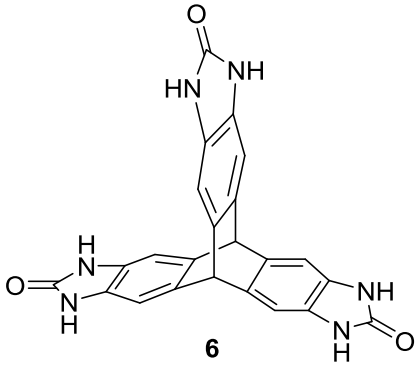

6

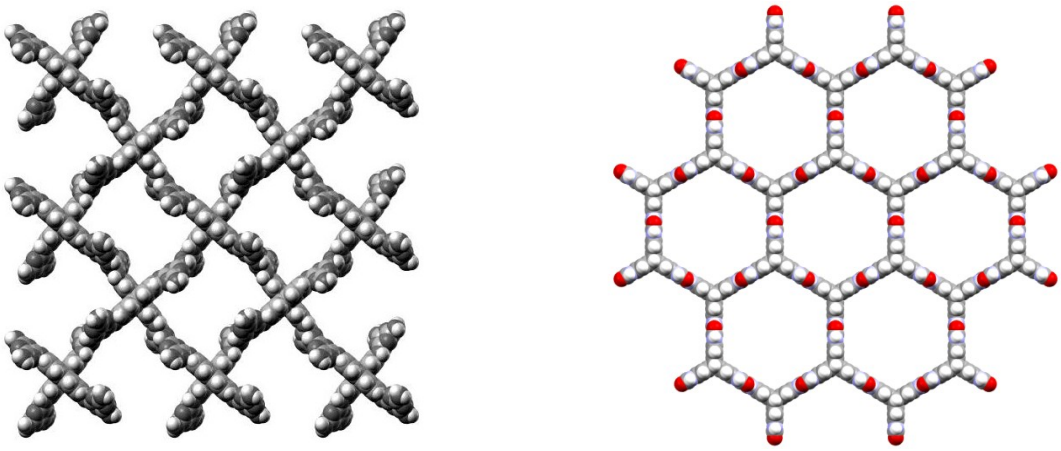

a **b**

Figure 11. Utilisation de la tectonique moléculaire pour générer des solides poreux. (a) Représentation de la structure cristalline du spirobifluorène **4.** (b) Représentation de la structure cristalline du triptycène **6.**

1.4 L'ingénierie cristalline en science des matériaux

L'organisation moléculaire est susceptible d'avoir un impact sur les propriétés de tous les matériaux utilisés à l'état solide tels les composés pharmaceutiques, les explosifs, les pigments et les conducteurs électriques; l'impossibilité de contrôler ou de prévoir cette organisation est un problème dans chacun de ces domaines. Les succès de la tectonique moléculaire dans la conception de solide poreux ne se transposent malheureusement pas à toutes les familles de matériaux, car ses synthons de prédilection ne sont pas compatibles à toutes les propriétés voulues. Des stratégies visant à guider l'association supramoléculaire ont émergé dans plusieurs domaines, mais leur portée est généralement restreinte à des petites familles de matériaux. Les composés explorés dans cette thèse étant principalement pertinents dans différentes sphères de l'électronique organique, la prochaine section se concentrera sur les façons dont l'organisation peut y affecter les propriétés et de comment elle peut être modulée.

1.4.1 L'ingénierie cristalline en électronique organique

Les petites molécules et les analogues supramoléculaires possédant un réseau π étendu ont trouvé des applications dans plusieurs branches de l'électronique organique. Ces composés sont particulièrement utiles dans les transistors à effet de champs, les cellules solaires et les diodes électroluminescentes. Dans ces dispositifs, la performance des composés est liée à leur capacité à participer dans la séparation, le transfert et le transport des charges. Dans une molécule de réseau π étendu, il y a typiquement des orbitales moléculaires occupées de haute énergie et des orbitales moléculaires vides de basse énergie, réduisant ainsi le gap et facilitant la perte ou le gain d'électrons. Pour que deux molécules participent à ces processus, elles doivent généralement être en proximité dans une orientation permettant un bon empilement de leurs réseaux π, car le recouvrement orbitalaire qui lui est associé maximise le couplage électronique intermoléculaire. Ainsi, une grande partie des efforts visant à contrôler l'organisation dans ce type de matériaux a été dirigée vers la promotion et l'optimisation des contacts intermoléculaires des systèmes π.[62-64]

Ce genre de travail est particulièrement développé dans la famille des oligoacènes car ces composés cristallisent généralement dans un motif à chevron contenant peu de contacts π et ainsi peu adapté à la percolation des charges.[65] Par exemple, l'ajout de groupement triisopropylsilyléthynyle (TIPS) au pentacène permet de passer d'une organisation dans laquelle les molécules sont presque orthogonales à une organisation où elles sont parallèles (Figure 12).[66] L'organisation est modifiée, car les groupements volumineux triisopropylsilyles entravent la formation des interactions C-H···π responsables de l'arrangement à chevron, mais leur maintient quelque peu à l'écart de l'acène par l'alcyne permet l'empilement des anneaux aromatiques. Lorsque des chaînes alkyles moins encombrantes sont employées, l'organisation redevient similaire à celle du pentacène et la mobilité électronique dans ces composés est réduite.[67] Cet exemple souligne aussi un autre aspect commun des stratégies d'ingénierie cristalline appliquées aux matériaux : les groupements ajoutés afin de moduler l'organisation contribuent rarement aux propriétés visées au-delà de leur rôle supramoléculaire. Les groupes TIPS permettent d'augmenter la solubilité et d'atteindre un arrangement optimal, mais

demeurent des groupes isolants. Il peut donc sembler contre-intuitif de les intégrer à un matériau afin d'augmenter sa conductivité. Ainsi, au défi de contrôler la nanostructure s'ajoute celui d'y arriver sans déprécier les propriétés moléculaires recherchées. Une façon de résoudre ce problème consiste à se pencher sur les façons dont les groupements responsables des caractéristiques moléculaires désirées peuvent aussi être utilisés pour diriger l'association des molécules. De telles connaissances pourraient être utilisées pour concevoir des matériaux en considérant à la fois les propriétés moléculaires et les propriétés supramoléculaires des fragments déterminants.

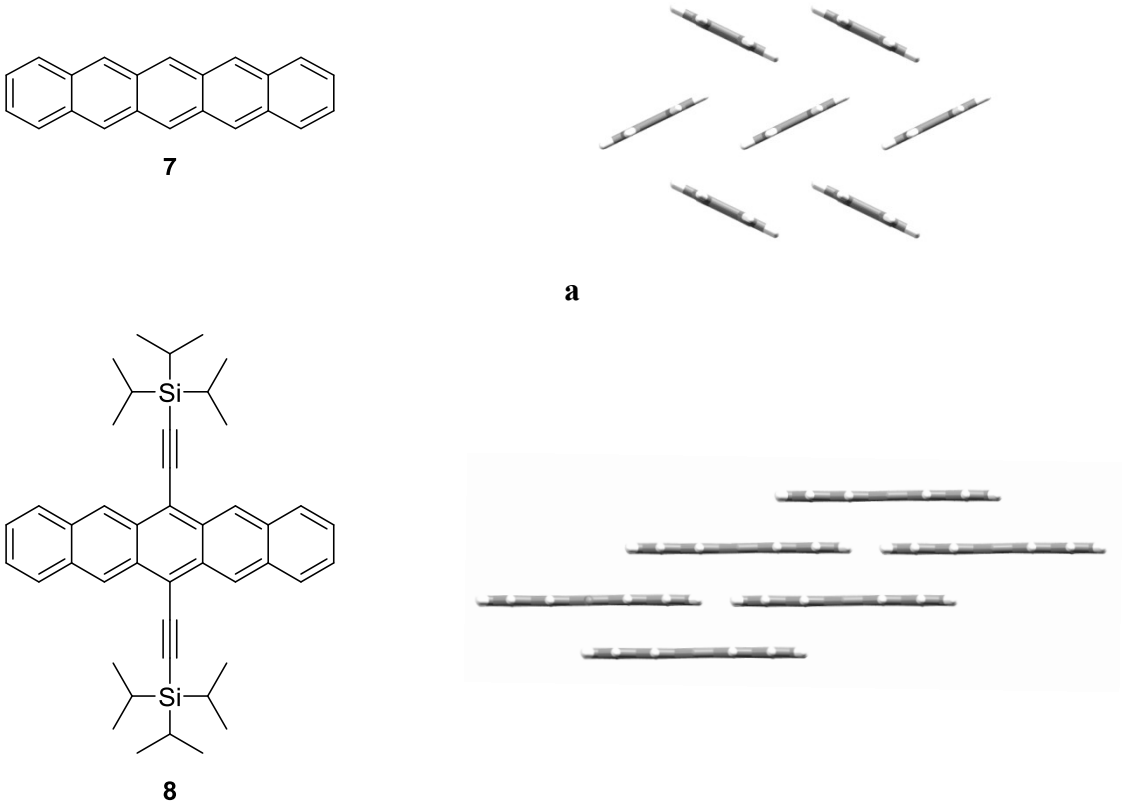

Figure 12. (a) Représentation de l'organisation cristalline du pentacène. (b) Organisation d'un dérivé modifié par des groupes TIPS. L'ajout de groupements volumineux défavorise la formation d'interactions C-H···π et permet ainsi de convertir l'arrangement à chevrons du pentacène en une organisation lamellaire. Les groupements TIPS sont ne sont pas représentés pour mieux montrer l'organisation des anneaux aromatiques.

1.4.1.1 Les cellules solaires organiques

Dans les dispositifs dont la couche active est composée d'une combinaison de substances, les défis associés au contrôle des arrangements moléculaires sont multipliés. Les cellules solaires organiques sont typiquement constituées d'un matériau qui absorbe la lumière, ce qui le conduit à un état excité, et qui transfère alors les électrons promus à une orbitale de plus haute énergie à un matériau accepteur (Figure 13). Ces électrons migrent ensuite vers l'anode alors que l'orbitale HOMO du composé donneur est repeuplée par la cathode.[68]

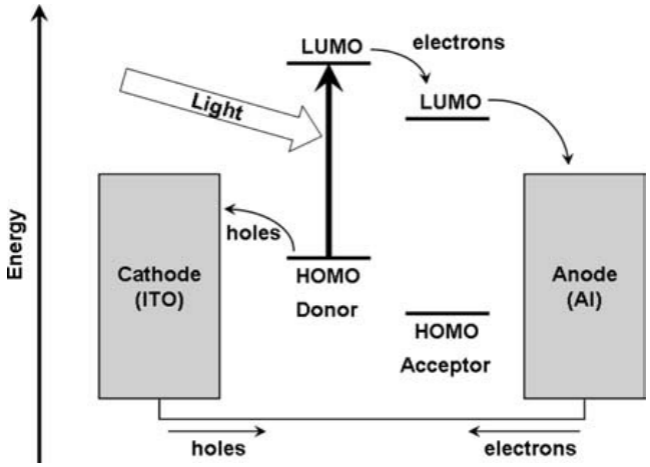

Figure 13. Schématisation du fonctionnement d'une cellule solaire organique. L'absorption lumineuse par le matériau donneur résulte en la promotion d'un électron de l'orbitale HOMO vers l'orbitale LUMO. Cet électron est alors à un niveau énergétique où le transfert vers le matériau accepteur est favorable et l'électron cascade jusqu'à l'anode. D'autres électrons sont réinjectés dans le matériau donneur par la cathode.[69]

Les matériaux donneurs sont généralement constitués d'unités riches en électrons et d'unités pauvres en électrons, combinées de façon à réduire le gap, à optimiser l'absorption lumineuse et à positionner les orbitales à des niveaux énergétiques favorisant les transferts électroniques vers l'accepteur et maximisant le voltage de la cellule.[70-72] Les fragments riches en électrons appartiennent par exemple aux familles des thiophènes (**9**) et des carbazoles (**11**) alors que les fragments pauvres en électrons sont souvent des thiadiazoles (**13-16**) ou des

cétopyrroles (**18-19**). Quelques exemples représentatifs de chaque catégorie sont présentés à la Figure 14. Parmi les groupes électroattracteurs, les dérivés du benzothiadiazole (**13**) sont particulièrement communs et des dérivés halogénés (**14**), des dérivés azotés (**15**) et des composés analogues possédant des réseaux aromatiques étendus (**16**) sont aussi utilisés.[73] L'exploration des matériaux accepteurs n'a originellement pas connu le même engouement que le développement des matériaux donneurs et les composés accepteurs ont pendant longtemps été limités à la famille des fullerènes. Les composés C_{60} (**20**) et C_{70} (**21**) ainsi que des dérivés fonctionnalisés pour faciliter leur manipulation (**22-23**), ont été utilisés extensivement pour leur bonne mobilité électronique, leur aptitude à promouvoir la séparation des charges et la stabilité de leur forme réduite.[74-76]

Les matériaux utilisés dans les cellules solaires doivent être conducteurs et les organisations moléculaires qui favorisent la percolation des charges, généralement des empilements π compacts, sont recherchées.[77, 78] L'impact de l'organisation sur les performances est particulièrement bien démontré par une série d'oligothiophènes rapportée par Fitzner et al. dans laquelle les molécules différent seulement par la substitution des thiophènes qui portent des hydrogènes, des groupes méthyles ou de groupes éthyles (Figure 15).[79] Bien que les composés montrent des propriétés pratiquement identiques en solution, le composé ayant l'organisation cristalline la plus dense produit des cellules solaires deux fois plus performantes.

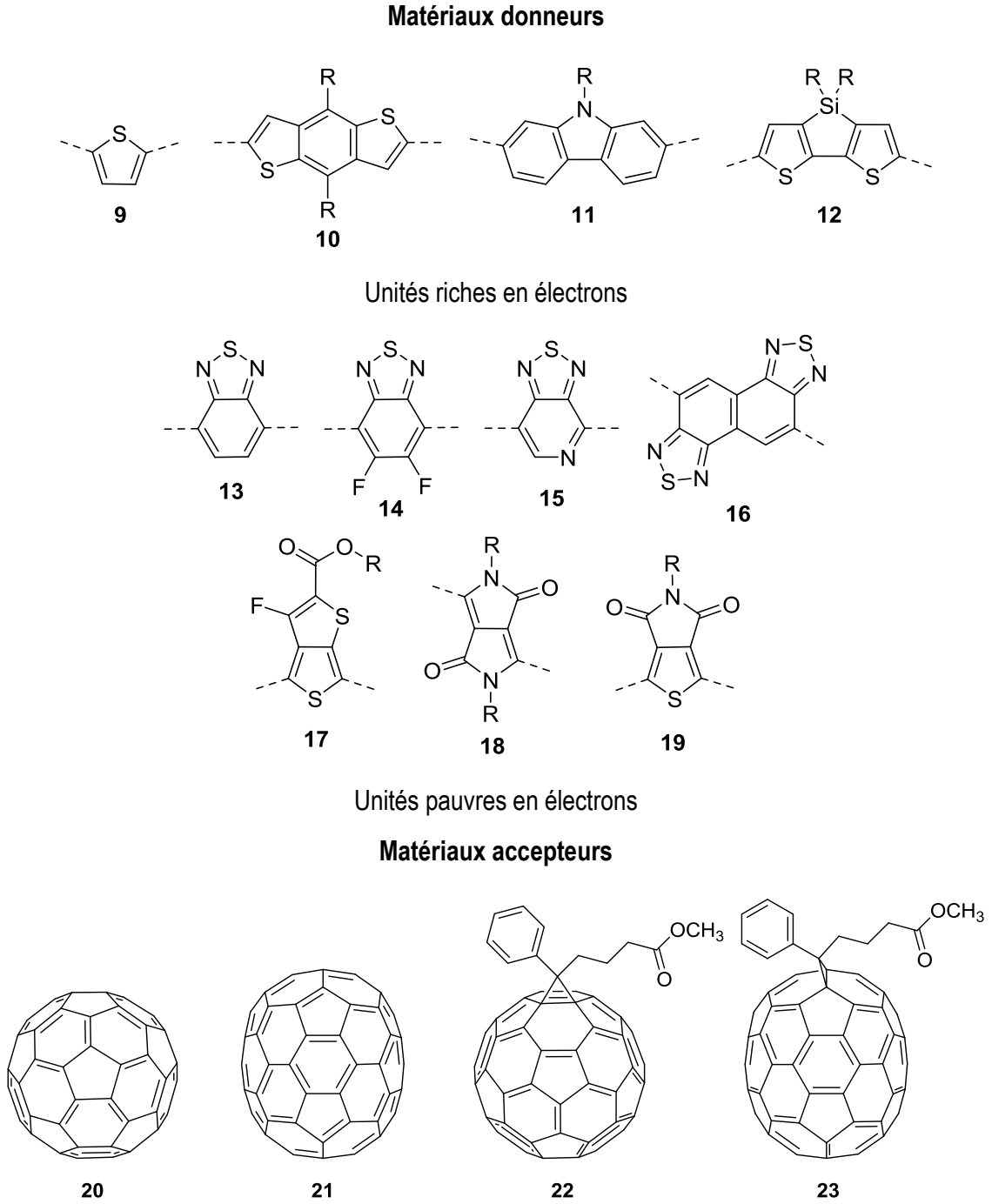

Figure 14. Exemples de matériaux typiquement employés dans la couche active des cellules solaires organiques. Les matériaux donneurs sont formés d'une combinaison de fragments électrodonneurs et électroaccepteurs et les matériaux accepteurs appartiennent généralement à la famille des fullerènes.

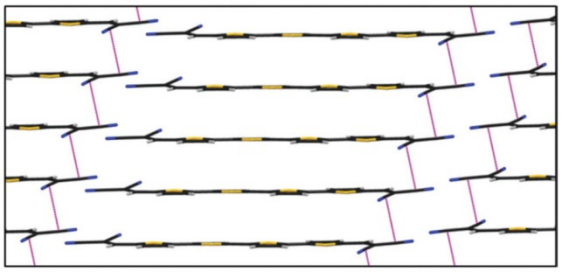

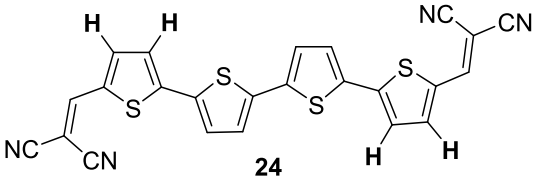

24

Efficacité énergétique : 1,5%

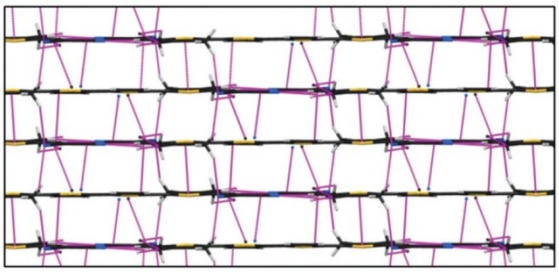

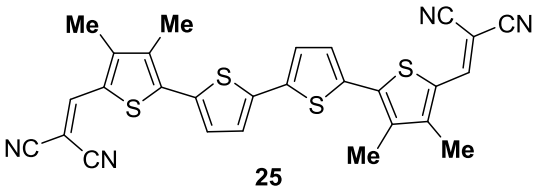

25

Efficacité énergétique : 3,8%

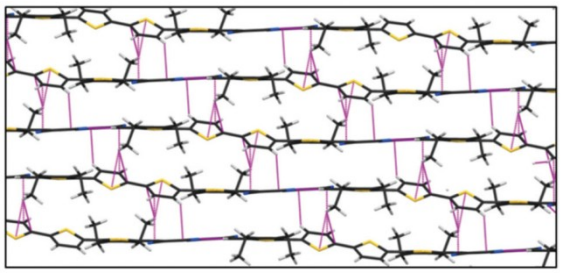

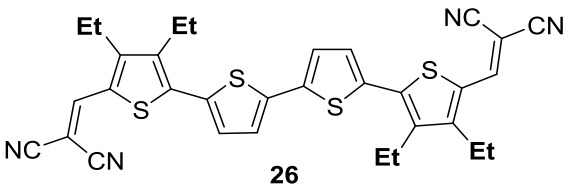

26

Efficacité énergétique : 1,5%

Figure 15. Corrélation entre l'organisation et les performances dans les cellules solaires organiques. Dans cette série de composés, le matériau ayant l'organisation la plus dense conduit aux meilleures efficacités énergétiques. L'efficacité énergétique correspond à la portion d'énergie lumineuse convertie en énergie électrique.

Dans ce type de dispositifs, les performances dépendent de surcroit de l'organisation de l'interface entre le composé donneur et le composé accepteur.[78, 80-82] Bien que l'on retrouve de plus en plus d'exemples qui corrèlent les arrangements moléculaires à l'hétérojonction aux rendements énergétiques, il existe actuellement peu de stratégies visant à contrôler cette organisation. Cela est notamment dû à la difficulté de déterminer la nanostructure de films composés de mélanges de substances et à l'influence impondérable de la morphologie des films sur les performances.[83,84] L'impact des arrangements

intermoléculaires à l'hétérojonction est notamment illustré par le rôle de la nature et de la position des chaînes alkyles dans le matériau donneur.[85] Ces groupements, intégrés pour augmenter la solubilité, peuvent influencer l'association avec le matériau accepteur par l'encombrement stérique. Ainsi, la présence de chaînes alkyles volumineuses sur la portion du matériau donneur où est localisée l'orbitale LUMO est nuisible, car les substituants entravent l'association avec le matériau accepteur et défavorisent de cette façon le transfert électronique (Figure 16). Dans des polymères à base de benzodithiophène et de thiènopyrrole-4,6-dione, la permutation de chaînes alkyles ramifiées et linéaires entre les parties pauvres et riches en électrons du matériau donneur fait varier les rendements énergétiques entre 1,7 et 8%.

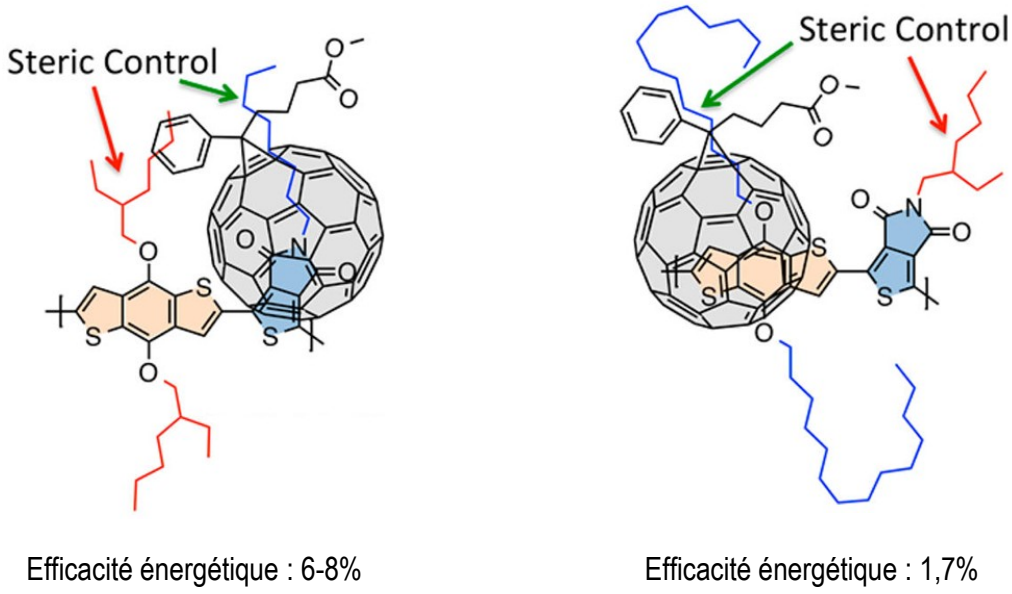

Figure 16. Corrélation entre l'organisation de l'hétérojonction et les performances dans les cellules solaires organiques. L'encombrement stérique provenant des chaînes alkyles solubilisantes peut diriger l'association entre le polymère et les fullerènes. Lorsque les chaînes les plus encombrantes sont placées sur la portion du polymère où se trouve l'orbitale LUMO, l'efficacité énergétique est réduite, car le transfert électronique entre le polymère et le fullerène est affectée.[85]

1.4.1.2 Les batteries rechargeables

Plusieurs matériaux organiques sont maintenant utilisés dans la fabrication d'électrodes, principalement dans la confection de cathodes dans les batteries rechargeables au lithium.[86-88] Le fonctionnent de ces dispositifs est analogue à celui des cellules galvaniques et repose sur la connexion de deux matériaux possédant des potentiels rédox différents et pouvant participer à des réactions d'oxydoréductions réversibles (Figure 17). Ces matériaux sont immergés dans un électrolyte et séparés par une membrane qui limite le transport ionique. Lors de la décharge, l'oxydation de l'anode génère des électrons ensuite utilisés dans la réduction de la cathode. L'équilibre des charges est assuré par la migration de l'électrolyte (Figure 18). Plusieurs classes de matériaux organiques ont été explorées dans la fabrication de cathode, tels les thioéthers, les organodisulfides ainsi que divers types de carbonyle.[89-92] Les composés quinonoïdes ont été l'objet d'un intérêt particulier, car ils prennent part à des réactions rédox réversibles impliquant plusieurs électrons et leur forme réduite est stabilisée par aromaticité (Figure 17).

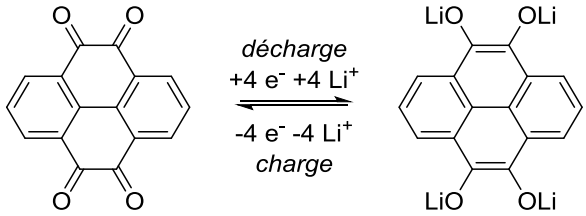

27 **28**

Figure 17. Exemple de composés organiques quinonoïdes pouvant être utilisés dans la fabrication de cathode dans les batteries rechargeables et réaction rédox qui lui est associée.[90]

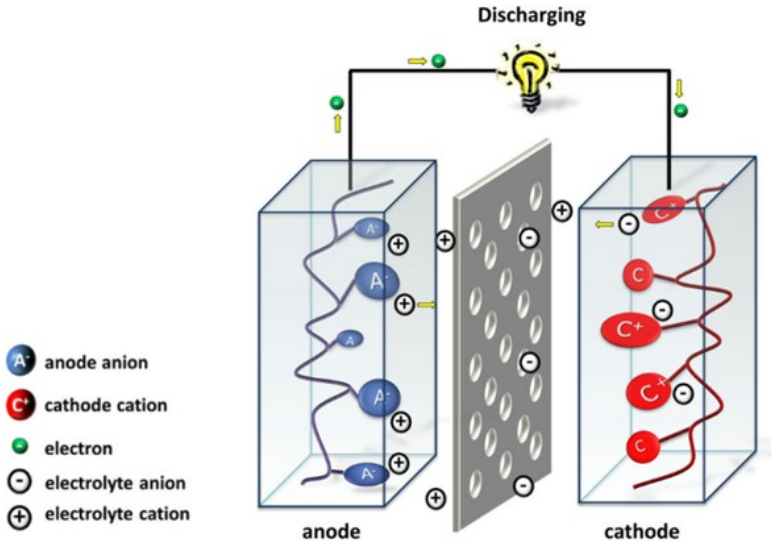

Figure 18. Schéma montrant le fonctionnement général d'une batterie rechargeable lors de la décharge. La différence de potentiel entre la cathode et l'anode promeut l'oxydation de l'anode. Les électrons produits sont transférés à la cathode et permettent sa réduction. La diffusion de l'électrolyte entre les électrodes assure la répartition des charges.[86]

Les matériaux constituant les électrodes doivent être structurés de façon à faciliter la diffusion des électrons et des ions. Actuellement, peu de stratégies s'attaquent directement à ces enjeux structuraux qui sont plutôt contournés par l'ajout d'additifs. L'influence de l'organisation moléculaire sur les performances peut alors cependant se manifester dans la structure de l'interface entre ces additifs et le composé actif. Par exemple, lorsque des nanotubes de carbone sont utilisés pour palier à la mauvaise conductivité du composé rédox, les molécules du composé actif peuvent s'autoassembler à leur surface grâce à leur système π étendu, ce qui favorise à la fois la migration des électrons et l'accessibilité des sites redox à l'électrolyte.[93]

1.5 Objectifs de la thèse

En chimie supramoléculaire, le tout est plus grand que la somme de ses parties : les caractéristiques d'un matériau ne sont pas toujours définies par les attributs de molécules isolées et émergent parfois seulement de leur collectivité. Les propriétés dépendent alors de l'organisation moléculaire et l'impossibilité de la prévoir est un obstacle majeur à notre habileté à concevoir des matériaux ayant des caractéristiques prédéfinies. Bien que différentes méthodes permettent de moduler l'organisation, leur portée est généralement limitée et les fragments employés sont souvent étrangers aux propriétés ultimement visées. Ainsi, les organisations favorables sont parfois atteintes aux dépens des propriétés moléculaires. Par conséquent, nous avons choisi d'étudier l'association moléculaire dans des familles de composés pertinentes en électronique organique et de nous pencher sur les façons dont les fragments moléculaires déterminant les propriétés intrinsèques attrayantes peuvent aussi être utilisés pour diriger l'association moléculaire. Nous avons aussi choisi de nous limiter à des composés structurellement apparentés et nous nous sommes focalisés sur des composés de forme quinonoïde qui combinent trois caractéristiques essentielles : (1) La présence d'un système-π étendu; (2) la capacité de s'engager dans diverses interactions intermoléculaires; et (3) un caractère électrodéficitaire favorisant des phénomènes de transfert de charge ou la participation dans des réactions rédox (Figure 19).

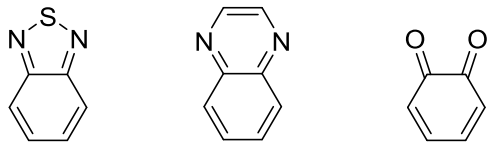

Figure 19. Exemples de structures de type quinonoïde.

Une première partie de la thèse se concentre sur l'association des thiadiazoles aromatiques. Ces unités sont communes à plusieurs matériaux optoélectroniques et se sont révélées particulièrement efficaces lorsqu'intégrées aux cellules solaires organiques. Afin

d'approfondir la pertinence de notre étude à cette technologie, nous avons aussi étudié la formation de co-cristaux entre des dérivés de thiadiazoles et des fullerènes, une autre classe de matériaux couramment intégrée dans ce type de dispositif. Cette section est suivie d'un chapitre qui détaille une partie des efforts synthétiques déployés dans la préparation des thiadiazoles. La seconde partie de la thèse se tourne vers des dérivés de triptycène portant des unités quinone et hydroquinone et sur les façons dont leur association et leurs propriétés rédox peuvent être utilisées de concert à l'état solide. Finalement, une dernière section discute de comment les composés explorés peuvent être intégrés à des matériaux et des dispositifs à la lumière de ce qui a été présenté.

1.6 Références

1. Whitesides, G. M.; Simanek, E. E.; Mathias, J. P.; Seto, C. T.; Chin, D. N.; Mammen, M.; Gordon, D. M. *Acc. Chem. Res.* **1995**, *28*, 37-44.
2. Desiraju, G. R. *Angew. Chem., Int. Ed.* **1995**, *34*, 2311-2327.
3. Lehn, J. M. *Angew. Chem., Int. Ed.* **1988**, *27*, 89-112.
4. Steed, J. W.; Turner, D. R.; Wallace, K. *Core concepts in supramolecular chemistry and nanochemistry*. John Wiley & Sons: New York, 2007.
5. Dunitz, J. D. *Pure Appl. Chem.* **1991**, *63*, 177-185.
6. Authier, A. *Early Days of X-ray Crystallography*. Oxford University Press: Oxford, 2013.
7. Friedrich, W.; Knipping, P.; von Laue, M. *Sitzungsberichte der Kgl. Bayer. Akad. der Wiss.* **1912**, 303.
8. Bragg, W. L. *Proc. Royal Soc. A* **1913**, *89*, 248-277.
9. Bragg, W. L. *Nature* **1912**, *90*, 410.
10. Bragg, W. L. *Proc. Camb. Philos. Soc.* **1913**, *17*, 43-57.
11. Bragg, W. H.; Bragg, W. L. *Nature* **1913**, *91*, 557.
12. Bragg, W. H.; Bragg, W. L. *Proc. Royal Soc. A* **1913**, *89*, 277-291.
13. Lonsdale, K. *Nature* **1928**, *122*, 810.
14. Bragg, W. H.; Bragg, W. L. The discovery of X-ray diffraction. In *Laue Diagrams, 25 Years of research on X-ray diffraction following Prof. Max von Laue discovery*, Indian Academy of Sciences: Bangalore, 1937; pp 9-10.
15. Watson, J. D.; Crick, F. H. C. *Nature* **1953**, *171*, 737.
16. Franklin, R. E.; Gosling, R. G. *Nature* **1953**, *171*, 740.
17. Wilkins, M. H. F.; Stokes, A. R.; Wilson, H. R. *Nature* **1953**, *171*, 738.
18. Pauling, L.; Corey, R. B. *J. Am. Chem. Soc.* **1950**, *72*, 5349-5349.
19. The Cambridge Structural Database (CSD). www.ccdc.cam.ac.uk.
20. Gibbs, J. W. *Trans. Connect. Acad. Sci.* **1878**, *3*, 343-524.
21. Gibbs, J. W. *Trans. Connect. Acad. Sci.* **1876**, *3*, 108-248.
22. Erdemir, D.; Lee, A. Y.; Myerson, A. S. *Acc. Chem. Res.* **2009**, *42*, 621-629.
23. Vekilov, P. G. *Cryst. Growth Des.* **2010**, *10*, 5007-5019.

24. Bøjesen, E. D.; Iversen, B. B. *CrystEngComm* **2016**, *18*, 8332-8353.
25. Schreiber, R. E.; Houben, L.; Wolf, S. G.; Leitus, G.; Lang, Z.-L.; Carbó, J. J.; Poblet, J. M.; Neumann, R. *Nature Chem.* **2017**, *9*, 369.
26. De Yoreo, J. J.; Gilbert, P. U. P. A.; Sommerdijk, N. A. J. M.; Penn, R. L.; Whitelam, S.; Joester, D.; Zhang, H.; Rimer, J. D.; Navrotsky, A.; Banfield, J. F.; Wallace, A. F.; Michel, F. M.; Meldrum, F. C.; Cölfen, H.; Dove, P. M. *Science* **2015**, *349*, aaa6760.
27. Mooij, W. T. M.; van Eijck, B. P.; Price, S. L.; Verwer, P.; Kroon, J. *J. Comput. Chem.* **1998**, *19*, 459-474.
28. Desiraju, G. R. *Nat. Mater.* **2002**, *1*, 77-79.
29. Desiraju, G. R. *J. Chem. Sci.* **2010**, *122*, 667-675.
30. Waldstein, P.; Blatz, L. A. *J. Phys. Chem.* **1967**, *71*, 2271-2276.
31. Cruz-Cabeza, A. J.; Bernstein, J. *Chem. Rev.* **2014**, *114*, 2170-2191.
32. Cruz-Cabeza, A. J.; Reutzel-Edens, S. M.; Bernstein, J. *Chem. Soc. Rev.* **2015**, *44*, 8619-8635.
33. Desiraju, G. R. *Cryst. Growth Des.* **2004**, *4*, 1089-1090.
34. Brog, J.-P.; Chanez, C.-L.; Crochet, A.; Fromm, K. M. *RSC Adv.* **2013**, *3*, 16905-16931.
35. Kersten, K.; Kaur, R.; Matzger, A. *IUCrJ* **2018**, *5*, 124-129.
36. *Co-crystals: Preparation, Characterization and Applications*. Aakeröy, C. B.; Sinha, A. S. ed.; The Royal Society of Chemistry: London, 2018.
37. Aakeroy, C. *Acta Crystallogr., Sect. B: Struct. Sci.* **2015**, *71*, 387-391.
38. Desiraju, G. R. *CrystEngComm* **2003**, *5*, 466-467.
39. Dunitz, J. D. *CrystEngComm* **2003**, *5*, 506-506.
40. Matsuda, H.; Osaki, K.; Nitta, I. *Bull. Chem. Soc. Jpn.* **1958**, *31*, 611-620.
41. Sakurai, T. *Acta Crystallogr.* **1965**, *19*, 320-330.
42. Sakurai, T. *Acta Crystallogr., Sect. B: Struct. Sci.* **1968**, *B 24*, 403-412.
43. Vishweshwar, P.; McMahon, J. A.; Bis, J. A.; Zaworotko, M. J. *J. Pharm. Sci.* **2006**, *95*, 499-516.
44. Pepinsky, R. *Phys. Rev.* **1955**, *100*, 971-971.
45. Schmidt, G. M. J. *Pure Appl. Chem.* **1971**, *27*, 647.

46. Wierda, D. A.; Feng, T. L.; Barron, A. R. *Acta Crystallogr., Sect. C: Cryst. Struct. Commun.* **1989**, *45*, 338-339.
47. Desiraju, G. R. *J. Am. Chem. Soc.* **2013**, *135*, 9952-9967.
48. Kitaigorodskii, A. I. *Molecular Crystals and Molecules*. Academic Press: New York, 1973.
49. Etter, M. C. *Acc. Chem. Res.* **1990**, *23*, 120-126.
50. Corey, E. J. *Pure Appl. Chem.* **1967**, *14*, 19-38.
51. Desiraju, G. R.; Murty, B. N.; Kishan, K. V. R. *Chem. Mater.* **1990**, *2*, 447-449.
52. Desiraju, G. R. *Chem. Commun.* **1997**, 1475-1482.
53. Das, D.; Desiraju, G. R. *Chem. Asian J.* **2006**, *1*, 231-244.
54. Wuest, J. D. *Chem. Commun.* **2005**, 5830-5837.
55. Hosseini, M. W. *CrystEngComm* **2004**, *6*, 318-322.
56. Simard, M.; Su, D.; Wuest, J. D. *J. Am. Chem. Soc.* **1991**, *113*, 4696-4698.
57. Maly, K. E.; Gagnon, E.; Maris, T.; Wuest, J. D. *J. Am. Chem. Soc.* **2007**, *129*, 4306-4322.
58. Helzy, F.; Maris, T.; Wuest, J. D. *Cryst. Growth Des.* **2008**, *8*, 1547-1553.
59. Helzy, F.; Maris, T.; Wuest, J. D. *J. Org. Chem.* **2016**, *81*, 3076-3086.
60. Beaudoin, D.; Blair-Pereira, J.-N.; Langis-Barsetti, S.; Maris, T.; Wuest, J. D. *J. Org. Chem.* **2017**, *82*, 8536-8547.
61. Fournier, J.-H.; Maris, T.; Wuest, J. D. *J. Org. Chem.* **2004**, *69*, 1762-1775.
62. Sutton, C.; Risko, C.; Brédas, J.-L. *Chem. Mater.* **2016**, *28*, 3-16.
63. Yao, Z. F.; Wang, J. Y.; Pei, J. *Cryst. Growth Des.* **2018**, *18*, 7-15.
64. Yassar, A. *Polym. Sci. Ser. C* **2014**, *56*, 4-19.
65. Anthony, J. E. *Chem. Rev.* **2006**, *106*, 5028-5048.
66. Anthony, J. E.; Brooks, J. S.; Eaton, D. L.; Parkin, S. R. *J. Am. Chem. Soc.* **2001**, *123*, 9482-9483.
67. Payne, M. M.; Parkin, S. R.; Anthony, J. E.; Kuo, C.-C.; Jackson, T. N. *J. Am. Chem. Soc.* **2005**, *127*, 4986-4987.
68. Brédas, J.-L.; Norton, J. E.; Cornil, J.; Coropceanu, V. *Acc. Chem. Res.* **2009**, *42*, 1691-1699.

69. Benanti, T. L.; Venkataraman, D. *Photosynth. Res.* **2006**, *87*, 73-81.
70. Scharber, M. C.; Mühlbacher, D.; Koppe, M.; Denk, P.; Waldauf, C.; Heeger, A. J.; Brabec, C. J. *Adv. Mater.* **2006**, *18*, 789-794.
71. Henson, Z. B.; Müllen, K.; Bazan, G. C. *Nature Chem.* **2012**, *4*, 699-704.
72. Li, Y. *Acc. Chem. Res.* **2012**, *45*, 723-733.
73. Wang, Y.; Michinobu, T. *J. Mater. Chem. C* **2016**, *4*, 6200-6214.
74. Yan, C.; Barlow, S.; Wang, Z.; Yan, H.; Jen, A. K. Y.; Marder, S. R.; Zhan, X. *Nat. Rev. Mater.* **2018**, *3*, 18003.
75. Hudhomme, P. *EPJ Photovolt.* **2013**, *4*, 40401.
76. Liu, T.; Troisi, A. *Adv. Mater.* **2013**, *25*, 1038-1041.
77. Rivnay, J.; Mannsfeld, S. C. B.; Miller, C. E.; Salleo, A.; Toney, M. F. *Chem. Rev.* **2012**, *112*, 5488-5519.
78. Brabec, C. J.; Heeney, M.; McCulloch, I.; Nelson, J. *Chem. Soc. Rev.* **2011**, *40*, 1185-1199.
79. Fitzner, R.; Elschner, C.; Weil, M.; Uhrich, C.; Körner, C.; Riede, M.; Leo, K.; Pfeiffer, M.; Reinold, E.; Mena-Osteritz, E.; Bäuerle, P. *Adv. Mater.* **2012**, *24*, 675-680.
80. Konarev, D. V.; Zubavichus, Y. V.; Valeev, E. F.; Slovokhotov, Y. L.; Shul'ga, Y. M.; Lyubovskaya, R. N. *Synth. Met.* **1999**, *103*, 2364-2365.
81. Ran, N. A.; Roland, S.; Love, J. A.; Savikhin, V.; Takacs, C. J.; Fu, Y.-T.; Li, H.; Coropceanu, V.; Liu, X.; Brédas, J.-L.; Bazan, G. C.; Toney, M. F.; Neher, D.; Nguyen, T.-Q. *Nat. Commun.* **2017**, *8*, 79.
82. Graetzel, M.; Janssen, R. A. J.; Mitzi, D. B.; Sargent, E. H. *Nature* **2012**, *488*, 304.
83. Lee, H.; Park, C.; Sin, D. H.; Park, J. H.; Cho, K. *Adv. Mater.* **2018**, *30*, 1800453.
84. Huang, Y.; Kramer, E. J.; Heeger, A. J.; Bazan, G. C. *Chem. Rev.* **2014**, *114*, 7006-7043.
85. Graham, K. R.; Cabanetos, C.; Jahnke, J. P.; Idso, M. N.; El Labban, A.; Ngongang Ndjawa, G. O.; Heumueller, T.; Vandewal, K.; Salleo, A.; Chmelka, B. F.; Amassian, A.; Beaujuge, P. M.; McGehee, M. D. *J. Am. Chem. Soc.* **2014**, *136*, 9608-9618.
86. Muench, S.; Wild, A.; Friebe, C.; Häupler, B.; Janoschka, T.; Schubert, U. S. *Chem. Rev.* **2016**, *116*, 9438-9484.
87. Xie, J.; Zhang, Q. *J. Mater. Chem. A* **2016**, *4*, 7091-7106.

88. Wuttke, S.; Medina, D. D.; Rotter, J. M.; Begum, S.; Stassin, T.; Ameloot, R.; Oschatz, M.; Tsotsalas, M. *Adv. Funct. Mater.* **2018**, *28*, 1801545.
89. Song, Z.; Zhou, H. *Energy Environ. Sci.* **2013**, *6*, 2280-2301.
90. Liang, Y.; Zhang, P.; Chen, J. *Chem. Sci.* **2013**, *4*, 1330-1337.
91. Liang, Y.; Tao, Z.; Chen, J. *Adv. Energy Mater.* **2012**, *2*, 742-769.
92. Häupler, B.; Wild, A.; Schubert, U. S. *Adv. Energy Mater.* **2015**, *5*, 1402034.
93. Lee, M.; Hong, J.; Kim, H.; Lim, H.-D.; Cho, S. B.; Kang, K.; Park, C. B. *Adv. Mater.* **2014**, *26*, 2558-2565.

Chapitre 2.

Organisation moléculaire de 2,1,3-benzothiadiazoles à l'état solide

Chapitre 2. Organisation moléculaire de 2,1,3-benzothiadiazoles à l'état solide.

Les benzothiadiazoles (**1**) sont des hétérocycles plats et pauvres en électrons dont la structure électronique est la mieux représentée par sa forme quinonoïde. Bien qu'ils aient d'abord été étudiés par les industries pharmaceutique et agrochimique, ils sont maintenant principalement utilisés comme unités pauvres en électrons dans des composés conjugués de type *push-pull* destinés à des applications optoélectroniques. Les benzothiadiazoles ont notamment été utilisés extensivement dans l'élaboration de matériaux pour les cellules solaires organiques où ils ont mené à certains des matériaux les plus performants.

1

Dans les dispositifs à couche mince, l'arrangement des molécules constituant la couche active affecte les performances des matériaux. Dans les cellules solaires, par exemple, les unités doivent être structurées de façon à optimiser l'absorption lumineuse, la séparation des charges et leur transport vers les électrodes. Il n'existe pas de stratégie générale permettant de contrôler cette organisation et les structures optimales sont généralement obtenues grâce à un processus d'essais-erreurs. Les thiadiazoles offrent une opportunité intéressante de diriger l'association, car ils peuvent prendre part à diverses liaisons supramoléculaires telles des interactions S···N, des interactions C-H···N et des interactions π. Il est cependant difficile d'évaluer comment les thiadiazoles pourraient être utilisés pour moduler l'organisation, car il existe peu d'études systématiques sur leurs modes d'association privilégiés. Nous avons ainsi entrepris la préparation d'une série de thiadiazoles et nous nous sommes penchés sur leur structure cristalline. De plus, puisqu'il s'agit d'une classe de molécules utilisée dans des matériaux optoélectroniques, nous avons aussi évalué d'autres caractéristiques pertinentes à ce

type d'applications telles l'absorption et l'émission lumineuse ainsi que les propriétés rédox. Finalement, les thiadiazoles étant principalement exploités dans les cellules solaires, nous nous sommes aussi attardés à leur association avec les fullerènes C_{60} et C_{70}, des accepteurs d'électrons communément utilisés dans ce type de dispositifs.

Molecular Organization of 2,1,3-Benzothiadiazoles in the Solid State

Sophie Langis-Barsetti, Thierry Maris, and James D. Wuest

The Journal of Organic Chemistry, **2017***, 82,* 5034-5045

Abstract

Derivatives of 2,1,3-benzothiadiazole (**1**) are widely used in many areas of science and are particularly valuable as components of active layers in various thin-film optoelectronic devices. Even more effective benzothiadiazoles are likely to result if a deeper understanding of their preferred patterns of molecular association can be acquired. To provide new insight, we have analyzed the structures of compounds in which multiple benzothiadiazole units are attached to well-defined planar and nonplanar molecular cores. Our results show that molecular organization can be controlled in complex structures by using directional S···N bonding of benzothiadiazole units and other characteristic interactions. Moreover, the observed structures are distinctly different from those of analogous arenes. Replacing benzene rings in arenes by thiadiazoles thereby provides a strategy for making new compounds with extended systems of π-conjugation and unique patterns of molecular organization, including the ability to co-crystallize with the fullerenes C_{60} and C_{70}.

Introduction

The synthesis of 2,1,3-benzothiadiazole (**1**) was first reported by Hinsberg in 1889.[2] Subsequent reviews of the chemistry of benzothiadiazoles have been published,[3] but the family of compounds has remained unfamiliar to many chemists. Increasingly, however, 2,1,3-benzothiadiazole units can be found in molecular structures with a broad spectrum of useful properties. For example, tizanidine is an adrenergic agonist widely prescribed as a muscle relaxant, and many other derivatives of 2,1,3-benzothiadiazole (**1**) have biological properties of interest.[4-7] In addition, 2,1,3-benzothiadiazole units have been incorporated as electron-poor moieties in various π-conjugated push-pull polymers and small molecules for use as luminescent materials and as components of thin-film optoelectronic devices, including light-emitting diodes, solar cells, field-effect transistors, and biosensors.[8-30] In fact, some of the best molecular materials devised so far for these applications are derivatives of 2,1,3-benzothiadiazole (**1**). As a result, the chemistry of 2,1,3-benzothiadiazoles is a subject of rapidly growing interest.

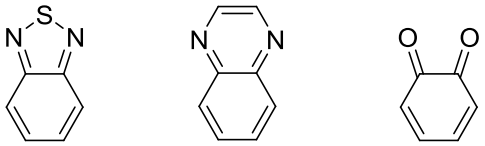

1 **2** **3**

In typical molecular thin-film optoelectronic devices, the components of the active layers must be properly organized on the nanometric scale to attain optimal efficiency. In photovoltaic devices, for example, the components must be arranged to absorb light, promote the separation of charges, and facilitate their transport to electrodes.[31-35] In many cases, suitable local molecular organization must be achieved without allowing the components to crystallize or undergo extensive separation of phases. Unfortunately, few guidelines are available to help direct the search for molecular components that meet these criteria, and

making effective new thin-film molecular devices is often a laborious undertaking requiring substantial experimentation.

Challenges inherent in creating predictably organized molecular structures are compounded in the case of 2,1,3-benzothiadiazoles by a lack of systematic investigations of their preferred motifs of association in the solid state. Representative crystallographic studies have confirmed that the atoms of C, N, and S in the 2,1,3-benzothiadiazole core are essentially coplanar and that intramolecular bonding is well represented by quinonoid structure **1**.[8,9,36-49] This preference is consistent with dipole moments measured for the increasingly polarized series of analogues naphthalene, quinoxaline (**2**), 2,1,3-benzothiadiazole (**1**), and 1,2-benzoquinone (**3**), which are 0, 0.51,[50,51] 1.8,[52] and 4.2 D,[53-55] respectively. Previously published structural studies show that 2,1,3-benzothiadiazoles can engage in various intermolecular interactions, including π-stacking, dipole-dipole interactions, C-H···π interactions, C-H···N interactions, and S···N interactions.[8,9,36-49] S···N interactions involving benzothiadiazoles can be considered to arise from various effects, including the electrostatic attraction of opposing partial charges and the interaction of S-N σ* orbitals with non-bonding orbitals centered on N.[56-59] The strength of S···N interactions appears to be similar to that of typical hydrogen bonds and has been calculated by dispersion-corrected DFT methods to be approximately 4 kcal/mol.[58] However, the relative importance of various interactions characteristic of 2,1,3-benzothiadiazoles remains unclear, and there are no reports of extensive efforts to use these interactions to direct the crystallization of complex 2,1,3-benzothiadiazoles in predetermined ways.

To provide deeper insight, we have synthesized compounds **4**-**8**, in which multiple 2,1,3-benzothiadiazole units are attached to well-defined planar and nonplanar molecular cores, and we have analyzed their structures by X-ray crystallography. Very few structures incorporating two or more 2,1,3-benzothiadiazole units have been reported previously.[8,9,43-49] Compounds **4**-**8** allow us to test the notion that neighboring molecules can be positioned predictably in complex structures by using directional interactions of 2,1,3-benzothiadiazole units. Moreover, the expected importance of S···N interactions makes it likely that the

molecular organization preferred by compounds **4**-**8** and related structures will be distinctly different from that of analogous aromatic hydrocarbons. Replacing benzene rings in arenes by thiadiazoles will thereby create new compounds with extended systems of π-conjugation, as found in conventional aromatic analogues, but also with novel optoelectronic properties arising in part from radically different patterns of association in condensed phases.[60] To ensure that our structural analyses of compounds **4**-**8** are relevant to studies in which the typical components of molecular thin-film devices must be properly organized, we have also examined co-crystallizations of triptycenetris(thiadiazole) **8** with the fullerenes C_{60} and C_{70}, which define a class of compounds widely used as electron acceptors in solar cells.

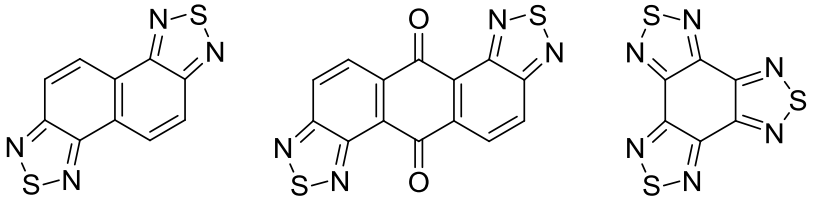

4 **5** **6**

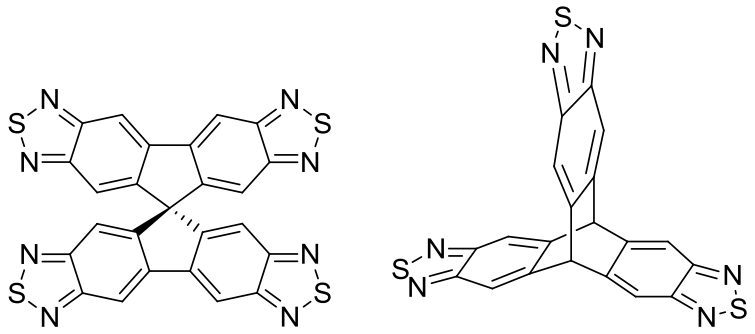

7 **8**

Results and Discussion

Syntheses of 2,1,3-Benzothiadiazoles 4-8.

Benzotris(thiadiazole) **6** was prepared by a published multistep method,[61] and triptycenetris(thiadiazole) **8** was also synthesized by a reported procedure.[43] Naphthobis(thiadiazole) **4** was previously synthesized by heating 1,5-naphthalenediol, 2,6-naphthalenediol, or brominated derivatives with the explosive reagent N_4S_4.[62] To avoid working with N_4S_4, we developed an alternative method in which the tetrahydrochloride salt of 1,2,5,6-naphthalenetetramine[63] was converted into bis(thiadiazole) **4** in 86% yield by treatment with $SOCl_2$ in pyridine (Scheme 1).[64] Anthraquinonebis(thiadiazole) **5** was prepared in 40% yield by the reaction of 1,2,5,6-tetraaminoanthracene-9,10-dione[65,66] with S_2Cl_2 in DMF (Scheme 1). 3,3',6,6'-Tetranitro-9,9'-spirobi[9*H*-fluorene]-2,2',7,7'-tetramine (**9**)[67] was reduced with $SnCl_2$ to give the corresponding octahydrochloride salt of octaamine **10** in 81% yield, and a subsequent reaction of the salt with S_2Cl_2 in DMF produced tetrakis(thiadiazole) **7** in 61% yield (Scheme 1). Although the syntheses of thiadiazoles **4**-**8** proved to be efficient, we found that significant effort was required to produce the compounds in high purity and subject them to full characterization. In particular, compounds **4** and **6** tended to crystallize rapidly in ways that trapped impurities in the lattice, compound **5** proved to be unstable in solution, and compounds **6** and **7** showed poor solubility.

Scheme 1

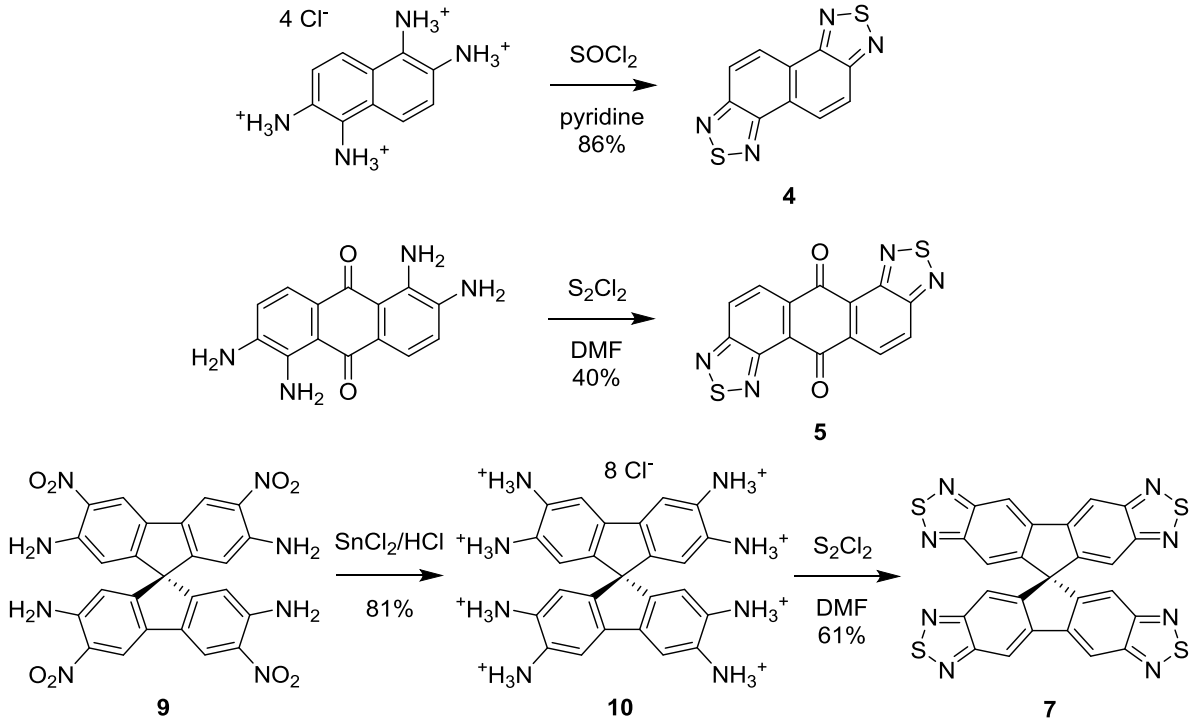
4 Cl-
NH3+
NH3+
+H3N
NH3+
SOCl2
pyridine
86%
4
O
NH2
NH2
H2N
NH2
O
S2Cl2
DMF
40%
5
O2N
NO2
H2N
NH2
H2N
NH2
O2N
NO2
9
SnCl2/HCl
81%
8 Cl-
+H3N
NH3+
+H3N
NH3+
+H3N
NH3+
+H3N
NH3+
10
S2Cl2
DMF
61%
7

Structure of Naphthobis(thiadiazole) 4.

Cooling a hot saturated solution of compound **4** in THF afforded rectangular orange crystals. Analysis by X-ray diffraction established that the crystals belonged to the monoclinic space group $P2_1/c$. Crystallographic parameters are provided in Table 1, and views of the structure appear in Figure 1. Molecules of compound **4** are virtually planar and are linked to form undulating flat tapes by pairs of short coplanar S···N contacts (3.08 Å), as shown in Figure 1a. The S···N contacts are significantly shorter than the sum of the van der Waals radii (3.35 Å)[68] and are characteristic features of the structures of many other 2,1,3-benzothiadiazoles.[8,9,36-49] Short contacts do not necessarily correspond to bonding interactions,[69] but the results of calculations and the widespread observation of short S···N contacts in the structures of other 2,1,3-benzothiadiazoles and related compounds provide strong evidence of an important directional bonding effect. The tapes observed in the structure of compound **4** are further linked by C-H···N interactions (2.61 Å) to create sheets (Figure 1a), which form π-stacks with a distance of 3.40 Å between the mean planes (Figure 1b).

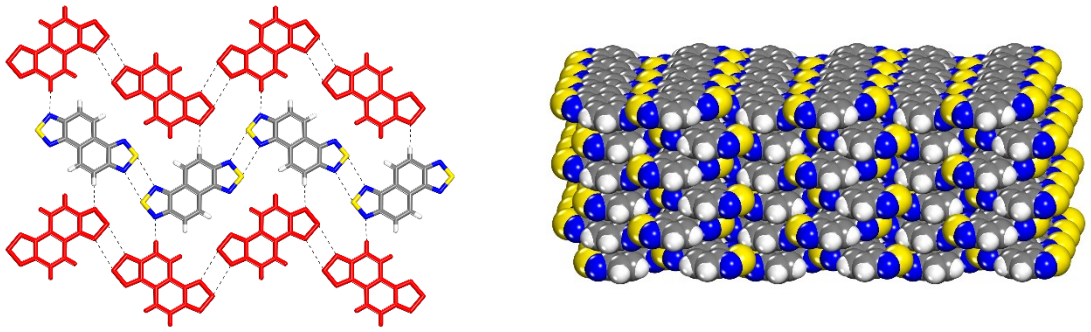

Figure 1. Representations of the structure of crystals of naphthobis(thiadiazole) **4** grown from THF. (a) View showing how undulating flat tapes held together by S···N interactions are further linked by C-H···N hydrogen bonds to form sheets. Two individual tapes are highlighted in red, and the most significant intermolecular interactions are represented by broken lines. (b) Space-filling view showing the π-stacking of sheets. Unless otherwise stated, atoms of carbon appear in gray, atoms of hydrogen in white, atoms of nitrogen in blue, and atoms of sulfur in yellow.

Table 1. Crystallographic data for 2,1,3-benzothiadiazoles **4**, **5**, **7**, and **8**.

compound	**4**	**5**	**7**	**8 • n DMSO**[a]
crystallization medium	THF	1,2-dichlorobenzene	mesitylene/MeOH	DMSO
formula	$C_{10}H_4N_4S_2$	$C_{14}H_4N_4O_2S_2$	$C_{25}H_8N_8S_4$	$C_{20}H_8N_6S_3$
crystal system	monoclinic	monoclinic	monoclinic	tetragonal
space group	$P2_1/c$	$P2_1/n$	$P2/c$	$I\bar{4}2d$
a (Å)	7.8092(3)	3.8045(1)	13.1602(7)	16.3407(3)
b (Å)	17.4192(7)	9.6098(3)	12.2830(6)	16.3407(3)
c (Å)	6.8514(3)	16.4052(4)	14.3308(7)	19.0557(4)
α (°)	90	90	90	90
β (°)	95.335(2)	92.4211(4)	111.651(2)	90
γ (°)	90	90	90	90
V (Å^3)	927.96(7)	599.25(3)	2153.1(2)	5088.2(2)
Z	4	2	4	8
ρ_{calcd} (g cm^{-3})	1.749	1.797	1.693	1.119
T (K)	100	150	100	100
μ (mm^{-1})	4.972	2.747	2.881	1.816
R_1, $I > 2\sigma$ (%)	4.92	4.59	5.40	3.60
R_1, all data (%)	5.01	4.91	5.65	3.77
ωR_2, $I > 2\sigma$ (%)	16.43	12.61	12.94	10.52
ωR_2, all data (%)	16.53	12.98	13.08	10.68
no. measured reflections	36551	16985	129206	27446
no. independent reflections	1758	1182	4962	2898
no. obs. reflections $I > 2\sigma$(I)	1689	1093	4693	2767

[a]Guests not identified unambiguously by crystallography are omitted from the composition. For details, see the Experimental Section.

Structure of Anthraquinonebis(thiadiazole) 5.

Cooling a hot saturated solution of compound **5** in 1,2-dichlorobenzene produced needles, which were found to belong to the monoclinic space group $P2_1/n$. Additional crystallographic data are presented in Table 1, and views of the structure are shown in Figure 2. As in the case of naphthobis(thiadiazole) **4**, molecules of extended analogue **5** are joined by multiple S···N bonds (3.08 Å) to form flat tapes (Figure 2a), which appear to be reinforced by O···S interactions (3.30 Å) that are slightly shorter than the sum of the van der Waals radii of the atoms involved (3.32 Å).[68] The tapes form π-stacks separated by a distance of 3.37 Å between the mean planes. Tapes in adjacent stacks lie at an angle of 37° and are connected by C-H···N and C-H···O interactions with H···N and H···O distances of 2.59 Å and 2.67 Å, respectively (Figure 2).

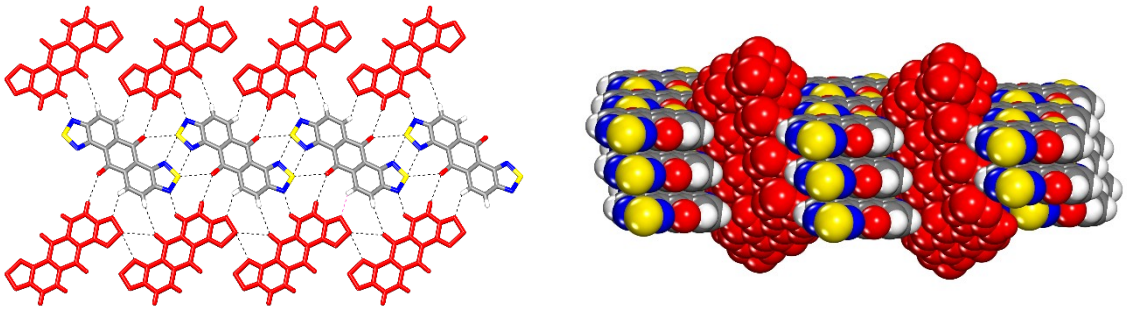

Figure 2. Representations of the structure of crystals of anthraquinonebis(thiadiazole) **5** grown from 1,2-dichlorobenzene. (a) View along the *a*-axis showing how S···N and O···S interactions link the molecules into tapes, and how adjacent tapes are joined by C-H···N and C-H···O interactions. Two adjacent tapes are highlighted in red, and the most significant interactions involving the central tape are represented by broken lines. (b) Space-filling view showing how the tapes are π-stacked and how adjacent stacks lie at an angle of 37°. Tapes in two stacks are highlighted in red. Unless otherwise indicated, atoms of carbon are shown in gray, atoms of hydrogen in white, atoms of nitrogen in blue, atoms of oxygen in red, and atoms of sulfur in yellow.

Structure of Benzotris(thiadiazole) 6.

The structure of crystals of compound **6** grown from THF was reported previously by Makarov et al. but not analyzed in detail.[44] We have found that pale yellow needles formed by crystallizing compound **6** from hot DMF or pyridine have the same structure. The molecular organization is analogous to arrangements favored by naphthobis(thiadiazole) **4** and anthraquinonebis(thiadiazole) **5**, as shown in Figure 3. Molecules of compound **6** are linked to give flat tapes by novel bifurcated S···N interactions (3.19 Å) in which single atoms of sulfur are shared by two nitrogen atoms (Figure 3a). The resulting tapes form π-stacks, with a distance of 3.37 Å between mean planes (Figure 3b). Tapes in adjacent stacks are canted at an angle of 43° and are linked by additional S···N contacts (3.09 and 3.11 Å).

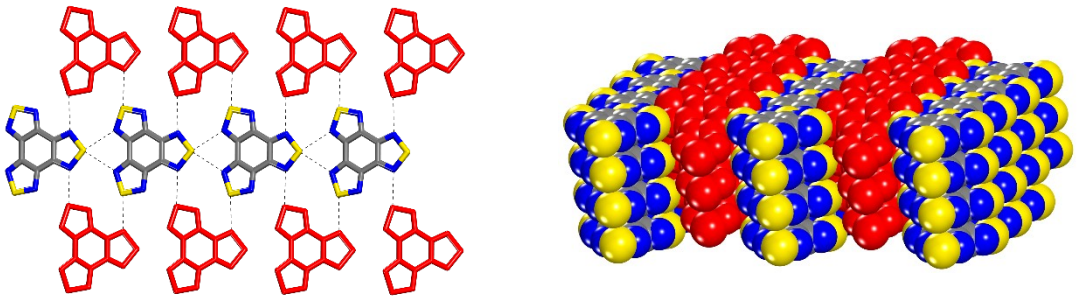

Figure 3. Representations of the structure of crystals of benzotris(thiadiazole) **6** grown from THF, DMF, or pyridine. (a) View showing how bifurcated S···N interactions link the molecules into tapes, and how adjacent tapes are joined by additional S···N interactions. Two adjacent tapes are highlighted in red, and significant interactions involving the central tape are represented by broken lines. (b) Space-filling view showing how the tapes are π-stacked and how adjacent stacks lie at an angle of 43°. Tapes in two stacks are highlighted in red. Unless otherwise stated, atoms of carbon are shown in gray, atoms of nitrogen in blue, and atoms of sulfur in yellow.

Structure of Spirobifluorenetetrakis(thiadiazole) 7.

Adding MeOH to a saturated solution of compound **7** in mesitylene induced the formation of rectangular yellow crystals, which were found to belong to the monoclinic space group *P*2*/c*. Additional crystallographic information is summarized in Table 1, and a representation of the structure appears in Figure 4. Molecules are linked to form undulating chains by alternating S···N interactions (3.05 Å) and π-stacking (3.35 Å for the shortest C···C distance). The chains are connected to form open sheets by additional S···N interactions (3.20 and 3.27 Å) and by C-H···N (2.60 Å) interactions. The sheets are stacked with an offset to allow spirobifluorenyl moieties to occupy the large openings defined by adjacent sheets.

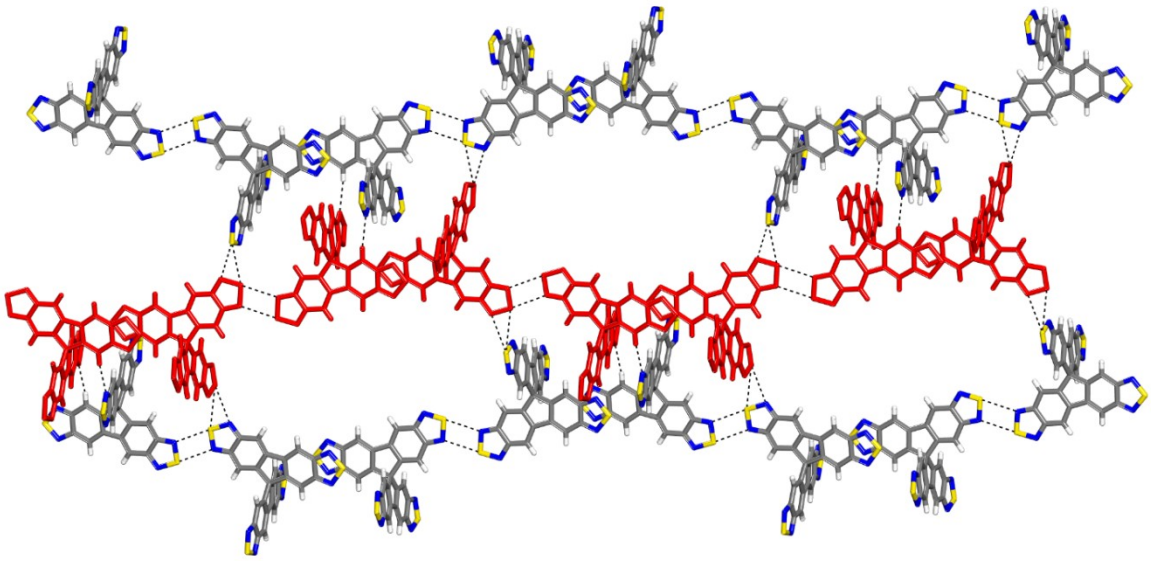

Figure 4. Representation of the structure of crystals of spirobifluorenetetrakis(thiadiazole) **7** grown from mesitylene/MeOH. Molecules are linked into undulating chains by alternating S···N interactions and π-stacking, and chains are connected to form open sheets by additional S···N interactions and by C-H···N interactions. One individual chain is highlighted in red, and the most significant interactions are represented by broken lines. Unless otherwise stated, atoms of carbon are shown in gray, atoms of hydrogen in white, atoms of nitrogen in blue, and atoms of sulfur in yellow.

Structures of Triptycenetris(thiadiazole) 8.

Mastalerz and coworkers recently reported the structure of crystals of compound **8** grown by sublimation.[43] In our own concurrent study of compound **8**, we found that cooling hot solutions in DMSO afforded the same polymorph obtained by sublimation, and a new solvated form was produced concomitantly. Molecular organization in the known unsolvated form is directed in part by S···N and C-H···N interactions, as observed in thiadiazoles **4**-**7**. In the case of triptycenetris(thiadiazole) **8**, molecules are linked into chains by an alternating pattern of weak reciprocal S···N contacts (3.30 Å) and C-H···N interactions (2.62 Å) aligned along the *a*-axis, as shown in Figure 5. Each chain is surrounded by four parallel neighboring chains that are each rotated by 90° with respect to the central chain. The neighboring chains are joined to the central chain by C-H···N interactions (2.49 and 2.61 Å).

Crystallizing triptycenetris(thiadiazole) **8** from DMSO concomitantly yielded a solvate,[70] in addition to the unsolvated form described above. Crystals of the solvate were found to belong to the tetragonal space group $I\bar{4}2d$. Other crystallographic data are provided in Table 1, and representations of the structure appear in Figure 6. No significant S···N interactions are present, and the structure can be described as being constructed from stacked chains, aligned perpendicularly along the *a*- and *b*-axes (Figure 6a). In the structure, thiadiazole rings are superimposed over benzene rings, with a distance of 3.84 Å between centroids, and C-H···N interactions (2.61 Å) help control the association of perpendicular chains (Figure 6b). Comparison of Figures 5a and 6a reveals that the overall molecular organization in the unsolvated and solvated forms is closely similar. However, molecules of triptycenetris(thiadiazole) **8** are less efficiently packed in the solvated form, leaving 38% of the volume of the crystals accessible for including guest molecules of DMSO, which are disordered.[71-73]

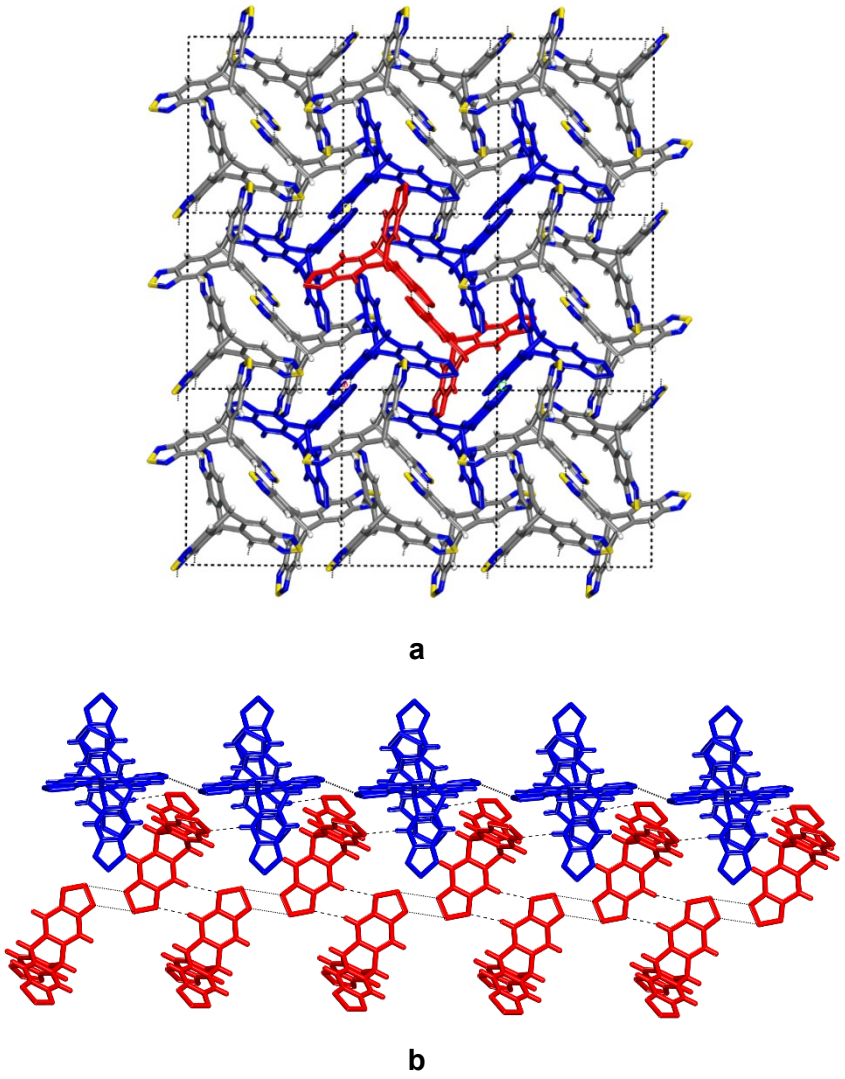

Figure 5. Representations of the structure of unsolvated crystals of triptycenetris(thiadiazole) **8** grown from DMSO or produced by sublimation. (a) View of a 3 × 3 × 3 array of unit cells as seen along the *a*-axis, showing the cross section of a central chain of molecules (red) linked by S···N and C-H···N interactions, with four adjacent chains (blue) that are rotated by 90°. Unless otherwise indicated, atoms of carbon are shown in gray, atoms of hydrogen in white, atoms of nitrogen in blue, and atoms of sulfur in yellow. (b) Detailed view of adjacent chains (red and blue), with key intrachain and interchain interactions represented by broken lines.

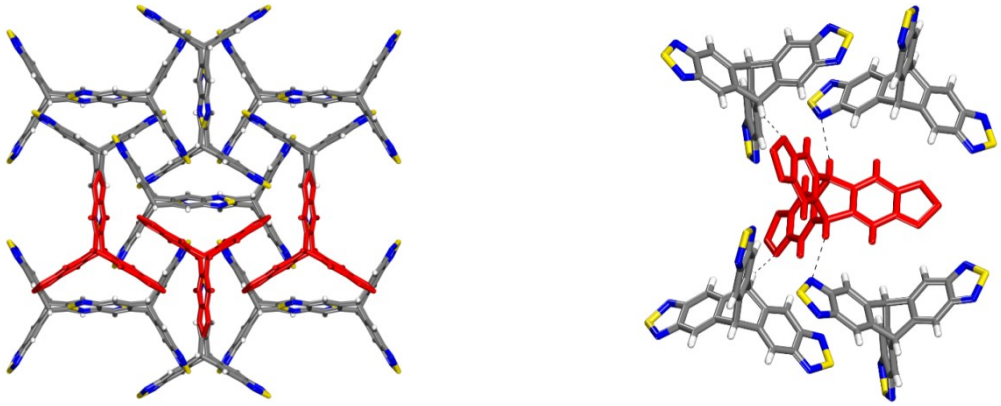

Figure 6. Representations of the structure of crystals of triptycenetris(thiadiazole) **8** grown from DMSO as a solvate. Unless otherwise indicated, atoms of carbon are drawn in gray, atoms of hydrogen in white, atoms of nitrogen in blue, and atoms of sulfur in yellow. Disordered molecules of DMSO are omitted. (a) View along the *c*-axis showing perpendicular chains of stacked molecules aligned along the *a*- and *b*-axes, with one chain highlighted in red. (b) Detailed view of interchain C-H···N interactions, showing a central molecule in red and four neighbors in perpendicular chains with atoms in normal colors.

The concomitant crystallization of unsolvated and solvated forms of triptycenetris(thiadiazole) **8**, along with their closely analogous molecular organization, suggests that the relatively rigid trigonal geometry of the compound precludes highly efficient packing. Indeed, the density of the unsolvated form (1.604 g/cm^3) is significant lower than those of naphthobis(thiadiazole) **4** (1.749 g/cm^3) and spirobifluorenetetrakis(thiadiazole) **7** (1.693 g/cm^3), despite similar percentages of C, N, and S. The structures of the two forms of triptycenetris(thiadiazole) **8** may help reveal the mechanism of crystallization by showing how solvent can be squeezed out of a solvated nucleus to produce a structurally analogous unsolvated form.[74-75]

It is instructive to compare the crystallization of thiadiazoles **4-7** with that of triptycenetris(thiadiazole) **8**. In the cases of compounds **4-7**, polymorphs or solvates were not

observed, even when crystallizations were carried out under various conditions. In addition, significant S···N interactions were found in the structures of all compounds **4**-**7**, as normally observed for benzothiadiazoles, whereas these characteristic interactions proved to be weak or even absent in the structures of triptycenetris(thiadiazole) **8**. Together, these findings suggest that the geometry of the rigid trigonal triptycenyl core of compound **8** may not let the benzothiadiazole units engage in their normal associative behavior, thereby directing crystallization away from preferred motifs of organization. This notion is further supported by the fact that compound **8** crystallizes as a solvate, and it suggests that compound **8** may be particularly suitable for co-crystallizations with other guests.

Structure of Co-Crystals Formed by Triptycenetris(thiadiazole) 8 and C_{60}.

We confirmed the ability of compound **8** to serve as a host by co-crystallizing it with fullerenes, which represent a class of compounds widely used as electron-accepting components in molecule-based solar cells and other devices. Layering a solution of compound **8** in mesitylene on top of a solution of C_{60} in the same solvent led to slow mixing and the growth of dark purple triangular crystals, which were found to have the approximate composition **8** • 0.5 C_{60} • 0.5 mesitylene[70] and to belong to the cubic space group $Pa\bar{3}$. Additional crystallographic parameters are summarized in Table 2, and representations of the structure are provided in Figure 7. Structural analysis was complicated by twinning of the co-crystals and disorder of all components. Each molecule of C_{60} is enveloped by six molecules of triptycenetris(thiadiazole) **8** (Figure 7a), and each concave face of compound **8** accommodates a molecule of C_{60} (Figure 7b). The driving force for the observed co-assembly of these dissimilar components is provided in part by the complementarity of their shapes, the interaction of their π-surfaces, and their inability to pack efficiently by themselves. Residual volume in the structure is occupied by disordered molecules of mesitylene.

On the basis of the measured diameter of C_{60} (7.10 Å) and the separation of layers in graphite (3.35 Å),[76] 6.90 Å can be considered to be the distance between the centroid of C_{60} and an atom of carbon in van der Waals contact. The separation of the centroids of two molecules of C_{60} in van der Waals contact is therefore 10.4 Å. Shorter distances can be

interpreted as the result of bonding interactions or as the compressive effects of molecular packing. In the structure of the co-crystal of compound **8** and C_{60}, distances from the centroid of the fullerene to the surrounding benzothiadiazole units can measured by using the centroids of either the thiadiazole rings or the benzene rings. In both cases, the distances are shorter than those expected for surfaces in van der Waals contact; for the thiadiazole rings, the centroid-centroid distances are 6.71 and 6.83 Å, and for the benzene rings the values are 6.83 and 6.86 Å. Each molecule of C_{60} is completely isolated from other fullerenes by intervening molecules of triptycenetris(thiadiazole) **8**, and the shortest centroid-centroid distances for C_{60} are 13.41 Å.

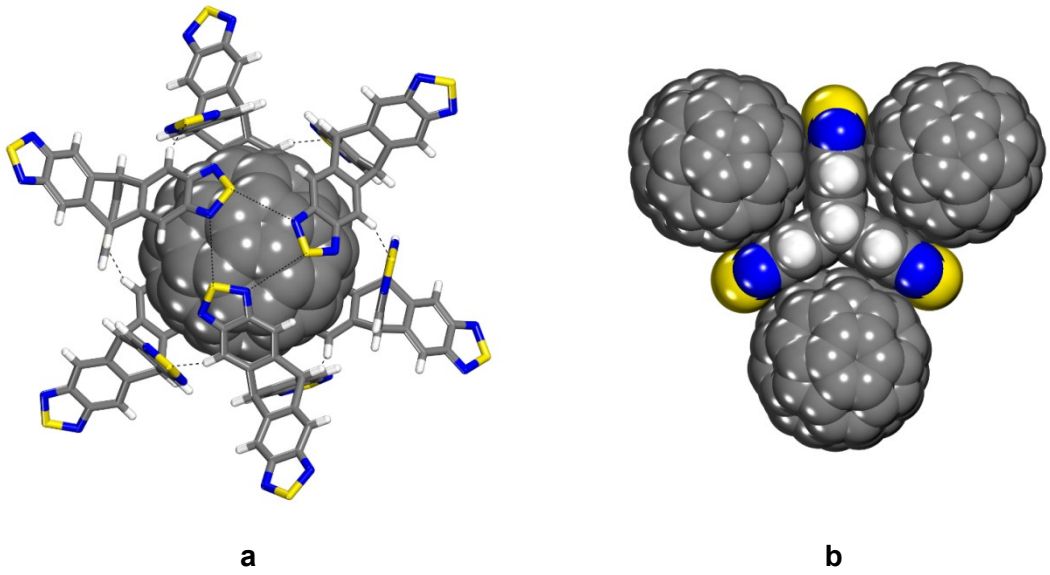

Figure 7. Representations of the structure of co-crystals of triptycenetris(thiadiazole) **8** and C_{60} grown from mesitylene with the approximate composition **8** • 0.5 C_{60} • 0.5 mesitylene. Atoms of carbon are shown in gray, atoms of hydrogen in white, atoms of nitrogen in blue, and atoms of sulfur in yellow. (a) View showing a central molecule of C_{60} surrounded by six molecules of compound **8**. Key S···N and C-H···S interactions are represented by broken lines. Disordered molecules of mesitylene are omitted. (b) View showing how all three concave faces of triptycenetris(thiadiazole) **8** are used to accommodate molecules of C_{60}.

Table 2. Crystallographic data for co-crystals of triptycenetris(thiadiazole) **8** with C_{60} and C_{70}.

compound	**8 • 0.5 C_{60} • 0.5 mesitylene**	**8 • 0.5 C_{70} • 1.5 CS_2**
crystallization medium	mesitylene	CS_2
	$C_{20}H_8N_6S_3$ • 0.5 C_{60} • 0.5	$C_{20}H_8N_6S_3$• 0.5 C_{70} • 1.5
formula	C_9H_{12}	CS_2
crystal system	cubic	cubic
space group	$Pa\bar{3}$	$Pa\bar{3}$
a (Å)	18.9035(9)	19.5040(3)
b (Å)	18.9035(9)	19.5040(3)
c (Å)	18.9035(9)	19.5040(3)
α (°)	90	90
β (°)	90	90
γ (°)	90	90
V (Å^3)	6755.0(10)	7419.4(3)
Z	4	4
ρ_{calcd} (g cm^{-3})	1.670	1.724
T (K)	100	100
μ (mm^{-1})	1.604	2.521
R_1, $I > 2\sigma$ (%)	0.1142	0.0641
R_1, all data (%)	0.1285	0.0686
ωR_2, $I > 2\sigma$ (%)	0.2763	0.1724
ωR_2, all data (%)	0.2869	0.1774
no. measured reflections	92123	77875
no. independent reflections	2714	2853
no. obs. reflections $I > 2\sigma$(I)	2619	2584

The shorter separation of thiadiazole rings and C_{60} in the structure of the co-crystal may be a consequence of the particular trigonal geometry of compound **8**, and it may also reflect the polarization of benzothiadiazoles and greater complementarity of the thiadiazole rings with the electron-accepting character of C_{60}. Related co-crystals of C_{60} with triptycene itself have been obtained under two sets of conditions, and their structures have been determined.[77-79] In both cases, each molecule of C_{60} interacts with the concave faces of two

molecules of triptycene and is therefore only partly enclosed. The centroid of the fullerene and the centroids of the two interacting benzene rings of triptycene are separated by 6.75 and 6.76 Å in one case,[79] and the values have not been reported in the other.[77,78] These distances are shorter than the corresponding separations in the co-crystal of triptycenetris(thiadiazole) **8** with C_{60}, supporting the conclusion that the more electron-deficient benzene rings in compound **8** are not optimally suited for forming strong π-interactions with electron acceptors such as fullerenes. Partially surrounded molecules of C_{60} in co-crystals with triptycene are free to interact with neighboring fullerenes, and the closest contacts (10.15 Å)[79] are significantly shorter than the normal van der Waals separation (10.4 Å).

In general, fullerenes have low solubility and a high tendency to self-associate,[80-84] so it is noteworthy that triptycenetris(thiadiazole) **8** co-crystallizes with C_{60} and produces a structure in which the fullerene components are kept apart. In contrast, triptycene itself does not segregate included fullerenes. This difference presumably arises in part because the molecular π-surface of compound **8** is almost twice as large as that of triptycene. Furthermore, the six enveloping molecules of compound **8** that surround each molecule of C_{60} in the co-crystal are directly bonded to one another by multiple S···N interactions (3.22 Å) and C-H···S hydrogen bonds (2.80 Å), thereby reinforcing the observed co-assembly. Of particular note is the interaction of two sets of three surrounding molecules of compound **8** to create cyclic trimers of thiadiazole units located on opposite faces of the enclosed molecule of C_{60} (Figure 7a). This motif is related to normal pairwise association of thiadiazoles, as observed in the structures of compounds **4**, **5**, **7**, and **8**, but to our knowledge cyclic trimers have not been previously reported. In the co-crystal, each molecule of compound **8** forms S···N and C-H···S interactions with a total of 12 neighbors to define a three-dimensional network in which 52% of the volume is available for the inclusion of C_{60} and mesitylene.[71-73] Although triptycene **8** and C_{60} co-crystallize readily, adding aliquots of C_{60} did not alter the ^{1}H NMR spectra of saturated solutions of compound **8** in $CS_2/CDCl_3$, suggesting that association is limited to the solid state.

Structure of the Co-Crystal Formed by Triptycenetris(thiadiazole) 8 and C_{70}.

Layering a solution of compound **8** in CS_2 on top of a solution of C_{70} in the same solvent induced the formation of dark red hexagonal crystals. The crystals proved to have the approximate composition **8** • 0.5 C_{70} • 1.5 CS_2,[70] to belong to the cubic space group $Pa\bar{3}$, and to be isostructural with the co-crystals formed by compound **8** and C_{60}. Additional crystallographic parameters are provided in Table 2, and the structure is represented by the images in Figure 8. Again, the fullerene is surrounded by six molecules of triptycenetris(thiadiazole) **8** (Figure 8a), and each concave face of compound **8** accommodates a molecule of C_{70} (Figure 8b); however, C_{70} is larger than C_{60}, so the surrounding molecules of compound **8** can no longer be in contact with each other, and the distinctive pattern of S···N and C-H···S interactions formed in the co-crystal with the smaller fullerene can no longer be maintained. This suggests that the primary driving force for the closely analogous co-assemblies of compound **8** with C_{60} and C_{70} is not the formation of S···N and C-H···S interactions, but rather the interaction of π-surfaces that have complementary shapes. Residual volume in the structure not occupied by molecules of triptycenetris(thiadiazole) **8** or C_{70} accommodates disordered molecules of CS_2.

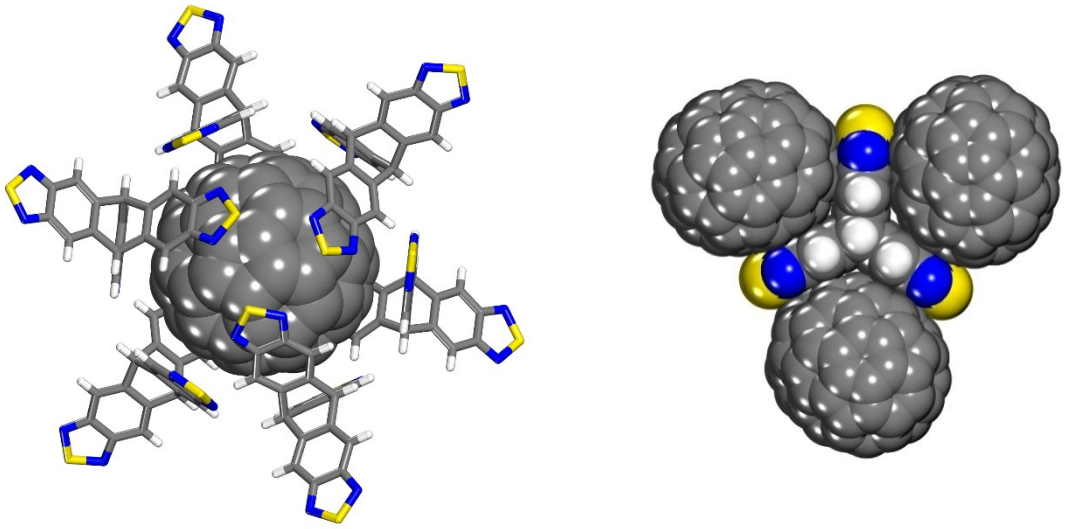

Figure 8. Representations of the structure of co-crystals of triptycenetris(thiadiazole) **8** and C_{70} grown from CS_2 with the approximate composition **8** • 0.5 C_{70} • 1.5 CS_2. Atoms of carbon are shown in gray, atoms of hydrogen in white, atoms of nitrogen in blue, and atoms of sulfur in yellow. (a) View showing a central molecule of C_{70} surrounded by six molecules of compound **8**. Disordered molecules of CS_2 are omitted. (b) View showing how all three concave faces of triptycenetris(thiadiazole) **8** accommodate molecules of C_{70}.

Comparison of Complex Benzothiadiazoles 4-6 with Simple Benzothiadiazole (1) and Analogous Arenes.

In previous work, the primary motivation for using 2,1,3-benzothiadiazole units to replace standard arene moieties in π-conjugated polymers and small molecules has been to alter optical and electronic properties. We have confirmed that useful properties of this type are retained by representative compounds with multiple benzothiadiazole units attached to well-defined molecular cores. In particular, Table 3 (reduction potentials) and Figure 9 (absorption and emission spectra) show that key properties of benzothiadiazoles **4**-**6** resemble those of benzothiadiazole (**1**) itself.

Table 3. Reduction potentials of benzothiadiazoles **1**, **4**, **5**, and **6**.[a]

compound	$E_{1/2}$ **(V)**
Benzothiadiazole **1**	-1.94 (reversible)
Naphthobis(thiadiazole) **4**	-1.67 (reversible), -2.45 (reversible)
Anthraquinonebis(thiadiazole) **5**	-0.71 (reversible), -1.29 (quasi-reversible), -1.97 (quasi-reversible)
Benzotris(thiadiazole) **6**	-1.64 (reversible), -2.21 (reversible)

[a]Measured using ~1 mM solutions in *N*-methyl-2-pyrrolidone containing tetrabutylammonium hexafluorophosphate (0.1 M) as supporting electrolyte. Potentials are reported with respect to the ferrocene/ferrocenium couple.

As expected, bis(thiadiazole) **4** and tris(thiadiazole) **6** are more easily reduced than benzothiadiazole (**1**), which reflects the more extended aromatic structures of compounds **4** and **6**, as well as the presence of multiple electron-withdrawing thiadiazole units. Once one thiadiazole unit in compounds **4** and **6** has been reduced, the second reduction requires a higher potential, as anticipated. Under the conditions used, the third reduction of tris(thiadiazole) **6** could not be observed. Anthraquinonebis(thiadiazole) **5** showed three reduction waves, with only the first being fully reversible. The ease of the first reduction suggests that it involves the quinone unit. No oxidation of any of the benzothiadiazoles could be observed within the range of accessible potentials. The absorption and emission spectra of bis(thiadiazole) **4** and tris(thiadiazole) **6** closely resemble those of benzothiadiazole (**1**) itself but have bathochromic shifts of the main bands. The absorption spectrum of anthraquinonebis(thiadiazole) **5** is more similar to that of anthraquinone, and no emission could be detected for this compound.

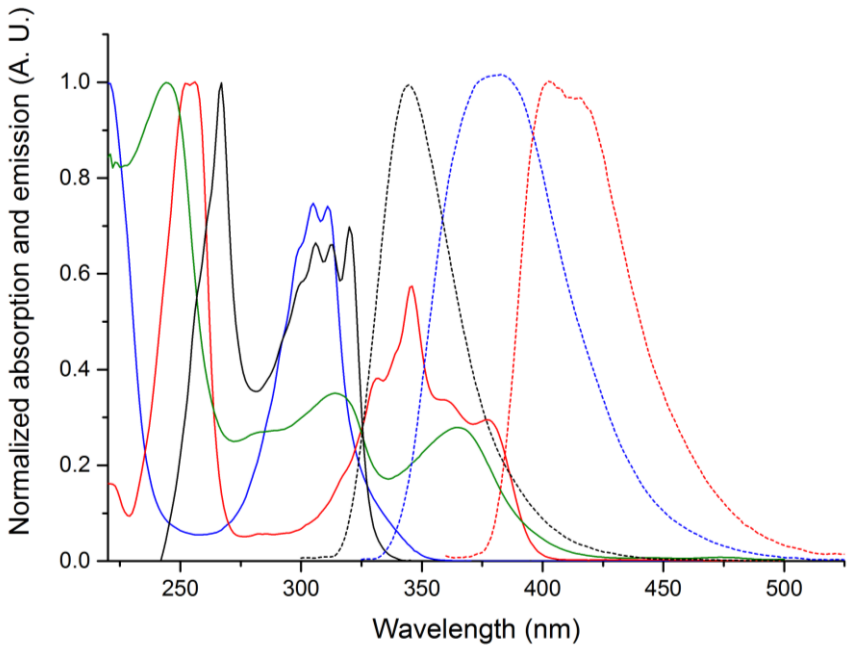

Figure 9. Absorption spectra (solid lines) and emission spectra (broken lines) of solutions of benzothiadiazole (**1**) (blue), naphthobis(thiadiazole) **4** (red), anthraquinonebis(thiadiazole) **5** (green), and benzotris(thiadiazole) **6** (black). All solutions were prepared in THF, with λ_{ex} = 310 nm for compound **1,** λ_{ex} = 256 nm for compound **4**, λ_{ex} = 257 nm for compound **5**, and λ_{ex} = 267 nm for compound **6**.

The redox properties of complex benzothiadiazoles reflect their pronounced preference for quinonoidal structures rather than alternatives with normal benzene rings (Scheme 2). Table 4 confirms this preference by presenting average bond lengths observed in the benzothiadiazole units of compounds **4**-**8**. C-C bonds *e* are systematically shorter than bonds *c*, *d*, and *f*, thereby confirming that complex benzothiadiazoles retain strong quinonoid character.

Scheme 2

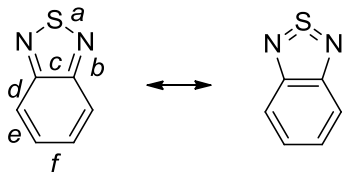

Table 4. Average bond lengths in benzothiadiazole units of compounds **4-8**.

bond	average bond lengths (Å)				
	4	**5**	**6**	**7**	**8**
a	1.62	1.61	1.63	1.62	1.63
b	1.34	1.35	1.35	1.35	1.35
c	1.44	1.44	1.43	1.44	1.44
d	1.43	1.43	1.45	1.42	1.42
e	1.35	1.36	-	1.37	1.36
f	1.43	1.43	-	1.44	1.44

The behavior of compounds **4-8** confirms that the presence of multiple 2,1,3-benzothiadiazole units in complex structures can alter optoelectronic properties in useful ways. In addition, the ability to engage in S···N bonding and other characteristic interactions allows benzothiadiazole units to direct molecular organization and make it diverge from patterns observed for analogous arenes. This can be confirmed by comparing the structures of benzothiadiazoles **4-8** with those of close analogues **11-15**. The structures of hydrocarbons **14** and **15** have not been reported, but those of chrysene (**11**),[85] dibenzanthraquinone **12**,[86] and triphenylene (**13**)[87] are known. All three compounds adopt herringbone arrangements directed in part by π-stacking and C-H···π interactions. In none of the three structures do two adjacent interacting molecules lie in the same plane. In contrast, coplanar chains of molecules held together by S···N bonding are observed in the structures of all three analogous

benzothiadiazoles **4**-**6**. These differences underscore the dual potential of 2,1,3-benzothiadiazole units to modulate individual molecular optoelectronic properties, as well as to help govern collective behavior controlled by overall molecular organization.

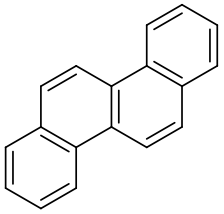

11

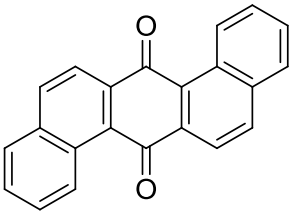

12

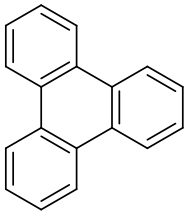

13

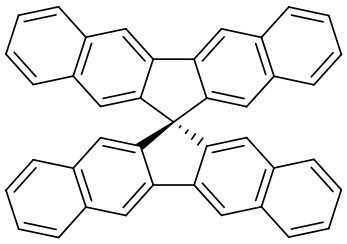

14

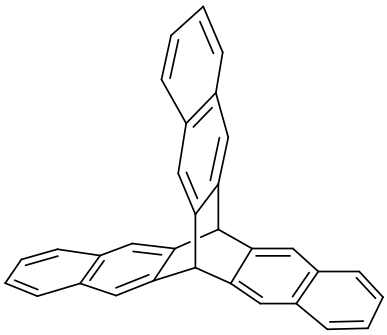

15

Conclusions

Materials with predetermined structures and properties can be built from molecular modules designed so that their topologies and interactions work in concert to control local organization.[88] This modular strategy is now widely used to create new materials for many purposes. The behavior of compounds **4**-**8**, in which multiple benzothiadiazole units are attached to well-defined planar and nonplanar molecular cores, shows that molecular organization can be controlled in complex structures by using directional S···N bonding and other characteristic interactions. The observed structures are distinctly different from those of analogous arenes. Replacing benzene rings in arenes by thiadiazoles thereby provides a strategy for making new compounds with extended systems of π-conjugation, characteristic optoelectronic properties, and unique patterns of molecular organization, including the ability to co-crystallize with fullerenes.

Experimental Section

Anhydrous oxygen-free solvents were obtained by passage through columns packed with activated alumina and supported Cu catalyst (Glass Contour, Irvine, CA). Reagents and all other solvents were purchased from commercial sources and used without further purification unless otherwise indicated. Full characterizations of known compounds **4** and **6** are included below to provide data not presented in earlier publications. Absorption and emission spectra were measured at 25 °C. Cyclic voltammograms were obtained using ~1 mM solutions in anhydrous *N*-methylpyrrolidinone (NMP) sparged with N_2. The working electrode was a Pt electrode, the counter electrode was a Pt wire, and the pseudo-reference electrode was an Ag wire.

N**aphtho[1,2-*c*:5,6-*c*']bis([1,2,5]thiadiazole) (4).**[62] Under N_2, $SOCl_2$ (0.45 mL, 6.2 mmol) was added to a solution of the tetrahydrochloride salt of 1,2,5,6-naphthalenetetraamine (0.501 g, 1.50 mmol)[63] in anhydrous oxygen-free pyridine (15 mL). The resulting dark orange mixture was heated at 75 °C for 3 h. Water (15 mL) was then added, followed by concentrated aqueous HCl until the supernatant was neutral (~15 mL). The precipitated solid was separated by filtration, washed with water, washed with 95% ethanol, and dried under vacuum at 50 °C to afford compound **4** (0.317 g, 1.29 mmol, 86%) as an orange solid. It was then crystallized from hot dioxane (55% recovery), and a small sample was sublimed for elemental analysis. Further purification can also be achieved by treatment with activated charcoal to afford a pale yellow solid. Single crystals for analysis by X-ray diffraction were grown by cooling a hot saturated solution of compound **4** in THF: mp 247-248 °C; FTIR (ATR) 3066, 1503, 1176, 860, 830, 740, 603, 503, 488 cm^{-1}; ^1H NMR (400 MHz, $CDCl_3$) δ 8.95 (d, ^3J = 9 Hz, 2H), 8.22 (d, ^3J = 9 Hz, 2H); ^{13}C NMR (100 MHz, $CDCl_3$) δ 154.8, 153.0, 127.2, 125.9, 121.3; UV-Vis (THF) λ_{max} (ε) 256 (47,400), 332 (18,100), 346 (24,200), 362 (15,700), 377 (14,000); Emission (THF, λ_{ex} 256 nm) λ_{em} 305, 338, 402 nm; CV (NMP, NBu_4PF_6) $E_{1/2}$ -1.67, -2.45 V (Fc/Fc^+); HRMS (ASAP-TOF) calcd for $C_{10}H_4N_4S_2$ + H *m/e* 244.9956, found 244.9966. Anal. Calcd for $C_{10}H_4N_4S_2$: C, 49.17; H, 1.65; N, 22.94; S, 26.25. Found: C, 49.12; H, 1.46; N, 23.17; S, 26.21. A sample recrystallized from THF was shown to be structurally homogeneous

by comparing the experimentally determined X-ray powder diffraction pattern of the bulk solid with the simulated pattern derived from analysis of a single crystal.

Anthra[1,2-*c*:5,6-*c*']bis([1,2,5]thiadiazole)-6,12-dione (5). A solution of 1,2,5,6-tetraaminoanthracene-9,10-dione (0.252 g, 0.939 mmol)[65,66] in dry DMF (5 mL) was added under N_2 to a solution of S_2Cl_2 (0.60 mL, 7.5 mmol) in DMF (5 mL), and the resulting mixture was stirred at 25 °C for 3 h. Water (15 mL) was then added, and the dark precipitate was separated by filtration and washed with hot toluene until elementary sulfur could no longer be detected by thin-layer chromatography. The solid was then crystallized from hot 1,2-dichlorobenzene (~90 mL) to give an initial crop of compound **5** as dark violet needles. Hexane was layered on top on the filtrate, and an additional portion of the product crystallized, giving a total amount of 0.123 g (0.379 mmol, 40%). A small sample was further purified for elemental analysis by sublimation. Further purification can also be achieved by treatment with activated charcoal to afford a yellow solid: mp > 300 °C; FTIR (ATR) 3238, 3084, 1664, 1275, 1262, 820 cm^{-1}; ^1H NMR (400 MHz, TFA-*d*/$CDCl_3$ 7:3) δ 8.68 (d, ^3J = 9 Hz, 2H), 8.55 (d, ^3J = 9 Hz, 2H); ^{13}C NMR (176 MHz, TFA-*d*/$CDCl_3$ 7:3) δ 185.1, 159.8, 151.8, 137.7, 130.7, 129.1, 125.3; UV-Vis (THF) λ_{max} 244, 314, 365 nm; CV (NMP, NBu_4PF_6) $E_{1/2}$ -0.71, -1.29, -1.97 V (Fc/Fc^+); HRMS (ASAP-TOF) calcd for $C_{14}H_4N_4O_2S_2$ + H *m/e* 324.9846, found 324.9854. Anal. Calcd for $C_{14}H_4N_4O_2S_2$: C, 51.85; H, 1.24; N, 17.27; S, 19.77. Found: C, 51.29; H, 1.26; N, 16.87; S, 19.72. The sample recrystallized from 1,2-dichlorobenzene was shown to be structurally homogeneous by comparing the experimentally determined X-ray powder diffraction pattern of the bulk solid with the simulated pattern derived from analysis of a single crystal.

Benzo[1,2-*c*:3,4-*c*':5,6-*c*'']tris([1,2,5]thiadiazole) (6). Compound **6** was prepared by the published method[61] and was crystallized from hot DMF: mp > 300 °C; FTIR (ATR) 1539, 1336, 833, 517 cm^{-1}; ^{13}C NMR (100 MHz, DMSO-d_6) δ 149.8; UV-Vis (THF) λ_{max} (ε) 267 (30,400), 306 (20,200), 313 (20,100), 320 (21,300) nm; Emission (THF, λ_{ex} 267 nm) λ_{em} 301, 344 nm; CV (NMP, NBu_4PF_6) $E_{1/2}$ -1.64, -2.21 V (Fc/Fc^+); HRMS (APCI) calcd for $C_6N_6S_3$ *m/e* 251.9344, found 251.9352. The sample recrystallized from DMF was shown to be

structurally homogeneous by comparing the experimentally determined X-ray powder diffraction pattern of the bulk solid with the simulated pattern derived from analysis of a single crystal.

9,9'-Spirobi[9*H*-fluorene]-2,2',3,3',6,6',7,7'-octamine (10) Octahydrochloride. A mixture of 3,3',6,6'-tetranitro-9,9'-spirobi[9*H*-fluorene]-2,2',7,7'-tetramine (**9**; 0.502 g, 0.902 mmol)[67] and $SnCl_2 \bullet 2\ H_2O$ (4.08 g, 18.1 mmol) in absolute ethanol (20 mL) and concentrated aqueous HCl (10 mL) was stirred under N_2 for 12 h at 90 °C. The mixture was then cooled in an ice bath, and the suspended solid was separated by filtration, washed with concentrated aqueous HCl, and dried under vacuum. The off-white solid was then dissolved in water (20 mL), and the solution was layered on concentrated aqueous HCl (40 mL). The resulting suspension was cooled at 0 °C and filtered. The product was dried under vacuum to give the octahydrochloride of 9,9'-spirobi[9*H*-fluorene]-2,2',3,3',6,6',7,7'-octamine (**10**) as a colorless crystalline solid (0.532 g, 0.731 mmol, 81%). The air-sensitive salt was stored under N_2 and used without further purification: FTIR (ATR) 3338, 3225, 2816, 2562, 1628, 1486, 1438 cm^{-1}; ^1H NMR (400 MHz, DMSO-d_6) δ 7.40 (s, 4H), 6.30 (s, 4H), 3.65 (br s, 24 H); HRMS (ASAP-TOF) calcd for $C_{25}H_{24}N_8$ + H *m/e* 437.2197, found 437.2186.

9,9'-Spirobi[fluoreno[2,3-*c*:6,7-*c*']bis([1,2,5]thiadiazole)] (7). Compound **7** was prepared from the octahydrochloride salt of octaamine **10** in 61% yield by the method described above for making compound **5**. Crystallization was achieved by adding MeOH to a saturated solution of compound **7** in mesitylene: mp > 300 °C; FTIR (ATR) 3058, 1519, 1243, 848, 860, 812 cm^{-1};^1H NMR (400 MHz, TFA-*d*/$CDCl_3$ 7:3) δ 8.84 (s, 4H), 7.51 (s, 4H); ^{13}C NMR (100 MHz, TFA-*d*/$CDCl_3$ 7:3) δ 157.3, 157.0, 155.9, 144.2, 119.4, 116.0, 65.0; HRMS (ASAP-TOF) calcd for $C_{25}H_8N_8S_4$ + H *m/e* 548.9833, found 548.9846.

T**riptycene[2,3-*c*:9,10-*c*':17,18-*c*'']tris([1,2,5]thiadiazole) (8).** The hexahydrochloride salt of 2,3,6,7,14,15-hexaaminotriptycene was first prepared by a published method[89] and was then crystallized with 90% recovery by layering an aqueous solution over concentrated aqueous

HCl. The salt was subsequently converted into triptycenetris(thiadiazole) **8** by the reported procedure.[44]

Co-Crystallization of Triptycenetris(thiadiazole) 8 and C_{60}. A solution of compound **8** (60 mg, 0.14 mmol) in mesitylene (50 mL) was layered over a solution of C_{60} (50 mg, 0.069 mmol) in mesitylene (125 mL). Dark purple co-crystals with the approximate composition **8** • 0.5 C_{60} • 0.5 mesitylene (53 mg, 0.062 mmol, 45%) appeared within a few hours. The sample was shown to be structurally homogeneous by comparing the experimentally determined X-ray powder diffraction pattern of the bulk solid with the simulated pattern derived from analysis of a single crystal.

Co-Crystallization of Triptycenetris(thiadiazole) 8 and C_{70}. An analogous procedure was carried out in CS_2 to yield dark red co-crystals of approximate composition **8** • 0.5 C_{70} • 1.5 CS_2 in 60% yield. The sample was shown to be structurally homogeneous by comparing the experimentally determined X-ray powder diffraction pattern of the bulk solid with the simulated pattern derived from analysis of a single crystal.

X-Ray Crystallographic Studies. Crystals of naphthobis(thiadiazole) **4** were analyzed using a Bruker Microstar diffractometer equipped with a Cu rotating anode generator (λ = 1.54178 Å). Data for all other crystals were collected on a Bruker Metaljet diffractometer using GaKα radiation (λ = 1.34139 Å). During all experiments, crystals were cooled (150 K for anthraquinonebis(thiadiazole) **5** and 100 K for all other samples) using an N_2 cryostream device. Frame integration was performed using SAINT,[90] and absorption correction was carried out using SADABS within the APEX2 suite of software.[91]

Structures were solved by direct methods using SHELXS[92] (for anthraquinonebis(thiadiazole) **5** and co-crystals formed by triptycenetris(thiadiazole) **8** and C_{60}) or by intrinsic phasing with SHELXT (in all other cases).[93] Refinements were carried out using SHELXL2016/6.[94] With one exception (the structure of co-crystals of compound **8** and C_{60}), all non-hydrogen atoms were refined anisotropically. Hydrogen atoms were placed in ideal positions and defined as

riding atoms with the exception of compound **5**, for which the hydrogen atoms were fully refined.

The sample used to analyze the structure of spirobifluorenetetrakis(thiadiazole) **7** was a two-component twin. Data reduction and scaling were applied on both components, but only reflections from the major twin component were used in the final refinement. In the structure of the DMSO solvate of triptycenetris(thiadiazole) **8**, the guest molecules are highly disordered, and the updated SQUEEZE routine implemented in PLATON was applied.[95] SQUEEZE found a void of 1930 $Å^3$ filled with 439 electrons. An unsolvated form crystallizes concomitantly and could not be separated easily by hand, so analysis of the composition of the solvate by other methods was not undertaken.

The structure of co-crystals of triptycenetris(thiadiazole) **8** and C_{60} grown from mesitylene was also refined as a two-component twin. Molecules of both compound **8** and C_{60} were found to be disordered. Disorder for compound **8** involved only two orientations, whereas molecules of C_{60} were found to be affected by orientational disorder in such a way that it was not possible to refine the anisotropic atomic displacement parameters to realistic values. A model involving six C_{60} molecules was refined as rigid body with a single isotropic atomic displacement parameter, thereby lowering the *R* factor to about 11%. In the case of co-crystals of compound **8** and C_{70} grown from CS_2, structural refinement involved two disordered C_{70} molecules, with their anisotropic atomic displacement parameters refined using proper restraints.

CCDC 1517237-1517244 contain the supplementary crystallographic data. These data can be obtained free of charge from the Cambridge Crystallographic Data Centre via www.ccdc.cam.ac.uk/data_request/cif.

Acknowledgments. We are grateful to the Natural Sciences and Engineering Research Council of Canada, the Ministère de l'Éducation du Québec, the Canada Foundation for

Innovation, the Canada Research Chairs Program, NanoQuébec, and Université de Montréal for financial support. In addition, we thank Dr. Daniel Beaudoin for helpful discussions.

Supporting Information Available: Selected ^{1}H and ^{13}C NMR spectra, additional data for representative compounds **4-6**, and further crystallographic information, including ORTEP drawings and tables of structural data in CIF format. This material is available free of charge via the Internet at http://pubs.acs.org.

Notes and References

1. Fellow of the Fonds de recherche du Québec-Nature et technologies (FRQNT).
2. Hinsberg, O. *Ber. Dtsch. Chem. Ges.* **1889**, *22*, 2895-2902.
3. Weinstock, L. M.; Shinkai, I. In *Comprehensive Heterocyclic Chemistry*; Katritzky, A. R., Rees, C. W., Eds.; Pergamon Press: Oxford, 1984; Vol. 4, pp 513-543.
4. Miranda, M. S.; Matos, M. A. R.; Morais, V. M. F.; Liebman, J. F. *J. Chem. Thermodynamics* **2012**, *50*, 30-36.
5. Piccionello, A. P.; Guarcello, A. *Curr. Bioact. Compd*. **2010**, *6*, 266-283.
6. Cozzolino, A. F.; Gruhn, N. E.; Lichtenberger, D. L; Vargas-Baca, I. *Inorg. Chem*. **2008**, *47*, 6220-6226.
7. Sayers, A. C.; Bürki, H. R.; Eichenberger, E. *Arzneim.-Forsch*. **1980**, *30*, 793-803.
8. Xia, D.; Wang, X.-Y.; Guo, X.; Baumgarten, M.; Li, M.; Müllen, K. *Cryst. Growth Des*. **2016**, *16*, 7124-7129.
9. Xia, D.; Guo, X.; Chen, L.; Baumgarten, M.; Keerthi, A.; Müllen, K. *Angew. Chem., Int. Ed*. **2016**, *55*, 941-944.
10. Jung, J. W.; Jo, J. W.; Jung, E. H.; Jo, W. H. *Org. Electron*. **2016**, *31*, 149-170.
11. Neto, B. A. D.; Carvalho, P. H. P. R.; Correa, J. R. *Acc. Chem. Res*. **2015**, *48*, 1560-1569.
12. Parker, T. C.; Patel, D. G.; Moudgil, K.; Barlow, S.; Risko, C.; Brédas, J.-L.; Reynolds, J. R.; Marder, S. R. *Mater. Horiz*. **2015**, *2*, 22-36.
13. Zhan, R.; Liu, B. *Macromol. Chem. Phys*. **2015**, *216*, 131-144.
14. Kim, J.; Han, A-R. Hong, J.; Kim, G.; Lee, J.; Shin, T. J.; Oh, J. H.; Yang, C. *Chem. Mater.* **2014**, *26*, 4933-4942.
15. Shi, Z.-F.; Black, H. T.; Dadvand, A.; Perepichka, D. F. *J. Org. Chem.* **2014**, *79*, 5858-5860.
16. Steckler, T. T.; Henriksson, P.; Mollinger, S.; Lundin, A.; Salleo, A.; Andersson, M. R. *J. Am. Chem. Soc.* **2014**, *136*, 1190-1193.
17. Li, Y.; Liu, T.; Liu, H.; Tian, M.-Z.; Li, Y. *Acc. Chem. Res.* **2014**, *47*, 1186-1198.
18. Gao, C.; Wang, L.; Li, X.; Wang, H. *Polym. Chem*. **2014**, *5*, 5200-5210.
19. Lin, Y.; Wang, H.; Li, Y.; Zhu, D.; Zhan, X. *J. Mater. Chem. A* **2013**, *1*, 14627-14632.

20. Neto, B. A. D.; Lapis, A. A. M.; da Silva Júnior, E. N.; Dupont, J. *Eur. J. Org. Chem*. **2013**, 228-255.
21. Yang, G.; Di, C.-a.; Zhang, G.; Zhang, J.; Xiang, J.; Zhang, D.; Zhu, D. *Adv. Funct. Mater*. **2013**, *23*, 1671-1676.
22. Wang, N.; Chen, Z.; Wei, W.; Jiang, Z. *J. Am. Chem. Soc.* **2013**, *135*, 17060-17068.
23. Osaka, I.; Shimawaki, M.; Mori, H.; Doi, I.; Miyazaki, E.; Koganezawa, T.; Takimiya, K. *J. Am. Chem. Soc.* **2012**, *134*, 3498-3507.
24. Zhang, Y.; Kim, C.; Lin, J.; Nguyen, T.-Q. *Adv. Funct. Mater*. **2012**, *22*, 97-105.
25. Lee, J.; Cho, S.; Seo, J. H.; Anant, P.; Jacob, J.; Yang, C. *J. Mater. Chem.* **2012**, *22*, 1504-1510.
26. Behramand, B.; Molin, F.; Gallardo, H. *Dyes Pigments* **2012**, *95*, 600-605.
27. Wang, M.; Hu, X.; Liu, P.; Li, W.; Gong, X.; Huang, F.; Cao, Y. *J. Am. Chem. Soc.* **2011**, *133*, 9638-9641.
28. Zhou, H.; Yang, L.; Price, S. C.; Knight, K. J.; You, W. *Angew. Chem., Int. Ed.* **2010**, *49*, 7992-7995.
29. Yamashita, Y. *Chem. Lett*. **2009**, *38*, 870-875.
30. Blouin, N.; Michaud, A.; Gendron, D.; Wakim, S.; Blair, E.; Neagu-Plesu, R.; Belletête, M.; Durocher, G.; Ye Tao, Y.; Leclerc, M. *J. Am. Chem. Soc.* **2008**, *130*, 732-742.
31. Jackson, N. E.; Savoie, B. M.; Marks, T. J.; Chen, L. X.; Ratner, M. A. *J. Phys. Chem. Lett*. **2015**, *6*, 77-84.
32. Haruk, A. M.; Mativetsky, J. M. *Int. J. Mol. Sci*. **2015**, *16*, 13381-13406.
33. Dang, M. T.; Hirsch, L.; Wantz, G.; Wuest, J. D. *Chem. Rev*. **2013**, *113*, 3734-3765.
34. Brabec, C. J.; Heeney, M.; McCulloch, I.; Nelson, J. *Chem. Soc. Rev.* **2011**, *40*, 1185-1199.
35. Bassani, D. M.; Jonusauskaite, L.; Lavie-Cambot, A.; McClenaghan, N. D.; Pozzo, J.-L.; Ray, D.; Vives, G. *Coord. Chem. Rev.* **2010**, *254*, 2429–2445.
36. Konstantinova, L. S.; Knyazeva, E. A.; Obruchnikova, N. V.; Gatilov, Y. V.; Zibarev, A. V.; Ratikin, O. A. *Tetrahedron Lett*. **2013**, *54*, 3075-3078.
37. Tomura, M.; Yamashita, Y. *Z. Kristallogr*. **2003**, *218*, 555-556.

38. Tomura, M.; Akhtaruzzaman, M.; Suzuki, K.; Yamashita, Y. *Acta Crystallogr*. **2002**, *C58*, o373-o375.
39. Suzuki, T.; Tsuji, T.; Okubo, T.; Okada, A.; Obana, Y.; Fukushima, T.; Miyashi, T.; Yamashita, Y. *J. Org. Chem*. **2001**, *66*, 8954-8960.
40. Mikhno, O. A.; Ezhkova, Z. I.; Zhdanov, G. S. *Kristallografiya* **1973**, *18*, 99-105.
41. Klimasenko, N. L.; Chetkina, L. A.; Ginzburg, S. L.; Neigauz, M. G.; Smelyanskaya, E. M. *J. Struct. Chem*. **1973**, 14, 94-100.
42. Luzzati, V. *Acta Crystallogr*. **1951**, *4*, 193-200.
43. Kohl, B.; Over, L. C.; Lohr, T.; Vasylyeva, M.; Rominger, F.; Mastalerz, M. *Org. Lett.* **2014**, *16*, 5596-5599.
44. Makarov, A. Y.; Zhivonitko, V. V.; Makarov, A. G.; Zikirin, S. B.; Bagryanskaya, I. Y.; Bagryansky, V. A.; Gatilov, Y. V.; Irtegova, I. G.; Shakirov, M. M.; Zibarev, A. V. *Inorg. Chem.* **2011**, *50*, 3017-3027.
45. Tam, T. L.; Li, H.; Wei, F.; Tan, K. J.; Kloc, C.; Lam, Y. M.; Mhaisalkar, S. G.; Grimsdale, A. C. *Org. Lett.* **2010**, *12,* 3340-3343.
46. Yamashita, Y.; Ono, K.; Tomura, M.; Tanaka, S. *Tetrahedron* **1997**, *53*, 10169-10178.
47. Ono, K.; Tanaka, S.; Yamashita, Y. *Angew. Chem., Int. Ed*. **1994**, *33*, 1977-1979.
48. Gieren, A.; Lamm, V.; Hübner, T.; Rabben, M.; Neidlein, R.; Droste, D. *Chem. Ber*. **1984**, *117*, 1940-1953.
49. Gieren, A.; Betz, H.; Hübner, T.; Lamm, V.; Neidlein, R.; Droste, D. *Z. Naturforsch.* **1984**, *39b*, 485-496.
50. Lumbroso, H.; Curé, J.; Konakahara, T.; Takagi, Y. *J. Mol. Struct*. **1980**, *68*, 293-305.
51. Hurley, J.; Le Fèvre, R. J. W. *J. Chem. Soc. B* **1967**, 824-827.
52. Tobiason, F. L.; Huestis, L.; Chandler, C.; Pedersen, S. E.; Peters, P. *J. Heterocycl. Chem*. **1973**, *10*, 773-778.
53. Borovikov, Yu. Ya.; Makovetskii, V. P.; Pivovarova, N. S.; Sivachek, T. E. *Zh. Obshch. Khim.* **1994**, *64*, 1192-1196.
54. Blackman, G. L.; Brown, R. D.; Porter, A. P. *J. Chem. Soc., Chem. Commun.* **1975**, 499.
55. Nagakura, S.; Kuboyama, A. *J. Am. Chem. Soc*. **1954**, *76*, 1003-1005.

56. Khan, I.; Panini, P.; Khan, S. U.-D.; Rana, U. A.; Andleeb, H.; Chopra, D.; Hameed, S.; Simpson, J. *Cryst. Growth Des.* **2016**, *16*, 1371-1386.
57. Adhikari, U.; Scheiner, S. *J. Phys. Chem. A* **2014**, *118*, 3183-3192.
58. Cozzolino, A. F.; Elder, P. J. W.; Lee, L. M.; Vargas-Baca, I. *Can. J. Chem*. **2013**, *91*, 338-347.
59. Pomogaeva, A.; Gu, F. L.; Imamura, A.; Aoki, Y. *Theor. Chem. Acc*. **2010**, *125*, 453-460.
60. Anthony, J. E. *Chem. Rev*. **2006**, *106*, 5028-5048.
61. Komin, A. P.; Carmack, M. *J. Heterocycl. Chem.* **1975**, *12*, 829-833.
62. Mataka, S.; Takahashi, K.; Ikezaki, Y.; Hatta, T.; Tori-i, A.; Tashiro, M. *Bull. Chem. Soc. Jpn.* **1991**, *64*, 68-73.
63. Langis-Barsetti, S.; Maris, T.; Wuest, J. D. *J. Org. Chem*., submitted for publication.
64. A similar route was recently reported by: Kawashima, K. (Sankyo Kasei Co., Japan). Method for Producing Naphthobisthiadiazole. WO 2014002969 A1, January 3, 2014.
65. Imai, K.; Kurihara, M.; Mathias, L.; Wittmann, J.; Alston, W. B.; Stille, J. K. *Macromolecules* **1973**, *6*, 158-162.
66. Bracke, W.; Marvel, C. S. *J. Polym. Sci. A* **1970**, *8*, 3177-3187.
67. Fournier, J.-H.; Maris, T.; Wuest, J. D. *J. Org. Chem.* **2004**, *69*, 1762-1775.
68. Bondi, A. *J. Phys. Chem.* **1964**, *68*, 441-451.
69. Jackson, N. E.; Savoie, B. M.; Kohlstedt, K. L.; de la Cruz, M. O.; Schatz, G. C.; Chen, L. X.; Ratner, M. A. *J. Am. Chem. Soc*. **2013**, *135*, 10475-10483.
70. Compositions of solvates and co-crystals were typically estimated by X-ray diffraction and further assayed by ^{1}H NMR spectroscopy of dissolved samples. Crystallization of triptycenetris(thiadiazole) **8** from DMSO produced concomitant solvated and unsolvated forms that could not be separated easily by hand, so the exact composition of the DMSO solvate was not determined.
71. The percentage of volume accessible to guests was estimated by the PLATON program (References 72 and 73). PLATON calculates the accessible volume by allowing a spherical probe of variable radius to roll over the van der Waals surface of the network. PLATON uses a default value of 1.20 Å for the radius of the probe, which is an appropriate model for small guests such as water. The van der Waals radii used to define

surfaces for these calculations are C: 1.70 Å, H: 1.20 Å, N: 1.55 Å, and S: 1.8 Å. The percentage of accessible volume is given by $100V_g/V$, where V is the volume of the unit cell and V_g is the guest-accessible volume as calculated by PLATON.

72. Spek, A. L. *PLATON, A Multipurpose Crystallographic Tool*; Utrecht University: Utrecht, The Netherlands, 2001.
73. van der Sluis, P.; Spek, A. L. *Acta Crystallogr.* **1990**, *A46*, 194-201.
74. Fucke, K.; McIntyre, G. J.; Lemée-Cailleau, M.-H.; Wilkinson, C.; Edwards, A. J.; Howard, J. A. K.; Steed, J. W. *Chem. Eur. J.* **2015**, *21*, 1036-1047.
75. Fucke, K.; Howard, J. A. K.; Steed, J. W. *Chem. Commun*. **2012**, *48*, 12065-12067.
76. Johnson, R. D.; Bethune, D. S.; Yannoni, C. S. *Acc. Chem. Res.* **1992**, *25*, 169-175.
77. Konarev, D. V.; Drichko, N. V.; Lyubovskaya, R. N.; Shul'ga, Y. M.; Litvinov, A. L.; Semkin, V. N.; Dubitsky, Y. A.; Zaopo, A. *J. Mol. Struct.* **2000**, *526*, 25-29.
78. Konarev, D. V.; Zubavichus, Y. V.; Valeev, E. F.; Slovokhotov, Y. L.; Shul'ga, Y. M.; Lyubovskaya, R. N. *Synth. Met*. **1999**, *103*, 2364-2365.
79. Veen, M. E.; Postma, P. M.; Jonkman, H. T.; Spek, A. L.; Feringa, B. L. *Chem. Commun*. **1999**, 1709-1710.
80. Kulkarni, P. P.; Jafvert, C. T. *Environ. Sci. Tech*. **2008**, *42*, 845-851.
81. Marcus, Y.; Smith, A. L.; Korobov, M. V.; Mirakyan, A. L.; Avramenko, N. V.; Stukalin, E. B. *J. Phys. Chem. B* **2001**, *105*, 2499-2506.
82. Beck, M. T.; Mándi, G. *Fullerene Sci. Tech*. **1997**, *5*, 291-310.
83. Ruoff, R. S.; Tse, D. S.; Malhotra, R.; Lorents, D. C. *J. Phys. Chem*. **1993**, *97*, 3379-3383.
84. Sivaraman, N.; Dhamodaran, R.; Kaliappan, I.; Srinivasan, T. G.; Vasudeva Rao, P. R.; Mathews, C. K. *J. Org. Chem*. **1992**, *57*, 6077-6079.
85. Burns, D. M.; Iball, J. *Proc. R. Soc. Lond. A* **1960**, *257*, 491-514.
86. Entwistle, R. F.; Iball, J.; Motherwell, W. D. S.; Thompson, B. P. *Acta Crystallogr.* **1969**, *B25*, 770-775.
87. Ahmed, F. R.; Trotter, J. *Acta Crystallogr*. **1963**, *16*, 503-508.
88. Wuest, J. D. *Chem. Commun*. **2005**, 5830-5837.
89. Mastalerz, M.; Sieste, S.; Cenić, M.; Oppel, I. M. *J. Org. Chem*. **2011**, *76*, 6389-6393.
90. Bruker, 2014. APEX2 and SAINT. Bruker AXS Inc. Madison, Wisconsin, USA.

91. Krause, L., Herbst-Irmer, R., Sheldrick, G. M., Stalke, D. *J. Applied Crystallogr.* **2015**, *48*, 3-10.
92. Sheldrick, G. M. *Acta Crystallogr*. **2008**, *A64*, 112-122.
93. Sheldrick, G. M. *Acta Crystallogr*. **2015**, *A71*, 3-8.
94. Sheldrick, G. M. *Acta Crystallogr*. **2015**, *C71*, 3-8.
95. Spek, A. L. *Acta Crystallogr*. **2015**, *C71*, 9-18.

2.3 Conclusions

Des molécules s'associant dans des motifs d'interaction bien définis peuvent être utilisées pour construire des matériaux possédant des architectures prédéterminées. L'un des obstacles associés à l'application de cette stratégie consiste à identifier des fragments moléculaires capables de diriger l'association dont les propriétés s'harmonisent avec celles du matériau final. L'association des composés **4**-**8** montre que les organisations adoptées par les thiadiazoles sont différentes de celles adoptées par les arènes analogues. Les structures cristallines de ces thiadiazoles révèlent aussi que ces composés sont généralement impliqués dans des interactions caractéristiques, dont les interactions S···N qui mènent souvent à l'apparition du synthon représenté à la Figure 10. Ces observations montrent que les dérivés du benzothiadiazole peuvent diriger l'association et qu'ils peuvent être utilisés pour former des matériaux possédant des propriétés optoélectroniques et supramoléculaires caractéristiques. Les propriétés supramoléculaires des thiadiazoles englobent de surcroit la possibilité de s'assembler avec les fullerènes.

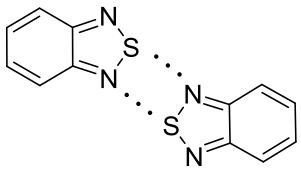

Figure 1. Structure d'un synthon observé dans la structure cristalline de plusieurs thiadiazoles.

Chapitre 3.

Synthèse de sels de naphtalènetétramine

Chapitre 3. Synthèse de sels de naphtalènetétramine

Notre capacité à étudier des matériaux est limitée par notre habileté à les synthétiser. Dans le cas des composés destinés à des applications technologiques, on désire aussi qu'ils puissent être préparés efficacement grâce à des synthèses courtes à haut rendement qui utilisent des réactifs accessibles et sécuritaires et des procédés de purification simples. Dans le chapitre 2, nous avons décrit comment le naphtobisthiadiazole **1** peut être préparé à partir de la naphtalènetétramine **2** afin d'éviter la manipulation du tétranitrure de tétrasoufre (N_4S_4). La naphtalènetétramine **2** est quant à elle obtenue via une courte synthèse qui nécessite la nitration d'un dérivé de la naphtalènediamine (**3**). Cette étape s'est révélée complexe et inefficace et nous nous sommes penchés sur les enjeux qui contrôlent l'issue de la réaction dans l'optique de pouvoir améliorer la synthèse des composés **1** et **2.** Ce chapitre décrit notre examen de l'étape de nitration. On y explore ultimement comment la nature du groupe protecteur influence la sélectivité de la nitration et de comment ces variations peuvent être exploitées afin de préparer sélectivement les tétramines **2** et **4**. Des études cristallographiques sont présentées pour plusieurs des produits, principalement afin de vérifier les structures et les conformations moléculaires et d'en extraire des informations sur le mécanisme de nitration.

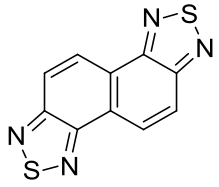

1

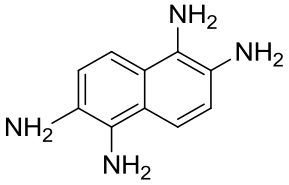

2

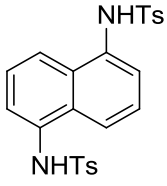

3

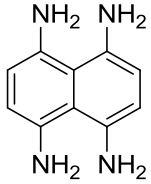

4

Synthesis of Salts of 1,2,5,6- and 1,4,5,8-Naphthalenetetramine

Sophie Langis-Barsetti, Thierry Maris, and James D. Wuest

ACS Omega, **2017**, *2*, 6023-6030

Abstract

1,2,5,6-Naphthalenetetramine (**1a**), its 1,4,5,8-isomer (**2a**), and their salts are valuable precursors for synthesizing nitrogen-containing arenes and other targets of interest. We describe how salts of tetramines **1a** and **2a** can be made from simple protected derivatives of 1,5-naphthalenediamine (**2d**) by sequences of regioselective dinitration, deprotection, and reduction. Various shortcomings of previously reported syntheses of tetramines **1a** and **2a** can thereby be avoided. In addition, we report structural studies that may help clarify the mechanism of nitration and resolve an earlier controversy about the regioselectivity observed in nitrations of derivatives of 1,5-naphthalenediamine (**2d**).

Introduction

1,2,5,6-Naphthalenetetramine (**1a**), its 1,4,5,8-isomer (**2a**), and their salts are useful as precursors of novel polymers,[1,2] azaarenes,[3] and other structures of interest.[4–9] In particular, tetramines **1a** and **2a** can be converted into bis(thiadiazole) **3**[10–12] and bis(thiadiazine) **4**,[6,7] respectively, which are related to compounds that have been widely incorporated in π-conjugated polymers and to small molecules used in luminescent materials and in thin-film optoelectronic devices, including light-emitting diodes, solar cells, field-effect transistors, and biosensors.[13–23]

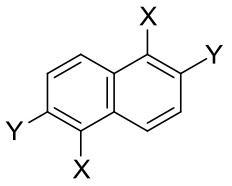

1a (X = Y = NH_2)
1b (X = NHTs; Y = NO_2)
1c (X = H, Y = Cl)
1d (X = NO_2, Y = Cl)
1e (X = NO_2, Y = NH_2)

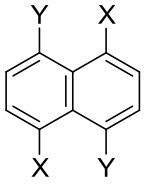

2a (X = Y = NH_2)
2b (X = Y = NO_2)
2c (X = NO_2, Y = H)
2d (X = NH_2, Y = H)
2e (X = NHTs, Y = H)
2f (X = NHTs, Y = NO_2)
2g (X = NH_2, Y = NO_2)
2h (X = NHCOMe, Y = H)
2i (X = NHCOMe, Y = NO_2)
2j (X = NHCbz, Y = H)
2k (X = NHCbz, Y = NO_2)

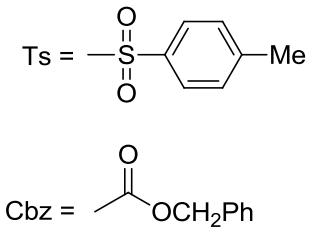

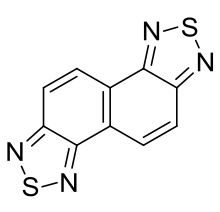

3

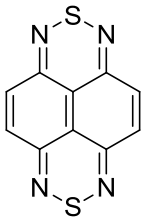

4

Unfortunately, previously published syntheses of naphthalenetetramines **1a** and **2a** have multiple undesirable features, and controversy has arisen about certain structural assignments. In particular, 1,4,5,8-naphthalenetetramine (**2a**) and salts have been prepared by

reducing 1,4,5,8-tetranitronaphthalene (**2b**),[24–27] an explosive compound produced in low yield by the dinitration of 1,5-dinitronaphthalene (**2c**), along with significant amounts of other nitrated products that must be separated. Another potential way to make tetramine **2a** is by dinitration of suitably protected derivatives of 1,5-naphthalenediamine (**2d**), followed by deprotection and reduction. In 1985, Nielsen et al. reported that the bis(4-methylbenzenesulfonamide) of 1,5-naphthalenediamine (compound **2e**)[28,29] reacted with $HNO_3/NaNO_2$ to give primarily the corresponding 4,8-dinitro derivative **2f**. Subsequent hydrolysis was alleged to produce 4,8-dinitro-1,5-naphthalenediamine (**2g**) in high yield.[30] Similarly, Nielsen et al. reported that the related dinitration of bis(acetamide) **2h**[31] gave mainly the 4,8-dinitro derivative **2i**, but their subsequent attempts to deprotect the dinitrated bis(acetamide) by hydrolysis were unsuccessful.[24,30]

More recent work by Sorokin et al. has suggested that dinitration of bis(4-methylbenzenesulfonamide) **2e** in fact gives the 2,6-dinitro derivative **1b**,[24] which can be subjected to hydrolysis and reduction to give 1,2,5,6-naphthalenetetramine (**1a**) in the form of its tetrahydrochloride salt.[1] In an alternative synthesis of tetramine **1a**,[1] 2,6-dichloronaphthalene (**1c**), itself the product of a multistep synthesis, was nitrated to give 2,6-dichloro-1,5-dinitronaphthalene (**1d**), which was converted into 1,5-dinitro-2,6-naphthalenediamine (**1e**) by high-pressure amination and subsequently into the tetrahydrochloride salt of tetramine **1a** by reduction and treatment with HCl.

We have reexamined the subject of 1,2,5,6-naphthalenetetramine (**1a**), its 1,4,5,8-isomer (**2a**), and their salts. The goal of our work has been to eliminate uncertainty about structural assignments, to provide new data that may help clarify the mechanism of nitration of derivatives of 1,5-naphthalenediamine (**2d**), and to find effective ways to make tetramines **1a** and **2a** without using explosive intermediates and inconvenient reactions.

Results and Discussion

The bis(4-methylbenzenesulfonamide) of 1,5-naphthalenediamine (compound **2e**) was dinitrated under the conditions ($HNO_3/NaNO_2$) used by Nielsen et al.[30] and later modified slightly by Sorokin and coworkers (Scheme 1).[24] We isolated the product in 27% yield after purification by crystallization from aqueous pyridine, and we confirmed that it was spectroscopically identical to the compound obtained previously by Nielsen, Sorokin, and their collaborators. However, Nielsen et al. reported that the product was the 4,8-dinitrated isomer **2f**, whereas Sorokin et al. identified the compound as the 2,6-dinitrated isomer **1b**. We crystallized the disputed product by cooling hot solutions in THF, and analysis by X-ray diffraction confirmed that dinitration occurs at the 2,6-positions to give compound **1b**, as claimed by Sorokin et al. Crystallographic details are provided in Table 1, and views of the structure appear in Figure 1.

Scheme 1

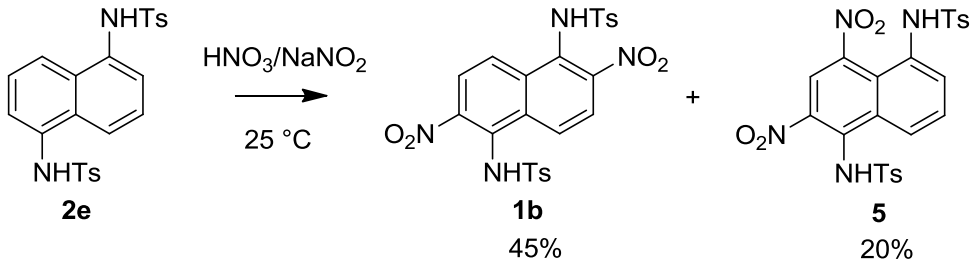

The observed conformation of bis(4-methylbenzenesulfonamide) **1b** (Figure 1a) is determined in part by a conspicuous pair of intramolecular N-H···O hydrogen bonds (2.24 Å) involving the sulfonamide and nitro groups. As expected, the 4-methylbenzenesulfonyl groups are forced out of the plane of the naphthyl core, and the sulfonamide nitrogen atoms are notably pyramidalized ($\Sigma_{\text{angles at N}} = 344°$). This is a characteristic property of related sulfonamides such as *N*-phenyl(4-methylbenzenesulfonamide).[32] In addition, the nitro groups are twisted by 34° out of the plane of the core. The naphthyl cores of compound **1b** are aligned along the *b*-axis to form parallel columns of slipped π-stacks with a separation of 3.58 Å

between mean planes. Adjacent columns are linked to form layers by C-H···O interactions (2.49 Å, as measured by H···O distance) involving sulfonyl groups and hydrogen atoms of the naphthyl units (Figure 1b). Packing of the layers is directed by interdigitated 4-methylphenyl groups and additional C-H···O interactions (2.48 and 2.53 Å, as measured by H···O distances) involving nitro and methyl groups (Figure 1c).

Table 1. Crystallographic data for compounds **1b**, **2k**, **5**, and **6**.

compound	**1b**	**2k**	**5**	**6**
crystallization medium	THF	THF	THF	THF/hexane
formula	$C_{24}H_{20}N_4O_8S_2$	$C_{26}H_{20}N_4O_8$	$C_{28}H_{28}N_4O_9S_2$	$C_{30}H_{28}N_4O_9$
crystal system	monoclinic	monoclinic	triclinic	monoclinic
space group	*C*2/*c*	$P2_1/c$	$P\bar{1}$	$P2_1/c$
a (Å)	25.4565(3)	21.374(2)	9.2281(3)	16.095(4)
b (Å)	5.6042(1)	5.9585(5)	10.7423(4)	21.593(5)
c (Å)	16.3639(2)	10.0311(8)	15.1969(5)	8.257(2)
α (°)	90	90	81.895(2)	90
β (°)	97.006(1)	92.402(4)	84.293(2)	101.741(11)
γ (°)	90	90	76.469(2)	90
V (Å^3)	2317.10(6)	1276.44(19)	1446.58(9)	2809.6(12)
Z	4	2	2	4
T (K)	100	150	150	150
ρ_{calc} (g cm^{-3})	1.595	1.344	1.443	1.391
λ (Å)	1.54178	1.54178	1.34139	1.34139
μ (mm^{-1})	2.630	0.858	1.425	0.561
R_1, $I > 2\sigma(I)$ (all)	0.0318	0.1252	0.0355	0.0978
R_1, all data	0.0323	0.1412	0.0416	0.1921
wR_2, $I > 2\sigma(I)$ (all)	0.0859	0.3727	0.0896	0.2271
wR_2, all data	0.0862	0.4018	0.0935	0.2893
measured reflections	22422	27338	34834	24254
independent reflections	2241	2425	6621	4070
observed reflections	2187	1850	5826	1961

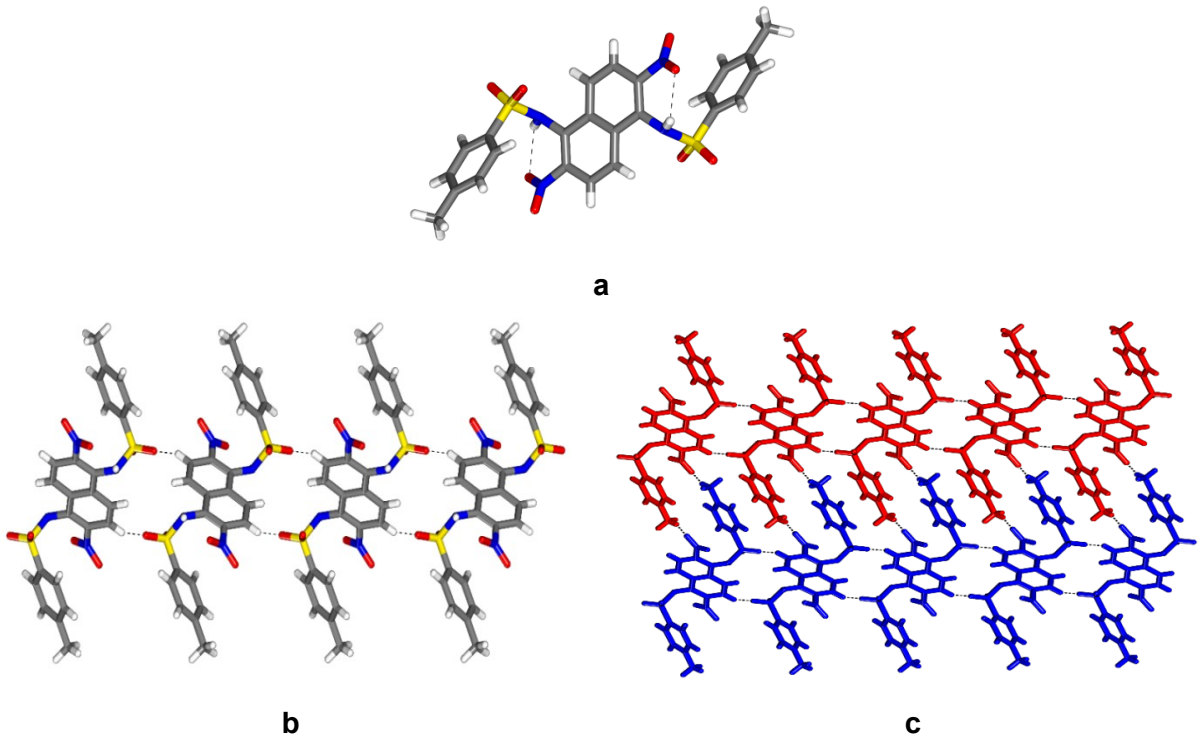

Figure 1. Representations of the structure of crystals of bis(4-methylbenzenesulfonamide) **1b** grown from THF. (a) View of the molecular conformation, which is controlled in part by the formation of intramolecular N-H···O hydrogen bonds involving the nitro and sulfonamide groups. (b) View of the structure along the direction of π-stacked naphthyl cores (*b*-axis), showing how C-H···O interactions link the stacks to form a layer. (c) View showing how the packing of adjacent layers (red and blue) is directed by interdigitated tolyl groups and additional C-H···O interactions involving nitro and methyl groups. Unless otherwise indicated, atoms of carbon are shown in gray, atoms of hydrogen in white, atoms of nitrogen in blue, atoms of oxygen in red, and atoms of sulfur in yellow. N-H···O hydrogen bonds and C-H···O interactions are represented by broken lines.

With the structure of the product of dinitration firmly established, the method of Nielsen, Sorokin, and their collaborators provides a reliable way to make compound **1b**. Although the yield is low, the product can be obtained in pure form by a simple procedure. Careful chromatographic separation of all products of nitration also yielded minor dinitro

compound **5**, and analysis of the total crude product by NMR spectroscopy indicated that the yields of major iomer **1b** and minor isomer **5** were 45% and 20%, respectively, before isolation. Crystallization of compound **5** from THF yielded a solvate of composition **5** • 1 THF, and its structure was determined by X-ray crystallography. Crystallographic details are summarized in Table 1, and views of the structure are presented in Figure 2.

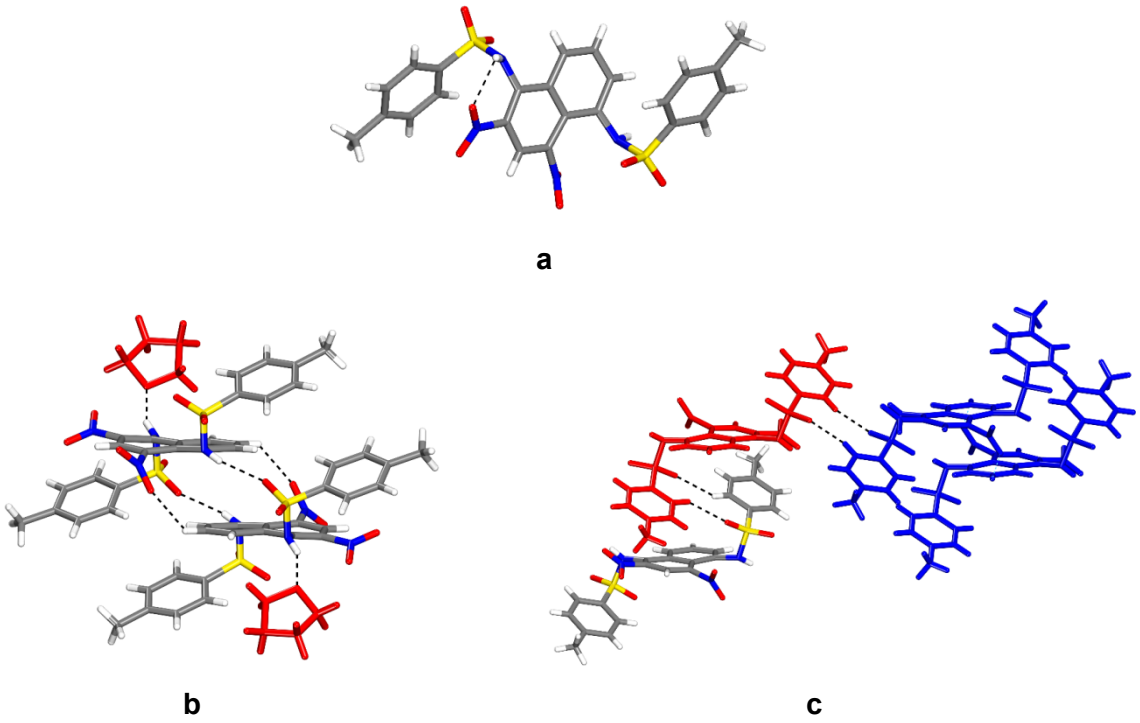

Figure 2. Representations of the structure of crystals of solvate **5** • 1 THF grown from THF. (a) View of the distorted molecular conformation of compound **5**, which is controlled in part by the formation of a single intramolecular N-H···O hydrogen bond involving a nitro group and a sulfonamide group. (b) View of dimer held together by N-H···O hydrogen bonds and C-H···O interactions, with hydrogen-bonded guest molecules of THF shown in red. (c) View showing how each molecule interacts with the next dimer in the same stack (red) and with a molecules in an adjacent stack of dimers (blue) by forming C-H···O interactions involving sulfonyl groups, and. Unless otherwise indicated, atoms of carbon are shown in gray, atoms of hydrogen in white, atoms of nitrogen in blue, atoms of oxygen in red, and atoms of sulfur in yellow. N-H···O hydrogen bonds and C-H···O interactions are represented by broken lines.

As in the case of bis(4-methylbenzenesulfonamide) **1b,** the conformation of isomer **5** is determined in part by the interaction of adjacent sulfonamide and nitro groups, but only one intramolecular N-H···O hydrogen bond (2.32 Å) is formed (Figure 2a). Introducing a nitro group at the 4-position significantly distorts the naphthalene core and produces a torsional angle of 174° along C_1-C_9-C_{10}-C_5. In addition, C-N bonds at the 4- and 5-positions are tilted out of the average plane of the core by 13° and 7°, respectively, in opposite directions. Pyramidalization of the sulfonamide nitrogen atoms ($\Sigma_{\text{angles at N}}$ = 348° and 337°) is similar to that observed in isomer **1b**, and the 4-methylbenzenesulfonyl groups are again forced out of the plane of the naphthyl core. Twisting of nitro groups out of the plane of the core is accentuated at the 4-position (55°), whereas the value at the 2-position (27°) resembles the one observed for isomer **1b**.

As shown in Figure 2b, molecules of compound **5** form dimers associated along the *b*-axis by N-H···O hydrogen bonds involving sulfonamide units (2.94 Å), as well as by offset π-stacking (3.41 Å between mean planes). The association is strengthened by C-H···O interactions between hydrogen atoms bonded to the naphthyl core and both a nitro group (2.65 Å) and a sulfonyl group (2.56 Å). The dimers are further linked to form stacks along the *b*-axis by reciprocal C-H···O interactions (2.39 Å) involving 4-methylbenzenesulfonyl groups (Figure 2c). Finally, adjacent stacks are linked by reciprocal C-H···O interactions (2.35 Å) involving 4-methylbenzenesulfonyl groups (Figure 2c), as well as by other C-H···O interactions. Guest molecules of THF are ordered and form N-H···O hydrogen bonds (2.77 Å) with sulfonamide groups (Figure 2b).

The bis(benzyl carbamate) of 1,5-naphthalenediamine (compound **2j**) reacted more slowly with $HNO_3/NaNO_2$ than the corresponding bis(4-methylbenzenesulfonamide) **2e**, and dinitration was therefore carried out at 25 °C, followed by a period of heating at 100 °C (Scheme 2). The major product was obtained as yellow needles in 18% yield after crystallization from THF. Analysis of the crystals by X-ray diffraction established that dinitration occurred at the 4 and 8 positions to give compound **2k**. Crystallographic data are presented in Table 1, and views of the structure are shown in Figure 3.

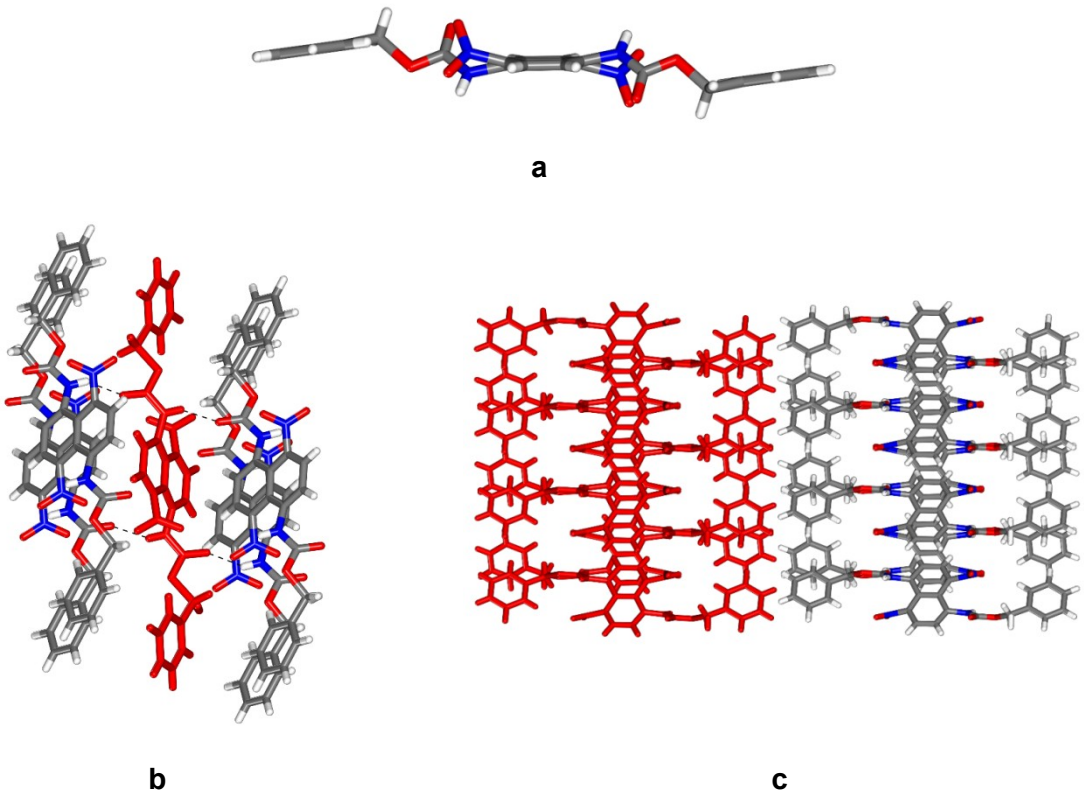

Figure 3. Representations of the structure of crystals of bis(benzyl carbamate) **2k** grown from THF. (a) View of the distorted molecular conformation of compound **2k**. (b) View showing that the structure can be considered to be composed of layers in which each molecule of compound **2k** is linked to four neighbors by four N-H···O hydrogen bonds involving the carbamoyl groups. The central molecule is shown in red, and hydrogen bonds are represented by broken lines. (c) View along the *c*-axis showing two adjacent layers, with one highlighted in red. Unless otherwise indicated, atoms of carbon are shown in gray, atoms of hydrogen in white, atoms of nitrogen in blue, and atoms of oxygen in red.

Scheme 2

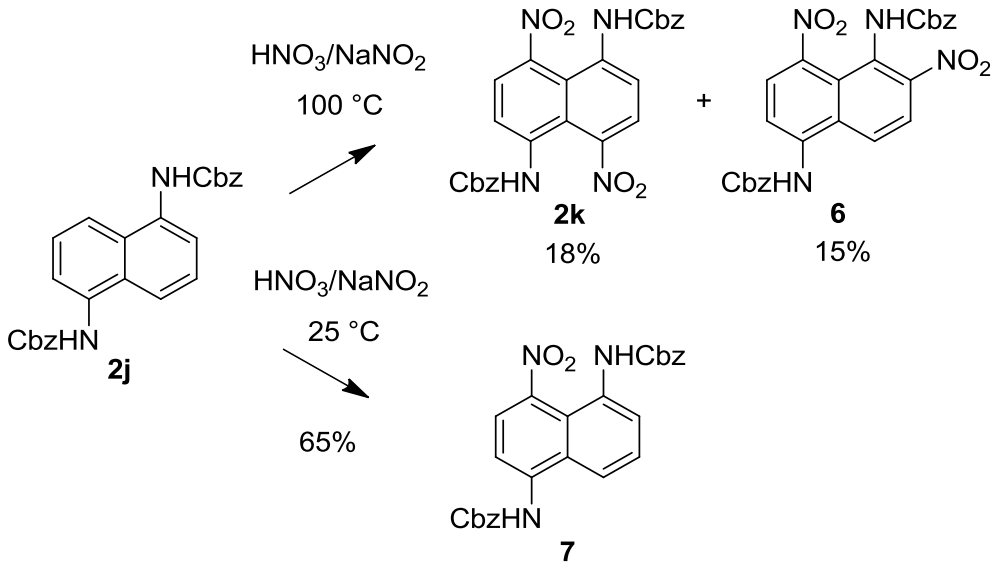

The conformation of bis(benzyl carbamate) **2k** shows that tetrasubstitution at the 1,4,5,8-positions causes significant distortions (Figure 3a). The naphthyl core is planar, and the atoms of nitrogen all adopt normal sp^2 hybridization. However, C-N bonds to the nitro groups are tilted out of the plane of the core by 17°, and C-N bonds to the carbamate groups are tilted in the opposite direction by 13°. Moreover, the nitro and carbamate groups are twisted out of the plane of the naphthyl core by 57° and 50°, respectively. The relatively high values of *R* shown in Table 1 reflect disorder of the benzyl groups over two positions. Molecules of compound **2k** associate to form layers held together in part by N-H···O hydrogen bonds (2.79 Å), which are a characteristic feature of the structures of related benzyl carbamates (Figure 3b).[33] Packing of adjacent layers is controlled by weak interactions of the benzyl groups (Figure 3c).

Although 2,6-dinitration of bis(4-methylbenzenesulfonamide) **2e** to give compound **1b** could be accomplished at 25 °C under the standard conditions ($HNO_3/NaNO_2$), 4,8-dinitration of bis(carbamate) **2j** to produce compound **2k** required heating at 100 °C. A similar reaction carried out at 25 °C led to formation of mononitro derivative **7** in 65% yield (Scheme 2). The

distorted structure of 4,8-dinitro derivative **2k** suggests that introduction of the first nitro group is facile but forces the adjacent carbamate group further out of the plane of the naphthyl core, leading to deactivation that makes dinitration difficult. Indeed, conversion of compound **7** into dinitrated product **2k** under the standard conditions ($HNO_3/NaNO_2$) required higher temperatures (Scheme 2).

4,8-Dinitro compound **2k** can be obtained in pure form by a simple method, so our procedure is useful, and the structure of the compound has been confirmed unambiguously. However, the yield is low, so we examined the crude product of direct dinitration at 100 °C in greater detail. Mononitro compound **7** was formed efficiently under milder conditions and can be converted into 4,8-dinitro derivative **2k** at higher temperatures, suggesting that it is an intermediate in further nitration. Subsequent crystallization of the crude product remaining after removing symmetric dinitro isomer **2k** produced a 1:1 THF solvate of 2,8-dinitro isomer **6**, which was isolated in 15% yield. Although dinitration of bis(benzyl carbamate) **2j** gave compounds **2k** and **6** in low yields (18% and 15%, respectively), the products could be isolated in pure crystalline form without chromatographic separation. Moreover, when the crude product of dinitration was examined by ^{1}H NMR spectroscopy, compounds **2k** and **6** were detected in yields of about 35% and 30%, respectively, and no other significant product is formed.

The structure assigned to 2,8-dinitro compound **6** was confirmed by X-ray crystallography. Views of the structure appear in Figure 4, and additional crystallographic data are summarized in Table 1.As observed in the structures of dinitro compounds **1b**, **2k**, and **5**, which have patterns of 1,2,5,6-, 1,4,5,8-, and 1,2,4,5-tetrasubstitution, respectively, the 1,2,5,8-tetrasubstitution found in bis(benzyl carbamate) **6** also causes significant molecular distortions (Figure 4a). In particular, the torsional angle defined by C_1-C_9-C_{10}-C_5 in the naphthyl core is 173°, and the nitro and carbamate groups are twisted out of the average plane. Molecules of compound **6** are linked to form columns parallel to the *c*-axis, both by N-H···O hydrogen bonds (2.91 Å) between carbamoyl units and by offset π-stacking with a separation of 3.65 Å between mean planes (Figure 4b). Packing of adjacent columns is determined by

various weak interactions. Guest molecules of THF form N-H···O hydrogen bonds (2.75 Å) with carbamoyl groups (Figure 4b). The relatively high values of *R* shown in Table 1 reflect disorder of the benzyl groups.

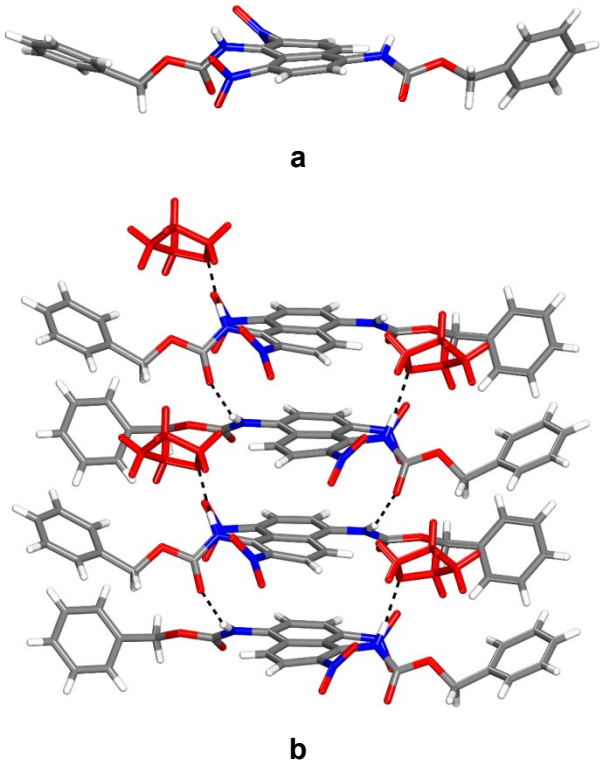

Figure 4. Representations of the structure of crystals of bis(benzyl carbamate) **6** grown from THF/hexane. (a) View of the distorted conformation of compound **6**, with only one orientation of the disordered benzyl groups drawn. (b) View showing part of a column of hydrogen-bonded and π-stacked molecules. Guest molecules of THF appear in red. Unless otherwise indicated, atoms of carbon are shown in gray, atoms of hydrogen in white, atoms of nitrogen in blue, and atoms of oxygen in red.

The mechanism of electrophilic aromatic nitration continues to be debated. In certain cases, it may involve direct reaction of NO_2^+ with the substrate to form a classic Wheland intermediate. However, suitably activated aromatic compounds can also undergo nitration by a

radical pathway initiated by electron transfer from the substrate to NO_2^+,[34–39] followed by coupling of the resulting aromatic radical cation with NO_2 to form a σ-bonded intermediate. In such cases, the position of nitration is dictated by the combined effects of non-uniform spin density in the aromatic radical cation and the stability of the intermediate. The regioselectivity of radical nitrations can thereby depend on the identity of substituents in subtle and unexpected ways. The observed preferences for 2,6-dinitration (in the case of bis(4-methylbenzenesulfonamide) **2e**) and for 4,8-dinitration (in the case of bis(carbamate) **2j**) presumably arise because the reactions occur by different mechanisms or because they both follow radical pathways, but the radical cations initially formed differ significantly in structure and distribution of spin density.

The yields of compounds **1b**, **2k**, **5**, and **6** are not high, but all are easily isolated in pure form by crystallization, their structures are firmly established, and sequences of deprotection and reduction allow preparation of 1,2,5,6- and 1,4,5,8-naphthalenetetramines **1a** and **2a**, as well as less symmetric isomers (Scheme 3). Dinitrated bis(4-methylbenzenesulfonamide) **1b** was deprotected in 93% yield by using H_2SO_4 as described by Nielsen et al.,[30] and the product **1e** was subsequently reduced by $SnCl_2$ to give the tetrahydrochloride salt of tetramine **1a** in 79% yield. Dinitrated bis(carbamate) **2k** was deprotected in 88% yield by using BBr_3, and the product **2g** was then reduced by $SnCl_2$ to give the tetrahydrochloride salt of tetramine **2a** in 55% yield. The salt was identified as the tetrahydrochloride on the basis of its elemental analysis, the composition of closely related salts,[40] and thermogravimetric analysis. Isolation of both naphthalenetetramines as their salts is an example of a widely-used strategy that avoids the need to work with highly air-sensitive free bases.[41]

Scheme 3

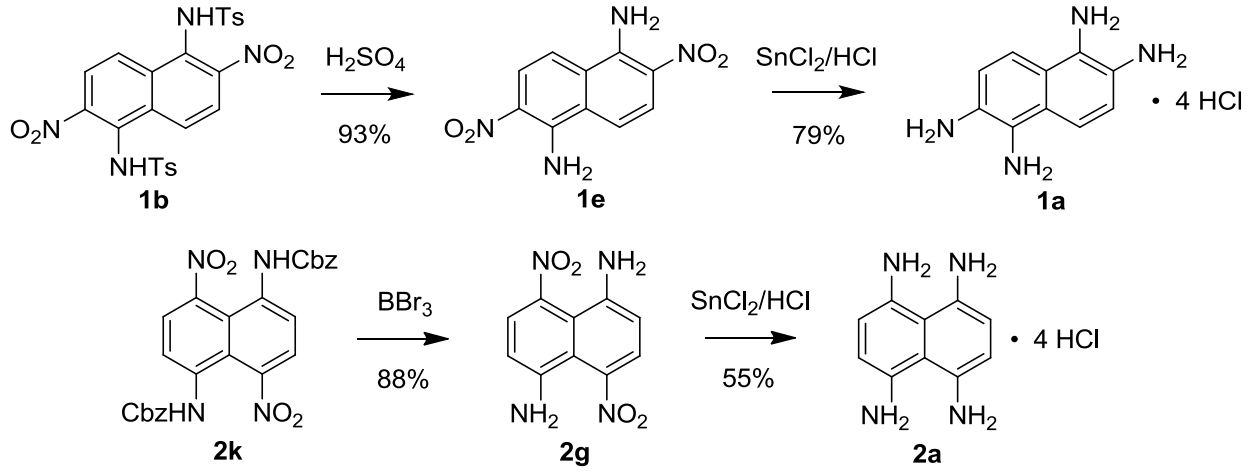

1,2,5,6-Naphthalenetetramine (**1a**), its 1,4,5,8-isomer (**2a**), and their salts are valuable precursors for synthesizing nitrogen-containing arenes and other targets of interest. We have found that salts of tetramines **1a** and **2a** can be made from simple protected derivatives of 1,5-naphthalenediamine (**2d**) by sequences of regioselective dinitration, deprotection, and reduction. Various shortcomings of previously reported syntheses of tetramines **1a** and **2a** can thereby be avoided. In addition, our studies provide new data that may help clarify the mechanism of nitration and resolve an earlier controversy about the regioselectivity observed in nitrations of 1,5-naphthalenediamine (**2d**).

Experimental Section

All reagents and solvents were obtained from commercial sources and used without further purification unless otherwise indicated. Compounds **1b**[24,30] and **1e**[24,30] were prepared by published procedures.

Bis(phenylmethyl) 1,5-Naphthalenediylcarbamate (2j). The compound was synthesized by a modification of the method reported by Festel et al.[42] Solutions of Na_2CO_3 (6.83 g, 64.4 mmol) in water (80 mL) and benzyl chloroformate (9.1 mL, 64 mmol) in dichloromethane (120 mL) were added to a solution of 1,5-naphthalenediamine (4.01 g, 25.4 mmol) in dichloromethane (400 mL). The mixture was stirred at 25 °C for 12 h, and then volatile components were removed by partial evaporation under reduced pressure to give a suspension. The off-white solid was separated by filtration, washed with water, and crystallized from hot dioxane to afford bis(phenylmethyl) 1,5-naphthalenediylcarbamate as colorless needles (**2j**; 9.10 g, 21.4 mmol, 84%).

***N*,*N*'-(2,4-Dinitronaphthalene-1,5-diyl)bis(4-methylbenzenesulfonamide) (5).** **B**is(4-methylbenzenesulfonamide) **1b** was nitrated as described by Nielsen et al.[30] to give a crude product containing compound **5** in 20% yield. Purification by flash chromatography (6:4 hexane:THF) and subsequent crystallization from THF provided *N*,*N*'-(2,4-dinitronaphthalene-1,5-diyl)bis(4-methylbenzenesulfonamide) (**5**) as yellow plates: mp 230 °C dec.; FTIR (ATR) 3283, 3249, 3129, 3040, 2958, 2991, 2028, 1534, 1336, 1162, cm^{-1}; ^1H NMR (400 MHz, DMSO-d_6) δ 11.16 (s, 1H), 10.11 (s, 1H), 8.57 (s, 1H), 7.69 (d, ^3J = 9 Hz, 1H), 7.42 (d, ^3J = 8 Hz, 2H), 7.38–7.30 (m, 5H), 7.26 (d, ^3J = 8 Hz, 2H), 6.69 (dd, ^3J = 7 Hz, ^4J = 1 Hz, 1H), 2.38 (s, 3H), 2.32 (s, 3H); ^{13}C NMR (100 MHz, DMSO-d_6) δ 143.7, 143.5, 136.8, 135.5, 133.0, 131.2, 130.7, 129.8 (2C), 129.6 (2C), 128.6, 127.2 (2C), 126.4 (2C), 125.3, 118.5, 21.0, 20.9; HRMS (ESI, TOF) calcd for $C_{24}H_{20}N_4O_8S_2 + NH_4^+$ *m/e* 574.1061, found 574.1044.

Bis(phenylmethyl) 4-Nitro-1,5-naphthalenediylcarbamate (7). A solution made by adding aqueous HNO_3 (70%, 3.5 mL) to acetic acid (50 mL) was then added to a solution of bis(phenylmethyl) 1,5-naphthalenediylcarbamate (**2j**; 1.03 g, 2.42 mmol) and $NaNO_2$ (0.055 g, 0.80 mmol) in acetic acid (50 mL). The mixture was stirred at 25 °C for 20 h and was then treated with water. The resulting precipitate was separated by filtration, washed with water and acetone, and crystallized from hot THF to give bis(phenylmethyl) 4-nitro-1,5-naphthalenediylcarbamate as a yellow solid (**7**; 0.740 g, 1.57 mmol, 65%): mp 237–238 °C; FTIR (ATR) 3272, 3064, 3033, 1696, 1543, 1505, 1417, 1346, 1244, 1073 cm^{-1}; ^1H NMR (400 MHz, DMSO-d_6) δ 10.13 (s, 1H), 9.38 (s, 1H), 8.22 (d, ^3J = 9 Hz, 1H), 7.94 (d, ^3J = 8 Hz, 1H), 7.83 (d, ^3J = 8 Hz, 1H), 7.69 (t, ^3J = 8 Hz, 1H), 7.57 (d, ^3J = 9 Hz, 1H), 7.49-7.34 (m, 9 H), 5.24 (s, 2H), 5.09 (s, 2H); ^{13}C NMR (100 MHz, DMSO-d_6) δ 154.9, 154.4, 143.6, 137.7, 136.7, 136.4, 131.7, 129.0, 128.7, 128.5, 128.3 (2C), 128.2, 127.8, 127.7, 127.2, 123.1, 122.3, 121.9, 118.1, 66.4, 65.9; HRMS (ESI, TOF) calcd for $C_{26}H_{21}N_3O_6 + NH_4^+$ *m/e* 489.1769, found 489.1717. Anal. Calcd for $C_{26}H_{21}N_3O_6$: C, 66.24; H, 4.49; N, 8.91. Found: C, 66.21; H, 4.45; N, 8.91.

Bis(phenylmethyl) 4,8-Dinitro-1,5-naphthalenediylcarbamate (2k). A solution prepared by adding aqueous HNO_3 (70%, 3.5 mL) to acetic acid (50 mL) was added to a solution of bis(phenylmethyl) 1,5-naphthalenediylcarbamate (**2j**; 1.02 g, 2.39 mmol) and $NaNO_2$ (0.053 g, 0.77 mmol) in acetic acid (50 mL). The mixture was stirred at 25 °C for 20 h and then at 100 °C for 3 h. The resulting suspension was cooled to 25 °C, treated with water, and filtered. The recovered solid was washed with water, washed with acetone, and crystallized from hot THF to give bis(phenylmethyl) 4,8-dinitro-1,5-naphthalenediylcarbamate as a pale yellow solid (**2k**; 0.222 g, 0.430 mmol, 18%): mp 255 °C dec; FTIR (ATR) 3273, 3064, 3041, 1516, 1702, 1515, 1499, 1244, 1228, 1144, 1075 cm^{-1}; ^1H NMR (400 MHz, DMSO-d_6) δ 9.81 (s, 2H), 8.16 (d, ^3J = 8 Hz, 2H), 7.72 (d, ^3J = 8 Hz, 2H), 7.39 (m, 10 H), 5.13 (s, 4H); ^{13}C NMR (100 MHz, DMSO-d_6) δ 155.1, 146.2, 137.2, 136.1, 129.2, 128.8, 128.5, 127.6, 125.3, 123.8, 67.0; HRMS (ESI, TOF) calcd for $C_{26}H_{20}N_4O_8 + NH_4^+$ *m/e* 534.1619, found 534.1626. Anal. Calcd for $C_{26}H_{20}N_4O_8$: C, 60.47; H, 3.90; N, 10.85. Found: C, 60.31; H, 3.86; N, 10.88.

Bis(phenylmethyl) 4,8-Dinitro-1,5-naphthalenediylcarbamate (2k). A solution prepared by adding aqueous HNO_3 (70%, 2.4 mL) to acetic acid (35 mL) was added to a solution of bis(phenylmethyl) 4-nitro-1,5-naphthalenediylcarbamate (**7**; 675 mg, 1.43 mmol) and $NaNO_2$ (35 mg, 0.51 mmol) in acetic acid (10 mL). The mixture was stirred at 100 °C for 3 h. The resulting suspension was then cooled to 25 °C, treated with water, and filtered. The recovered solid was washed with water, washed with acetone, and crystallized from hot THF to provide bis(phenylmethyl) 4,8-dinitro-1,5-naphthalenediylcarbamate as a pale yellow solid (**2k**; 163 mg, 0.315 mmol, 22%).

Bis(phenylmethyl) 2,8-Dinitro-1,5-naphthalenediylcarbamate (6). Bis(phenylmethyl) 1,5-naphthalenediylcarbamate (**2j**) was dinitrated at 100 °C under conditions described above, and the acetone extracts produced during purification of the primary product were subjected to evaporation under reduced pressure. The residue was dissolved in THF, and layering hexane over the solution induced crystallization of bis(phenylmethyl) 2,8-dinitro-1,5-naphthalenediylcarbamate in the form of yellow needles (**6**; 0.185 g, 0.358 mmol, 15%): mp 185 °C dec.; FTIR (ATR) 3287, 3145, 3032, 2952, 2885, 2058, 2005, 1736, 1703, 1523, 1210 cm^{-1}; ^1H NMR (400 MHz, $CDCl_3$) δ 8.18 (d, ^3J = 8 Hz, 1H), 7.99 (d, ^3J = 9 Hz, 1H), 7.92–7.88 (m, 2H), 7.72 (s, 1H), 7.52 (s, 1H), 7.46–7.35 (m, 10H), 5.29 (s, 2H), 5.07 (s, 2H); ^{13}C NMR (100 MHz, $CDCl_3$) δ 153.5, 145.4, 145.2, 137.1, 135.3, 135.2, 129.0, 128.9 (2C), 128.8 (2C), 128.7, 128.6, 128.4, 127.2, 125.8, 123.4, 122.1, 121.1, 119.0, 68.7, 68.4; HRMS (ESI, TOF) calcd for $C_{26}H_{20}N_4O_8 + NH_4^+$ *m/e* 534.1619, found 534.1623.

4,8-Dinitro-1,5-naphthalenediamine (2g). A suspension of bis(phenylmethyl) 4,8-dinitro-1,5-naphthalenediylcarbamate (**2k**; 322 mg, 0.623 mmol) in dichloromethane (15 mL) was stirred at 0 °C and treated dropwise with a solution of BBr_3 (1.0 M, 1.3 mL, 1.3 mmol) in dichloromethane. The resulting suspension was stirred at 25 °C for 3 h, treated with water, and stirred for 15 min. Volatiles were removed by evaporation under reduced pressure, and the residual solid was washed with water and dried under vacuum to give 4,8-dinitro-1,5-naphthalenediamine as a red solid (**2g**; 136 mg, 0.548 mmol, 88%). Further purification was achieved by crystallization from hot absolute ethanol: mp 230 °C dec; FTIR (ATR) 3431,

3343, 3257, 3065, 3041, 1516, 1454, 1247 cm^{-1}; ^1H NMR (400 MHz, DMSO-d_6) δ 8.02 (d, ^3J = 9 Hz, 2H), 6.84 (d, ^3J = 9 Hz, 2H), 6.55 (s, 4H); ^{13}C NMR (100 MHz, DMSO-d_6) δ 149.5, 135.9, 128.9, 115.5, 110.1; HRMS (APCI, TOF) calcd for $C_{10}H_8N_4O_4$ - H *m/e* 247.0473, found 247.0453.

1,4,5,8-Naphthalenetetramine Tetrahydrochloride (2a • 4 HCl). A mixture of 4,8-dinitro-1,5-naphthalenediamine (**2g**; 106 mg, 0.427 mmol) and $SnCl_2$ • 2 H_2O (972 mg, 4.30 mmol) in ethanol (7.5 mL) and concentrated aqueous HCl (2.5 mL) was stirred at 90 °C under N_2 for 12 h and was then cooled to 0 °C. The resulting suspension was filtered, and the recovered solid was washed with HCl and dried under vacuum to afford crude 1,4,5,8-naphthalenetetramine tetrahydrochloride as an off-white solid (**2a** • 4 HCl; 78 mg, 0.23 mmol, 55%). Further purification could be accomplished by dissolving the product in water and adding the solution to concentrated aqueous HCl. The salt was stored under dry N_2: mp 100 °C dec; FTIR (ATR) 3034, 2905, 2817, 2728, 2693, 2587, 2532, 1125, 629 cm^{-1}; ^1H NMR (400 MHz, DMSO-d_6) δ 7.12 (s, 4H), 3.59 (br s, 12H); ^{13}C NMR (100 MHz, DMSO-d_6) δ 131.8, 122.2, 118.6; HRMS (ESI, TOF) calcd for $C_{10}H_{12}N_4$ + H^+ *m/e* 189.1135, found 189.1135. Anal. Calcd for $C_{10}H_{16}Cl_4N_4$: C, 35.95; H, 4.83; N, 16.77. Found: C, 35.95; H, 4.80; N, 15.93.

1,2,5,6-Naphthalenetetramine Tetrahydrochloride (1a • 4 HCl). A mixture of 2,6-dinitro-1,5-naphthalenediamine (**13**; 1.02 g, 4.11 mmol) and $SnCl_2$ • 2 H_2O (9.05 g, 40.1 mmol) in ethanol (40 mL) and concentrated aqueous HCl (12 mL) was stirred at 90 °C under N_2 for 12 h and was then cooled to 0 °C. The resulting suspension was filtered, and the recovered solid was washed with HCl and dried under vacuum to provide crude 1,2,5,6-naphthalenetetramine tetrahydrochloride as a beige solid. The product was then dissolved in water (~100 mL), and the solution was poured into warm, vigorously stirred concentrated aqueous HCl (~100 mL). The mixture was cooled to 25 °C, and the resulting suspension was cooled further to 0 °C. The precipitated solid was separated by filtration, washed with HCl, and dried under vacuum to afford a purified sample of 1,2,5,6-naphthalenetetramine tetrahydrochloride (**1a** • 4 HCl; 1.08 g, 3.23 mmol, 79%). The salt was stored under dry N_2. ^1H NMR (400 MHz, DMSO-d_6) δ 7.50

(d, ^{3}J = 9 Hz, 2H), 7.23 (d, ^{3}J = 9 Hz, 2H), 4.17 (br s, 12H). Additional characterization was reported by Stille and coworkers.[1]

Supporting Information Available: ^{1}H and ^{13}C NMR spectra of compounds **1a** • 4 HCl, **2a** • 4 HCl, **2g**, **2j**, **5**, and **6**, as well as additional crystallographic details, including ORTEP drawings and tables of structural data in CIF format. This material is available free of charge via the Internet at http://pubs.acs.org.

Acknowledgments. We are grateful to the Natural Sciences and Engineering Research Council of Canada, the Ministère de l'Éducation du Québec, the Canada Foundation for Innovation, the Canada Research Chairs Program, NanoQuébec, and Université de Montréal for financial support.

Author Information

Corresponding Author

*E-mail: james.d.wuest@umontreal.ca

E-mail: sophie.langis-barsetti@umontreal.ca

E-mail: thierry.maris@umontreal.ca

Notes. The authors declare no competing financial interest.

‡ Fellow of the Fonds de recherche du Québec–Nature et technologies (FRQNT).

References

1. Imai, K.; Kurihara, M.; Mathias, L.; Wittmann, J.; Alston, W. B.; Stille, J. K. *Macromolecules* **1973**, *6*, 158–162.
2. Arnold, F. E.; Van Deusen, R. L. *Polymer Lett*. **1968**, *6*, 815–819.
3. Geib, S.; Martens, S. C.; Zschieschang, U.; Lombeck, F.; Wadepohl, H.; Klauk, H.; Gade, L. H. *J. Org. Chem*. **2012**, *77*, 6107–6116.
4. Vitske, V.; König, C.; Hübner, O.; Kaifer, E.; Himmel, H.-J. *Eur. J. Inorg. Chem*. **2010**, 115–126.
5. Lebkücher, A.; Rybina, A.; Herten, D.-P.; Hübner, O.; Wadepohl, H.; Kaifer, E.; Himmel, H.-J. *Z. Anorg. Allg. Chem.* **2011**, *637*, 547–555.
6. Gieren, A.; Lamm, V.; Haddon, R. C.; Kaplan, M. L. *J. Am. Chem. Soc.* **1979**, *101*, 7277–7281.
7. Haddon, R. C.; Kaplan, M. L.; Marshall, J. H. *J. Am. Chem. Soc.* **1978**, *100*, 1235–1239.
8. Wudl, F.; Kaplan, M. L.; Teo, B. K.; Marshall, J. *J. Org. Chem.* **1977**, *42*, 1666–1667.
9. Dawans, F.; Marvel, C. S. *J. Polym. Sci., Part A: Polym. Chem.* **1965**, *3*, 3549–3571.
10. Langis-Barsetti, S.; Maris, T.; Wuest, J. D. *J. Org. Chem*. **2017**, *82* 5034–5045.
11. Mataka, S.; Takahashi, K.; Ikezaki, Y.; Hatta, T.; Tori-i, A.; Tashiro, M. *Bull. Chem. Soc. Jpn.* **1991**, *64*, 68–73.
12. Kawashima, K. (Sankyo Kasei Co., Japan). Method for Producing Naphthobisthiadiazole. WO 2014002969 A1, January 3, 2014.
13. Jung, J. W.; Jo, J. W.; Jung, E. H.; Jo, W. H. *Org. Electron*. **2016**, *31*, 149–170.
14. Neto, B. A. D.; Carvalho, P. H. P. R.; Correa, J. R. *Acc. Chem. Res*. **2015**, *48*, 1560–1569.
15. Parker, T. C.; Patel, D. G.; Moudgil, K.; Barlow, S.; Risko, C.; Brédas, J.-L.; Reynolds, J. R.; Marder, S. R. *Mater. Horiz*. **2015**, *2*, 22–36.
16. Zhan, R.; Liu, B. *Macromol. Chem. Phys*. **2015**, *216*, 131–144.
17. Li, Y.; Liu, T.; Liu, H.; Tian, M.-Z.; Li, Y. *Acc. Chem. Res.* **2014**, *47*, 1186–1198.
18. Li, Y. *Acc. Chem. Res.* **2012**, *45*, 723–733.
19. Gao, C.; Wang, L.; Li, X.; Wang, H. *Polym. Chem*. **2014**, *5*, 5200–5210.

20. Neto, B. A. D.; Lapis, A. A. M.; da Silva Júnior, E. N.; Dupont, J. *Eur. J. Org. Chem*. **2013**, 228–255.
21. Behramand, B.; Molin, F.; Gallardo, H. *Dyes Pigments* **2012**, *95*, 600–605.
22. Chen, J.; Cao, Y. *Acc. Chem. Res.* **2009**, *42*, 1709–1718.
23. Yamashita, Y. *Chem. Lett*. **2009**, *38*, 870–875.
24. Sorokin, V. I.; Ozeryanskii, V. A.; Pozharskii, A. F. *Russ. J. Org. Chem*. **2002**, *38*, 699–708.
25. Hinze, W. L.; Liu, L.-J.; Fendler, J. H. *J. Chem. Soc. Perkin Trans. 2* **1975**, 1751–1767.
26. Ward, E. R.; Johnson, C. D. *J. Chem. Soc.* **1961**, 4314–4321.
27. Ward, E. R.; Johnson, C. D.; Day, L. A. *J. Chem. Soc.* **1959**, 487–493.
28. Bayer, R. W.; O'Reilly, E. J., Jr. *J. Org. Chem*. **1958**, *23*, 746–747.
29. Hodgson, H. H.; Whitehurst, J. S. *J. Chem. Soc*. **1945**, 202–204.
30. Nielsen, A. T.; DeFusco, A. A.; Browne, T. E. *J. Org. Chem.* **1985***, 50,* 4211–4218.
31. Buu-Hoi. N. P. *Bull. Soc. Chim. Fr.* **1945**, *12*, 587–593.
32. Gowda, B. T.; Foro, S.; Nirmala, P. G.; Terao, H.; Fuess, H. *Acta Crystallogr*. **2009**, *E65*, o1219.
33. Mata, I.; Molins, E.; Amat, M.; Llor, N.; Checa, B. *Acta Crystallogr*. **2012**, *C68*, o114–o118.
34. Kenner, J. *Nature* **1945**, *156*, 369–370.
35. Perrin, C. L. *J. Am. Chem. Soc.* **1977**, *99*, 5516–5518.
36. Peluso, A.; Del Re, G. *J. Phys. Chem.* **1996**, *100*, 5303–5309.
37. Esteves, P. M.; Carneiro, J. W. d. M.; Cardoso, S. P.; Barbosa, A. G. H.; Laali, K. K.; Rasul, G.; Prakash, G. K. S.; Olah, G. A. *J. Am. Chem. Soc.* **2003**, *125*, 4836–4849.
38. de Queiroz, J. F.; Carneiro, J. W. d. M.; Sabino, A. A.; Sparrapan, R.; Eberlin, M. N.; Esteves, P. M. *J. Org. Chem*. **2006**, *71*, 6192–6203.
39. Shopsowitz, K.; Lelj, F.; MacLachlan, M. J. *J. Org. Chem*. **2011**, *76*, 1285–1294.
40. Ekstrand, Å, G. *Ber. Dtsch. Chem. Ges.* **1888,** *20*, 1353–361.
41. Mastalerz, M.; Sieste, S.; Cenić, M.; Oppel, I. M. *J. Org. Chem*. **2011**, *76*, 6389–6393.
42. Festel, G.; Eisenbach, C. D. *J. Prakt. Chem*. **1999**, *341*, 29–36.

3.3 Conclusions

Notre étude de la nitration de la naphtalènediamine **2e** n'a ultimement pas mené à un meilleur rendement pour la formation du produit **1b** et ainsi à une synthèse plus efficace du naphtobisthiadiazole **3**. Elle a cependant permis d'éclaircir plusieurs facettes du processus de nitration notamment en établissant avec certitude la régiosélectivité de la réaction et en illustrant l'impact de la nature des groupements protecteurs sur la position de nitration. De plus, les composés nitrés **1b** et **2k** peuvent être utilisés pour former les tétramines **1a** et **2a**, qui peuvent ensuite servir de précurseurs à d'autres composés d'intérêt dont différents types d'arènes azotés. Bien que les rendements des étapes de nitration soient peu élevés, ces voies synthétiques possèdent d'autres aspects pratiques comme des modes de purification simples, l'utilisation de réactifs accessibles et la formation d'intermédiaires stables et sécuritaires.

Chapitre 4.

Les dérivés quinonoïdes du triptycène : des solides cristallins et perméables pouvant participer à des réactions redox

Chapitre 4. Les dérivés quinonoïdes du triptycène : des solides cristallins et perméables pouvant participer à des réactions redox

L'évolution de notre compréhension de l'association moléculaire doit beaucoup aux quinones et aux hydroquinones. Le premier co-cristal jamais rapporté était constitué à parts égales de 1,4-benzoquinone et de 1,4-hydroquinone.[1] De plus, la compilation des études cristallographiques des quinones dans les années soixante-dix a permis d'établir que les liens C-H···O peuvent diriger l'association moléculaire.[2] Finalement, la nature des clathrates a été établie par la résolution de la structure du composé d'inclusion formé par la 1,4-hydroquinone et le sulfure d'hydrogène.[3] Ce sont cependant pour leurs propriétés rédox que les quinones ont été le plus étudiées et il est ainsi peu étonnant qu'elles soient à l'avant-garde des molécules organiques explorées pour former les électrodes des batteries organiques. Comme dans la plupart des matériaux électroniques organiques, les molécules utilisées dans ces dispositifs doivent être positionnées de façon à favoriser la percolation des charges. Dans les batteries organiques, les matériaux constituant les électrodes doivent de plus permettre la diffusion de l'électrolyte et cette organisation doit pouvoir être maintenue au fils des réactions rédox. Dans le but d'étudier des molécules qui pourraient à la fois participer à des réactions d'oxydoréduction et former des réseaux ouverts, nous avons choisi de préparer une série de composés dans laquelle des quinones et des hydroquinones sont intégrées au squelette du triptycène, car cette structure rigide et trigonale prévient fréquemment la formation d'empilements compacts. Nous avons ensuite examiné les organisations supramoléculaires adoptées par ces composés et nous sommes attardés à leurs propriétés rédox en solution et à l'état solide.

---

[1] Wöhler, F. *Liebigs Ann.* **1844**, *51*, 145–163.
[2] Bernstein, J.; Cohen, M. D.; Leiserowitz, L. The Structural Chemistry of Quinones. In *The Chemistry of Quinonoid Compounds*; Patai, S., Ed.; Patai's Chemistry of Functional Groups, John Wiley & Sons: New York, 1974; Vol. 1, pp 37–110.
[3] Palin, D. E.; Powell, H. M. *Nature* **1945**, *156*, 334

Triptycene 1,2-Quinones and Quinols. Permeable Crystalline Redox-Active Molecular Solids

Sophie Langis-Barsetti, Thierry Maris, and James D. Wuest

The Journal of Organic Chemistry, **2018**, *83*, 15426–15437

Abstract

Suitably designed quinones and quinols are promising modules for the programmed construction of ordered redox-active molecular solids. To explore this potential, we have synthesized compounds **1**–**4**, in which multiple 1,2-benzoquinone and 1,2-quinol units are attached to a triptycene core. The resulting molecules have topologies that disfavor efficient packing, and structural studies show that they crystallize to form open networks held together by characteristic attractive intermolecular forces, including O-H···O hydrogen bonds, C-H···O interactions, π-stacking, and dipolar interactions. Remarkably, the resulting solids are permeable and can undergo reversible redox reactions without loss of crystallinity. Our work may thereby help lead to the design of robust carbon-based batteries with electrodes derived from quinones, quinols, and other redox-active molecules abundantly produced by nature.

Introduction

Quinones and hydroquinones (known historically as quinols) play a uniquely important role in chemistry, in part because of their widespread occurrence in nature and their characteristic ability to engage in redox reactions.[2,3] In addition, these compounds take part in diverse intermolecular interactions and thereby show strongly associative behavior, allowing them to serve as useful modules in the programmed construction of ordered molecular materials.[4] In particular, the participation of these compounds in charge-transfer interactions and π-stacking has been used to produce assemblies with radicals[5,6] and with aromatic compounds.[7–9] Quinones and quinols can also form hydrogen-bonded networks with a variety of partners, including heterocycles,[8,10] phenols,[9,11–15] and other classes of compounds.[16–18] The first example of the phenomenon of co-crystallization, reported by Wöhler in 1844,[19] was produced by combining 1,4-benzoquinone and 1,4-hydroquinone in a 1:1 ratio. The resulting structure, known as quinhydrone, features an open network held together by a combination of hydrogen bonds and charge-transfer interactions.[20–22]

However, surprisingly little effort has been made so far to build on this promising foundation by designing more complex quinones and quinols for use in the modular construction of new molecular materials.[23–27] Moreover, the chemistry of 1,4-benzoquinones and hydroquinones has been explored much more extensively than that of the isomeric 1,2-benzoquinones and their reduced forms,[28] despite the potential of all of these compounds to engage in similar intermolecular interactions and to serve as modules in supramolecular construction.[29,30] In particular, the historic work of Wöhler provides a strong motivation for studying the co-crystallization of 1,2-benzoquinones with catechols, but little work of this type has been reported.[31–32] We have therefore undertaken a study to assess the utility of 1,2-benzoquinones and the corresponding catechols in the modular assembly of complex redox-active molecular structures held together by hydrogen bonds, charge-transfer interactions, and other forces. Of particular interest is the possibility of using such modules to make porous crystalline solids for use as electrodes in carbon-based batteries.[33–36]

In addition to being redox-active, 1,2-benzoquinones can also take part in Diels-Alder reactions, leading to the formation of dimers,[37,38] or by undergoing sequences of hydration, tautomerization, and autoxidation to give hydroxy-substituted 1,4-benzoquinones and other products.[39,40] To avoid these degradative pathways, we elected to study suitably substituted 1,2-benzoquinones. Moreover, to favor the formation of open networks created by modular assembly, we decided to attach multiple 1,2-benzoquinone and catechol units to molecular cores with shapes designed to inhibit efficient packing. In this way, we identified triptycene(trisquinone) **1** and reduced forms **2**–**4** as compounds of particular interest as modules for supramolecular construction. Triptycenes are attractive choices because their characteristic rigid trigonal topology interferes with close molecular packing and thereby favors the formation of open structures with significant volume available for the inclusion of guests.[41] Moreover, triptycenes **1**–**4** provide relatively simple symmetric structures that incorporate multiple 1,2-benzoquinone and catechol units, all freely exposed on the molecular periphery in a way that lets them form characteristic intermolecular interactions without significant interference. Simpler triptycenes with quinone and catechol moieties have been prepared by White and MacLachlan for use in constructing molecular assemblies,[42,43] but no structural analyses of the triptycenes themselves have been reported.

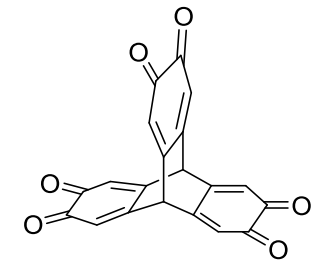

1

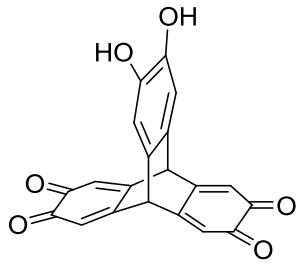

2

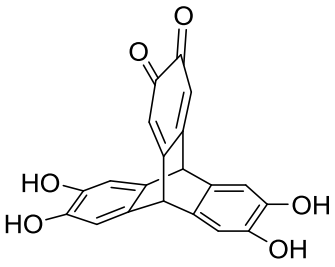

3

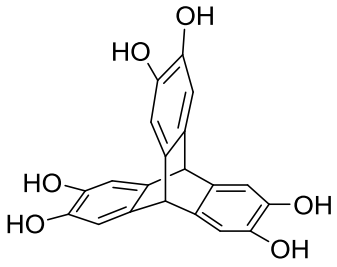

4

Results and Discussion

Syntheses of Triptycenes 1–4.

Ghanem et al. reported using BBr_3 to convert the known hexamethoxytriptycene **5** into triptycene(triscatechol) **4** (Scheme 1), but no characterization of the product was reported.[44] We prepared triscatechol **4** from precursor **5** by a modified procedure in which only three equivalents of BBr_3 were used, because the demethylation of *ortho* methoxy substituents is known to occur via cyclic borate intermediates.[45] In triptycene derivatives, controlled stepwise oxidation of the three aromatic rings is possible because electronic effects are communicated transannularly.[46,47] Notably, Chen and collaborators reported the progressive oxidation of an analogue of triscatechol **4** with nitric acid by varying the concentration of oxidant and the length of contact.[47] Nitric acid was also used by Han and coworkers to prepare an analogue of trisquinone **1**, but they reported only a partial characterization of the product.[48] To avoid possible side reactions involving nitration and ring opening,[49] and to better control the extent of oxidation, we decided to treat triscatechol **4** with other agents, and we achieved the synthesis of compounds **1**–**3** in a selective manner, as summarized in Scheme 1.

Scheme 1

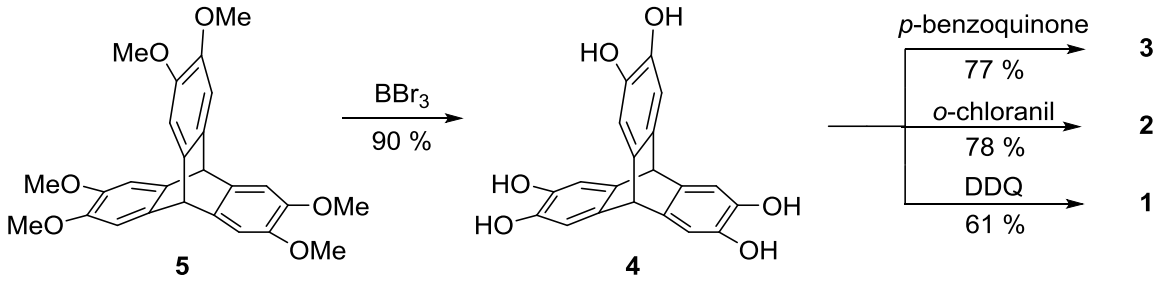

Although 1,4-benzoquinones are typically less powerful oxidants than their 1,2-benzoquinone counterparts,[50,51] each catechol unit in triscatechol **4** is substituted by an electron-donating tetrahydroxy-9,10-dihydroanthracenyl scaffold, and 1,4-benzoquinone can in fact be used to effect a single oxidation to give monoquinone **3** in 77% yield. Oxidation to produce bisquinone **2** occurred in 78% yield when triscatechol **4** was treated with tetrachloro-

1,2-benzoquinone (*o*-chloranil), whereas *p*-chloranil was ineffective. These reactions are highly selective, and only a single product of oxidation was observed in the crude mixtures. No significant amounts of starting material, intermediates, or over-oxidized compounds were observed, even after extended periods of time or in the presence of excess oxidant. Finally, 2,3-dichloro-5,6-dicyano-1,4-benzoquinone (DDQ) oxidized triscatechol **4** to give trisquinone **1** in 61% yield. Compounds **1**–**4** all proved to be stable in the solid state, although triscatechol **4** is slightly air-sensitive, and quinones **1**–**3** decomposed slowly in solution, especially when exposed to heat or light.[52] All characterizations were therefore performed using freshly prepared solutions, and crystallizations were carried out in the dark.

Absorption and Emission Properties of Triptycenes 1–4.

Absorption and emission spectra of compounds **1**–**4** are shown in Figure 1. All four compounds absorb near 290 nm, and the band shifts bathochromically from trisquinone **1** to triscatechol **4** as electron-donating catechol units are added to the triptycene core. Quinones **1**–**3** show additional absorption near 380 nm, leading to spectra that superimpose the characteristic features of catechol itself (λ_{max} = 277 nm) and those of 1,2-benzoquinone (λ_{max} = 273, 377 nm).[53,54] Monoquinone **3** also exhibits an important charge-transfer band around 480 nm, which is typical of triptycene donor-acceptor systems,[46,47,55] and bisquinone **2** shows a band that is similar but less intense. Emission spectra for compounds **2**–**4** reflect the relative positions of their absorption bands near 290 nm. Emission from trisquinone **1** is bathochromically shifted, but spectra of compound **1** were recorded in DMF to circumvent poor solubility in CH_3CN, and the observed shift may be solvent-induced.

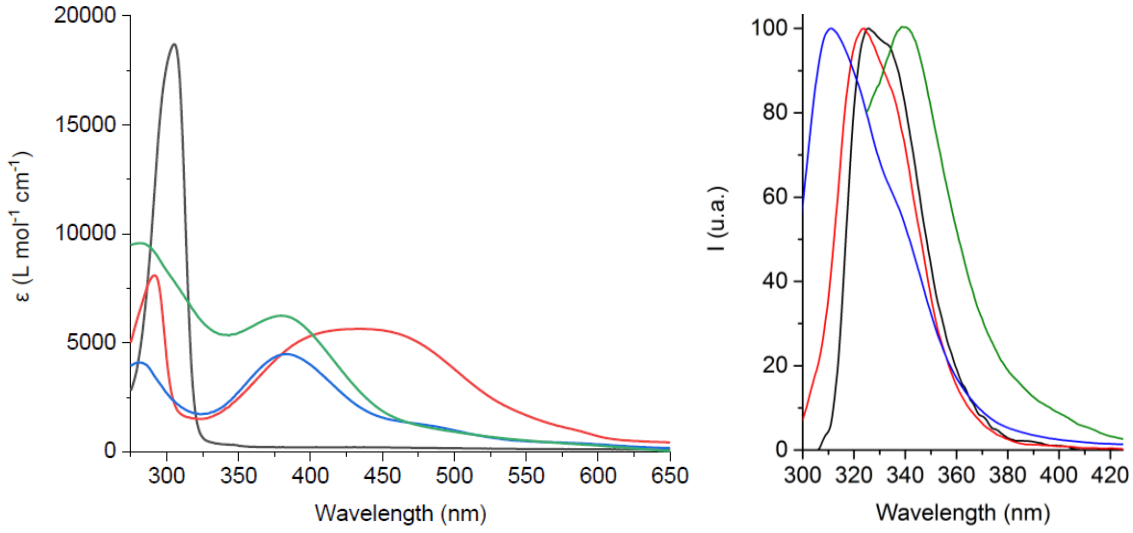

Figure 1. Absorption spectra (left) and normalized emission spectra (right) of solutions of triptycene(trisquinone) **1** (green), bisquinone **2** (blue), monoquinone **3** (red), and triscatechol **4** (black). Compound **1** was dissolved in DMF, and compounds **2**–**4** were dissolved in CH_3CN, with λ_{ex} = 280 nm for compounds **1** and **2**, λ_{ex} = 290 nm for compound **3**, and λ_{ex} = 300 nm for compound **4**.

Structure of Triptycene(trisquinone) 1.

Layering CH_3CN on a solution of trisquinone **1** in DMSO induced the formation of red crystals, which were found to belong to the hexagonal space group $P6_3$. Additional crystallographic information is summarized in Table 1, and a representation of the structure appears in Figure 2. Dipolar interactions between canted oxygen atoms and dienes (3.03 Å for the shortest C···O distance) underlie organization of molecules of compound **1** to form sheets (Figure 2a). Adjacent sheets are linked in an offset arrangement by C-H···O interactions (2.46–2.48 Å) involving oxygen atoms and hydrogen atoms of the quinone units (Figure 2b), thereby defining parallel hexagonal channels. The channels contain disordered molecules of CH_3CN, and 17% of the total volume of the crystals is accessible to guests.[56–58] Direct removal of the guests under reduced pressure leads to the loss of crystallinity, and we have not yet been able to prepare a guest-free crystalline solid constructed from trisquinone **1**.

Table 1. Crystallographic data for triptycenes **1**–**4**.

compound	**1 • CH_3CN**	**2 • 1.5 dioxane**	**3 • 3.5 dioxane**	**4**[a]
crystallization medium	DMSO/CH_3CN	dioxane/PhMe	dioxane/hexane	Me-THF
formula	$C_{20}H_8O_6$ • C_2H_3N	$C_{20}H_{10}O_6$ • 1.5 $C_4H_8O_2$	$C_{20}H_{12}O_6$ • 3.5 $C_4H_8O_2$	$C_{20}H_{14}O_6$
crystal system	hexagonal	monoclinic	monoclinic	hexagonal
space group	$P6_3$	$P2_1/c$	$I2/a$	$P\bar{6}2c$
a (Å)	15.7405(3)	17.2624(5)	24.0009(11)	13.3732(7)
b (Å)	15.7405(3)	8.6308(2)	8.5212(4)	13.3732(7)
c (Å)	11.9054(3)	16.1531(5)	31.560(2)	10.8212(7)
α (°)	90	90	90	90
β (°)	90	109.286(2)	93.151(2)	90
γ (°)	120	90	90	120
V (Å^3)	2554.53(12)	2271.57(11)	6444.8(6)	1676.0(2)
Z	6	4	8	2
ρ_{calcd} (g cm^{-3})	1.503	1.399	1.354	0.694[b]
T (K)	150	150	150	150
μ (mm^{-1})	0.599	0.574	0.560	0.276
$R_1, I > 2\sigma$	0.0968	0.0539	0.0811	0.0488
R_1, all data	0.2556	0.1298	0.2113	0.1623
$\omega R_2, I > 2\sigma$	0.1035	0.0654	0.1295	0.0493
ωR_2, all data	0.2804	0.1397	0.2532	0.1635
measured reflections	38684	29785	40908	37342
independent reflections	3924	4327	5526	1279
obs. reflections	3184	3615	3431	1248

[a] Guests not identified unambiguously by crystallography are omitted from the composition. [b] Calculated without contributions from guests.

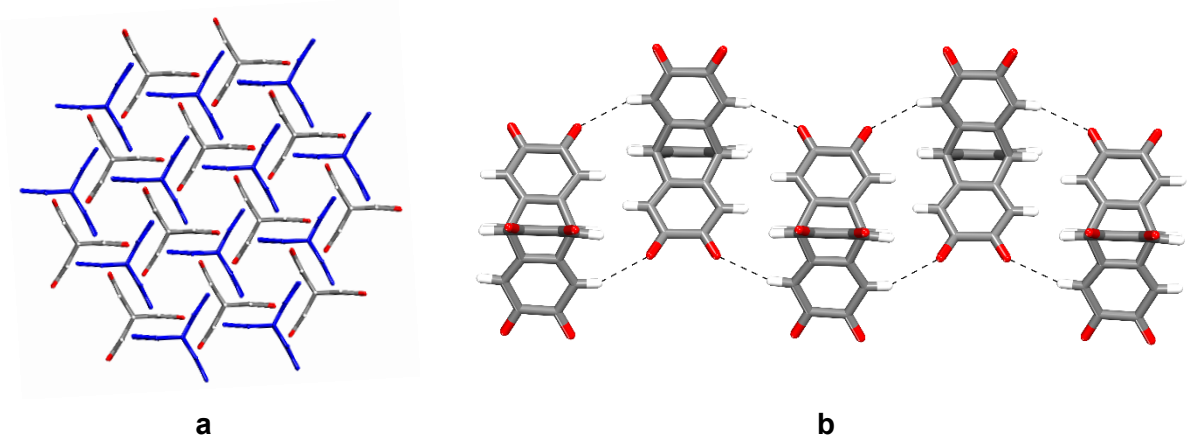

Figure 2. Representations of the structure of crystals of triptycene(trisquinone) **1** grown from DMSO/CH_3CN. (a) View down the *c*-axis showing two adjacent offset sheets, one with all molecules drawn in blue. The offset sheets define parallel hexagonal channels. (b) View down the *b*-axis showing molecules in five adjacent sheets and revealing how the sheets are connected by C-H···O interactions. The most significant interactions are represented by broken lines. Unless otherwise indicated, atoms of carbon are shown in gray, atoms of hydrogen in white, and atoms of oxygen in red. Included molecules of solvent are omitted.

Structure of Triptycene(bisquinone) 2.

The addition of toluene, chloroform, or ether to a saturated solution of bisquinone **2** in dioxane afforded rectangular dark orange crystals. Analysis by X-ray diffraction established that the crystals belonged to the monoclinic space group $P2_1/c$. Crystallographic parameters are provided in Table 1, and views of the structure appear in Figure 3. Molecules of compound **2** are connected by O-H···O hydrogen bonds (O···O distance = 2.735 Å) between quinone and catechol units to form undulating tapes. The tapes are further linked into sheets by C-H···O interactions (H···O distance = 2.50 Å) involving the bridgehead hydrogens and quinone moieties (Figure 3a). The sheets in turn are paired by additional C-H···O interactions (H···O distance = 2.38 Å) and by dipolar interactions between oxygen atoms and electron-deficient carbon atoms incorporated in the quinone units (2.90 Å for the shortest C···O distance). It is interesting to note that the quinone units involved as donors in these dipolar interactions are

planar, whereas the acceptor quinones are not, and their adjacent carbonyl groups form a dihedral angle of 17º. Additional cohesion within the sheets is provided by short C···O interactions (2.77 Å) involving the oxygen atoms of well-ordered molecules of included dioxane and electron-deficient carbon atoms in the distorted quinone units. Pairs of sheets are isolated from one another by layers of partly ordered molecules of dioxane (Figure 3b). In total, 42% of the volume of the crystal is accessible to guests.[56]

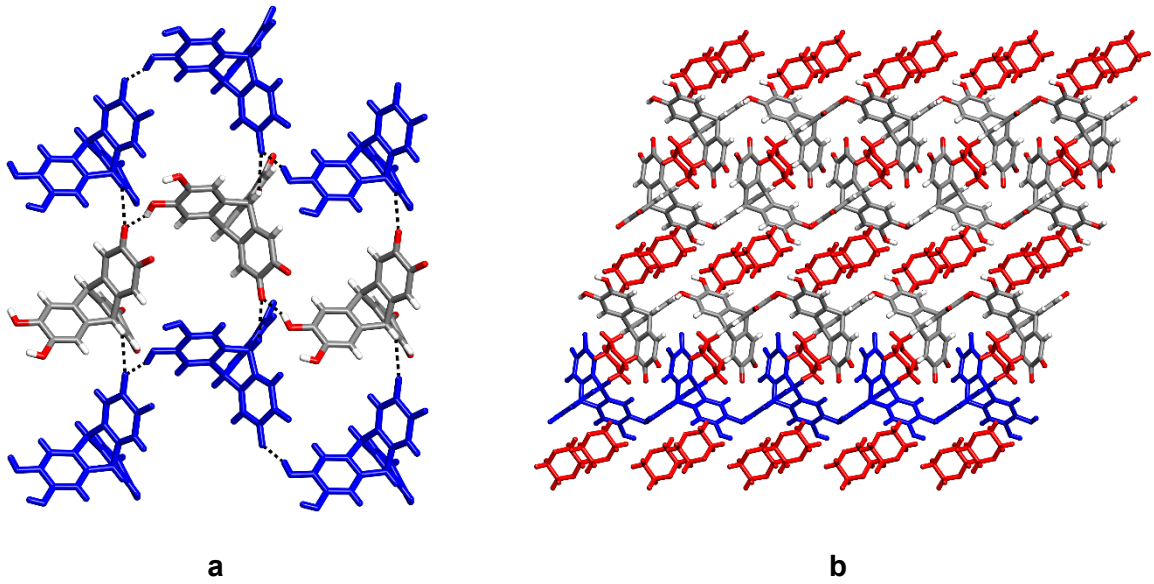

Figure 3. Representation of the structure of crystals of triptycene(bisquinone) **2** grown from dioxane/toluene. (a) View showing how undulating hydrogen-bonded tapes are further linked by C-H···O interactions to form sheets. Two individual tapes are highlighted in blue, and the most significant intermolecular interactions are represented by broken lines. (b) View down the *b*-axis showing how paired sheets are isolated from one another by layers of dioxane. One individual sheet is highlighted in blue, and all molecules of dioxane appear in red. Unless stated otherwise, atoms of carbon are shown in gray, atoms of hydrogen in white, and atoms of oxygen in red.

Crystallization of bisquinone **2** from a mixture of THF and hexane provided a pseudopolymorph in which the quinone units are less strikingly deformed.[59] As a result, the

torsion observed in the structure of crystals grown from dioxane may not be an inherent feature of compound **2** but may rather be a consequence of molecular packing or the result of multiple C···O interactions involving dioxane. However, distorted 1,2-benzoquinones have been noted by other researchers; for example, Fukin et al. observed a torsion angle of 34º between the carbonyl groups in 4,5-dimethoxy-3,6-di-*tert*-butyl-1,2-benzoquinone.[60]

Structure of Triptycene(monoquinone) 3.

Allowing vapors of hexane to diffuse into a solution of monoquinone **3** in dioxane induced the formation of dark red plates, which were found to belong to the monoclinic space group *I*2/*a*. Additional crystallographic data are presented in Table 1, and views of the structure are shown in Figure 4. Like bisquinone **2**, monoquinone **3** crystallizes to form a structure built from sheets separated by layers of included molecules of dioxane. Molecules of compound **3** form pairs held together by π-stacking of quinone units (centroids separated by 3.65 Å) and by C-H···π interactions involving hydrogen atoms of quinone units and the π-systems of catechol units (H···centroid distance = 2.38 Å). The pairs are further linked into sheets by multiple intermolecular O-H···O hydrogen bonds and C-H···O interactions (Figure 4). In particular, bifurcated O-H···O hydrogen bonds (O···O distances of 2.86 and 2.89 Å) are formed along the *b*-axis, with the two oxygen atoms of quinone units acting as a bidentate acceptor and an OH group of catechol units acting as donor. In addition, C-H···O interactions along the *b*-axis link oxygen atoms of quinone units with aromatic hydrogens and bridgehead hydrogens (H···O distances of 2.42 and 2.63 Å). Along the *a*-axis, intermolecular O-H···O hydrogen bonds between catechol units (O···O distance = 2.81 Å) and C-H···O interactions between catechol oxygen atoms and aromatic hydrogen atoms (H···O distance = 2.56 Å) reinforce the sheets. The structure is also strengthened by interactions of monoquinone **3** with oxygen atoms of included molecules of dioxane, which form O···H-O hydrogen bonds with catechol units (O···O distance = 2.76 Å), O···C interactions with quinone units (O···centroid distance = 2.78 Å), and various O···H-C interactions. Approximately 59% of the volume of the crystal is accessible to guests.[56]

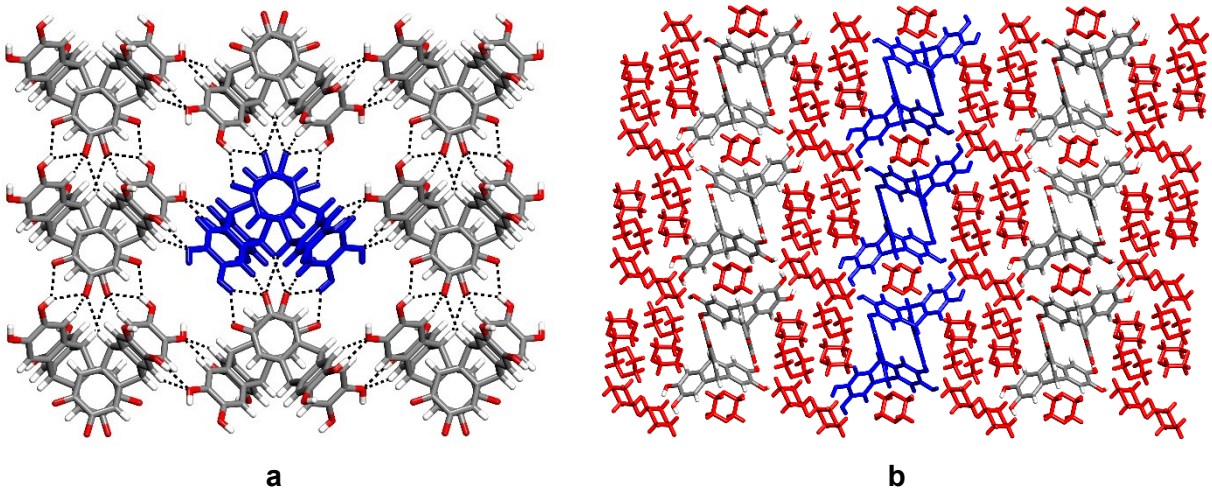

Figure 4. Representation of the structure of crystals of triptycene(monoquinone) **3** grown from dioxane/hexane.(a) View showing how π-stacked pairs are further associated by multiple O-H···O hydrogen bonds and C-H···O interactions to form sheets. An individual pair is highlighted in blue, and various intermolecular interactions are represented by broken lines. (b) View down the *b*-axis showing how sheets are isolated from one another by layers of dioxane. One individual sheet is highlighted in blue, and all molecules of dioxane appear in red. Unless stated otherwise, atoms of carbon are shown in gray, atoms of hydrogen in white, and atoms of oxygen in red.

Structure of Triptycene(triscatechol) 4.

Cooling a saturated solution of triscatechol **4** in methyltetrahydrofuran (Me-THF) yielded colorless needles that were found to belong to the hexagonal space group $P\bar{6}2c$. Other crystallographic data are provided in Table 1, and representations of the structure appear in Figure 5. Molecules of compound **4** can be considered to be packed in sheets in the *ab*-plane without forming any noteworthy intra-sheet interactions (Figure 5a), but adjacent sheets are linked along the *c*-axis by multiple O-H···O hydrogen bonds (O···O distances in the range 2.71–2.73 Å). In this way, each molecule of triscatechol **4** participates in a total of six intermolecular O-H···O hydrogen bonds.

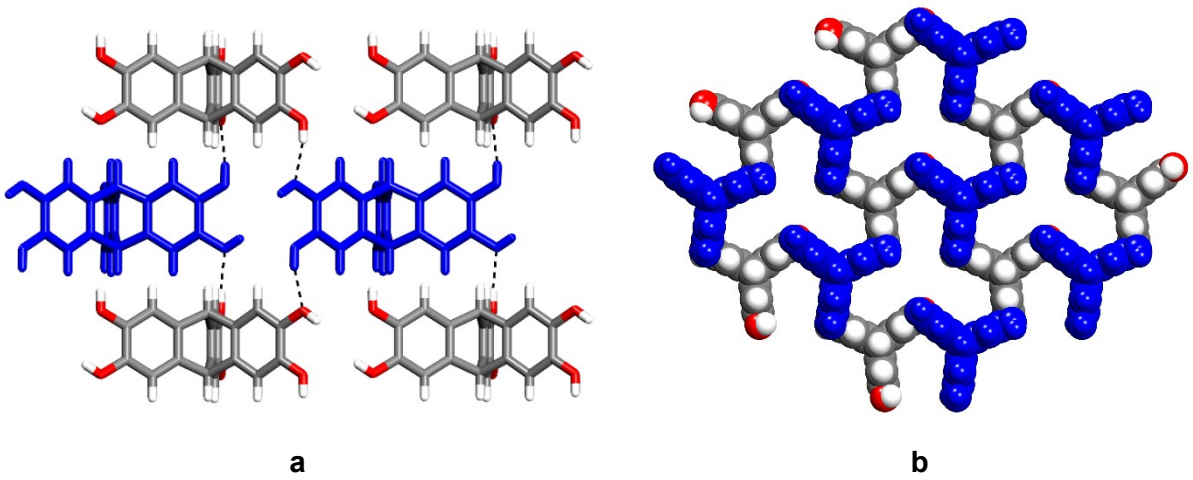

Figure 5. Representation of the structure of crystals of triptycene(triscatechol) **4** grown from Me-THF.(a) Side view of part of three offset sheets, showing how molecules in adjacent sheets are connected by O-H···O hydrogen bonds. Molecules in one sheet are highlighted in blue, and hydrogen bonds are represented by broken lines. (b) Space-filling view along the *c*-axis showing the presence of trilobate channels defined by two adjacent sheets, with one sheet highlighted in blue. Unless stated otherwise, atoms of carbon are shown in gray, atoms of hydrogen in white, and atoms of oxygen in red. Disordered molecules of included solvent are not shown.

Adjacent sheets are offset in a way that defines large trilobate channels (Figure 5b). The channels are filled with disordered molecules of solvent, and 63% of the total volume of the crystals is accessible to guests.[56] Larger fractions of guest-accessible volumes have been observed in other molecular crystals, particularly those of proteins.[61–63] However, the structure of triptycene(triscatechol) **4** is noteworthy because the molecule has a simple, open, symmetric topology and consists of only 26 non-hydrogen atoms. Our observations underscore the inherent difficulty of finding effective ways to pack molecules that have awkward topologies and must simultaneously take part in multiple directional interactions. Molecules of this type are typically programmed by their topologies and interactions to form open networks with significant volumes available for the inclusion of guests.

In addition to the structures described above in detail, pseudopolymorphs with similar molecular organization were also obtained by crystallizing triscatechol **4** from dioxane/hexane and by crystallizing bisquinone **2** and monoquinone **3** from THF/hexane.[59] The additional pseudopolymorphs differ primarily in the extent of inclusion of molecules of solvent. In particular, structures produced by crystallization from dioxane are more highly solvated than those obtained from THF, possibly because the extra atom of oxygen in dioxane provides an additional site of hydrogen bonding. In all cases, molecules of triptycenes **1**–**4** are linked by interactions typical of quinones and quinols, including O-H···O hydrogen bonds, C-H···O interactions, π-stacking, and dipolar interactions.[4,23] Crystals obtained under all conditions include molecules of solvent and typically have large guest-accessible volumes in the form of channels or layers. We attribute this behavior to the relatively rigid trigonal geometry of the triptycenyl core of compounds **1**–**4**, which cannot be packed efficiently in ways that allow the quinone and quinol units to engage in their preferred modes of association. As a result, normal patterns of crystallization are disrupted, and molecules of compounds **1**–**4** are forced to create open networks with significant fractions of volume occupied by guests. Moreover, because the compounds cannot crystallize in ways that simultaneously satisfy the demands of topology and directional intermolecular interactions, there is no overriding preference for a particular pattern of molecular organization, and the compounds have significant opportunities to crystallize in various pseudopolymorphic forms.

The prototypical 1:1 co-crystallization of 1,4-benzoquinone and hydroquinone to give quinhydrone led us to attempt co-crystallizations of different triptycenes **1**–**4.** Of special interest to us were co-crystallizations of pairs in which the numbers of complementary quinone and quinol units are properly balanced. Unfortunately, however, attempted co-crystallization of trisquinone **1** and triscatechol **4** was thwarted by disproportionation (Scheme 2), and pronounced differences in solubility prevented us from co-crystallizing compounds **2** and **3**. Disproportionation also occurred in mixtures containing compounds **1** and **3** or compounds **2** and **4** (Scheme 2).

Scheme 2

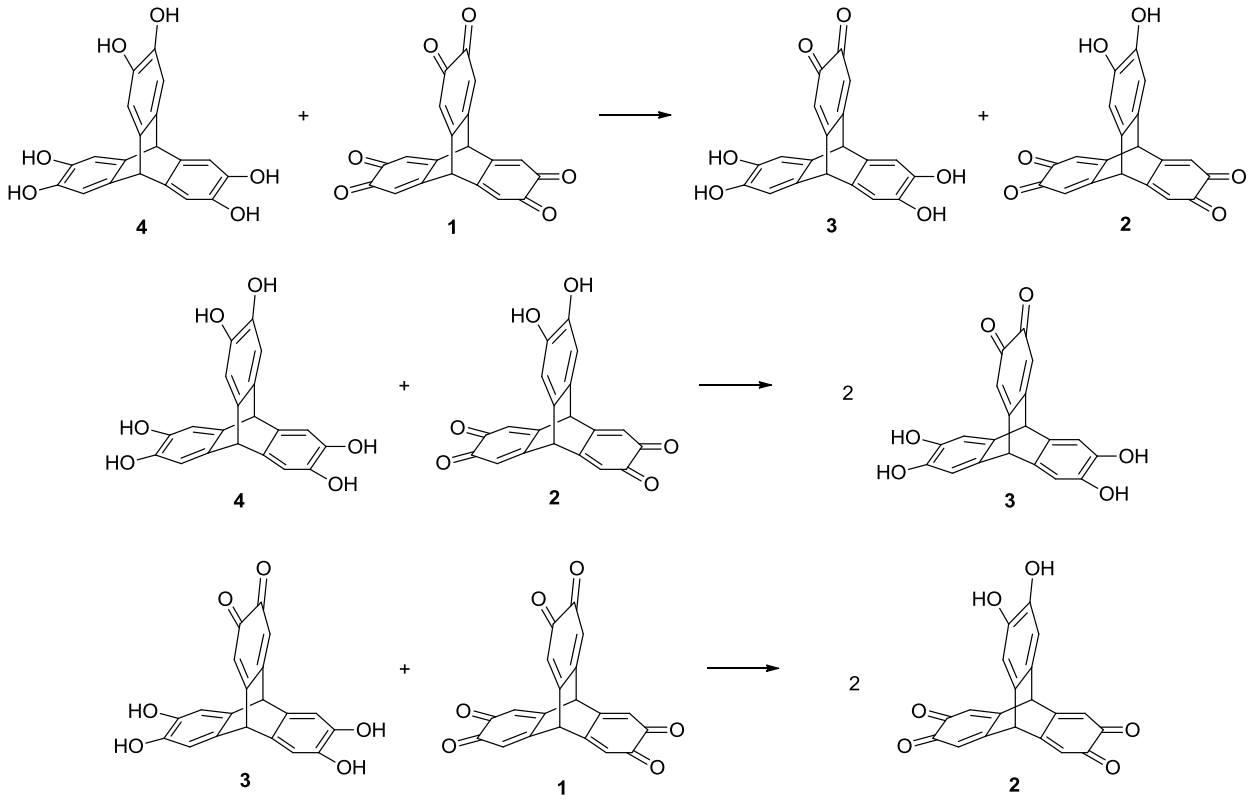

Redox Properties of Triptycenes 1–4 in Solution.

The highly selective syntheses of mono-, bis-, and trisquinones **1**–**3** by controlled oxidation prompted us to study the electrochemical behavior of the compounds in more detail. Cyclic voltammograms of solutions of trisquinone **1** and triscatechol **4** in DMF are presented in Figure 6. Redox potentials were assessed by square-wave voltammetry to allow the potential of non-reversible events to be measured more accurately. Square-wave voltammograms are shown in Figure 7, and redox potentials are summarized in Table 2, along with the properties of 1,2-benzoquinone and catechol as model compounds. The effect of transannular interactions on the redox properties of triptycene derivatives of 1,4-benzoquinone is well documented.[46,64–66] This behavior is mirrored in our redox data for related triptycene derivatives of 1,2-benzoquinone, and three distinct redox events were found for all compounds **1**–**4**.

Table 2. Redox potentials of triptycenes **1**–**4**.[a]

Compound	Reduction (V)	Oxidation (V)
1,2-Benzoquinone	-0.78 -0.69[b]	-
Trisquinone **1**	-1.05, -0.79, -0.58 -0.91,[b] -0.63,[b] -0.49[b]	-
Bisquinone **2**	-0.79,[b] -0.64[b]	0.48
Monoquinone **3**	-0.75[b]	0.35, 0.49
Triscatechol **4**	-	0.16, 0.35, 0.50
Catechol	-	0.49

[a]Measured by square-wave voltammetry in DMF solutions (~1 mM) containing tetrabutylammonium hexafluorophosphate (0.1 M) as supporting electrolyte. Potentials are reported with respect to the ferrocene/ferrocenium couple. [b] Values recorded in DMF solutions containing 1% MeCOOH.

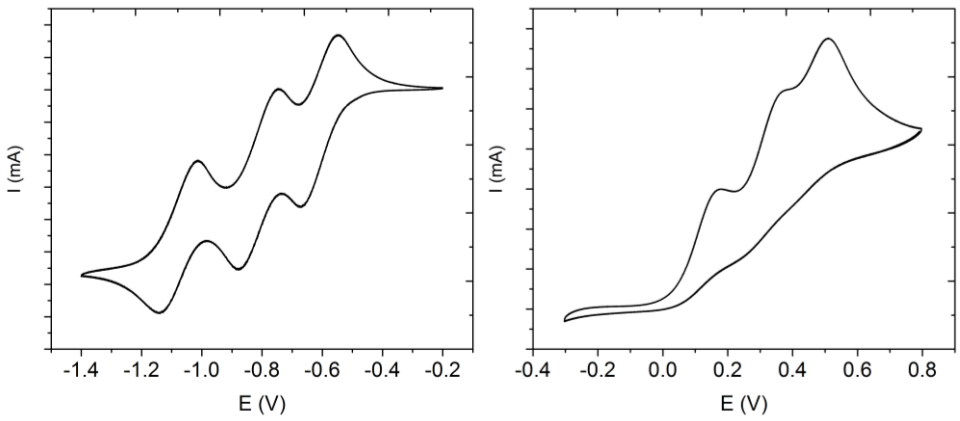

Figure 6. Cyclic voltammograms of solutions of triptycene(trisquinone) **1** (Figure 6a) and triptycene(triscatechol) **4** (Figure 6b) in DMF (~1 mM) containing tetrabutylammonium hexafluorophosphate (0.1 M) as supporting electrolyte. The voltammograms were recorded at a scan rate of 100 mV/s, and potentials are reported with respect to the ferrocene/ferrocenium couple.

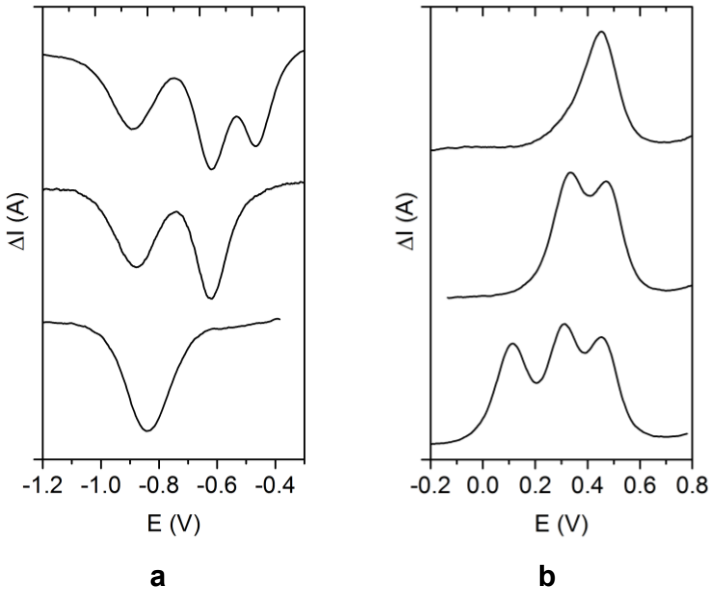

Figure 7. (a) Square-wave voltammograms showing the reduction waves of solutions of compounds **1**–**3** (top to bottom) in DMF containing 1% MeCOOH. (b) Square-wave voltammograms showing the oxidation waves of compounds **2**–**4** from top to bottom. All voltammograms were recorded in DMF solutions (~1 mM) containing tetrabutylammonium hexafluorophosphate (0.1 M) as supporting electrolyte. The voltammograms were recorded at a scan rate of 20–50 mV/s, and potentials are reported with respect to the ferrocene/ferrocenium couple.

Quinones typically undergo one-electron reduction in aprotic media.[50,51,67–69] Solutions of triptycene(trisquinone) **1** in DMF exhibit three reversible reduction waves corresponding to the formation and oxidation of semiquinone anions. Addition of MeCOOH shifts reduction to slightly more positive potentials, increases the intensity of the signals, and leads to a loss of reversibility. We attribute these changes to a transition to a two-electron process in which the resulting catecholate dianion is rapidly protonated by MeCOOH and is therefore no longer available for the return wave. The redox behavior of quinones and quinols is notoriously complex, however, and more detailed studies will be necessary to confirm the origin of our observations. In pure DMF, the reduction profiles of bisquinone **2** and monoquinone **3**

appeared to be complicated by the effect of intra- and intermolecular proton transfers, and the addition of MeCOOH simplifed the voltammograms. Under these conditions, an irreversible reduction wave was observed for each quinone unit at potentials similar to those needed to reduce trisquinone **1**. In all media examined, the first reductions of triptycenequinones **1** and **2** occurred at a lower potential than that observed for 1,2-benzoquinone.[53] This behavior presumably results from the electron-withdrawing effect of other quinone units in the compounds.

Cyclic voltammograms of compounds **2**–**4** in DMF show one, two, and three irreversible oxidation waves, respectively, and addition of MeCOOH had little effect on the oxidation profiles. The irreversibility of the transformations is most likely due to deprotonation of the highly unstable protonated quinones formed during the oxidation.[66–69] Oxidation potentials are consistent throughout the triptycene series, with equivalent oxidations taking place at nearly identical potentials for each compound. The substituted 9,10-dihydroanthracene scaffold can be seen to act as an electron-donating group, with all oxidation potentials being below those of catechol itself.

Redox Reactions of Triptycenes 1–4 as Crystalline Solids.

Our structural studies of compounds **1**–**4** establish that the triptycenyl topology, along with the characteristic ability of quinones and quinols to engage in multiple intermolecular interactions, gives rise to the formation of open networks composed of redox-active molecules. This special combination of features suggested that materials derived from compounds **1**–**4** might be able to serve as electrodes in carbon-based batteries and led us to study their redox behavior in the solid state. We found that exposure to vapors of H_2NNH_2 reduced quinones **1**–**3** to triscatechol **4**, both in solution and in the solid state. Correspondingly, vapors of HNO_3 (produced by 70% aqueous acid) could be used to oxidize solid samples of catechols **2**–**4.** Under these conditions, the redox reactions take place without the formation of significant amounts of by-products. Moreover, the progress of reactions can be assessed by visual inspection because the color of samples changes. For example, when dark purple crystals of the THF solvate of monoquinone **3** (Figure 8a) were exposed to vapors

of H_2NNH_2, triscatechol **4** was formed as a colorless solid that retained the morphology of the initial crystals (Figure 8b). No significant cracking was observed, and the resulting product was shown by polarized light microscopy to retain crystallinity. X-ray powder diffraction confirmed that the product of solid-state reduction is microcrystalline, and comparison with the characteristic pattern produced by crystals of monoquinone **3** established that the initial molecular organization is retained despite the change in composition (Figure 9). As a result, solid-state reduction under these conditions produces triscatechol **4** in crystalline form, with the molecules now arranged as they were in crystals of monoquinone **3**. Notably, the resulting structure of triscatechol **4** is not the same as that of crystals grown directly from solution. Analogous oxidations could be carried out by treating the Me-THF solvate of triscatechol **4** with HNO_3 to form monoquinone **3**. However, preventing the initial product from undergoing further oxidation was challenging, and the product was less highly crystalline.

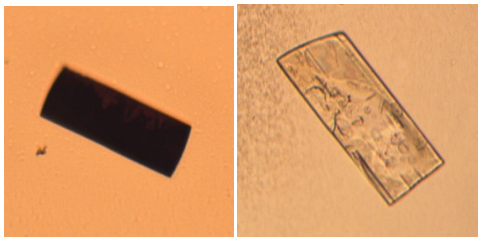

a **b**

Figure 8. Micrographs showing a dark purple crystal of monoquinone **3** grown from THF/hexane (Figure 8a) and a colorless crystal of triscatechol **4** resulting from solid-state reduction caused by exposure to vapors of H_2NNH_2 (Figure 8b).

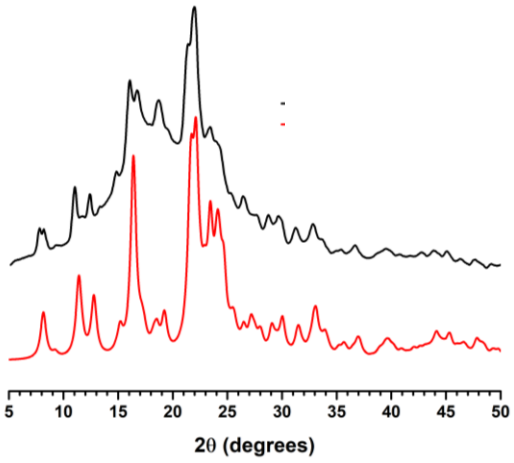

Figure 9. Comparison of the X-ray powder diffraction pattern (black trace) of a microcrystalline sample of triscatechol **4** (as produced by the solid-state reduction of crystals of monoquinone **3**) with the simulated pattern derived from the crystal structure of the THF solvate of compound **3** (red trace).

To understand how such processes occur, we examined the structure of the THF solvate of monoquinone **3** in detail and confirmed that it resembles the pseudopolymorphic solvate of dioxane (Figure 4). Again, π-stacking of quinone units creates pairs that are further linked into sheets by multiple intermolecular O-H···O hydrogen bonds and C-H···O interactions (Figure 10a). The sheets are connected by additional O-H···O hydrogen bonds, and molecules of THF are included between the layers (Figure 10b).

Topotactic processes in which crystals of small molecules react with added agents to give new compounds in crystalline form are very rare.[70–73] Moreover, we are not aware of any previous reports showing that transformations of this type can be carried out reversibly. Topotactic processes accompanied by changes in chemical composition cannot be dismissed as mere chemical curiosities; in fact, they promise to help solve key problems in emerging areas of technology. Of particular importance is the challenge of creating a new generation of green batteries that are cheap, rechargeable, and entirely derived from renewable carbon-based resources. In such devices, redox reactions must take place reversibly without substantially altering molecular organization in the electrodes.

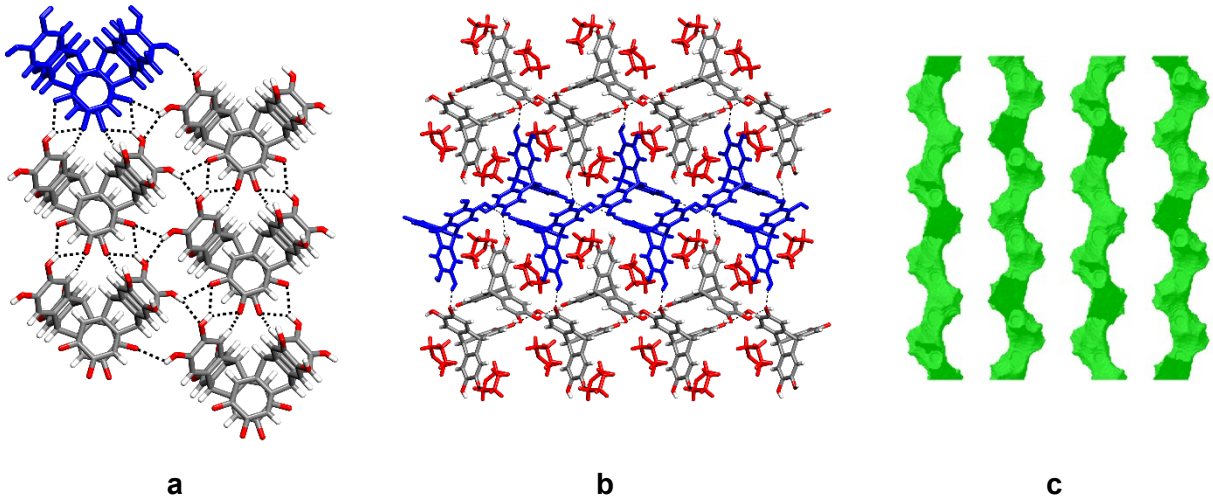

Figure 10. Representation of the structure of crystals of triptycene(monoquinone) **3** grown from THF/hexane. (a) View showing how π-stacked pairs are further joined by O-H···O hydrogen bonds and C-H···O interactions to form sheets. An individual π-stacked pair is highlighted in blue, and other significant intermolecular interactions are represented by broken lines. (b) View along the *c*-axis showing how sheets are connected by O-H···O hydrogen bonds and how molecules of THF are included between the layers. One individual sheet is highlighted in blue, and all molecules of THF appear in red. (c) View along the *a*-axis, showing layers in the *ac*-plane in which included molecules of THF occupy parallel channels (green). Unless otherwise stated, atoms of carbon are shown in gray, atoms of hydrogen in white, and atoms of oxygen in red.

Previous examples of topotactic processes occurring with changes in chemical composition suggest that molecular packing must normally be inefficient, so that external agents can penetrate the initial crystals and by-products can exit. Moreover, the crystals must be held together by intermolecular interactions that are strong enough to inhibit dissolution, disfavor unwanted molecular reorientation, and maintain the integrity of the crystals despite internal stresses generated by compositional and structural changes. In crystals of monoquinone **3**, the volume accessible to guests defines layers composed of parallel individual channels with the approximate dimensions 4 × 6 $Å^2$ (Figure 10c). These channels

include THF and are therefore wide enough to allow smaller molecules such as H_2NNH_2 and HNO_3 to diffuse throughout the crystal and to reduce or oxidize molecules of monoquinone **3**.

Exposing crystals of compound **3** to vapors of H_2NNH_2 for periods longer than those needed to effect complete conversion into triscatechol **4** caused fracturing along the longest axis (Figure S1). Indexing the crystal faces revealed that the fractures are aligned with the planes containing channels of THF. This finding is consistent with the hypothesis that H_2NNH_2 penetrates the crystals by entering the channels, replaces molecules of THF, and reduces host **3** to triscatechol **4**. These changes introduce stresses that are most easily relieved by fracturing the crystals along the planes of weakest bonding, which are those rich in included molecules of solvent.

Processes in which single crystals of simple molecular compounds are transformed by exposure to a suitable reagent into structurally related crystals of a different compound are highly uncommon. Moreover, no such transformations are known to be reversible or to involve interconversion of the constituent molecules by redox reactions. For these reasons, our results offer important evidence that it may be possible to engineer carbon-based rechargeable batteries analogous to the current generation of lithium-ion analogues, but with inorganic electrodes replaced by molecular solids that can undergo reversible redox processes without disruptive structural changes. Earlier studies have highlighted the potential of quinones and their reduced forms to serve as components in carbon-based batteries.[33–36,74,75] Our work takes a significant further step by showing how suitable quinones and quinols can be designed so that they form robust permeable crystals able to take part in reversible redox reactions without significant changes in molecular organization. In future work, we hope to reveal how related materials can be derived inexpensively from the large number of quinonoid compounds produced renewably by nature.

Conclusions

Suitably designed quinones and their reduced forms can serve as modules for the rational construction of ordered redox-active carbon-based solids. Our study of triptycenes **1**–**4** has revealed that attaching multiple quinone and quinol units to cores chosen to disfavor efficient packing can give rise to compounds that are programmed to form open networks held together by characteristic attractive intermolecular forces, including O-H···O hydrogen bonds, C-H···O interactions, π-stacking, and dipolar interactions. Remarkably, the resulting materials can undergo reversible redox reactions without losing crystallinity. In this way, our work helps define a path leading to the design of robust rechargeable carbon-based batteries incorporating electrodes derived from quinones, quinols, and other redox-active molecules that are abundantly produced by nature.

Experimental Section

Anhydrous oxygen-free solvents were obtained by passage through columns packed with activated alumina and supported Cu catalyst (Glass Contour, Irvine, CA). Reagents and all other solvents were purchased from commercial sources and used without further purification unless otherwise indicated. 1,2-Benzoquinone[76] and hexamethoxytriptycene **5**[44] were synthesized according to published procedures. A full characterization of known compound **4** is presented below to provide data not included in earlier publications.

NMR spectra were recorded at 20 °C, using a spectrometer operating at 400 MHz for ^{1}H NMR spectra and at 100 MHz for ^{13}C NMR spectra. Chemical shifts are reported in parts per million relative to tetramethylsilane, with the signal of residual undeuterated solvent used as an internal standard. Cyclic voltammograms were obtained using solutions in dry N_2-sparged dimethylformamide (DMF) or in DMF containing 1% acetic acid, with tetrabutylammonium hexafluorophosphate (TBAP) as the supporting electrolyte (0.1 M). The

working electrode was a glassy carbon electrode, the counter-electrode was a Pt wire, and the pseudo-reference electrode was an Ag wire. The concentration of the compounds examined was ~1 mM, and ferrocene/ferrocenium was used as an internal standard.

2,3,6,7,14,15-Hexahydroxytriptycene (4). Compound **4** was synthesized by modifying the method reported by Ghanem et al.[44] A solution of 2,3,6,7,14,15-hexamethoxytriptycene (**5**; 2.01 g, 4.63 mmol) in dichloromethane (100 mL) was stirred at 0 °C under N_2 and treated dropwise with a solution of BBr_3 (1.0 M, 16 mL, 16 mmol) in dichloromethane. The mixture was stirred at 25 °C for 18 h, treated with water, and stirred for 15 min. The resulting precipitate was separated by filtration, washed with water, and dried under vacuum to give 2,3,6,7,14,15-hexahydroxytriptycene (**4**; 1.47 g, 4.20 mmol, 91%) as a nearly colorless solid. Further purification could be achieved by crystallization from hot dioxane. Single crystals for analysis by X-ray diffraction were grown by adding hexane to a saturated solution of compound **4** in dioxane or by cooling a saturated solution in Me-THF: mp > 300 °C; FTIR (ATR) 3542, 3462, 3278, 3191, 1610, 1485, 1449 cm^{-1}; ^1H NMR (400 MHz, DMSO-d_6) δ 8.40 (s, 6H), 6.71 (s, 6H), 4.88 (s, 2H); $^{13}C\{^1H\}$ NMR (100 MHz, DMSO-d_6) δ 141.0, 137..8, 111.6, 51.0; UV-Vis (CH_3CN) λ_{max} (ε) 305 (18,700); Emission (THF, λ_{ex} 300 nm) λ_{em} 326 nm; SWV (DMF, NBu_4PF_6) $E_{1/2}$ 0.16, 0.35, 0.50 V (Fc/Fc^+); HRMS (APCI-TOF) *m/z* $[M - H]^-$ calcd for $C_{20}H_{13}O_6$ 349.0712, found 349.0714.

6,7,14,15-Tetrahydroxy-9,10-dihydro-9,10-[1,2]benzenoanthracene-2,3-dione (3). 1,4-Benzoquinone (0.232 g, 2.15 mmol) was added to a suspension of 2,3,6,7,14,15-hexahydroxytriptycene (**4**; 0.509 g, 1.45 mmol) in THF (10 mL). The mixture was stirred at 25 °C for 20 h, and volatiles were then removed by evaporation under reduced pressure. The residue was triturated with water, and the resulting dark purple solid was separated by filtration and dried under vacuum to afford 6,7,14,15-tetrahydroxy-9,10-dihydro-9,10-[1,2]benzenoanthracene-2,3-dione (**3**; 0.385 g, 1.11 mmol, 77%). Further purification could be achieved by crystallization induced by allowing hexane to diffuse slowly into a saturated solution of compound 3 in THF in the dark: mp > 300 °C; FTIR (ATR) 3397, 3254, 3129, 3054, 2956, 2808, 1673, 1639, 1617, 1590, 1572, 1499, 1460 cm^{-1};^1H NMR (400 MHz,

DMSO-d_6) δ 9.01 (s, 4H), 6.81 (s, 4H), 6.24 (s, 2H), 5.03 (s, 2H); $^{13}C\{^1H\}$ NMR (100 MHz, DMSO-d_6) δ 180.3, 153.4, 144.8, 130.3, 119.6, 111.9, 48.9; UV-Vis (CH_3CN) λ_{max} (ε) 291 (8090), 435 (5640); Emission (CH_3CN, λ_{ex} 290 nm) λ_{em} 324 nm; SWV (DMF/AcOH 1%, NBu_4PF_6) $E_{1/2}$ -0.75, 0.35, 0.49 V (Fc/Fc^+); HRMS (APPI-TOF) *m/z* $[M + H]^+$ calcd for $C_{20}H_{13}O_6$ 349.0712, found 349.0711.

14,15-Dihydroxy-9,10-dihydro-9,10-[1,2]benzenoanthracene-2,3,6,7-tetraone (2). *o*-Chloranil (0.352 g, 1.43 mmol) was added to a suspension of 2,3,6,7,14,15-hexahydroxytriptycene (**4**; 0.198 g, 0.565 mmol) in anhydrous oxygen-free dioxane (10 mL). The mixture was stirred at 25 °C for 20 h, and volatiles were then removed by evaporation under reduced pressure. The residue was then triturated with dichloromethane, and the resulting dark orange solid was separated by filtration, washed with dichloromethane, and dried under vacuum to afford 14,15-dihydroxy-9,10-dihydro-9,10-[1,2]benzenoanthracene-2,3,6,7-tetraone (**2**; 0.155 g, 0.448 mmol, 79%). Further purification could be achieved by crystallization induced by allowing toluene, ether, or chloroform to diffuse slowly into a saturated solution of compound **2** in dioxane in the dark: mp > 300 °C; FTIR (ATR) 3371, 3079, 2954, 1682, 1658, 1645, 1595, 1576, 1507, 1454 cm^{-1}; ^1H NMR (400 MHz, DMSO-d_6) δ 9.36 (s, 2H), 6.84 (s, 2H), 6.42 (s, 4H), 5.04 (s, 2H); $^{13}C\{^1H\}$ NMR (100 MHz, DMSO-d_6) δ 179.3, 150.1, 146.8, 126.0, 122.9, 112.4, 48.3; UV-Vis (CH_3CN) λ_{max} (ε) 280 (4100), 383 (4480), 480 (1230); Emission (CH_3CN, λ_{ex} 280 nm) λ_{em} 311 nm; SWV (DMF/AcOH 1%, NBu_4PF_6) $E_{1/2}$ -0.79, -0.64, 0.48 V (Fc/Fc^+); HRMS (ESI-TOF) *m/z* $[M - H]^-$ calcd for $C_{20}H_9O_6$ 345.0399, found 345.0390.

9,10-Dihydro-9,10-[1,2]benzenoanthracene-2,3,6,7,14,15-hexaone (1). 2,3-Dichloro-5,6-dicyano-1,4-benzoquinone (1.55 g, 6.83 mmol) was added to a suspension of 2,3,6,7,14,15-hexahydroxytriptycene (**4**; 0.198 g, 0.565 mmol) in anhydrous oxygen-free THF (15 mL) under an atmosphere of N_2. The mixture was stirred at 25 °C for 20 h, and the resulting suspension was filtered. The filtrate was washed with THF and dried under vacuum to afford 9,10-dihydro-9,10-[1,2]benzenoanthracene-2,3,6,7,14,15-hexaone as a yellow solid (**1**; 0.119

g, 0.346 mmol, 61%). Further purification to afford red crystals of compound **1** could be achieved by allowing CH_3CN to diffuse slowly into a saturated solution in DMSO: mp > 300 °C; FTIR (ATR) 3060, 3078, 2954, 1682, 1658, 1645, 1595, 1576, 1507, 1454 cm^{-1}; ^1H NMR (400 MHz, DMSO-d_6) δ 6.57 (s, 6H), 5.04 (s, 2H); $^{13}C\{^1H\}$ NMR (100 MHz, DMSO-d_6) δ 178.8, 147.1, 125.5, 48.1; UV-Vis (DMF) λ_{max} (ε) 281 (10,100), 380 (6740); Emission (DMF, λ_{ex} 280 nm) λ_{em} 339 nm; SWV (DMF, NBu_4PF_6) $E_{1/2}$ -1.03, -0.79, -0.60 V (Fc/Fc^+); HRMS (APCI-TOF) *m/z* $[M]^-$ calcd for $C_{20}H_8O_6$, 344.0321, found 344.0317.

Solid-State Redox Reactions. Freshly prepared dark purple crystals of monoquinone **3**, grown from solutions in THF, were placed in a 4 mL vial, which was then transferred to a 20 mL vial containing 1 mL of hydrazine hydrate. The larger vial was then sealed with a cap, and after about 15 min vapors of hydrazine had reached the crystals and begun to react. As soon as the solid sample had turned completely colorless, the small vial was removed, and the crystals were placed on the stage of a polarized-light microscope. As shown in the Supporting Information, the crystals retained their initial morphology, displayed birefringence, and yielded a well-resolved X-ray powder diffraction pattern. However, individual crystals were not sufficiently ordered to allow their structure to be determined by single-crystal X-ray diffraction. All other solid-state redox experiments were carried in a similar way, and the identity of the products was confirmed by recording their NMR spectra, which matched those of authentic samples.

Notes

The authors declare no competing financial interest.

Supporting Information

The Supporting Information is available free of charge on the ACS Publications website at DOI: 10.1021/acs.joc.8b02706. Description of representative solid-state redox experiments,

^{1}H and ^{13}C NMR spectra of triptycenes **1**−**4**, voltammograms, absorption/emission spectra, and additional crystallographic details, including ORTEP drawings (PDF). Structural data for compounds **1**−**4** (CIF).

Acknowledgments

We are grateful to the Natural Sciences and Engineering Research Council of Canada, the Ministère de l'Éducation du Québec , the Canada Foundation for Innovation , the Canada Research Chairs Program, and the Université de Montréal for financial support.

References

1. Fellow of the Fonds de recherche du Québec–Nature et technologies (FRQNT).
2. *The Chemistry of Quinonoid Compounds*; Patai, S., Ed.; Patai's Chemistry of Functional Groups, John Wiley & Sons: New York, 1974.
3. *The Chemistry of the Quinonoid Compounds*; Patai, S.; Rappoport, Z., Eds.; Patai's Chemistry of Functional Groups, John Wiley & Sons: New York, 1988.
4. Bernstein, J.; Cohen, M. D.; Leiserowitz, L. The Structural Chemistry of Quinones. In *The Chemistry of Quinonoid Compounds*; Patai, S., Ed.; Patai's Chemistry of Functional Groups, John Wiley & Sons: New York, 1974; Vol. 1, pp 37–110.
5. Nobusawa, M.; Akutsu, H.; Yamada, J.-i.; Nakatsuji, S. *Chem. Lett.* **2008**, *37*, 788–789.
6. Nakatsuji, S.; Nobusawa, M.; Suzuki, H.; Akutsu, H.; Yamada, J.-i. *J. Org. Chem*. **2009**, *74*, 9345–9350.
7. Klärner, F. G.; Burkert, U.; Kamieth, M.; Boese, R.; Benet-Buchholz, J. *Chem. Eur. J.* **1999**, *5*, 1700–1707.
8. Aoyama, Y.; Endo, K.; Anzai, T.; Yamaguchi, Y.; Sawaki, T.; Kobayashi, K.; Kanehisa, N.; Hashimoto, H.; Kai, Y.; Masuda, H. *J. Am. Chem. Soc.* **1996**, *118,* 5562–5571.
9. Ukegawa, T.; Kinuta, T.; Sato, T.; Tajima, N.; Kuroda, R.; Matsubara, Y.; Imai, Y. *Tetrahedron* **2010**, *66*, 8756–8762.
10. Murata, T.; Morita, Y.; Yakiyama, Y.; Fukui, K.; Yamochi, H.; Saito, G.; Nakasuji, K. *J. Am. Chem. Soc.* **2007**, *129*, 10837–10846.
11. Arimura, T.; Nishioka, T.; Ide, S.; Suga, Y.; Sugihara, H.; Murata, S.; Tachiya, M. *J. Photochem. Photobiol. A* **2001,** *145*, 123–128.
12. Reddy, D. S.; Dewa, T.; Endo, K.; Aoyama, Y. *Angew. Chem. Int. Ed.* **2000**, *39*, 4266–4268.
13. Imai, Y.; Tajima, N.; Sato, T.; Kuroda, R. *Chirality* **2002**, *14*, 604–609.
14. Imai, Y.; Kamon, K.; Kinuta, T.; Tajima, N.; Sato, T.; Kuroda, R.; Matsubara, Y. *Cryst. Growth Des.* **2008**, *8*, 3493–3496.
15. Toda, F.; Senzaki, M.; Kuroda, R. *Chem. Commun.* **2002**, 1788–1789.

16. Zhang, C.; Yang, Z.; Zhou, X.; Zhang, C.; Ma, Y.; Xu, J.; Zhang, Q.; Nie, F.; Li, H. *Cryst. Growth Des.* **2014**, *14*, 3923−3928.
17. Fleischman, S. G.; Kuduva, S. S.; McMahon, J. A.; Moulton, B.; Bailey Walsh, R. D.; Rodríguez-Hornedo, N.; Zaworotko, M. J. *Cryst. Growth Des.* **2003**, *3*, 909–919.
18. Hunter, C. A.; Shannon, R. J. *Chem. Commun.* **1996**, 1361–1362.
19. Wöhler, F. *Liebigs Ann.* **1844**, *51*, 145–163.
20. Matsuda, H.; Osaki, K.; Nitta, I. *Bull. Chem. Soc. Jpn.* **1958**, *31*, 611–620.
21. Sakurai, T. *Acta Crystallogr.* **1965**, *19*, 320–330.
22. Sakurai, T. *Acta Crystallogr.* **1968**, *B24*, 403–412.
23. Patil, A. O.; Pennington, W. T.; Desiraju, G. R.; Curtin, D. Y.; Paul, I. C. *Mol. Cryst. Liq. Cryst.* **1986**, *134*, 279–304.
24. Joshi, B. S.; Rho, T.; Rinaldi, P. L.; Liu, W.; Wagler, T. A.; Newton, M. G.; Lee, D.; Pelletier, S. W. *J. Chem. Crystallogr.* **1997***, 27,* 553–559.
25. Yamamura, K.; Kawashima, T.; Eda, K.; Tajima, F.; Hashimoto, M. *J. Mol. Struct.* **2005**, *737*, 1–6.
26. Hashimoto, M.; Takagi, H.; Yamamura, K. *Tetrahedron Lett.* **1999**, *40*, 6037–6040.
27. Nakasuji, K.; Sugiura, K.; Kitagawa, T.; Toyoda, J.; Okamoto, H.; Okaniwa, K.; Mitani, T.; Yamamoto, H.; Murata, I.; Kawamoto, A.; Tanaka, J. *J. Am. Chem. Soc.* **1991,** *113,* 1862–1864.
28. Griffith, W. P. *Transition Met. Chem.* **1993**, *18*, 250–256.
29. Fishwick, C. W. G.; Jones, D. W. *ortho*-Quinonoid compounds. In *The Chemistry of the Quinonoid Compounds*; Patai, S.; Rappoport, Z., Eds.; Patai's Chemistry of Functional Groups, John Wiley & Sons, Inc.: New York, 1988; Vol. 2, pp 403–453.
30. Nair, V.; Menon, R. S.; Biju, A. T.; Abhilash, K. G. *Chem. Soc. Rev*. **2012**, *41*, 1050–1059.
31. Calderazzo, F.; Forte, C.; Marchetti, F.; Pampaloni, G.; Pieretti, L. *Helv. Chim. Acta* **2004**, *87*, 781–789.
32. Satha, P.; Purohit, C. S. *Proc. Natl. Acad. Sci., India, Sect. A Phys. Sci.* **2014**, *84*, 221–225.

33. Wu, Y.; Zeng, R.; Nan, J.; Shu, D.; Qiu, Y.; Chou, S.-L. *Adv. Energy Mater*. **2017**, *7*, 1700278.

34. Zhao, Q.; Zhu, Z.; Chen, J. *Adv. Mater*. **2017**, *29*, 1607007.

35. Miroshnikov, M.; Divya, K. P.; Babu, G.; Meiyazhagan, A.; Arava, L. M. R.; Ajayan, P. M.; John, G. *J. Mater. Chem. A* **2016**, *4*, 12370–12386.

36. Häupler, B.; Wild, A.; Schubert, U. S. *Adv. Energy Mater*. **2015**, *5*, 1402034.

37. Harley-Mason, J.; Laird, A. H. *J. Chem. Soc.* **1958**, 1718–1719.

38. Patchett, A. A.; Witkop, B. *J. Org. Chem.* **1957**, *22,* 1477–1484.

39. Adler, E.; Andersson, G. *Liebigs Ann. Chem.* **1976,** 1435–1447.

40. Mandal, S.; Lee, Y.; Purdy, M. M.; Sayre, L. M. *J. Am. Chem. Soc.* **2000,** *122,* 3574–3584.

41. Chong, J. H.; MacLachlan, M. J. *Chem. Soc. Rev.* **2009**, *38*, 3301–3315.

42. White, N. G.; MacLachlan, M. J. *Chem. Sci.* **2015**, *6*, 6245–6249.

43. White, N. G.; MacLachlan, M. J. *Cryst. Growth Des.* **2015**, *15*, 5629−5636.

44. Ghanem, B. S.; Hashem, M.; Harris, K. D. M.; Msayib, K. J.; Xu, M.; Budd, P. M.; Chaukura, N.; Book, D.; Tedds, S.; Walton, A.; McKeown, N. B. *Macromolecules* **2010**, *43*, 5287–5294.

45. McOmie, J. F. W.; Watts, M. L.; West, D. E. *Tetrahedron* **1968**, *24*, 2289–2292.

46. Iwamura, H.; Makino, K. *J. Chem. Soc., Chem. Commun.* **1978**, 720–721.

47. Zhao, J.-M; Lu, H.-Y.; Cao, J.; Jiang, Y.; Chen, C.-F. *Tetrahedron Lett.* **2009**, *50*, 219–222.

48. Zhao, Y.-C.; Cheng, Q.-Y.; Zhou, D.; Wang, T.; Han, B.-H. *J. Mater. Chem.* **2012**, *22*, 11509–11514.

49. Baumgärtner, K.; Rominger, F.; Mastalerz, M. *J. Org. Chem*. **2015**, *80*, 8881−8886.

50. Chambers, J. Q. Electrochemistry of Quinones. In *The Chemistry of Quinonoid Compounds*; Patai, S., Ed.; Patai's Chemistry of Functional Groups, John Wiley & Sons: New York, 1974; Vol. 1, pp 737–791.

51. Chambers, J. Q. Electrochemistry of Quinones. In *The Chemistry of the Quinonoid Compounds*; Patai, S.; Rappoport, Z., Eds.; Patai's Chemistry of Functional Groups, John Wiley & Sons: New York, 1988; Vol. 2, pp 719–757.

52. Shurygina, M. P.; Kurskii, Yu. A.; Druzhkov, N. O.; Chesnokov, S. A.; Abakumov, G. A. *High Energ. Chem*. **2010**, *44,* 234–238.

53. Albarran, G.; Boggess, W.; Rassolov, V.; Schuler, R. H. *J. Phys. Chem. A* **2010,** *114,* 7470–7478.

54. Voltammograms and absorption spectra of 1,2-benzoquinone and catechol are provided in the Supporting Information for comparison.

55. Murata, I. *Pure Appl. Chem.* **1983**, *55*, 323–330.

56. The percentage of volume accessible to guests was estimated by the PLATON program (References 57 and 58). PLATON calculates the accessible volume by allowing a spherical probe of variable radius to roll over the van der Waals surface of the network. PLATON uses a default value of 1.20 Å for the radius of the probe, which is an appropriate model for small guests such as water. The van der Waals radii used to define surfaces for these calculations are C: 1.70 Å, H: 1.20 Å, and O: 1.52 Å. The percentage of accessible volume is given by $100V_g/V$, where V is the volume of the unit cell and V_g is the guest-accessible volume as calculated by PLATON.

57. Spek, A. L. *PLATON, A Multipurpose Crystallographic Tool*; Utrecht University: Utrecht, The Netherlands, 2001.

58. van der Sluis, P.; Spek, A. L. *Acta Crystallogr.* **1990**, *A46*, 194–201.

59. Crystallographic data for pseudopolymorphs of compounds **2**, **3**, and **4** are presented in the Supporting Information.

60. Fukin, G. K.; Cherkasov, A. V.; Shurygina, M. P.; Druzhkov, N. O.; Kuropatov, V. A.; Chesnokov, S. A.; Abakumov, G. A. *Struct. Chem*. **2010**, *21*, 607–611.

61. Pulido, A.; Chen, L.; Kaczorowski, T.; Holden, D.; Little, M. A.; Chong, S. Y.; Slater, B. J.; McMahon, D. P.; Bonillo, B.; Stackhouse, C. J.; Stephenson, A.; Kane, C. M.; Clowes, R.; Hasell, T.; Cooper, A. I.; Day, G. M. *Nature* **2017**, *543*, 657–664.

62. Mastalerz, M.; Oppel, I. M. *Angew. Chem. Int. Ed.* **2012**, *51*, 5252–5255.

63. Fournier, J.-H.; Maris, T.; Wuest, J. D. *J. Org. Chem.* **2004**, *69*, 1762−1775.

64. Talipov, M. R.; Navale, T. S.; Rathore, R. *Angew. Chem. Int. Ed.* **2015**, *54*, 14468–14472.

65. Yamamura, K.; Miyake, H.; Himeno, S.; Inagaki, S.; Nakasuji, K.; Murata, I. *Chem. Lett.* **1988**, *17*, 1819–1822.

66. Russell, G. A.; Suleman, N. K.; Iwamura, H.; Webster, O. W. *J. Am. Chem. Soc*. **1981,** *103*, 1560–1561.

67. Gupta, N.; Linschitz, H. *J. Am. Chem. Soc.* **1997**, *119,* 6384–6391.

68. Quan, M.; Sanchez, D.; Wasylkiw, M. F.; Smith, D. K. *J. Am. Chem. Soc.* **2007**, 129, 12847–12856.

69. Lin, Q.; Li, Q.; Batchelor-McAuley, C.; Compton, R. G. *J. Phys. Chem. C* **2015**, *119*, 1489−1495.

70. Paul, I. C.; Curtin, D. Y. *Science* **1975**, *187*, 19–26.

71. Braga, D.; Grepioni, F. Polymorphism, Crystal Transformations and Gas-Solid Reactions. In *Crystal Design: Structure and Function;* Desiraju, G. R.; Ed.; Perspectives in Supramolecular Chemistry, John Wiley & Sons: New York, 2003; Vol. 7, pp 325–373.

72. Brunet, P.; Demers, E.; Maris, T.; Enright, G. D.; Wuest, J. D. *Angew. Chem. Int. Ed.* **2003**, *42*, 5303−5306.

73. Le Fur, E.; Demers, E.; Maris, T.; Wuest, J. D. *Chem. Commun.* **2003**, 2966−2967.

74. For recent references, see: Liang, Y.; Jing, Y.; Gheytani, S.; Lee, K.-Y.; Liu, P.; Facchetti, A.; Yao, Y. *Nat. Mater*. **2017**, *16*, 841−848.

75. Kwon, J. E.; Hyun, C.-S.; Ryu, Y. J.; Lee, J.; Min, D. J.; Park, M. J.; An, B.-K.; Park, S. Y. *J. Mater. Chem. A* **2018**, *6*, 3134−3140.

76. Zhang, M. Y.; Barrow, R. A. *Org. Lett.* **2017**, *19*, 2302−2305.

4.3 Conclusions

Les quinones et les hydroquinones peuvent être utilisées pour former des solides organiques organisés pouvant participer à des réactions d'oxydoréduction. Notre étude des triptycènes **1**-**4** révèle que les interactions caractéristiques des quinones et des hydroquinones peuvent diriger l'association pour former des organisations poreuses lorsque ces unités sont intégrées à des squelettes conçus pour défavoriser un empilement compact. Les solides résultants sont perméables et peuvent prendre part à des réactions rédox dans leur forme cristalline. Certains de ces solides peuvent remarquablement participer à ces processus en maintenant leur organisation. Ces résultats sont particulièrement intéressants dans le contexte des batteries organiques où les matériaux constituant les électrodes doivent être structurés de façon à permettre la diffusion de l'électrolyte et où cette organisation doit subsistée suite au cycle d'oxydoréduction.

Chapitre 5.

Perspectives

Chapitre 5. Perspectives

Les chapitres précédents fournissent des informations utiles sur l'association et la préparation de thiadiazoles, de quinones et d'hydroquinones. Ces nouvelles connaissances peuvent servir de fondations à la conception de nouveaux matériaux et de nouvelles méthodes d'organisation. Plusieurs des composés explorés pourraient être testés dans des dispositifs et d'autres ouvrent la voie à l'exploration de nouvelles façons de structurer les matériaux.

5.1 Matériaux à base de thiadiazoles

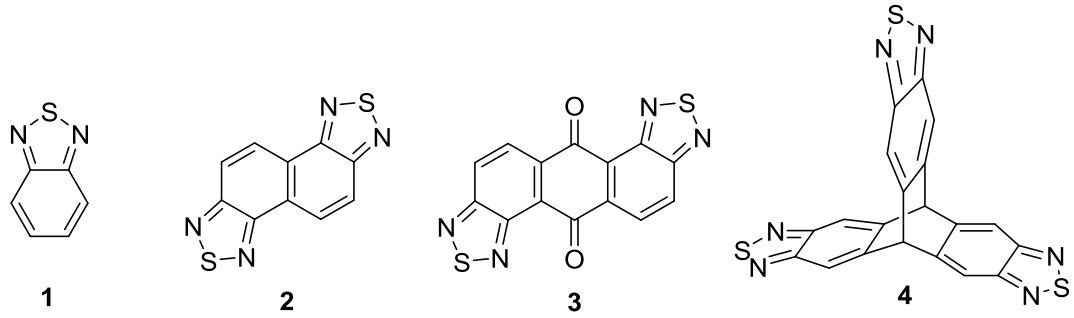

Bien que notre étude des thiadiazoles se soit concentrée sur leur association, nous avons aussi élargi cette famille de composés et rendu certaines molécules plus accessibles en revisitant leur synthèse. Certaines de ces unités, particulièrement le naphtobisthiadiazole **2** et l'anthraquinonebisthiadiazole **3**, peuvent être intégrées à des matériaux en tant que fragments pauvres en électrons de façon analogue à la manière dont le benzothiadiazole (**1**) est utilisé.[1] Les réseaux π étendus des thiadiazoles **2** et **3** permettent de générer des matériaux possédant un plus petit gap, une orbitale HOMO plus basse en énergie et des organisations plus favorables à la percolation des charges que les matériaux similaires contenant le thiadiazole **1**.[2-4] Ainsi, le naphtalène **2** a déjà été intégré à plusieurs polymères ayant ensuite mené à des cellules solaires très performantes dont les rendements énergétiques excédent 10% (Figure 1).[5-8] L'anthraquinone **3** a aussi commencé à attirer de l'intérêt et un analogue réduit a

récemment été copolymérisé avec une série de thiophènes pour former un nouveau matériau donneur (**6**) pour les cellules solaires. Les dispositifs fabriqués avec ce polymère ont produit des taux de conversion énergétique prometteurs atteignant jusqu'à 5,6%.[4]

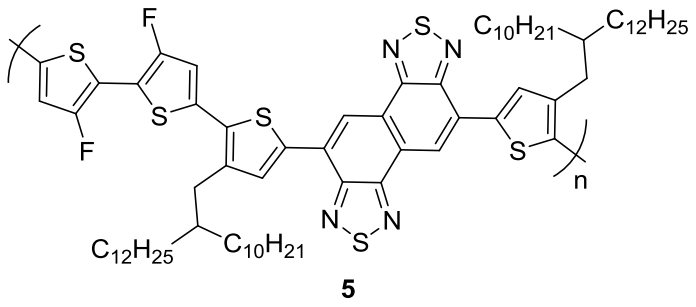

5

Efficacité énergétique : 10,5%[7]

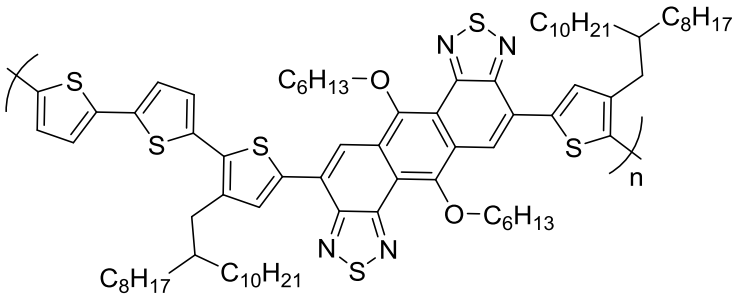

6

Efficacité énergétique : 5,6%[4]

Figure 1. Structures de matériaux incluant le naphtalène **2** et l'anthraquinone **3** ayant été utilisés dans des cellules solaires organiques.

De plus, les thiadiazoles peuvent être combinés à d'autres unités pauvres en électrons pour former des semi-conducteurs de type *n*.[1, 9] De tels polymères à base de benzothiadiazole (**1**) ont notamment été utilisés comme matériaux accepteurs dans des cellules solaires et des matériaux analogues à base de naphtobisthiadiazole **2** ont aussi été rapportés.[2,10,11] L'anthraquinone **3** et des composés apparentés pourraient également être intégrés à ce type de matériaux. Des substances semblables au thiadiazole **3** possédant une portion aromatique plus

étendue, comme le composé **7**, ont aussi été étudiées seules comme conducteur moléculaire de type *n*. [12, 13] Bien que les thiadiazoles puissent être intégrés à différents types de matériaux, leur utilisation est concentrée aux dispositifs à couches minces dans lesquels l'organisation des molécules de la couche active affecte les propriétés. Ainsi, les connaissances acquises sur les modes d'association privilégiés des thiadiazoles demeurent pertinentes et peuvent se révéler utiles pour comprendre et contrôler l'association moléculaire dans ces nouveaux matériaux.

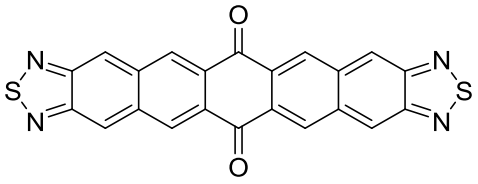

7

5.1.1 Association avec les fullerènes

Dans les cellules solaires organiques, les performances dépendent de la proportion d'électrons excités transférés du matériau donneur vers le matériau accepteur. Ce phénomène dépend à son tour de la qualité de l'interface entre ces composés.[14-16] Les dérivés de benzothiazole qui sont intégrés au matériau donneur comme unité pauvre en électrons, ils portent généralement l'orbitale LUMO des composés finaux. Ainsi, les systèmes dans lesquels le thiadiazole est placé en proximité de l'accepteur d'électrons sont prometteurs, car cette organisation devrait favoriser les transferts électroniques. La structure du co-cristal que nous avons obtenu entre le triptycène **4** et les fullerènes C_{60} et C_{70} suggère que l'autoassemblage est une stratégie qui pourrait permettre d'obtenir de tels arrangements malgré la mauvaise compatibilité électronique de ces composés. Il pourrait être intéressant de préparer une petite molécule *push-pull* à base du thiadiazole **4** ou d'un autre thiadiazole intégré à un squelette concave et d'étudier si l'association avec les fullerènes perdure dans un système plus complexe et si elle peut être exploitée dans un dispositif.[17] Plus généralement, ces d'études amènent à sonder comment la morphologie et la nanostructure de l'hétérojonction peuvent être contrôlées en créant une complémentarité supramoléculaire entre les matériaux donneurs et accepteurs.

5.2 Matériaux à base de quinones et d'hydroquinones

Outre les caractéristiques propres à son organisation, la triptycène trisquinone **8** possède plusieurs caractéristiques attrayantes pour la formation de cathode et des composés similaires ont déjà été utilisés pour former des électrodes.[18] Le triptycène **8** est notamment un composé très peu soluble, ce qui prévient la dégradation des électrodes par leur dissolution dans l'électrolyte. Il s'agit de surcroit d'une molécule contenant plusieurs unités rédox unies par seulement deux atomes de carbone ce qui en fait une molécule où une faible portion de la masse est inactive. La capacité de la trisquinone **8** à emmagasiner des charges sera testée sous peu dans un dispositif.

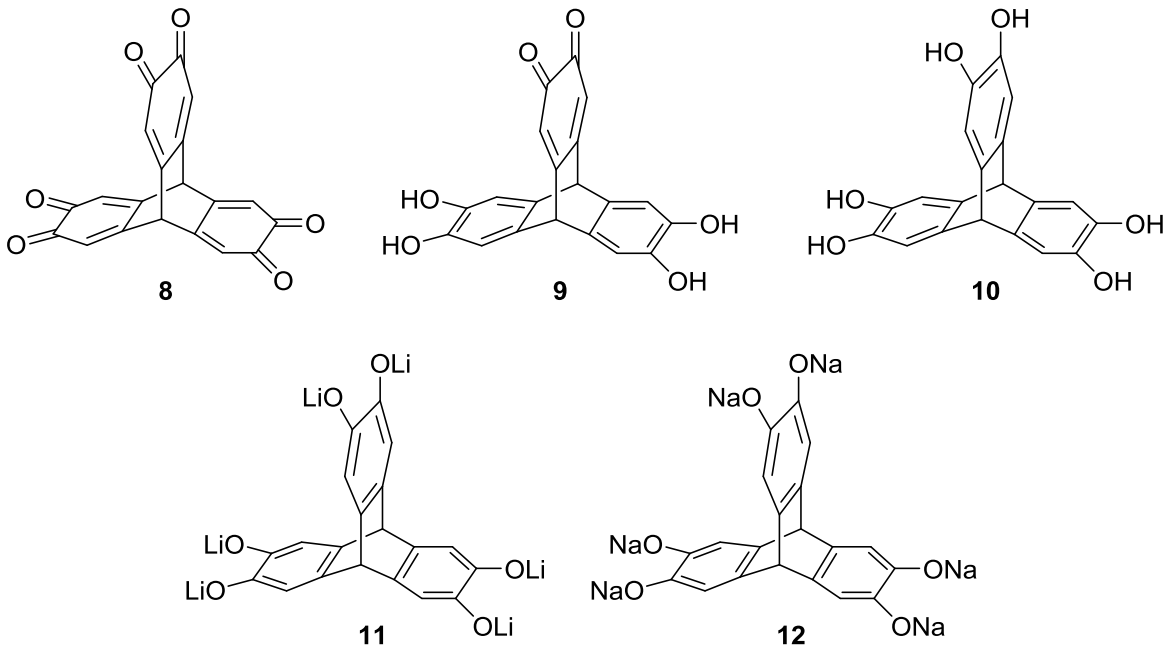

5.2.1 Utilisation des liens Li-O et Na-O pour contrôler l'organisation

Le contrôle de l'organisation dans les électrodes constituées de matériaux organiques pose un défi particulier : les molécules doivent être orientées de façon à faciliter la diffusion des charges et des ions et cette organisation doit de surcroit être maintenue au fil des réactions

d'oxydoréduction. De telles stabilités des arrangements moléculaires sont rares. La réduction de la monoquinone **9** vers le triscatechol **10** présentée dans le chapitre 4 en constitue le seul exemple pour des composés organiques. Dans les batteries rechargeables au lithium exploitant la réduction de quinones, le produit issu de la réaction n'est cependant pas une hydroquinone, mais plutôt le sel de lithium correspondant. Pour mieux comprendre les défis associés au contrôle de l'organisation, il pourrait être pertinent de synthétiser ce type de sel et de se pencher sur leur structure cristalline. Une analyse cristallographique du composé **11** pourrait permettre d'observer si ces sels adoptent des organisations semblables à celle de leur analogue protonné. Plus généralement, nous proposons une étude sur comment la permutation des atomes d'hydrogène pour des atomes de lithium modifie le type d'arrangement adopté. L'ingénierie cristalline reposant sur l'exploitation des ponts hydrogène est bien développée, mais une approche analogue qui exploite des interactions ioniques Li-O reste à inventer. Les structures contenant des ions de lithium sont aussi intrinsèquement intéressantes, car ces cations sont généralement impliqués dans une sphère de coordination complexe[19] pouvant mener à des interactions fortes et à la formation de solides robustes et poreux.[20-22] De plus, bien que le développement des batteries organiques se soit principalement engagé dans la recherche de batterie au lithium, plusieurs dispositifs s'appuient plutôt sur la chimie du sodium et des études analogues pourraient être conduites sur ces sels (**12**). Ainsi, la préparation et la caractérisation des composés **11** et **12** forment une opportunité intéressante de mieux comprendre les enjeux structuraux associés aux électrodes organiques et ouvrent de surcroit la porte à l'exploration de nouvelles façons de diriger l'association grâce aux liens ioniques Li-O et Na-O.

5.2.2 Nouvelles quinones et hydroquinones

Les caractéristiques fondamentales permettant aux dérivés quinonoïdes du triptycène de mener à des réseaux ouverts pouvant participer à des réactions rédox sont relativement simples : multiples portions quinone ou hydroquinone sont présentes, ces fragments sont la source des propriétés rédox et des interactions supramoléculaires dirigeant l'association, et le squelette auquel ces unités sont greffées doit défavoriser un empilement compact. Ces

éléments ne sont pas restreints aux dérivés du triptycène et d'autres noyaux pourraient mener à des composés possédant ces caractéristiques. Par exemple, les dérivés du spirobifluorène (**13**) explorés plus tôt dans la thèse pourraient aussi permettre de générer de tels composés, illustrés par les exemples **14** et **15**. Ainsi, cette stratégie mérite d'être étendue et plusieurs autres systèmes susceptibles de mener à des solides poreux pouvant prendre part à des transformations rédox pourraient être préparés. Alternativement, les structures pourraient aussi être diversifiées en se tournant vers les dérivés de l'isomère 1,4 de la benzoquinone qui pourraient offrir des caractéristiques rédox et supramoléculaires analogues. De plus, dans l'optique de préparer des systèmes plus accessibles et moins couteux, il pourrait être intéressant de se tourner vers les quinones et les hydroquinones extraites de la biomasse. Comme pour les systèmes à base de triptycène, ces nouveaux composés pourraient être étudiés pour leur organisation et leur comportement rédox à l'état solide, mais pourraient aussi être testés dans des dispositifs et utilisés pour former les sels de lithium analogues.

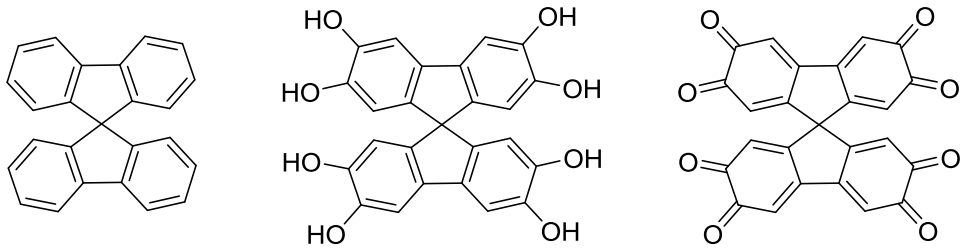

13 **14** **15**

5.3 Conclusions

Le travail présenté dans cette thèse s'est concentré sur la préparation et l'association de divers thiadiazoles, quinones et hydroquinones, mais amène aussi à s'engager dans de nouvelles directions. Certains des composés explorés pourraient être testés dans des dispositifs, soit en étant intégrés à des matériaux plus complexes dans le cas des thiadiazoles ou directement dans le cas de la trisquinone **8**. Cette dernière sera testée dans une batterie organique sous peu. Les études conduites sur l'association moléculaire mènent quant à elles à l'exploration de nouvelles façons de structurer les matériaux utilisés dans différentes sphères

de l'électronique organique. Ainsi, notre travail sur l'assemblage entre les fullerènes et les thiadiazoles peut servir de point départ à l'étude des façons dont l'hétérojonction des cellules solaires organiques peut être structurée grâce au design supramoléculaire. Aussi, l'étude de sels de lithium dérivés des hydroquinones pourrait mener à une meilleure compréhension des enjeux structuraux liés aux électrodes organiques et offre l'opportunité d'approfondir nos connaissances sur comment les liens Li-O peuvent diriger l'association moléculaire. Finalement, l'habileté des dérivés quinonoïdes du triptycène à former des réseaux rédox perméables invite à explorer de nouveaux systèmes conçus grâce à une stratégie similaire. Ces nouveaux composés pourraient être obtenus en exploitant des squelettes analogues au triptycène comme le spirobifluorène, en se tournant vers les dérivés de la 1,4-benzoquinone ou en étudiant des composés extraits de la biomasse.

5.4 Références

1. Du, J.; Biewer, M. C.; Stefan, M. C. *J. Mater. Chem. A* **2016**, *4*, 15771-15787.
2. Osaka, I.; Takimiya, K. *Adv. Mater.* **2017**, *29*, 1605218.
3. Wang, Y.; Michinobu, T. *J. Mater. Chem. C* **2016**, *4*, 6200-6214.
4. Mori, H.; Nishinaga, S.; Takahashi, R.; Nishihara, Y. *Macromolecules* **2018**, *51*, 5473-5484.
5. Liu, Y.; Zhao, J.; Li, Z.; Mu, C.; Ma, W.; Hu, H.; Jiang, K.; Lin, H.; Ade, H.; Yan, H. *Nat. Commun.* **2014**, *5*, 5293.
6. Lee, J.; Sin, D. H.; Moon, B.; Shin, J.; Kim, H. G.; Kim, M.; Cho, K. *Energy Environ. Sci.* **2017**, *10*, 247-257.
7. Kawashima, K.; Fukuhara, T.; Suda, Y.; Suzuki, Y.; Koganezawa, T.; Yoshida, H.; Ohkita, H.; Osaka, I.; Takimiya, K. *J. Am. Chem. Soc.* **2016**, *138*, 10265-10275.
8. Vohra, V.; Kawashima, K.; Kakara, T.; Koganezawa, T.; Osaka, I.; Takimiya, K.; Murata, H. *Nat. Photonics* **2015**, *9*, 403-409.
9. Parker, T. C.; Patel, D. G.; Moudgil, K.; Barlow, S.; Risko, C.; Bredas, J.-L.; Reynolds, J. R.; Marder, S. R. *Mater. Horizons* **2015**, *2*, 22-36.
10. Nakano, M.; Osaka, I.; Takimiya, K. *Macromolecules* **2015**, *48*, 576-584.
11. Ie, Y.; Sasada, S.; Karakawa, M.; Aso, Y. *Org. Lett.* **2015**, *17*, 4580-4583.
12. Xia, D.; Wang, X.-Y.; Guo, X.; Baumgarten, M.; Li, M.; Müllen, K. *Cryst. Growth Des.* **2016**, *16*, 7124-7129.
13. Shi, Z.-F.; Black, H. T.; Dadvand, A.; Perepichka, D. F. *J. Org. Chem.* **2014**, *79*, 5858-5860.
14. Huang, Y.; Kramer, E. J.; Heeger, A. J.; Bazan, G. C. *Chem. Rev.* **2014**, *114*, 7006-7043.
15. Lee, H.; Park, C.; Sin, D. H.; Park, J. H.; Cho, K. *Adv. Mater.* **2018**, *30*, 1800453.
16. Ryno, S. M.; Ravva, M. K.; Chen, X.; Li, H.; Brédas, J.-L. *Adv. Energy Mater.* **2017**, *7*, 1601370.
17. Ball, M.; Zhong, Y.; Wu, Y.; Schenck, C.; Ng, F.; Steigerwald, M.; Xiao, S.; Nuckolls, C. *Acc. Chem. Res.* **2015**, *48*, 267-276.

18. Kwon, J. E.; Hyun, C.-S.; Ryu, Y. J.; Lee, J.; Min, D. J.; Park, M. J.; An, B.-K.; Park, S. Y. *J. Mater. Chem. A* **2018**, *6*, 3134-3140.
19. Olsher, U.; Izatt, R. M.; Bradshaw, J. S.; Dalley, N. K. *Chem. Rev.* **1991**, *91*, 137-164.
20. Abrahams, B. F.; Grannas, M. J.; Hudson, T. A.; Robson, R. *Angew. Chem., Int. Ed.* **2010**, *49*, 1087-1089.
21. Zheng, S.-T.; Li, Y.; Wu, T.; Nieto, R. A.; Feng, P.; Bu, X. *Chem. Eur. J.* **2010**, *16*, 13035-13040.
22. Zhao, X.; Wu, T.; Zheng, S.-T.; Wang, L.; Bu, X.; Feng, P. *Chem. Commun.* **2011**, *47*, 5536-5538.

Chapitre 6.

Conclusions

Chapitre 6. Conclusions

«*What would the properties of materials be if we could really arrange the atoms the way we want them? [...] I can't see exactly what would happen, but I can hardly doubt that when we have some control of the arrangement of things on a small scale we will get an enormously greater range of possible properties that substances can have, and of different things that we can do.*»

-Richard Feynman, 1959

Lors de sa conférence intitulée «*There is plenty of room at the bottom*»[1], le physicien Richard Feynman suggérait une conception ascendante des matériaux, l'approche *bottom-up*, et présageait ainsi une des voies dans laquelle la science allait s'engager durant les décennies suivantes. Feynman imaginait cependant que l'habileté de structurer l'échelle nanométrique allait découler de progrès effectués en microscopie et dans d'autres sphères de la physique ou de l'ingénierie. Il ne semblait pas entrevoir le rôle central que la chimie allait jouer dans l'évolution de notre habileté à contrôler les arrangements moléculaires grâce au développement de l'autoassemblage. En effet, la chimie supramoléculaire a fait plusieurs pas de géants depuis les années cinquante, et la tectonique moléculaire permet désormais de concevoir des molécules s'assemblant dans des organisations prédéfinies. La portée de l'approche des tectons est cependant limitée. Il est nécessaire de diversifier les fragments moléculaires capables de diriger l'association afin de pouvoir contrôler l'organisation à l'aide d'unités dont les propriétés moléculaires sont compatibles à différents types de matériaux. Dans le cadre de cette thèse, nous avons étudié les architectures adoptées par des composés quinonoïdes afin de sonder s'ils peuvent être utilisés pour diriger l'association dans les matériaux où ils sont exploités pour leurs propriétés moléculaires.

Nous nous sommes d'abord concentrés sur des dérivés du benzothiadiazole. Ces unités sont fréquemment employées dans différents matériaux optoélectroniques destinés à des dispositifs à couche mince, particulièrement les cellules solaires organiques dans lesquels l'organisation des molécules formant la couche active affecte les performances. Avant nos études, il était difficile d'estimer comment les thiadiazoles peuvent être utilisés pour diriger l'association, car peu d'études systématiques sur leurs modes d'association privilégiés ont été rapportées. Nos études cristallographiques de composés dans lesquels plusieurs unités benzothiadiazole sont attachées à des noyaux rigides de différentes topologies montrent que l'organisation moléculaire peut être contrôlée dans des structures complexes par des liens S···N et d'autres interactions distinctives. Ces observations montrent que ces hétérocycles peuvent être utilisés pour former des matériaux possédant des propriétés optoélectroniques et supramoléculaires caractéristiques. Lorsqu'ils sont intégrés à un squelette adéquat, les thiadiazoles peuvent de surcroit co-cristalliser avec les fullerènes.

Notre travail sur les thiadiazoles a aussi exigé la préparation de nouveaux composés et l'élaboration de nouvelles synthèses. Certains des thiadiazoles présentés dans la thèse peuvent être intégrés à des matériaux en tant que fragments pauvres en électrons de façon analogue à la manière dont le benzothiadiazole lui-même est utilisé. Les performances exceptionnelles des matériaux à base de naphtobisthiadiazole nous ont poussées à tenter de perfectionner notre synthèse de ce composé. Le rendement global étant limité par celui de l'étape de nitration, nous nous sommes attardés à cette réaction. Notre travail a permis de mieux cerner la régiosélectivité de cette étape problématique et a mené à une préparation accessible et sélective des isomères 1,2,5,6 et 1,4,5,8 de la naphtalènetétramine.

Nous nous sommes ensuite penchés sur l'organisation des quinones, dont les propriétés rédox les ont placées au centre des matériaux explorés dans la nouvelle génération de batteries organiques. Afin d'examiner si les quinones et les hydroquinones peuvent être utilisées pour former les réseaux robustes et ouverts requis par cette technologie, nous les avons greffées sur un squelette triptycène afin de défavoriser un empilement moléculaire efficace. Les

interactions caractéristiques des quinones et des hydroquinones peuvent alors diriger l'édification de solides perméables pouvant participer à des réactions d'oxydoréduction. De façon particulièrement pertinente aux batteries organiques et de façon inédite, ces solides cristallins peuvent participer à ces réactions en maintenant leur organisation.

Globalement, notre travail sur les quinones et les thiadiazoles a contribué à approfondir notre compréhension de leurs modes d'association et a éclairci comment les interactions et les topologies de ces composés peuvent être utilisées de concert afin de diriger l'association vers le type d'organisation requise par les technologies où ils sont utilisés.

6.1 Références

1. Feynman, R. P. *Engineering and Science* **1960**, *23*, 22-36.

Annexe A

Informations supplémentaires

Chapitre 2

Organisation moléculaire
de 2,1,3-benzothiadiazoles à l'état solide.

Supporting Information

Molecular Organization of 2,1,3-Benzothiadiazoles in the Solid State

Sophie Langis-Barsetti, Thierry Maris, and James D. Wuest*

Contents

Page

Instrumentation

NMR spectra were recorded at 25 °C in DMSO-d_6, trifluoroacetic acid-*d*, or $CDCl_3$ using (1) a spectrometer operating at 400 MHz for ^1H NMR spectra and at 100 MHz for ^{13}C NMR spectra or (2) an instrument operating at 700 MHz for ^1H NMR spectra and at 176 MHz for ^{13}C NMR spectra. Chemical shifts are reported in parts per million relative to tetramethylsilane, with the signal of residual undeuterated solvent used as an internal standard. Cyclic voltammograms were obtained using solutions in N_2-purged dry *N*-methyl-2-pyrrolidone (NMP), with tetrabutylammonium hexafluorophosphate (TBAP) as the supporting electrolyte (0.1 M). The working electrode was a Pt electrode, the counter electrode was a Pt wire, and the pseudo-reference electrode was an Ag wire. The concentration of analyte was ~1 mM for benzothiadiazole (**1**), naphthobis(thiadiazole) **4**, and benzotris(thisdiazole) **6**.

The X-ray powder diffraction patterns of microcrystalline samples of naphthobis(thiadiazole) **4**, anthraquinonebis(thiadiazole) **5**, and benzotris(thiadiazole) **6** were measured in reflection geometry using a diffractometer (θ-θ setting) equipped with an XYZ platform and a 2D gas detector. X-rays were generated using a conventional sealed-tube source with a Cu anode producing CuKα radiation (λ = 1.54178 Å). The samples were gently ground and placed on a flat polymeric sample holder. The data collection involved acquisition of two different sections with increasing angular position, giving a set of two different two-dimensional X-ray diffraction frames that were integrated and combined to produce the final X-ray powder diffraction pattern. Calculated X-ray powder diffraction patterns were generated from *SHELX* files produced by analyses of single crystals, using Mercury software from the Cambridge Crystallographic Data Centre.[1] A unique value for the FWHM of the diffraction peaks was adjusted in order to get a better match between the resolution of the experimental and calculated patterns.

NMR Spectra

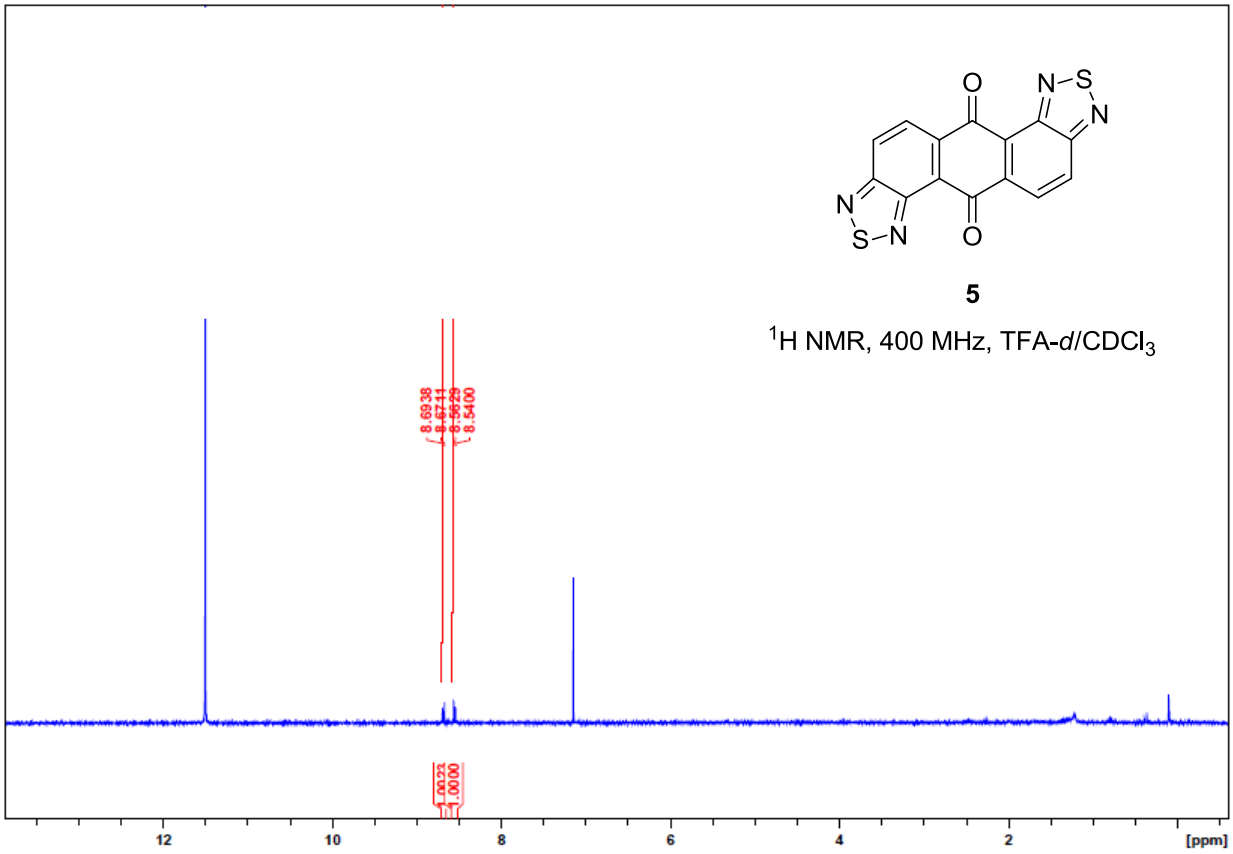

(Signals at high frequencies are from impurities in TFA-*d*)

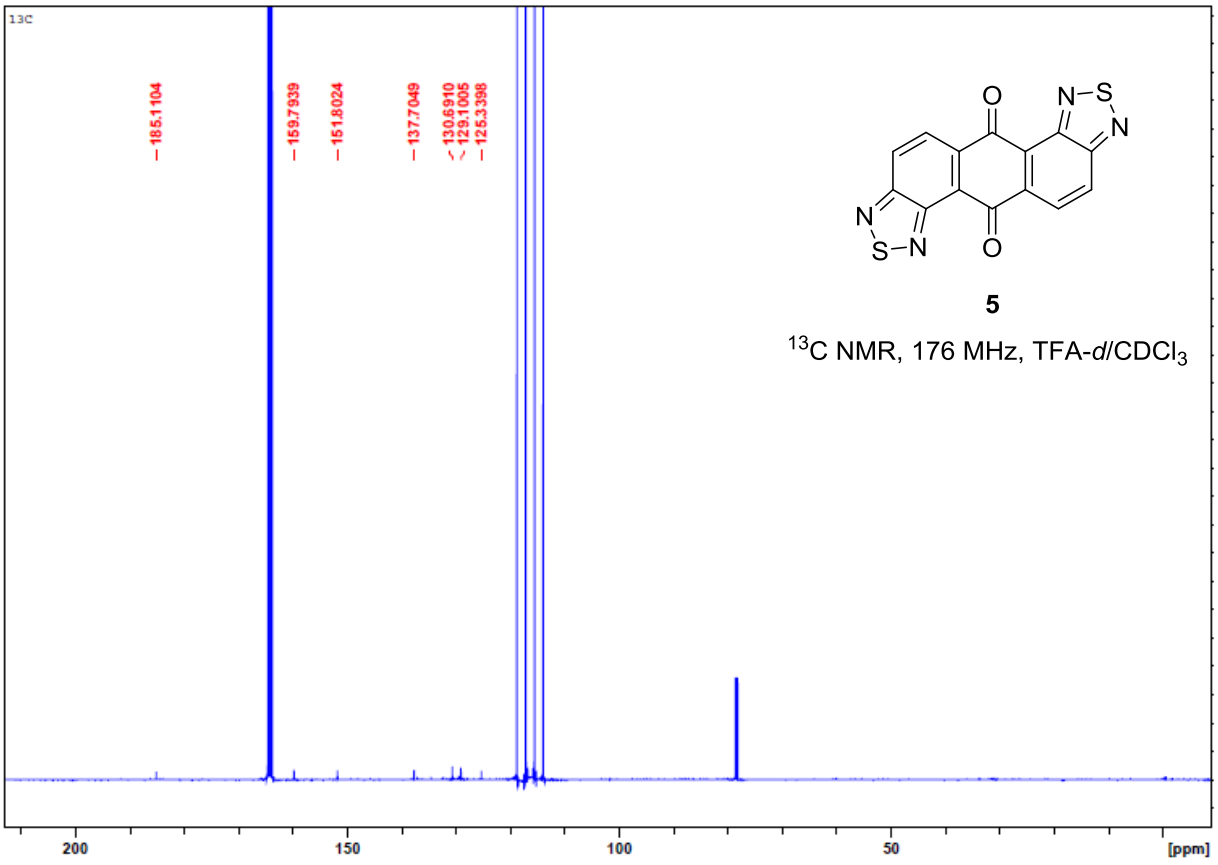

5

^{13}C NMR, 176 MHz, TFA-*d*/$CDCl_3$

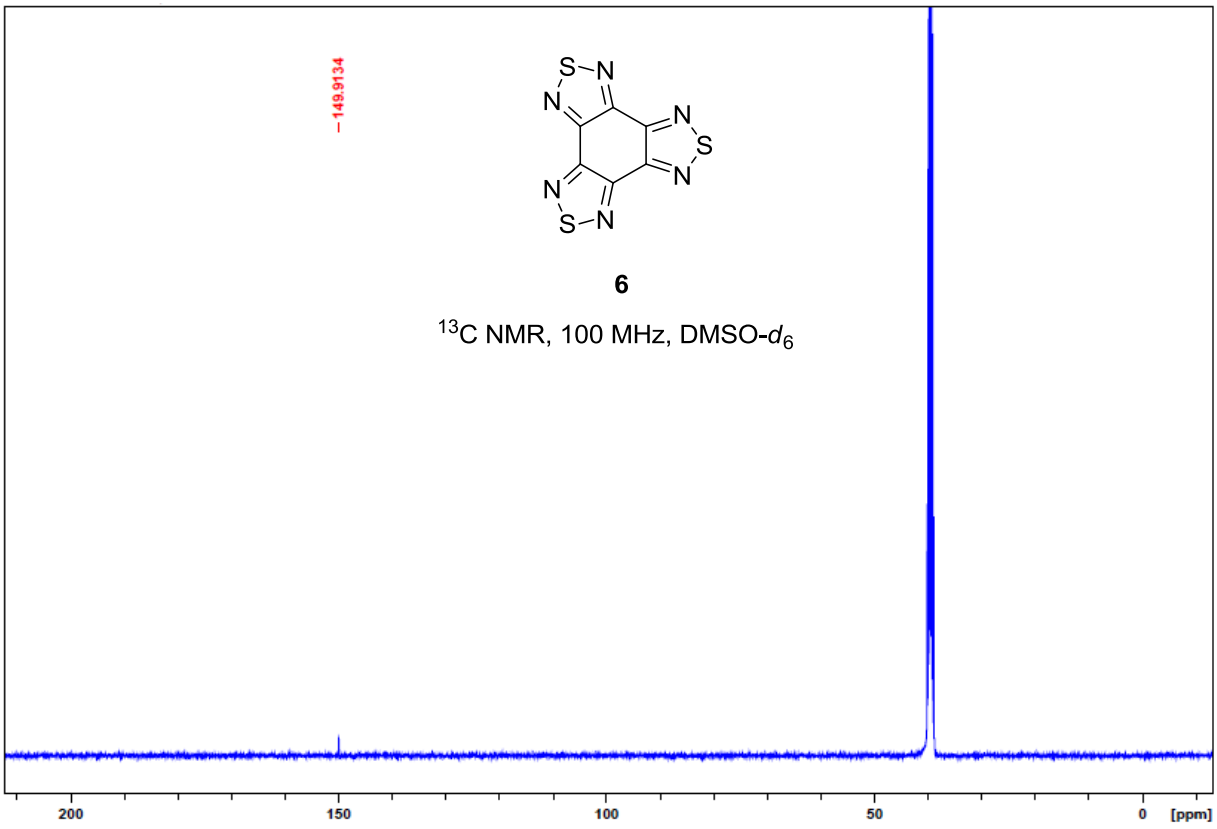

6

^{13}C NMR, 100 MHz, DMSO-d_6

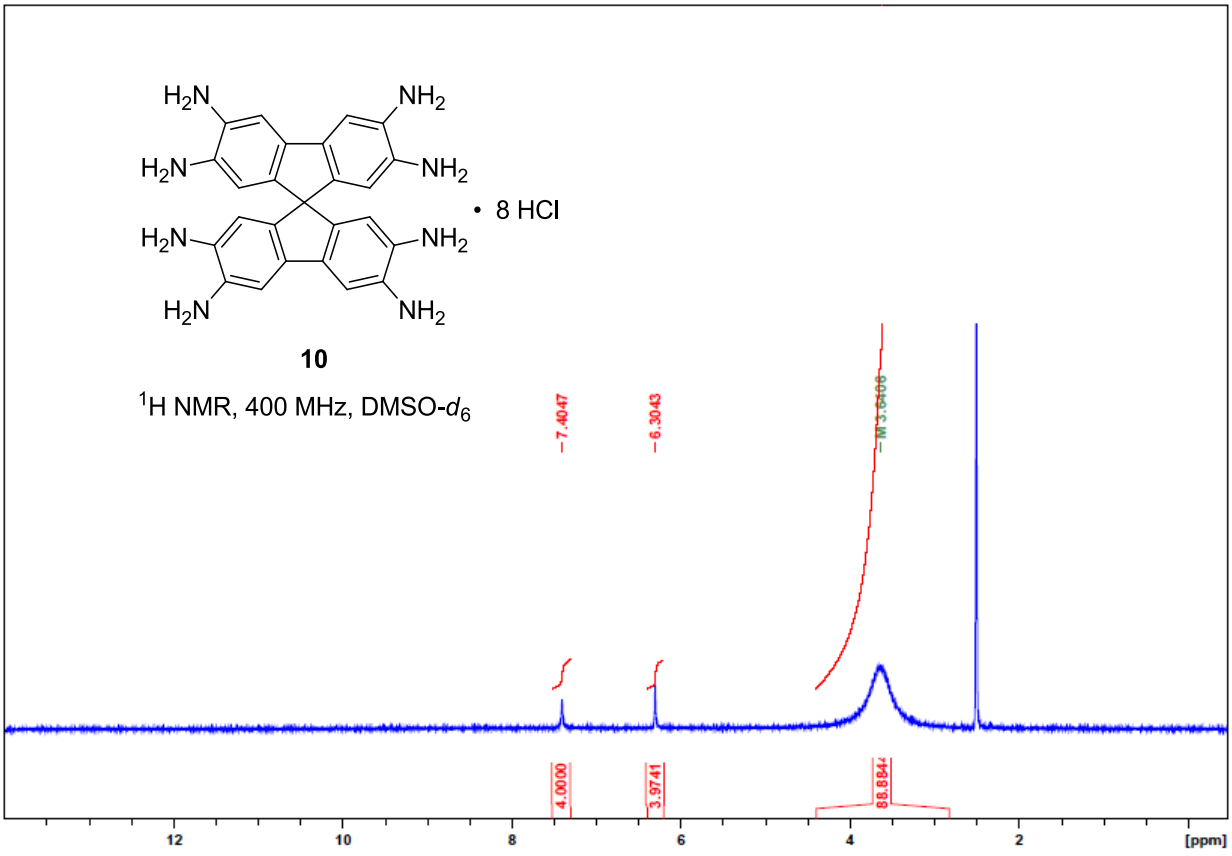
• 8 HCl
10
1H NMR, 400 MHz, DMSO-d6
7.4047
6.3043
3.5406
4.0000
3.9741
88.884
12
10
8
6
4
2
[ppm]

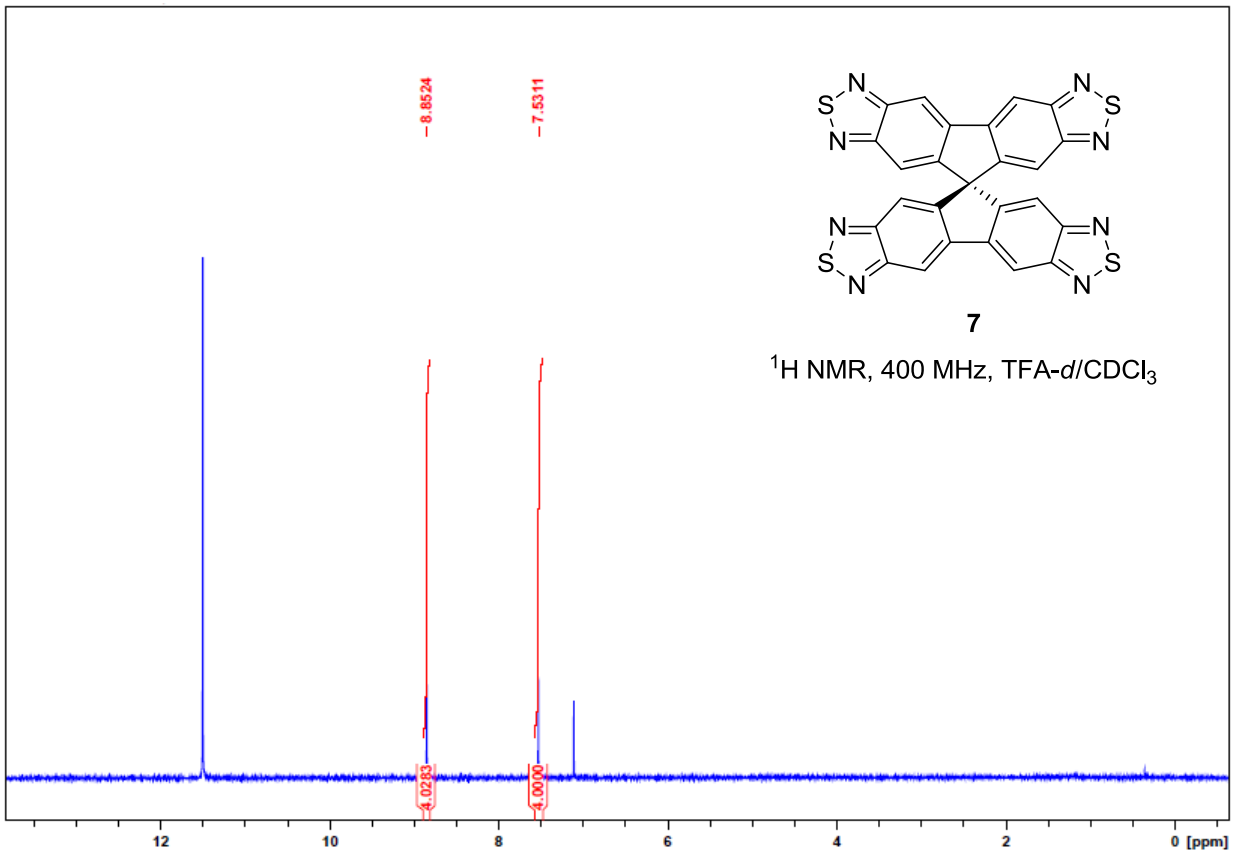

7

^{1}H NMR, 400 MHz, TFA-*d*/$CDCl_3$

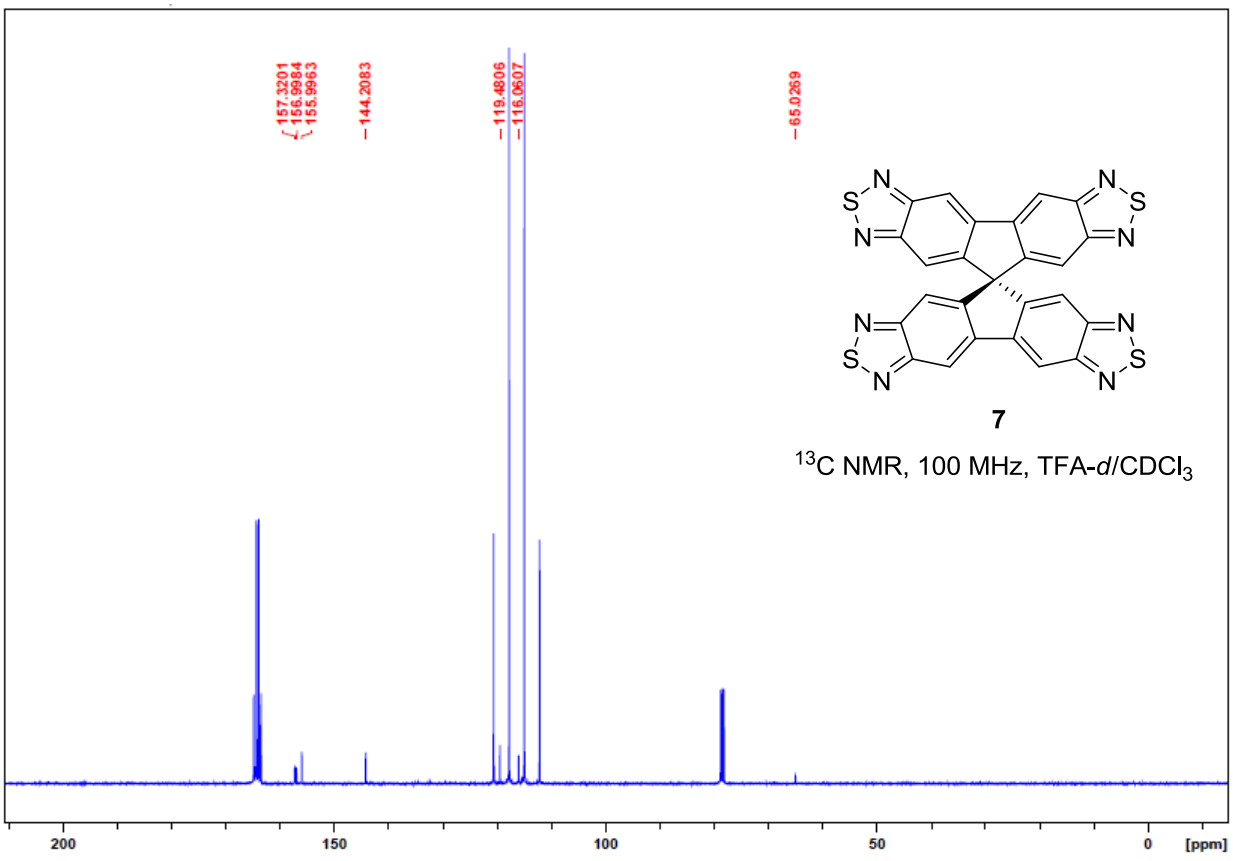

7

^{13}C NMR, 100 MHz, TFA-*d*/$CDCl_3$

Cyclic Voltammograms

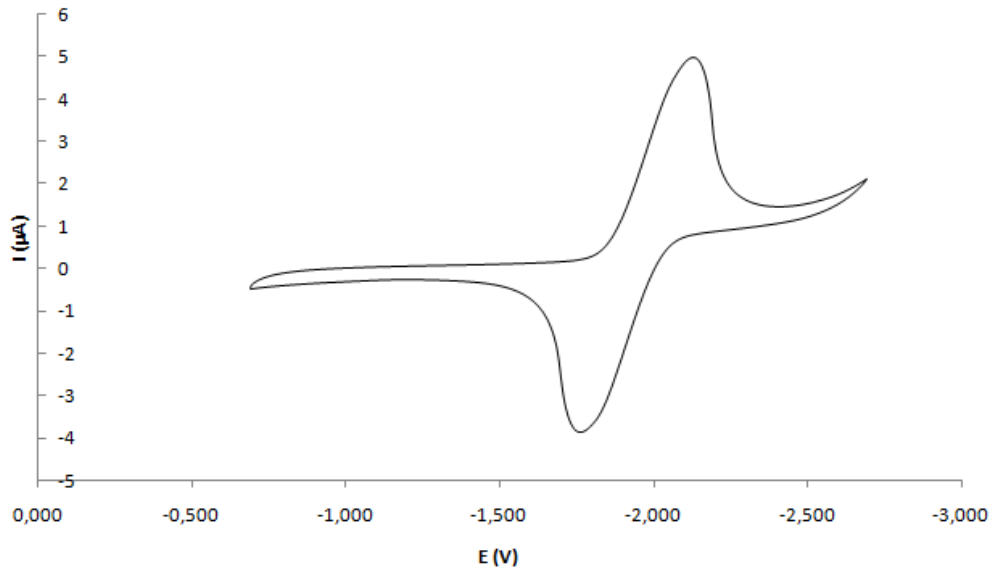

Figure S1. Cyclic voltammogram of benzothiadiazole (**1**) dissolved in NMP containing 0.1 M TBAP (scan rate = 50 mV/s). Potentials are reported with respect to the Fc/Fc^+ couple.

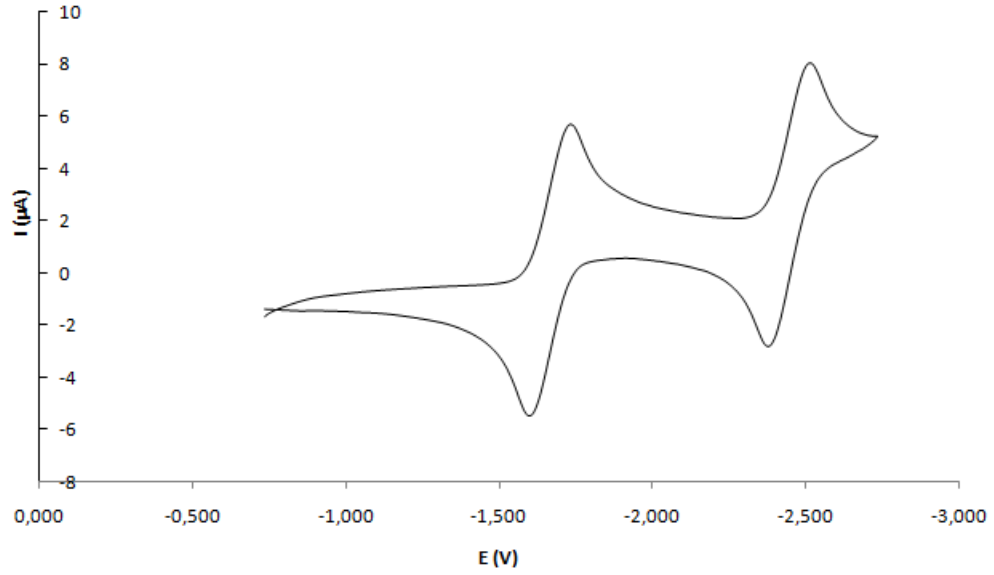

Figure S2. Cyclic voltammogram of naphthobis(thiadiazole) **4** dissolved in NMP containing 0.1 M TBAP (scan rate = 50 mV/s). Potentials are reported with respect to the Fc/Fc^+ couple.

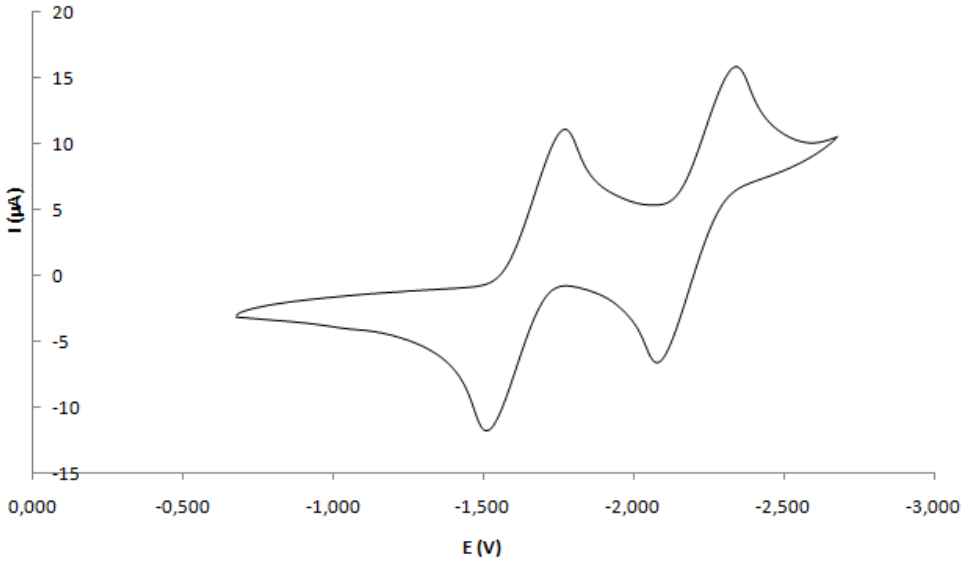

Figure S3. Cyclic voltammogram of benzotris(thiadiazole) **6** dissolved in NMP containing 0.1 M TBAP (scan rate = 50 mV/s). Potentials are reported with respect to the Fc/Fc^+ couple.

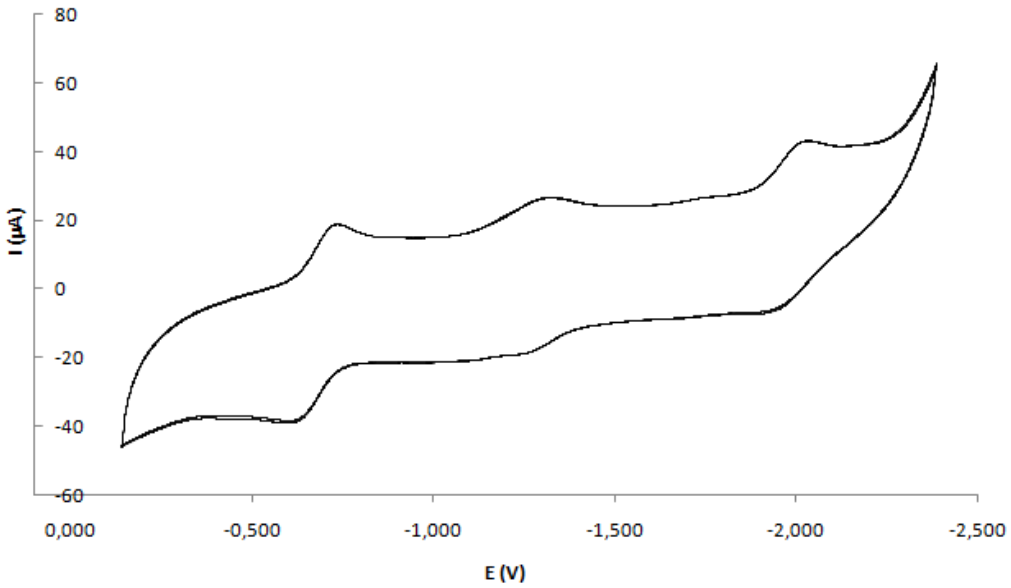

Figure S4. Cyclic voltammogram of anthraquinonebis(thiadiazole) **5** dissolved in NMP containing 0.1 M TBAP (scan rate = 200 mV/s). Potentials are reported with respect to the Fc/Fc^+ couple.

X-Ray Powder Diffraction Patterns

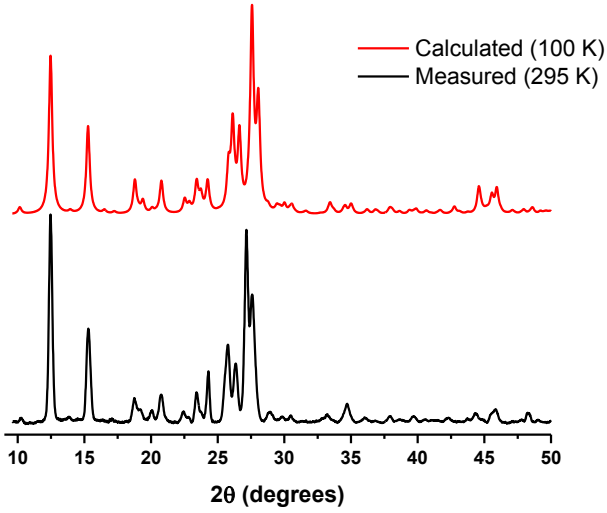

Figure S5. Comparison of experimental and calculated X-ray powder diffraction patterns of naphthobis(thiadiazole) **4.** Black: X-ray powder diffraction pattern of a microcrystalline sample of compound **4** measured at 295 K. Red: Calculated X-ray powder diffraction pattern based on the crystal structure of compound **4** determined at 100 K.

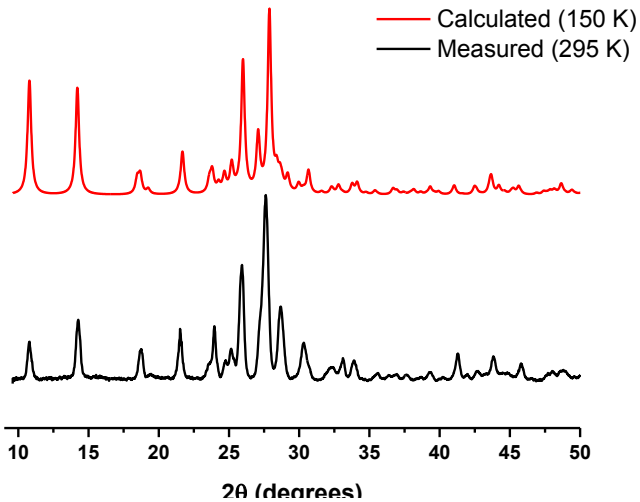

Figure S6. Comparison of experimental and calculated X-ray powder diffraction patterns of anthraquinonebis(thiadiazole) **5.** Black: X-ray powder diffraction pattern of a microcrystalline sample of compound **5** measured at 295 K. Red: Calculated X-ray powder diffraction pattern based on the crystal structure of compound **5** determined at 100 K.

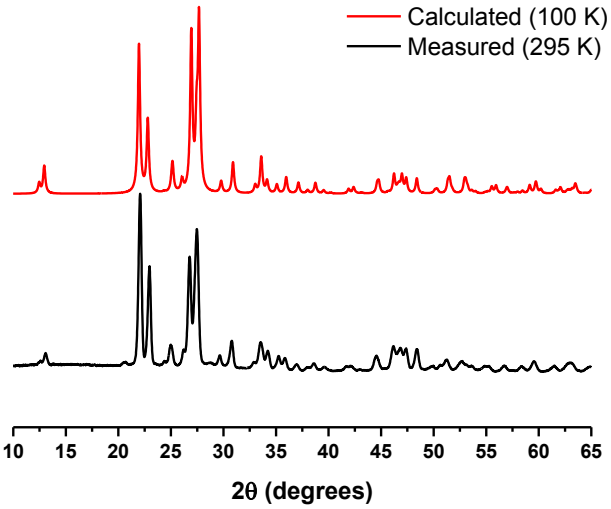

Figure S7. Comparison of experimental and calculated X-ray powder diffraction patterns of benzotris(thiadiazole) **6** . Black: X-ray powder diffraction pattern of a microcrystalline sample of compound **6** measured at 295 K. Red: Calculated X-ray powder diffraction pattern based on the crystal structure of compound **6** determined at 100 K.

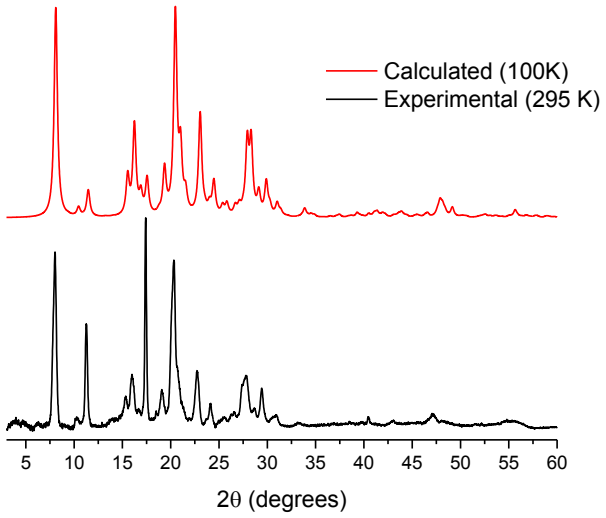

Figure S8. Comparison of experimental and calculated X-ray powder diffraction patterns of the co-crystals of triptycenetris(thiadiazole) **8** and C_{60}**.** Black: X-ray powder diffraction pattern of a microcrystalline sample of co-crystals of compound **8** and C_{60} measured at 295 K. Red: Calculated X-ray powder diffraction pattern based on the structure of the co-crystals of compound **8** and C_{60} measured at 100 K.

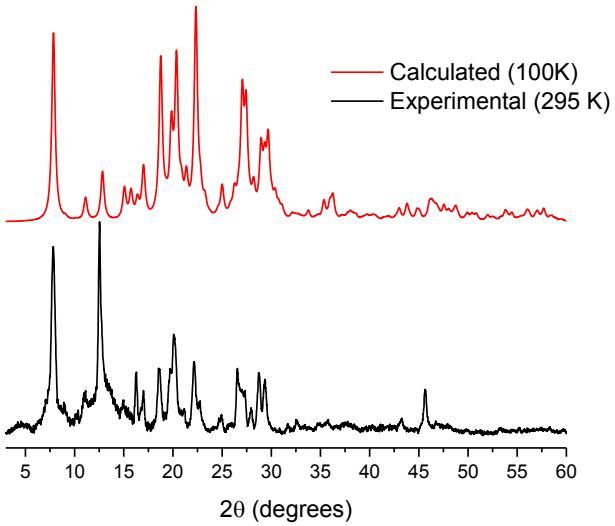

Figure S9. Comparison of experimental and calculated X-ray powder diffraction patterns of the co-crystals of triptycenetris(thiadiazole) **8** and C_{70}**.** Black: X-ray powder diffraction pattern of a microcrystalline sample of the co-crystals of compound **8** and C_{70} measured at 295 K. Red: Calculated X-ray powder diffraction pattern based on the structure of the co-crystals of compound **8** and C_{70} determined at 100 K.

Additional Crystallographic Details

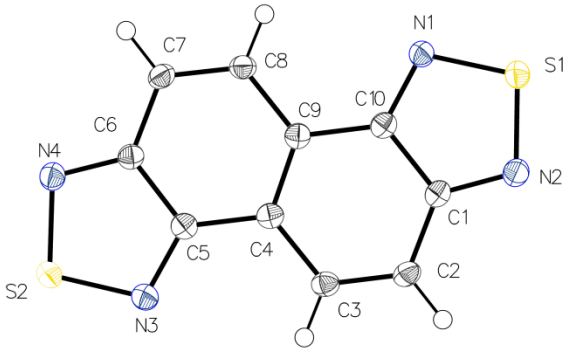

Figure S10. Thermal atomic displacement ellipsoid plot of the structure of crystals of naphthobis(thiadiazole) **4** grown from THF. The ellipsoids of non-hydrogen atoms are drawn at the 50% probability level, and hydrogen atoms are represented by a sphere of arbitrary size.

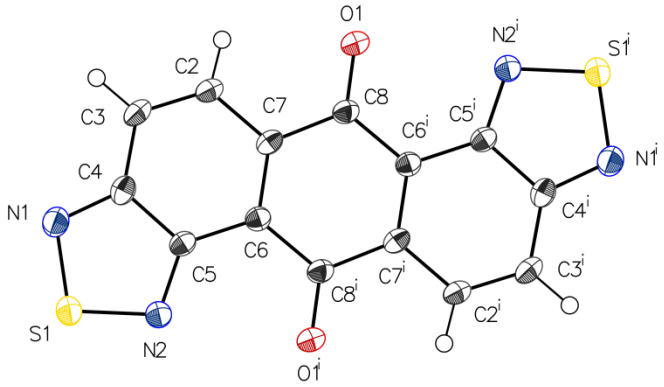

Figure S11. Thermal atomic displacement ellipsoid plot of the structure of crystals of anthraquinonebis(thiadiazole) **5** grown from 1,2-dichlorobenzene. The ellipsoids of non-hydrogen atoms are drawn at the 50% probability level, and hydrogen atoms are represented by a sphere of arbitrary size. Symmetry code (i): 1-x, 2-y, 2-z.

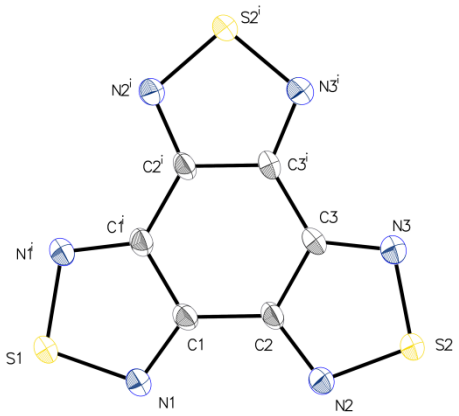

Figure S12. Thermal atomic displacement ellipsoid plot of the structure of crystals of benzotris(thiadiazole) **6** grown from DMF. The ellipsoids of non-hydrogen atoms are drawn at the 50% probability level, and hydrogen atoms are represented by a sphere of arbitrary size. Symmetry code (i): 1-x, y, z.

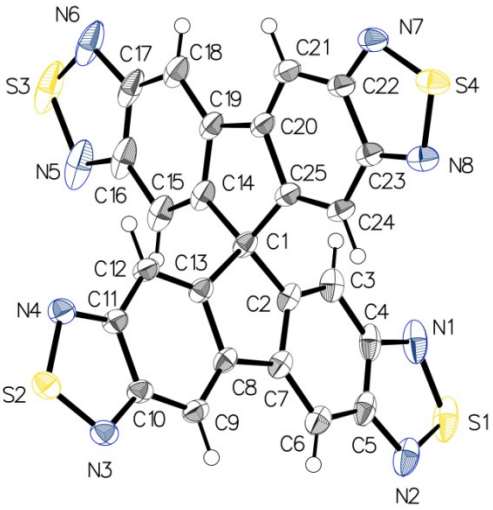

Figure S13. Thermal atomic displacement ellipsoid plot of the structure of crystals of spirobifluorenetetrakis(thiadiazole) **7** grown from mesitylene/MeOH. The ellipsoids of non-hydrogen atoms are drawn at the 50% probability level, and hydrogen atoms are represented by a sphere of arbitrary size.

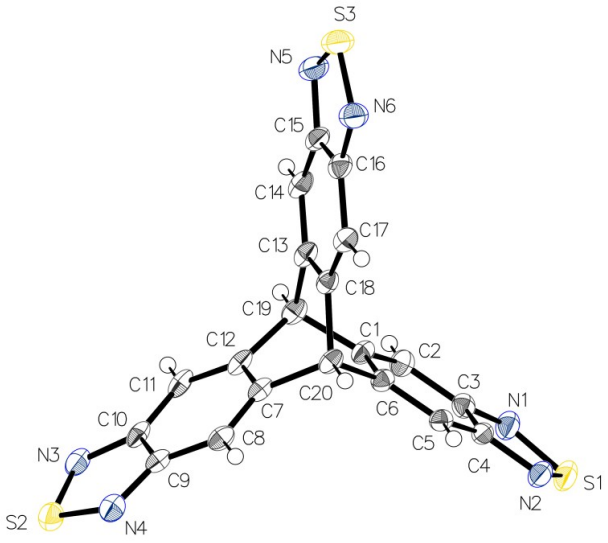

Figure S14. Thermal atomic displacement ellipsoid plot of the structure of unsolvated crystals of triptycenetris(thiadiazole) **8** grown from DMSO. The ellipsoids of non-hydrogen atoms are drawn at the 50% probability level, and hydrogen atoms are represented by a sphere of arbitrary size.

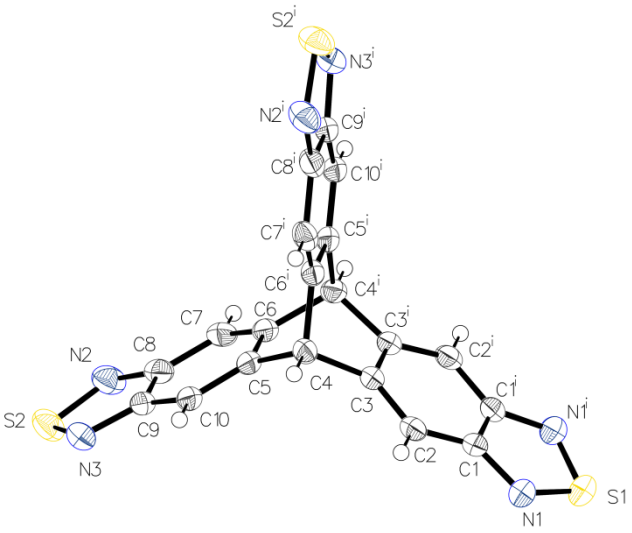

Figure S15. Thermal atomic displacement ellipsoid plot of the structure of crystals of the DMSO solvate of triptycenetris(thiadiazole) **8** grown from DMSO. The ellipsoids of non-hydrogen atoms are drawn at the 50% probability level, and hydrogen atoms are represented by a sphere of arbitrary size. Symmetry code (i): x, 3/2-y, 5/4-z.

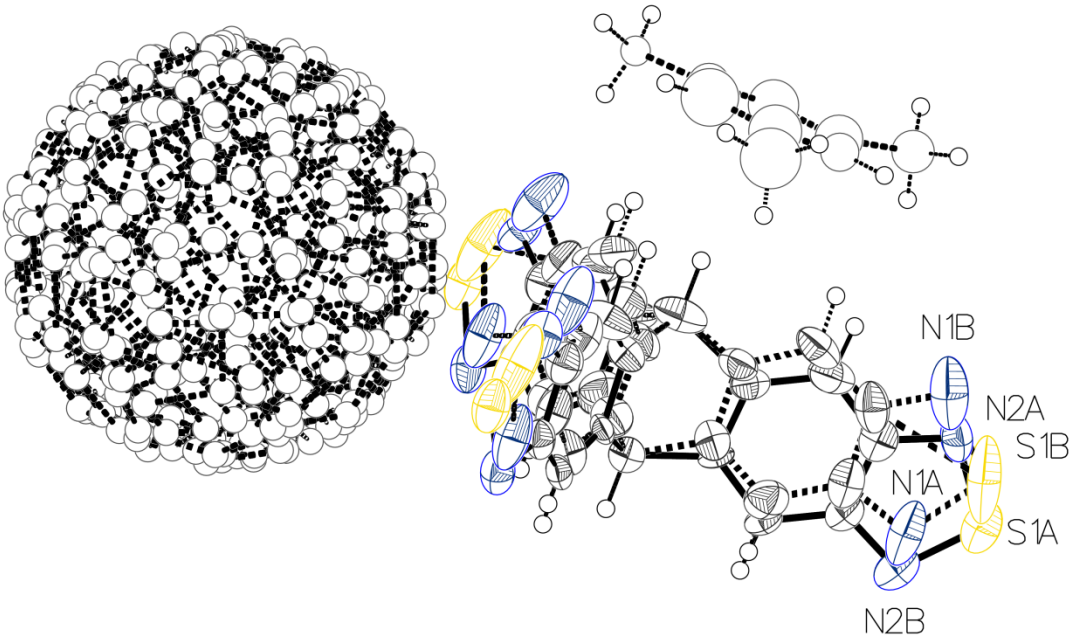

Figure S16. Thermal atomic displacement ellipsoid plot of the partial structure of co-crystals of of triptycenetris(thiadiazole) **8** and C_{60} grown from mesitylene. The ellipsoids of non-hydrogen atoms are drawn at the 50% probability level. Disordered atoms of C_{60} and guest molecules are represented by a sphere scaled at 50% of the probability level of the isotropic atomic displacement parameters. Hydrogen atoms are represented by a sphere of arbitrary size.

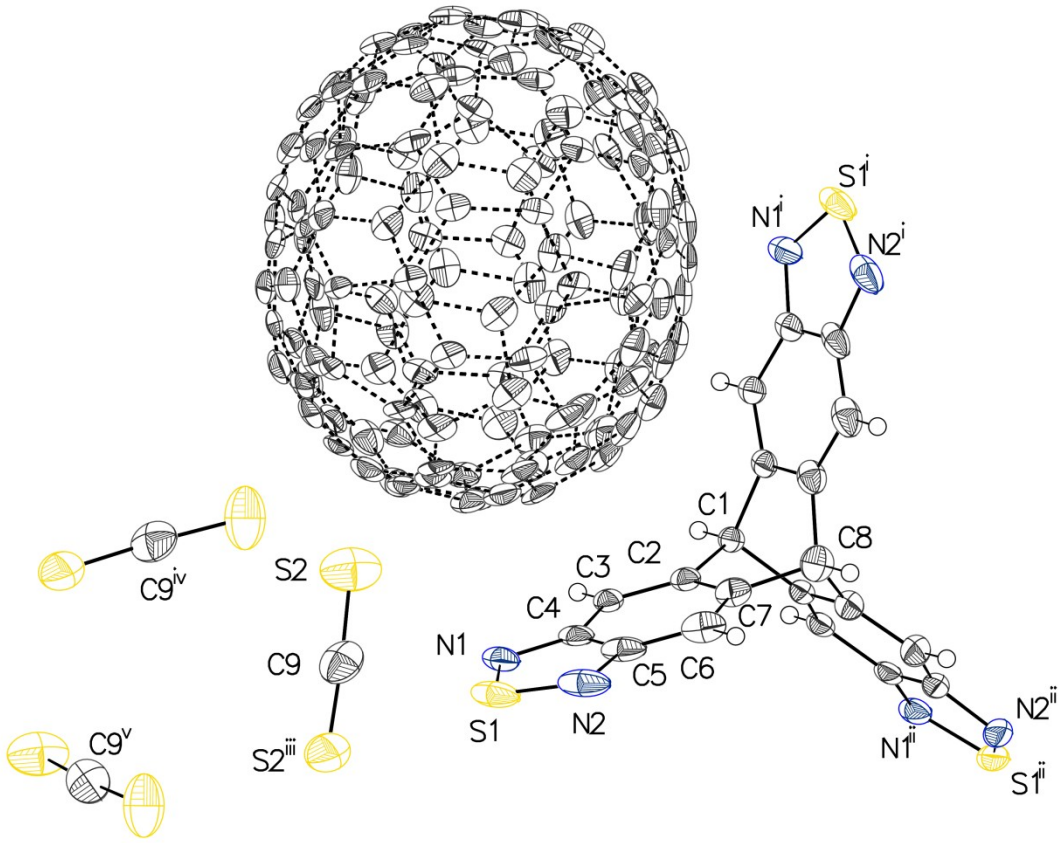

Figure S17. Thermal atomic displacement ellipsoid plot of the partial structure of co-crystals of triptycenetris(thiadiazole) **8** and C_{70} grown from CS_2. The ellipsoids of non-hydrogen atoms are drawn at the 50% probability level, and hydrogen atoms are represented by a sphere of arbitrary size. Symmetry code (i): y, z, x (ii): z, x, y (iii): ½+y, z, ½-x; (iv): ½-y, -z, ½+x; (v): ½+z, ½-x, -y.

Reference

1. Macrae, C. F.; Edgington, P. R.; McCabe, P.; Pidcock, E.; Shields, G. P.; Taylor, R.; Towler, M.; van de Streek, J. *J. Appl. Crystallogr.* **2006***, 39*, 453-457.

Annexe B

Informations supplémentaires

Chapitre 3

Synthèse de sels de naphtalènetétramine

Supporting Information

Synthesis of Salts of 1,2,5,6- and 1,4,5,8-Naphthalenetetramine

Sophie Langis-Barsetti, Thierry Maris, and James D. Wuest*

Contents Page

Instrumentation

NMR spectra were recorded at 25 °C using a spectrometer operating at 400 MHz for ^{1}H NMR spectra and at 100 MHz for ^{13}C NMR spectra. Chemical shifts are reported in parts per million relative to tetramethylsilane, with the signal of residual undeuterated solvent used as an internal standard.

The structure of crystals of bis(4-methylbenzenesulfonamide) **1b** was analyzed at 100 K, using a diffractometer equipped with a Cu microfocus source (λ = 1.54178 Å). Data for crystals of bis(benzyl carbamate) **2k** were collected at 150 K using a diffractometer equipped with a Cu rotating anode generator. The structures of compounds **5** and **6** were analyzed at 150 K using a Bruker Venture Metaljet diffractometer equipped with a liquid Ga jet source generator (λ = 1.34138 Å). Frame integration was performed using *SAINT*,[1] and absorption correction was carried out using *SADABS*[2] within the *APEX2* suite of software.[1]

Structures were solved by direct methods using *SHELXS*[3] for compounds **1b** and **2k,** and *SHELXT*[4] for compounds **5** and **6**. Refinements were carried out using *SHELXL2016/6*.[5] All non-hydrogen atoms were refined anisotropically. All hydrogen atoms were placed in ideal positions and defined as riding atoms, except for the hydrogen atom bonded to nitrogen in bis(4-methylbenzenesulfonamide) **1b**, which was located from the difference Fourier map and fully refined. Parts of bis(4-methylbenzenesulfonamide) **1b** and the THF solvate of compound **6** proved to be disordered and were refined over two orientations with distances and anisotropic atomic displacement parameters refined using proper restraints.

CCDC 1518001, 1518002, 1550607, and 1550608 contain the supplementary crystallographic data. These data can be obtained free of charge from the Cambridge Crystallographic Data Centre via www.ccdc.cam.ac.uk/data_request/cif.

NMR Spectra

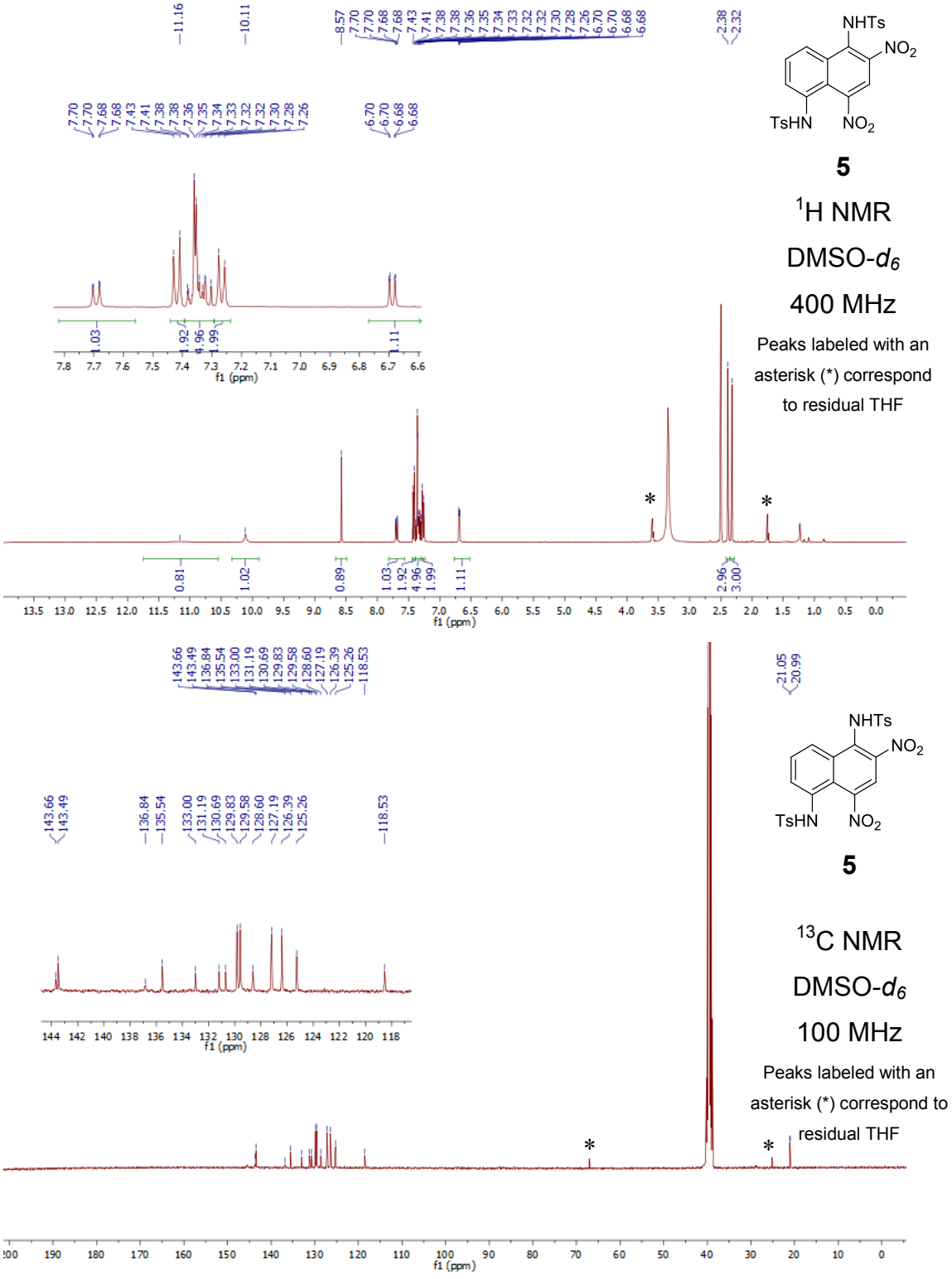

Figure S1. ^{1}H and ^{13}C NMR spectra of compound **5**.

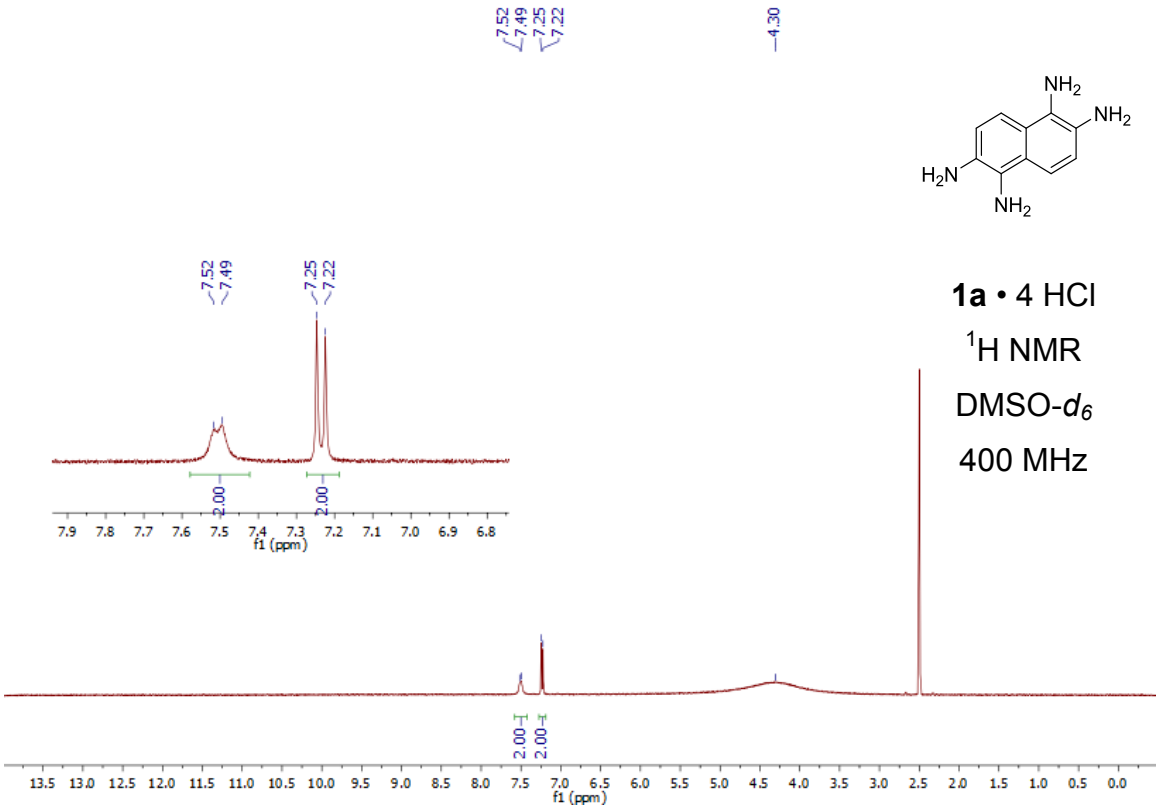

Figure S2. ^{1}H NMR spectrum of compound **1a** • 4 HCl.

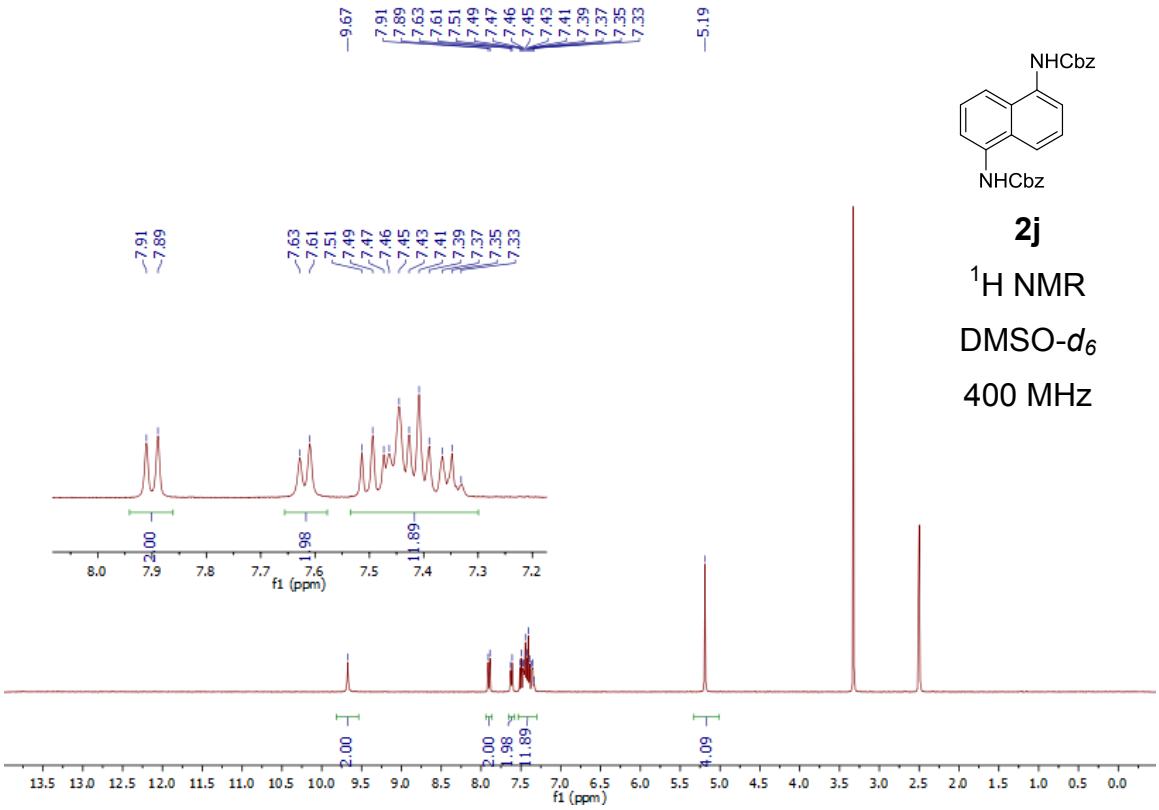

Figure S3. ^{1}H NMR spectrum of compound **2j**.

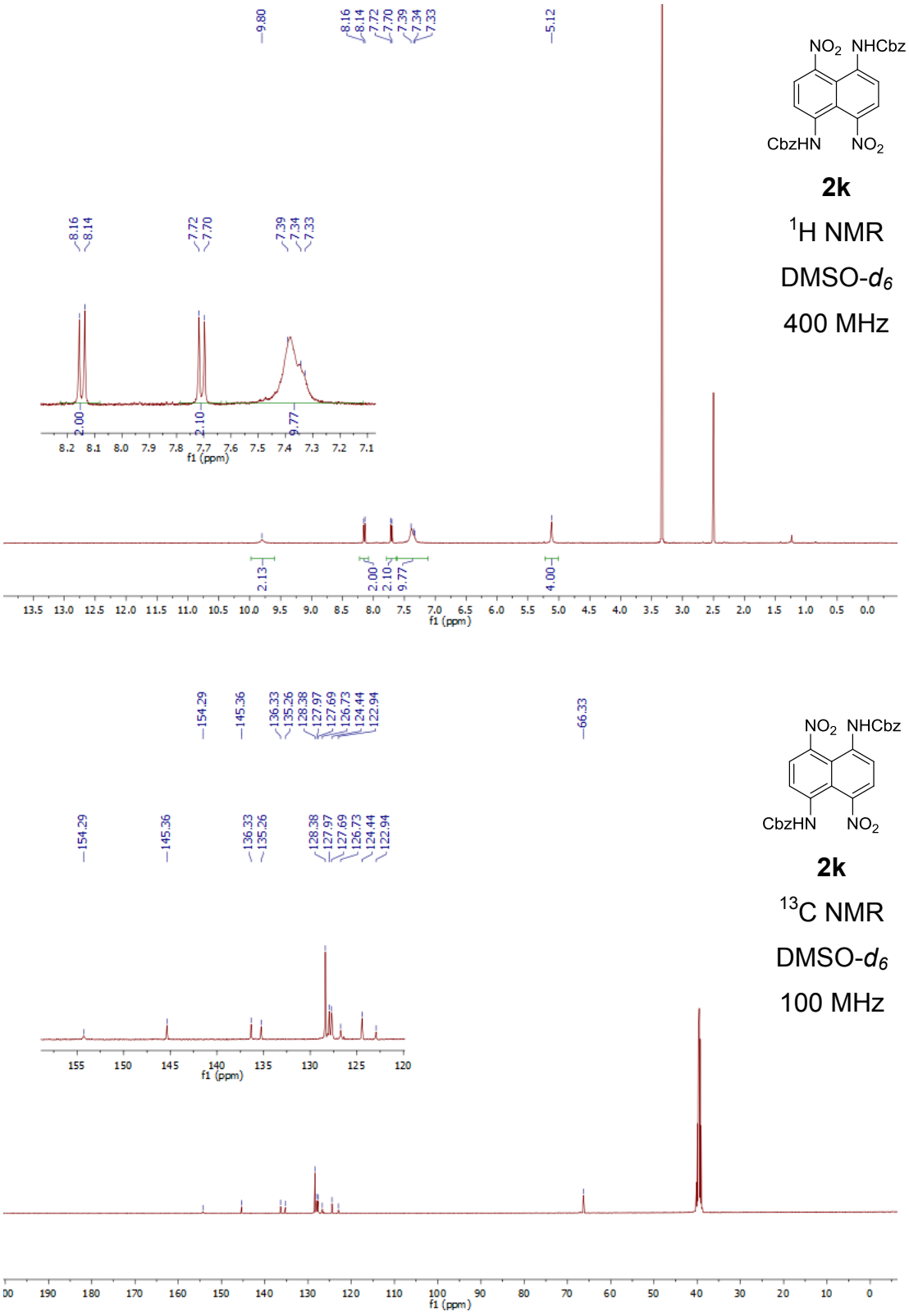

Figure S4. ^{1}H and ^{13}C NMR spectra of compound **2k**.

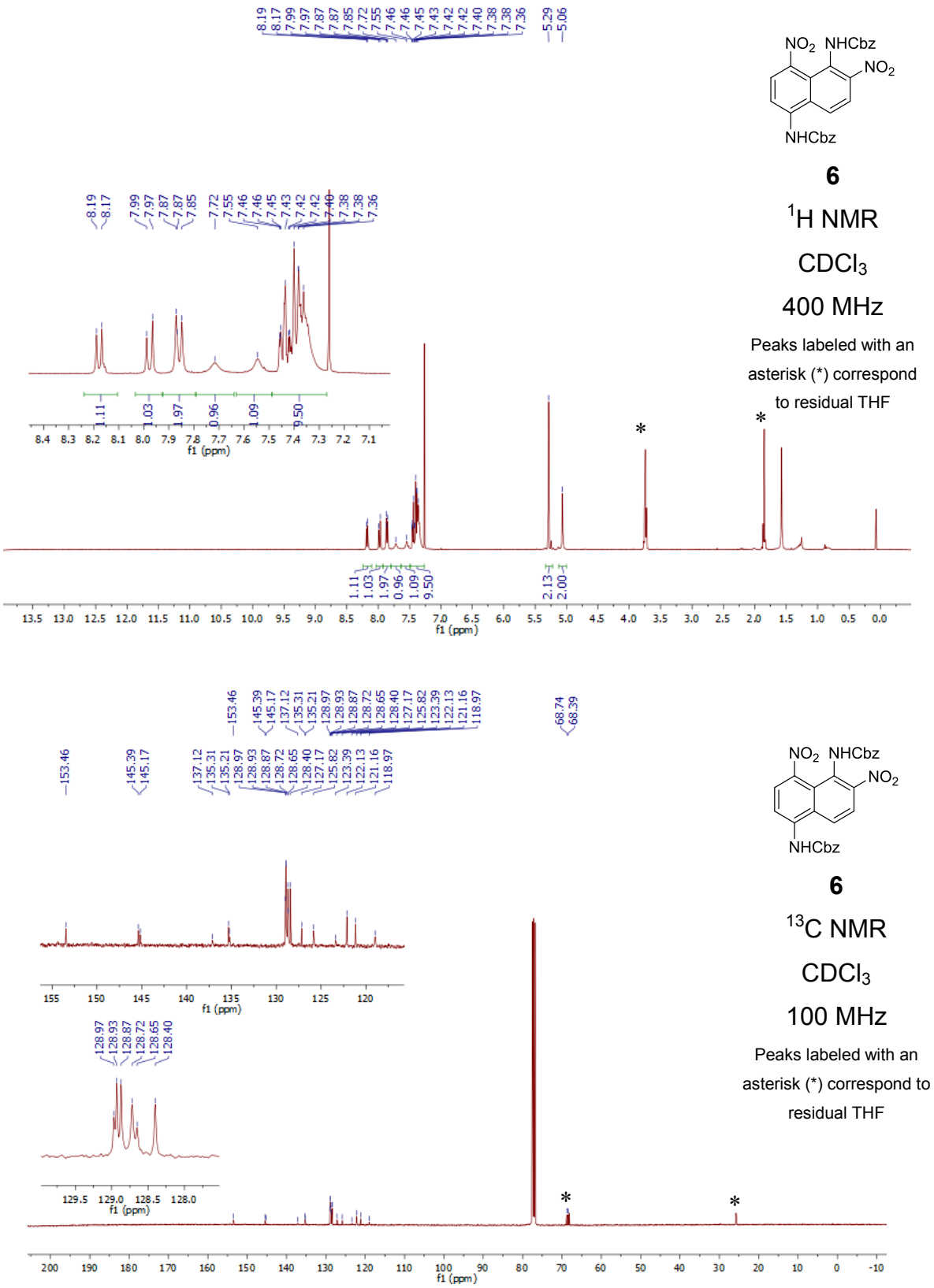

Figure S5. ^{1}H and ^{13}C NMR spectra of compound **6**.

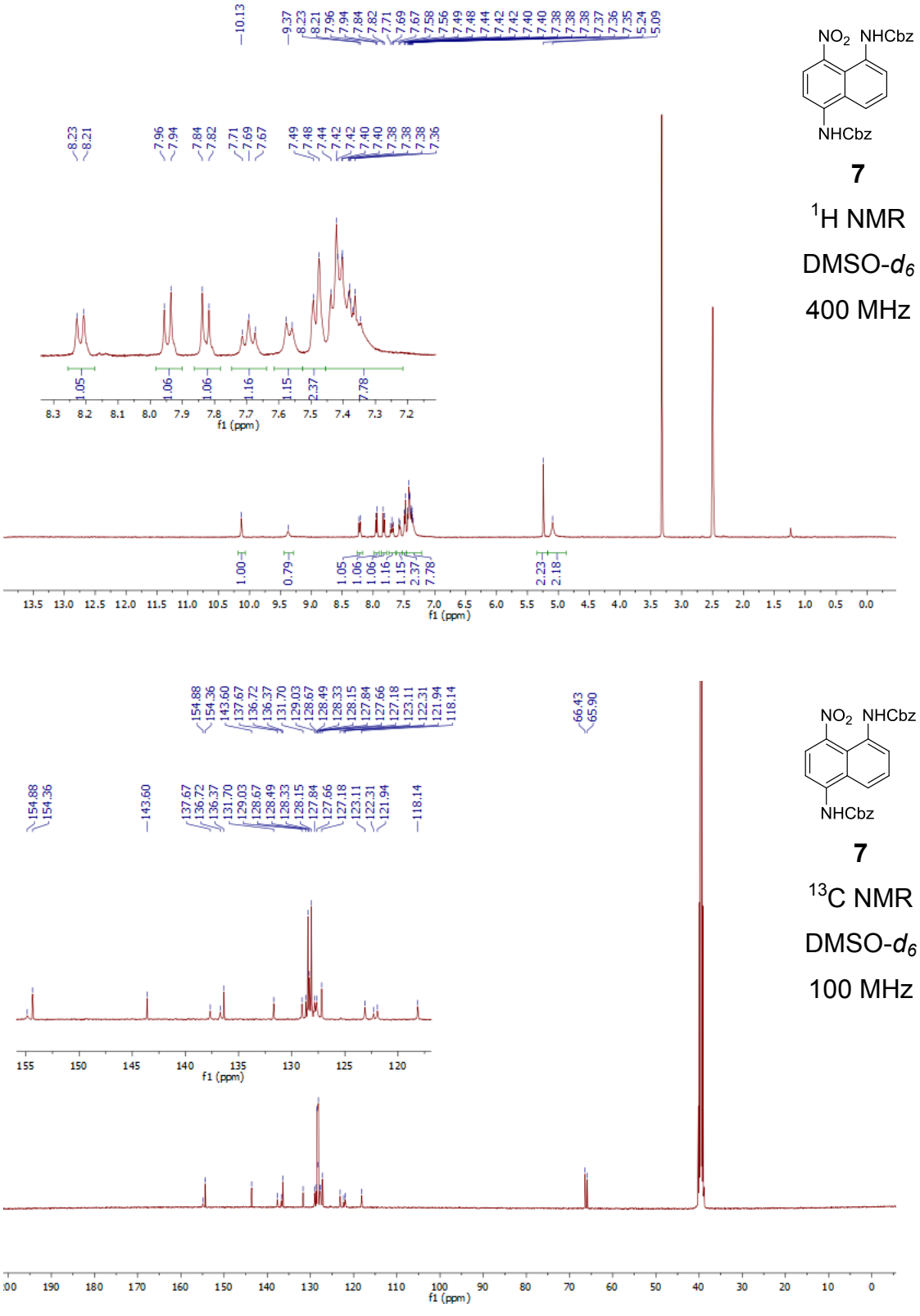

Figure S6. ^{1}H and ^{13}C NMR spectra of compound **7**.

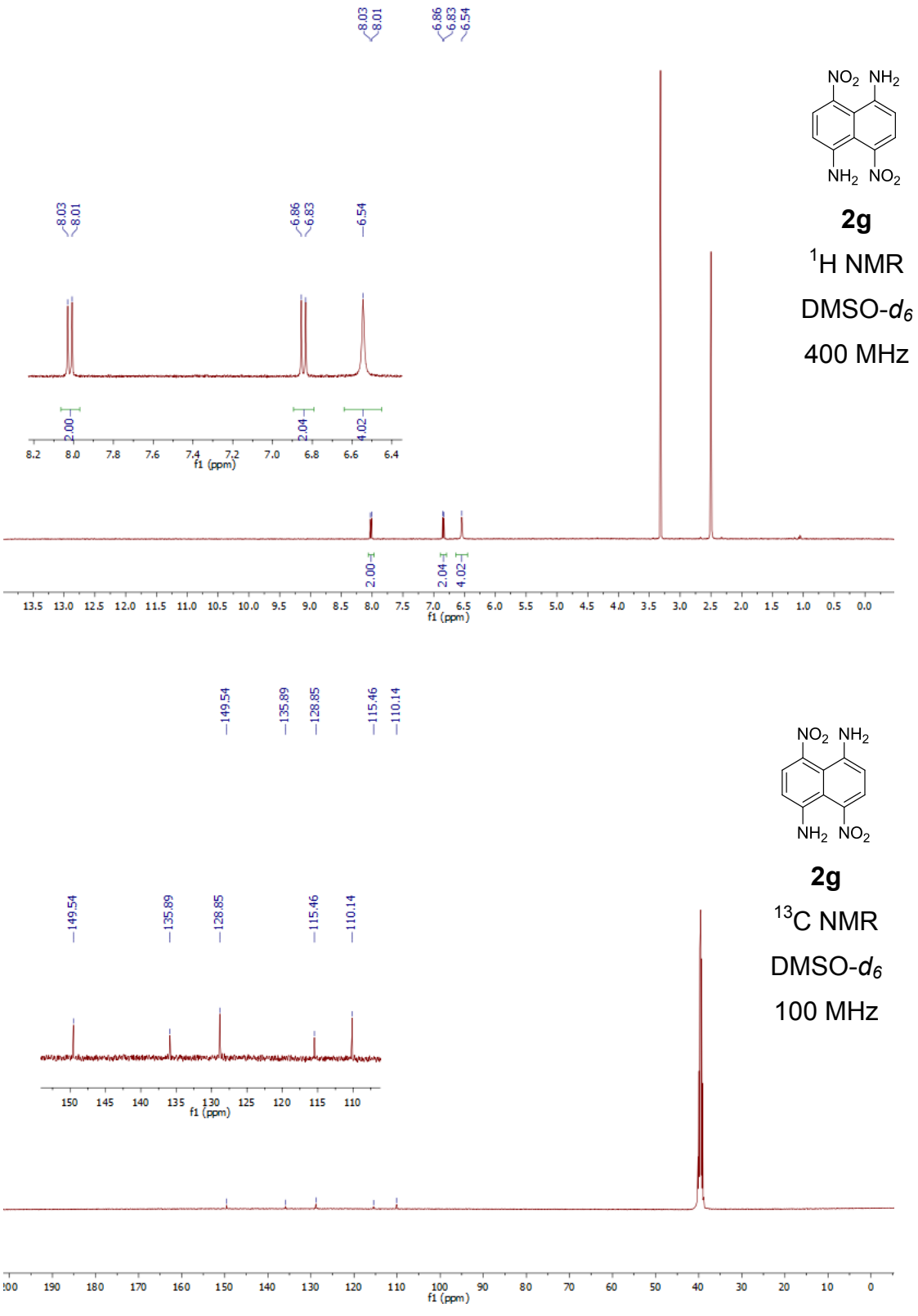

Figure S7. ^{1}H and ^{13}C NMR spectra of compound **2g**.

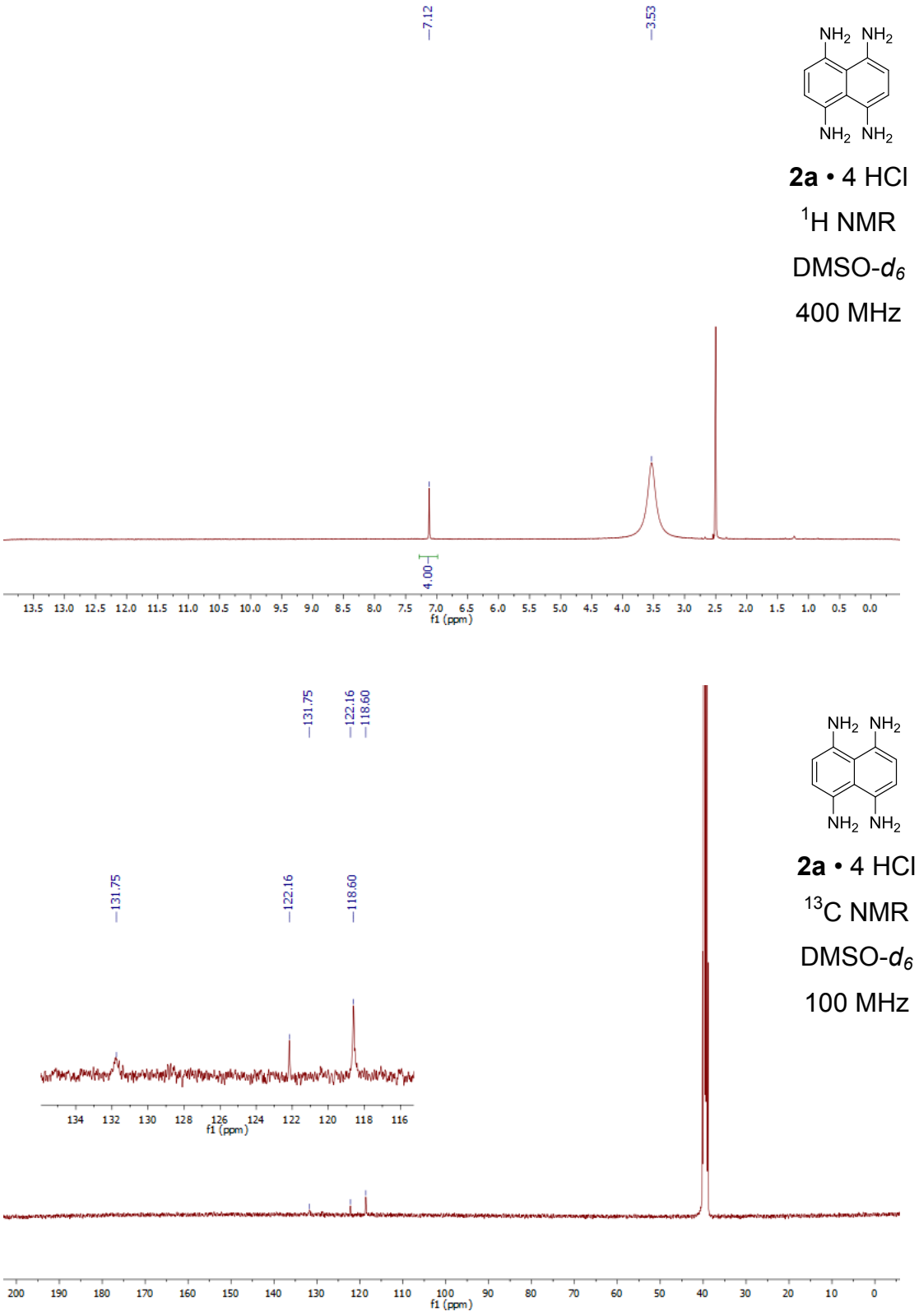

Figure S8. ^{1}H and ^{13}C NMR spectra of compound **2a** • 4 HCl.

Thermogravimetric Analysis

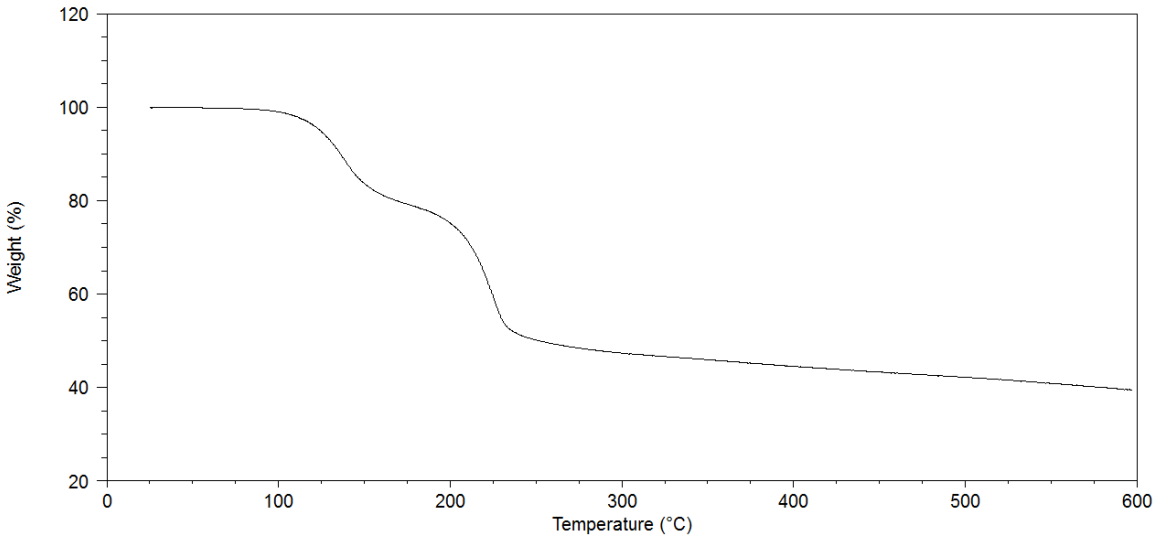

Figure S9. Thermogravimetric analysis of compound **2a** • 4 HCl. The weight loss in the range 100–150 °C corresponds to the loss of two equivalents of HCl.

Additional Crystallographic Details

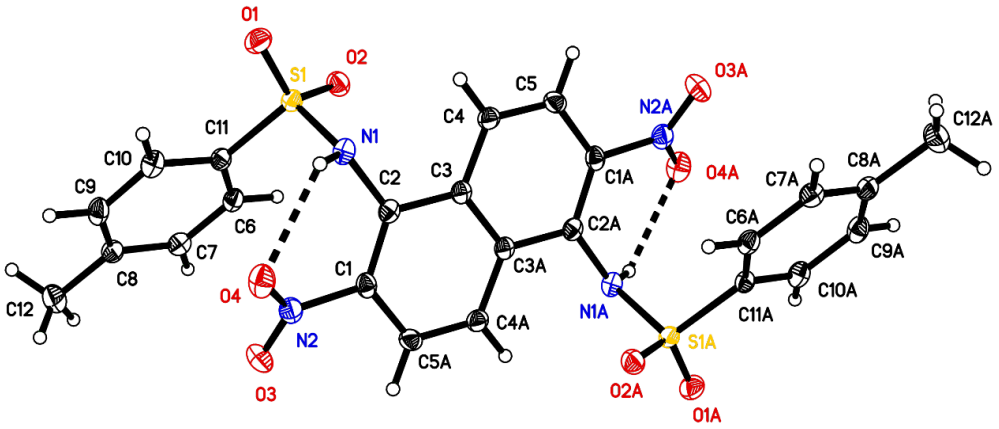

Figure S10. Thermal atomic displacement ellipsoid plot of the partial structure of bis(4-methylbenzenesulfonamide) **1b**, with intramolecular hydrogen bonds shown as black dotted lines. The ellipsoids of non-hydrogen atoms are drawn at the 50% probability level, and hydrogen atoms are represented by a sphere of arbitrary size. Atoms labeled with the suffix A are generated by the symmetry operation 1-*x*, -*y*, 1-*z*.

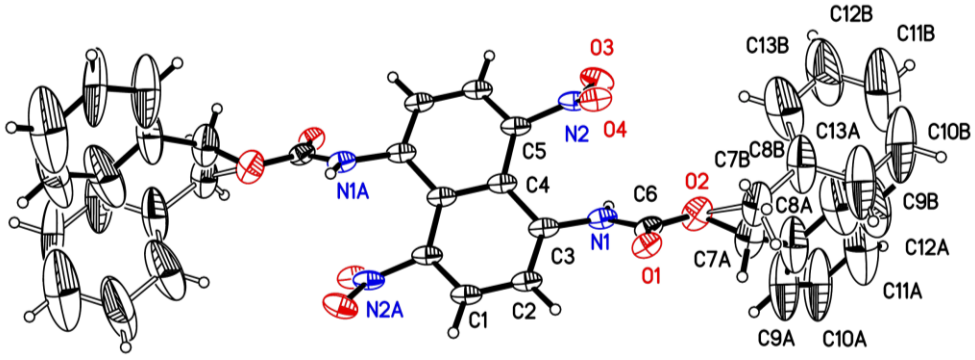

Figure S11. Thermal atomic displacement ellipsoid plot of the partial structure of bis(benzyl carbamate) **2k.** The ellipsoids of non-hydrogen atoms are drawn at the 50% probability level, and hydrogen atoms are represented by a sphere of arbitrary size. Atoms from the different parts of the disordered phenyl groups are labeled with the suffix A and B. The second half of the molecule is generated by the symmetry operation 1-*x*, 1-*y*, 1-*z*.

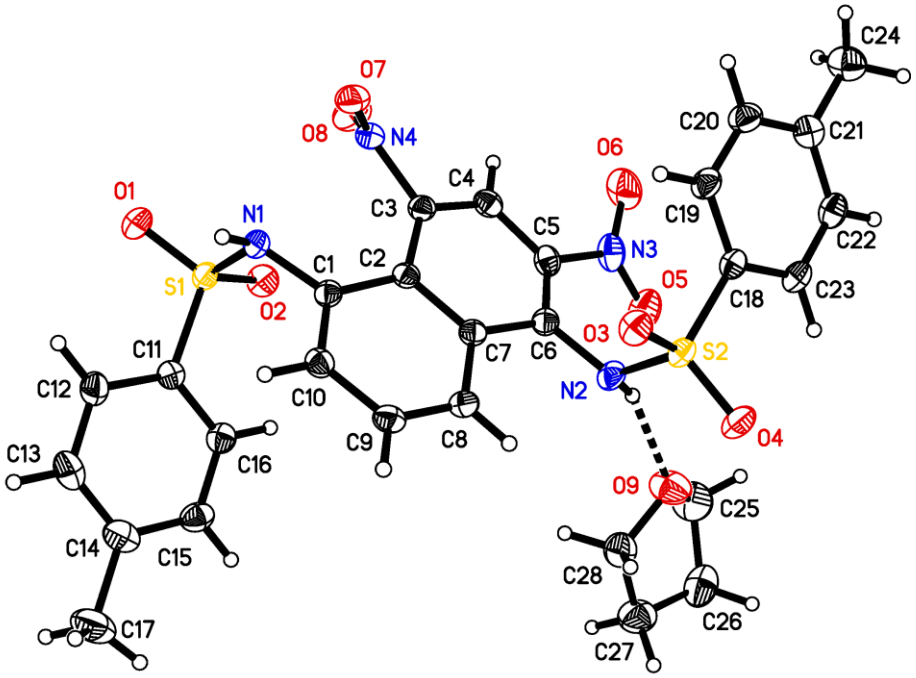

Figure S12. Thermal atomic displacement ellipsoid plot of the partial structure of crystals of solvate **5** • 1 THF grown from THF, with an intramolecular hydrogen bond shown as a black dotted line. The ellipsoids of non-hydrogen atoms are drawn at the 50% probability level, and hydrogen atoms are represented by a sphere of arbitrary size.

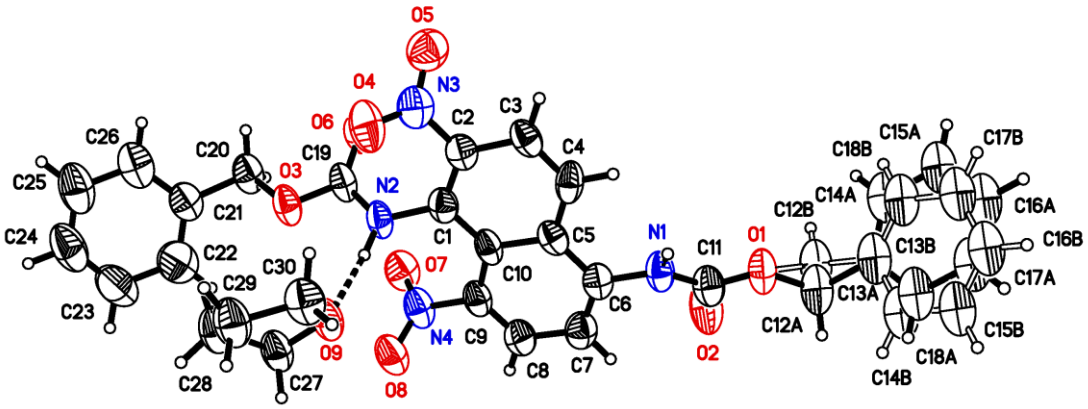

Figure S13. Thermal atomic displacement ellipsoid plot of the partial structure of crystals of the 1:1 THF solvate of compound **6,** with an intramolecular hydrogen bond shown as a black dotted line. The ellipsoids of non-hydrogen atoms are drawn at the 50% probability level, and hydrogen atoms are represented by a sphere of arbitrary size. Atoms from the different parts of the disordered groups are labeled with the suffixes A and B.

References

1. Bruker, 2014. APEX2 and SAINT. Bruker AXS Inc. Madison, Wisconsin, USA.
2. Krause, L.; Herbst-Irmer, R.; Sheldrick, G. M.; Stalke, D. *J. Appl. Crystallogr.* **2015**, *48*, 3–10.
3. Sheldrick, G. M. *Acta Crystallogr*. **2008**, *A64*, 112–122.
4. Sheldrick, G. M. *Acta Crystallogr*. **2015**, *A71*, 3–8.
5. Sheldrick, G. M. *Acta Crystallogr*. **2015**, *C71*, 3–8.

Annexe C

Informations supplémentaires

Chapitre 4

Les dérivés quinonoïdes du triptycène : des solides cristallins et perméables pouvant participer à des réactions redox

Supporting Information

Triptycene 1,2-Quinones and Quinols.

Permeable Crystalline Redox-Active Molecular Solids

Sophie Langis-Barsetti, Thierry Maris, and James D. Wuest*

Contents

Page

Instrumentation

NMR spectra were recorded at 20 °C, using a spectrometer operating at 400 MHz for ^{1}H NMR spectra and at 100 MHz for ^{13}C NMR spectra. Chemical shifts are reported in parts per million relative to tetramethylsilane, with the signal of residual undeuterated solvent used as an internal standard. Cyclic voltammograms were obtained using solutions in dry N_2-sparged dimethylformamide (DMF) or in DMF containing 1% acetic acid, with tetrabutylammonium hexafluorophosphate (TBAP) as the supporting electrolyte (0.1 M). The working electrode was a glassy carbon electrode, the counter-electrode was a Pt wire, and the pseudo-reference electrode was an Ag wire. The concentration of the compounds examined was ~1 mM, and ferrocene/ferrocenium was used as an internal standard. The concentrations of the solutions used to record UV-vis absorption and emission spectra were between 2×10^{-5} M and 4×10^{-5} M.

Solid-State Redox Reactions

Figure S1 shows how exposure of dark purple crystals of triptycene(monoquinone) **3** to vapors of hydrazine hydrate leads to reduction and transformation into colorless crystalline triptycene(triscatechol) **4**. The crystals retained their initial morphology (Figure S1), showed birefringence, and yielded a well-resolved X-ray powder diffraction pattern. All other solid-state redox experiments were carried in a similar way, and the identity of the products was confirmed by recording their ^{1}H NMR spectra, which matched those of authentic samples. Figure S2 shows the X-ray powder diffraction pattern of the crystalline product of oxidation obtained by exposing crystalline triscatechol **4** to vapors of HNO_3. Representative NMR spectra are shown in Figures S3 and S4. All solid-state redox reactions take place without the formation of other significant products, and the reactions can be reversed by adding the appropriate oxidant or reductant.

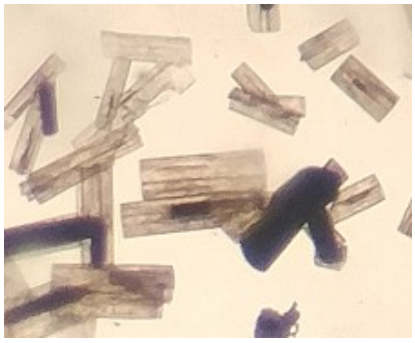

Figure S1. Micrograph showing colorless crystalline triptycene(triscatechol) **4** resulting from the solid-state reduction of crystals of triptycene(monoquinone) **3** caused by exposure to vapors of H_2NNH_2. Note the cracking of crystals along their longest axis.

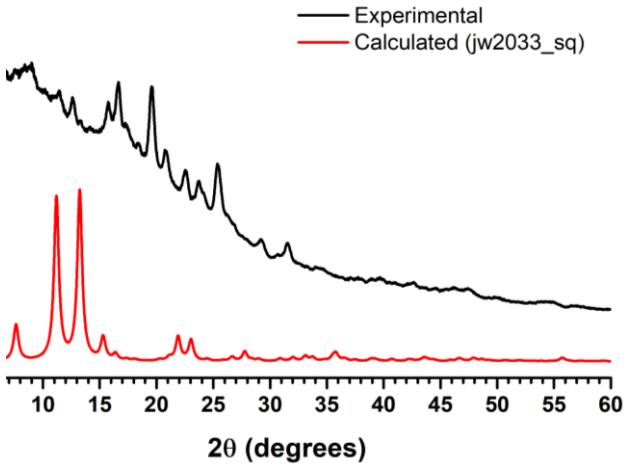

Figure S2. Comparison of the X-ray powder diffraction pattern (black trace) of a microcrystalline sample of a mixture of triptycenequinones **2** and **3** (produced by the solid-state oxidation of crystals of triscatechol **4**) with the simulated pattern derived from the crystal structure of the Me-THF solvate of compound **4** (red trace). Analysis of the sample by ^{1}H NMR spectroscopy revealed it was composed of 75% of monoquinone **3**, 20% of bisquinone **2**, and 5% of triscatechol **4**.

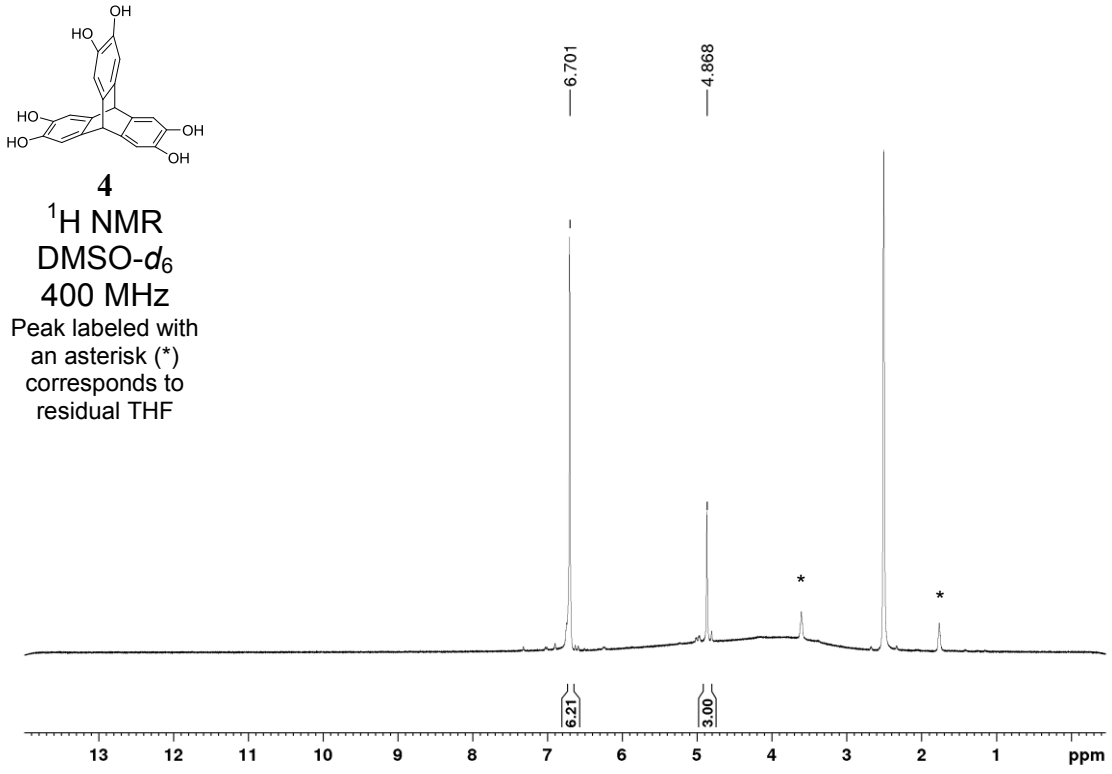

Figure S3. ^{1}H NMR spectrum of a crude sample of triptycene(triscatechol) **4** produced by the solid-state reduction that occurs when crystals of triptycene(monoquinone) **3** are exposed to vapors of hydrazine hydrate.

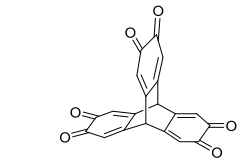

1

^{1}H NMR

DMSO-d_6

400 MHz

Peak labeled with an asterisk (*) corresponds to residual dioxane

Figure S4. ^{1}H NMR spectrum of a crude sample of triptycene(trisquinone) **1** produced by the solid-state oxidation that occurs when crystals of triptycene(triscatechol) **4** are exposed to vapors of HNO_3.

NMR Spectra

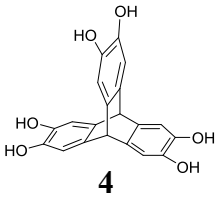

4

^{1}H NMR
DMSO-d_6
400 MHz

Peak labeled with an asterisk (*) corresponds to residual dioxane

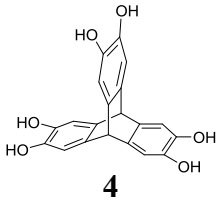

4

^{13}C NMR
DMSO-d_6
100 MHz

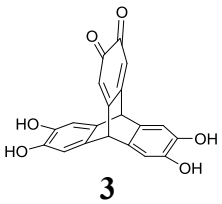

3

^{1}H NMR
DMSO-d_6
400 MHz

Peaks labeled with an asterisk (*) correspond to residual THF

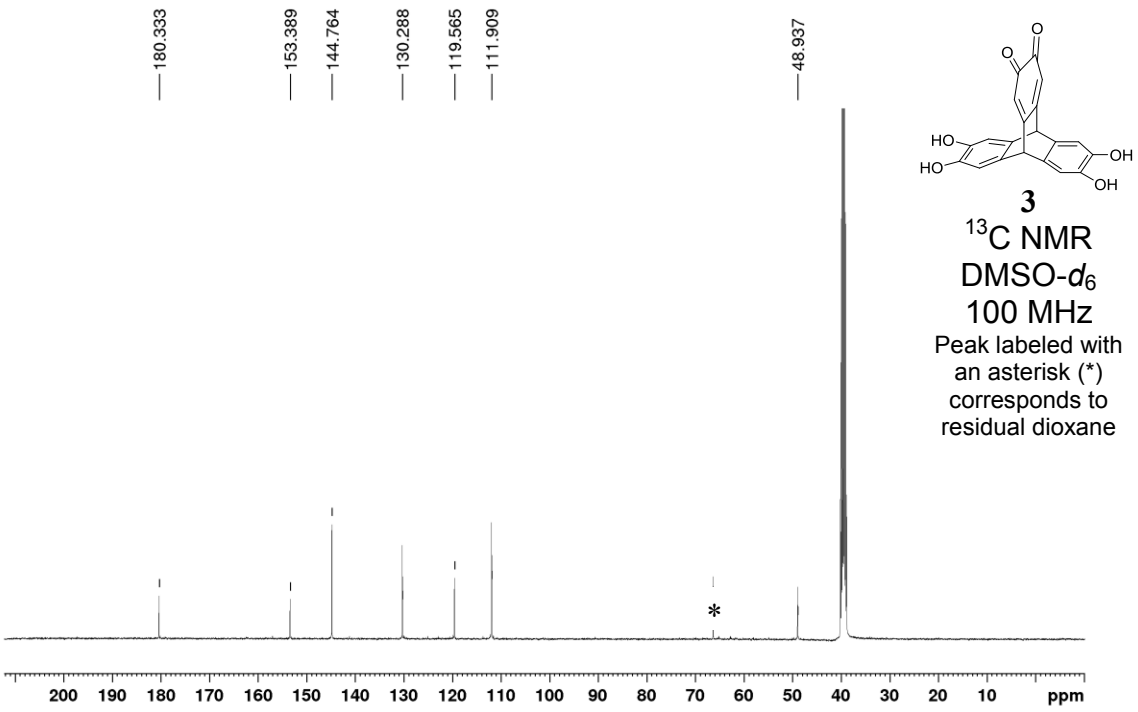

3

^{13}C NMR
DMSO-d_6
100 MHz

Peak labeled with an asterisk (*) corresponds to residual dioxane

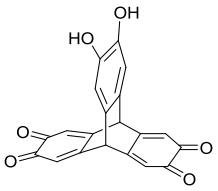

2

^{1}H NMR
DMSO-d_6
400 MHz

Peak labeled with an asterisk (*) corresponds to residual dioxane

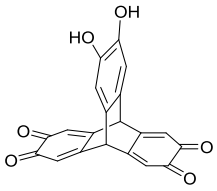

2

^{13}C NMR
DMSO-d_6
100 MHz

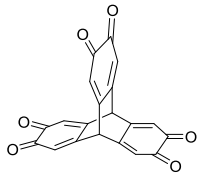

1
^{1}H NMR
DMSO-d_6
400 MHz

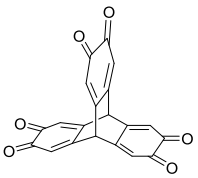

1
^{13}C NMR
DMSO-d_6
100 MHz

Voltammograms

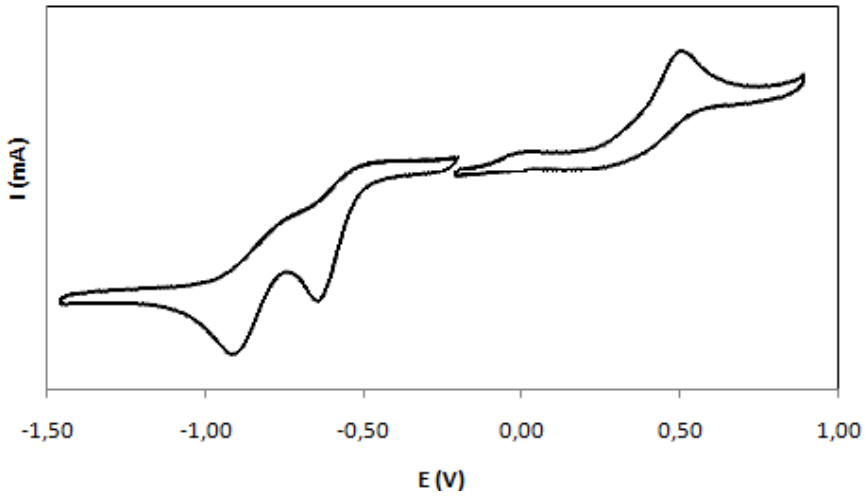

Figure S5. Cyclic voltammogram of triptycene(bisquinone) **2** (0.1 M TBAP in DMF/MeCOOH 1%, scan rate = 100 mV/s). Potentials are reported with respect to the ferrocene/ferrocenium couple.

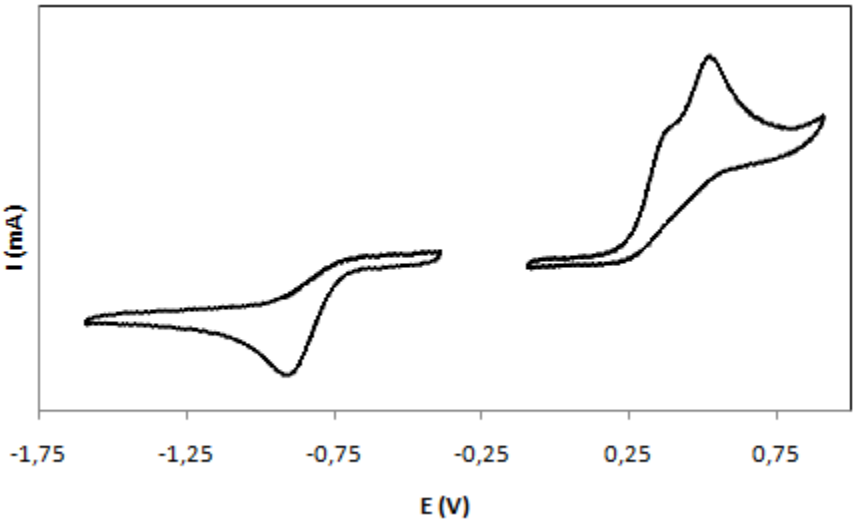

Figure S6. Cyclic voltammogram of triptycene(monoquinone) **3** (0.1 M TBAP in DMF/MeCOOH 1%, scan rate = 100 mV/s). Potentials are reported with respect to the ferrocene/ferrocenium couple.

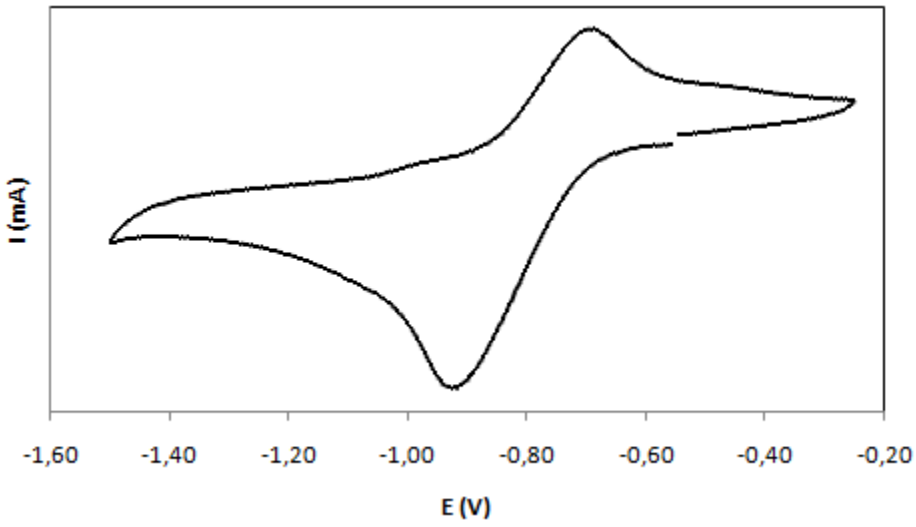

Figure S7. Cyclic voltammogram of 1,2-benzoquinone (0.1 M TBAP in DMF, scan rate = 200 mV/s). Potentials are reported with respect to the ferrocene/ferrocenium couple.

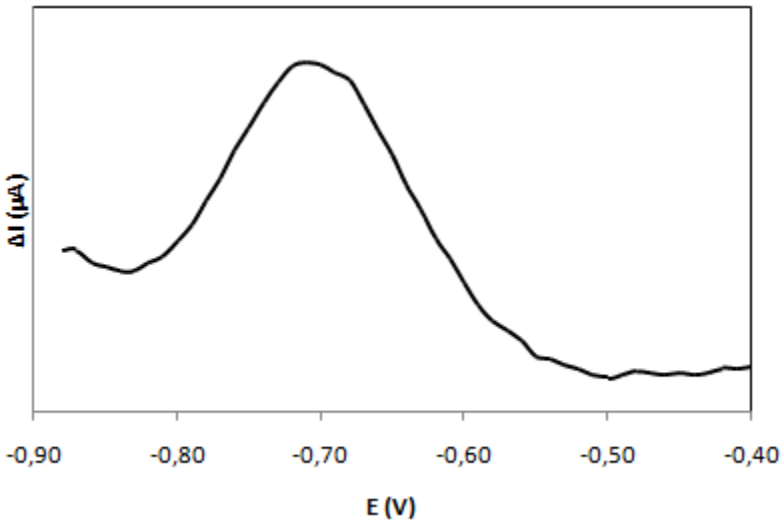

Figure S8. Square-wave voltammogram of 1,2-benzoquinone (0.1 M TBAP in DMF/MeCOOH 1%, scan rate = 100 mV/s). Potentials are reported with respect to the ferrocene/ferrocenium couple.

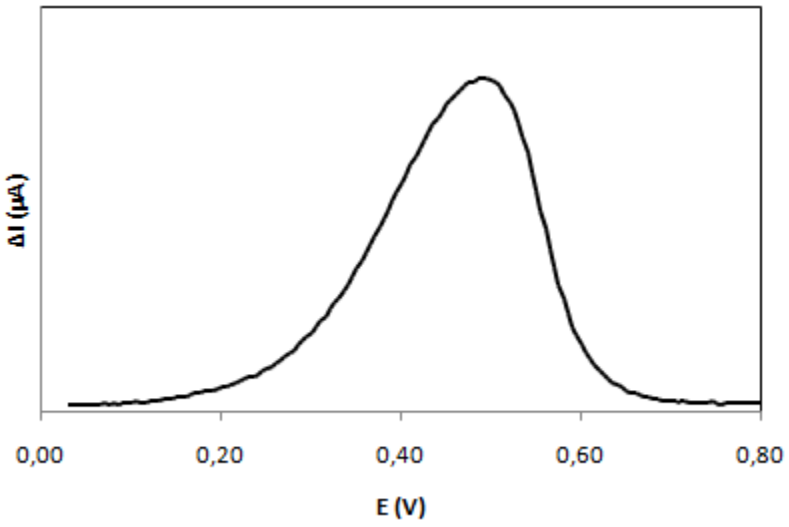

Figure S9. Square-wave voltammogram of catechol (0.1 M TBAP in DMF, scan rate = 100 mV/s). Potentials are reported with respect to the ferrocene/ferrocenium couple.

Absorption and Emission Spectra

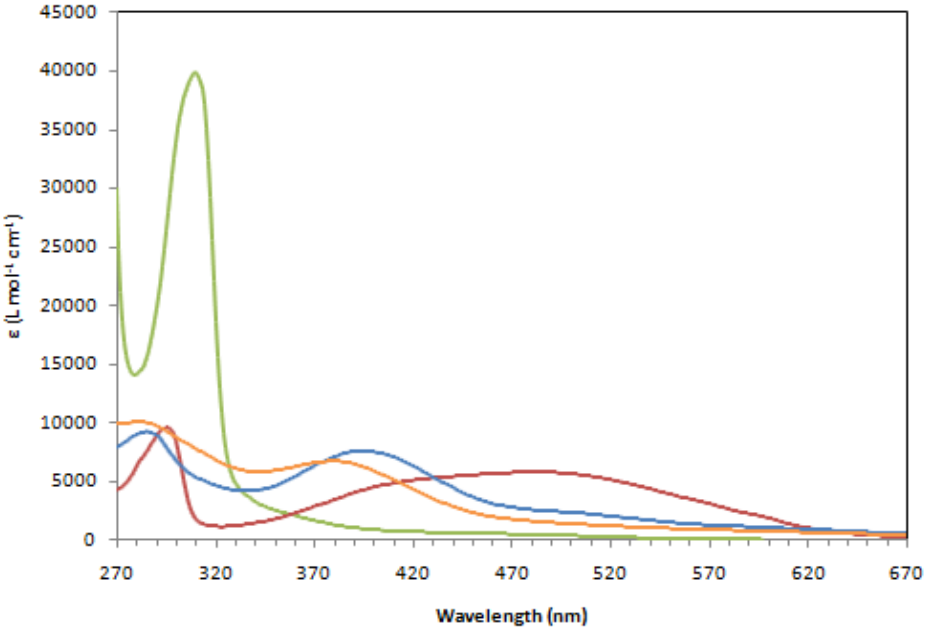

Figure S10. Absorption spectra of solutions of triptycene(trisquinone) **1** (yellow), bisquinone **2** (blue), monoquinone **3** (red), and triscatechol **4** (green) in DMF.

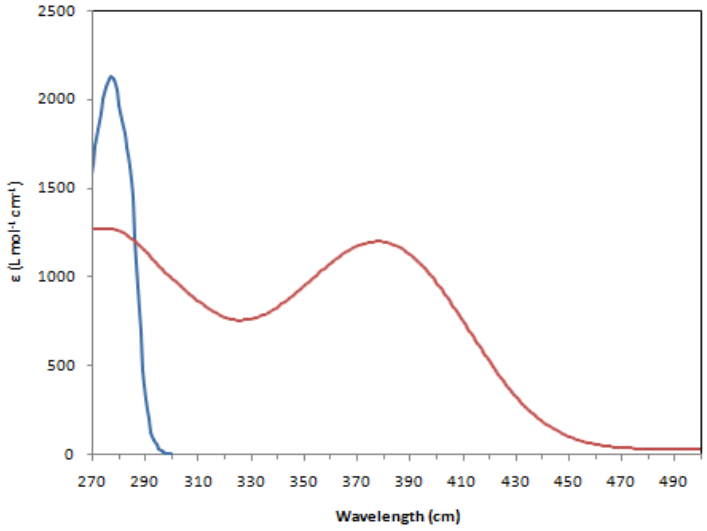

Figure S11. Absorption spectra of solutions of catechol (blue) in MeCN and 1,2-benzo quinone (red) in DMF.

Additional Crystallographic Details

Table S1. Additional Crystallographic Data for Triptycenes **2**–**4**.

Compound	**2 • THF**	**3 • THF**	**4 • 4.5 dioxane**
crystallization medium	THF/hexane	THF/hexane	dioxane
formula	$C_{24}H_{18}O_7$	$C_{24}H_{20}O_7$	$C_{38}H_{50}O_{15}$
crystal system	monoclinic	orthorhombic	triclinic
space group	$P2_1/c$	$Fdd2$	$P\bar{1}$
a (Å)	18.2472(6)	21.3113(8)	11.6237(9)
b (Å)	8.4518(3)	43.3656(17)	13.3004(10)
c (Å)	12.4155(4)	8.4955(3)	13.6633(10)
α (°)	90	90	62.625(3)
β (°)	93.856(2)	90	81.097(4)
γ (°)	90	90	82.543(4)
V (Å^3)	1910.40(11)	7851.3(5)	1849.1(2)
Z	4	16	2
ρ_{calcd} (g cm^{-3})	1.455	1.423	1.341
T (K)	120	100	100
μ (mm^{-1})	0.57	0.562	0.556
$R_1, I > 2\sigma$ (%)	0.0737	0.0535	0.0671
R_1, all data (%)	0.1680	0.1477	0.1431
$\omega R_2, I > 2\sigma$ (%)	0.1010	0.0547	0.1066
ωR_2, all data (%)	0.1853	0.1490	0.1629
no. measured reflections	47522	37484	46841
no. independent reflections	4389	4359	8458
no. observed reflections	3237	4212	5851

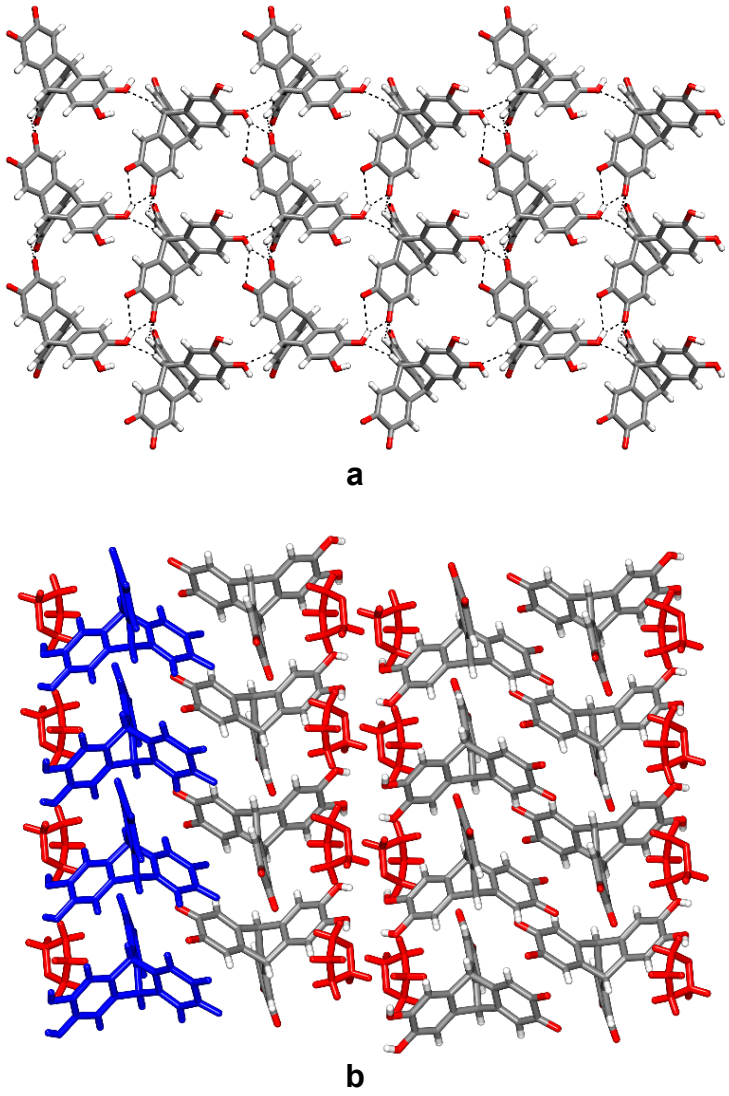

Figure S12. Representations of the structure of crystals of triptycene(bisquinone) **2** grown from THF/hexane. (a) View showing how O-H···O hydrogen bonds and C-H···O interactions link the molecules into sheets. Significant intermolecular interactions are represented by broken lines. (b) View showing (1) how sheets are paired by dipolar interactions between atoms of oxygen and electron-deficient atoms of carbon in quinone units and (2) how paired sheets are separated by layers of included solvent. One individual sheet is highlighted in blue, and molecules of THF are shown in red. Unless otherwise stated, atoms of carbon are shown in gray, atoms of hydrogen in white, and atoms of oxygen in red.

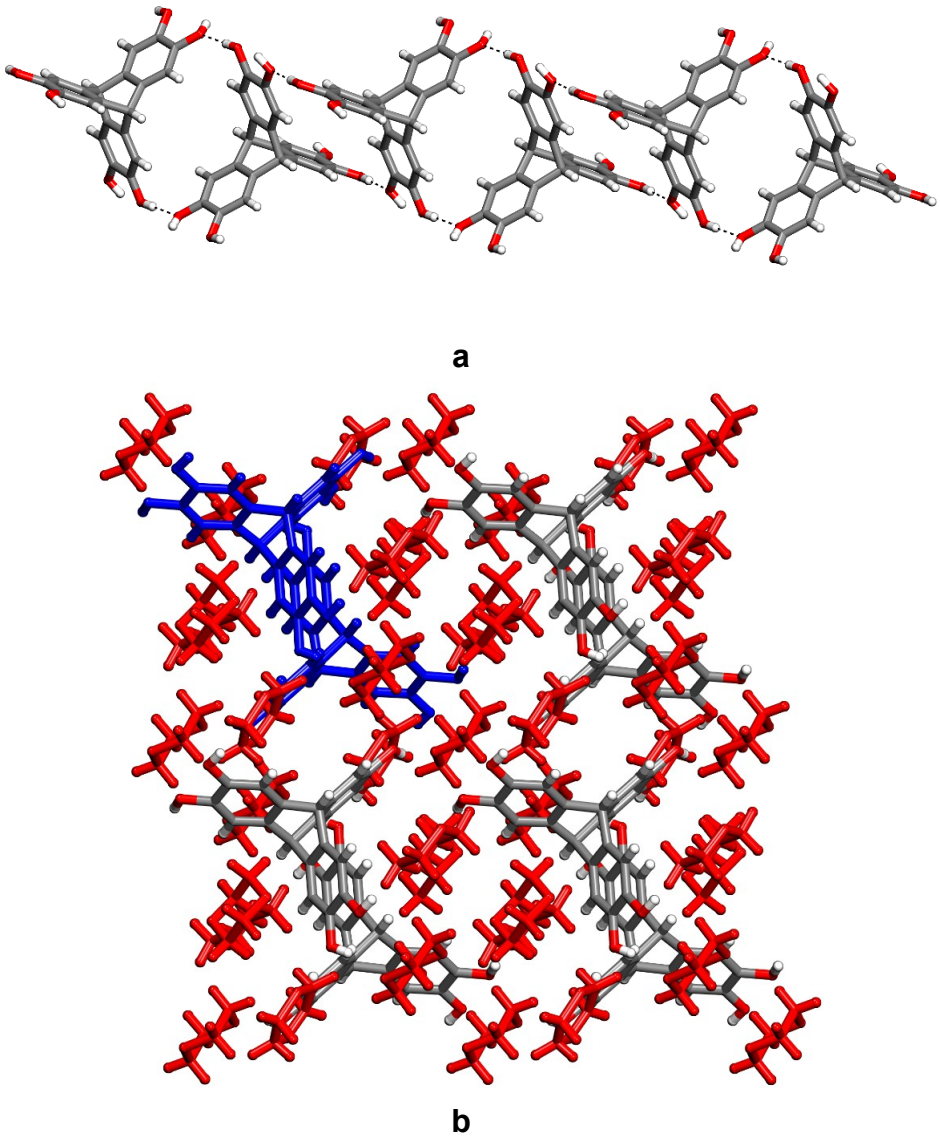

Figure S13. Representations of the structure of crystals of triptycene(triscatechol) **4** grown from dioxane/hexane. (a) View showing how O-H···O hydrogen bonds link the molecules into chains. Significant intermolecular interactions are represented by broken lines. (b) View down the *b*-axis showing how chains are isolated by domains of included solvent. In total, 65% of the volume of the crystal is accessible to guests. One individual chain is highlighted in blue, and molecules of dioxane are shown in red. Unless otherwise stated, atoms of carbon appear in gray, atoms of hydrogen in white, and atoms of oxygen in red.

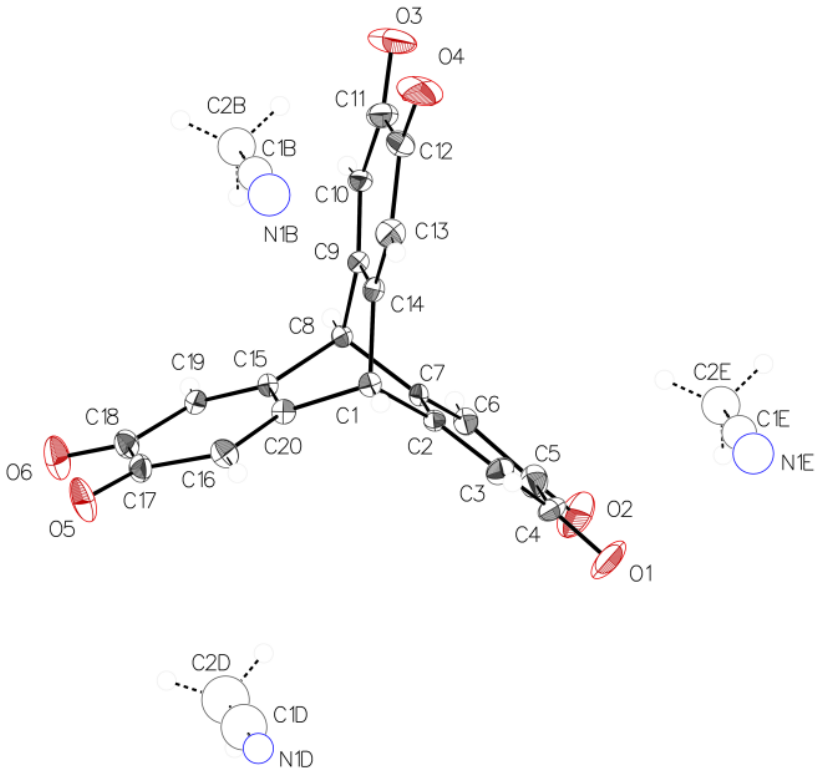

Figure S14. Thermal atomic displacement ellipsoid plot of the structure of crystals of triptycene(trisquinone) **1** grown from DMSO/MeCN. The ellipsoids of non-hydrogen atoms are drawn at the 50% probability level, and hydrogen atoms are represented by a sphere of arbitrary size.

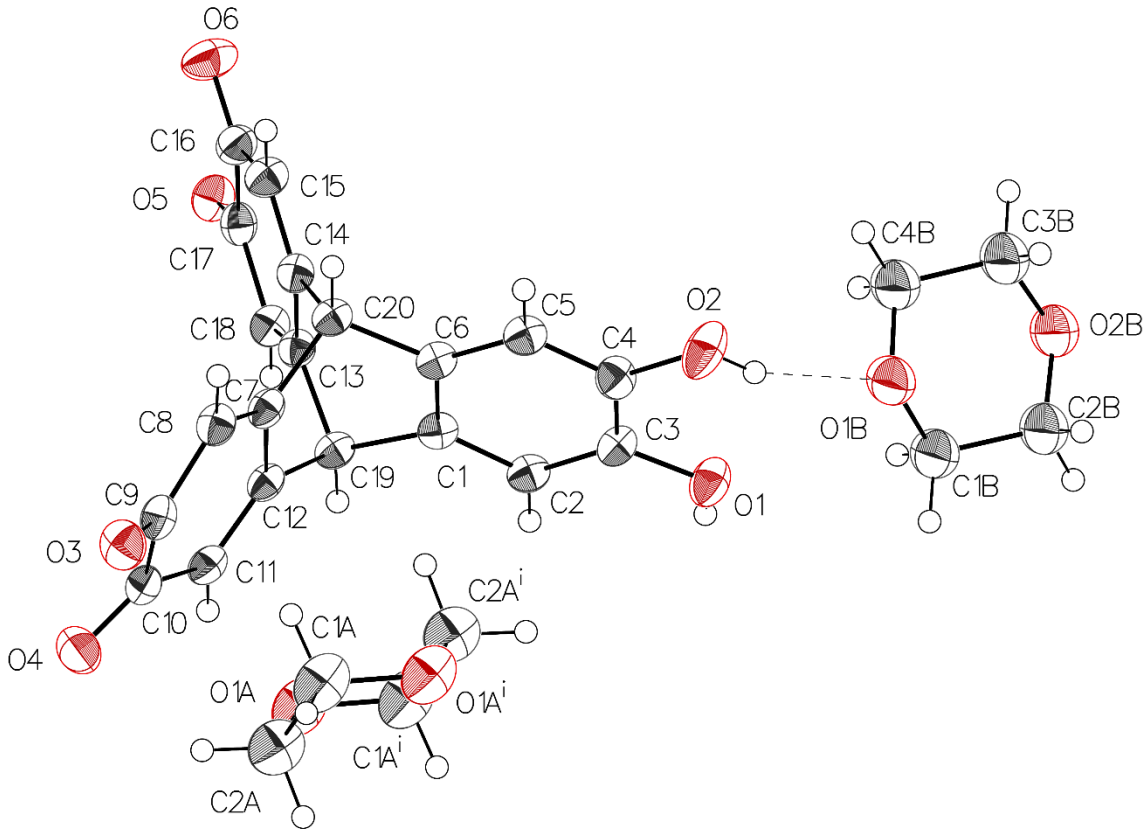

Figure S15. Thermal atomic displacement ellipsoid plot of the structure of crystals of triptycene(bisquinone) **2** grown from dioxane/hexane. The ellipsoids of non-hydrogen atoms are drawn at the 50% probability level, and hydrogen atoms are represented by a sphere of arbitrary size. Only one part of the disordered molecule of dioxane is shown. Symmetry code (i): -x, 2-y, 1-z.

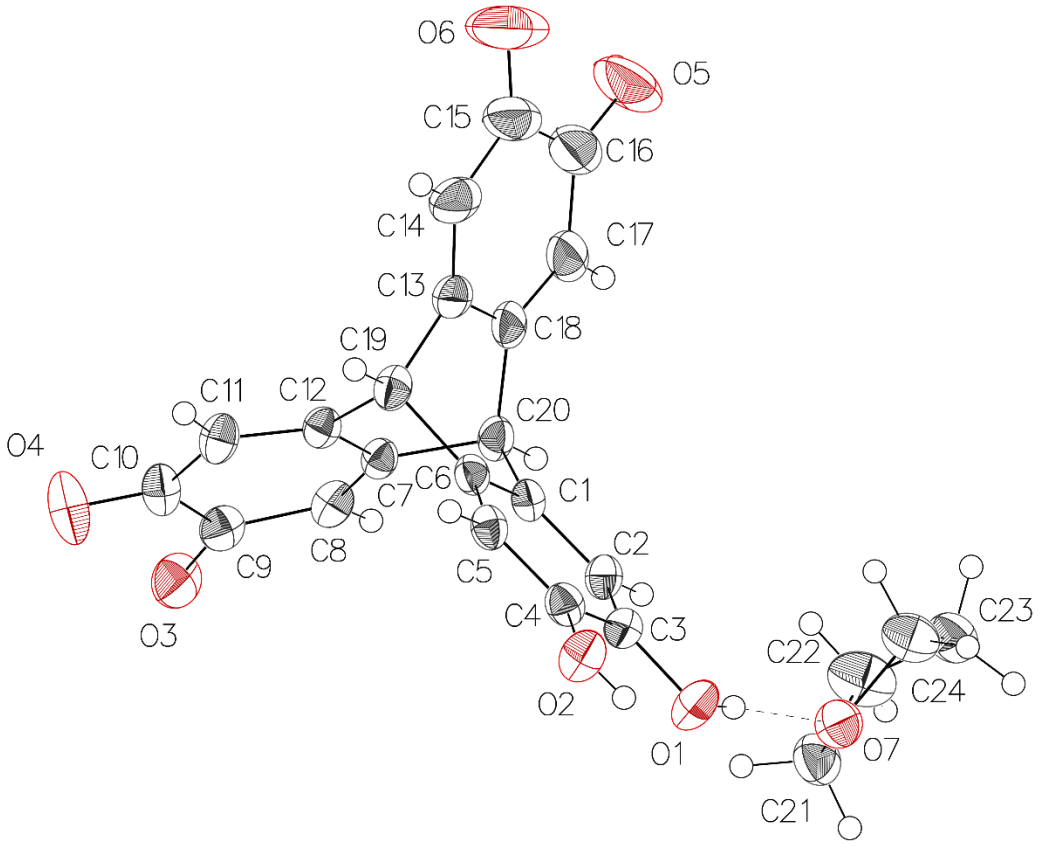

Figure S16. Thermal atomic displacement ellipsoid plot of the structure of crystals of triptycene(bisquinone) **2** grown from THF/hexane. The ellipsoids of non-hydrogen atoms are drawn at the 50% probability level, and hydrogen atoms are represented by a sphere of arbitrary size.

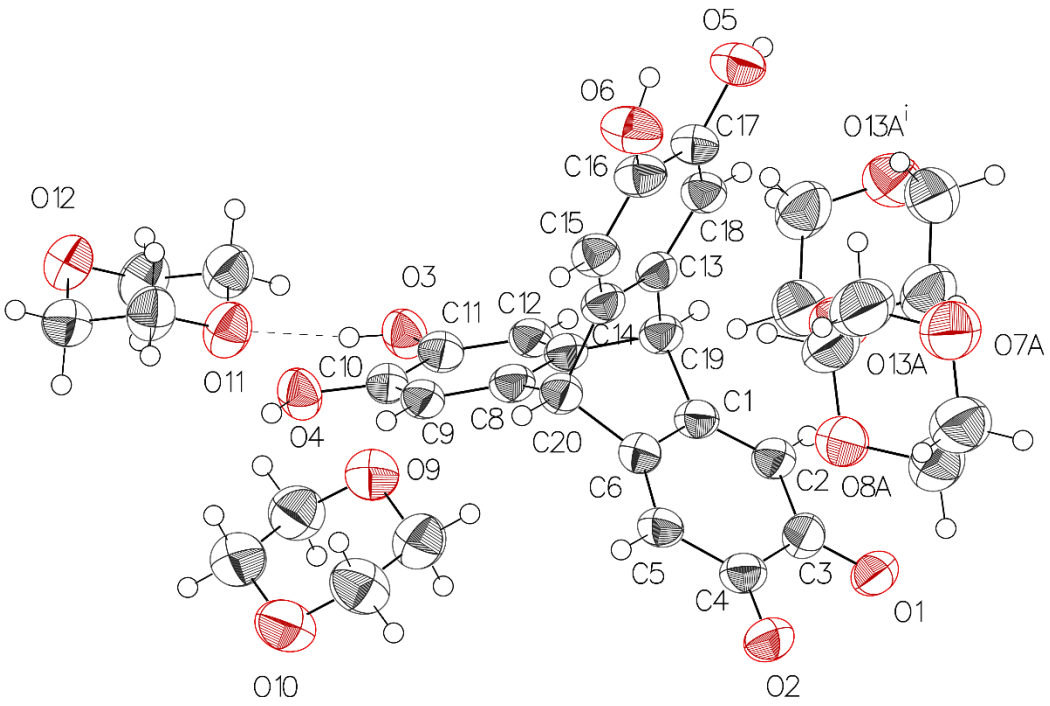

Figure S17. Thermal atomic displacement ellipsoid plot of the structure of crystals of triptycene(monoquinone) **3** grown from dioxane/hexane. The ellipsoids of non-hydrogen atoms are drawn at the 50% probability level, and hydrogen atoms are represented by a sphere of arbitrary size. Symmetry code (i): 1-x, 2-y, 1-z.

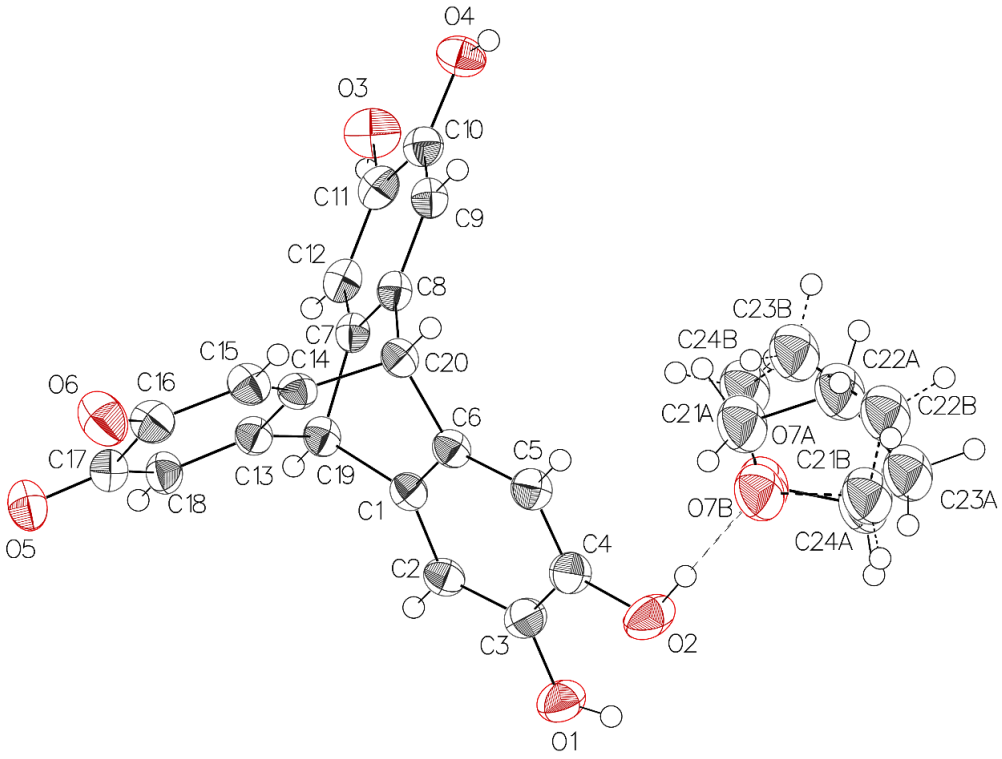

Figure S18. Thermal atomic displacement ellipsoid plot of the structure of crystals of triptycene(monoquinone) **3** grown from THF/hexane. The ellipsoids of non-hydrogen atoms are drawn at the 50% probability level, and hydrogen atoms are represented by a sphere of arbitrary size.

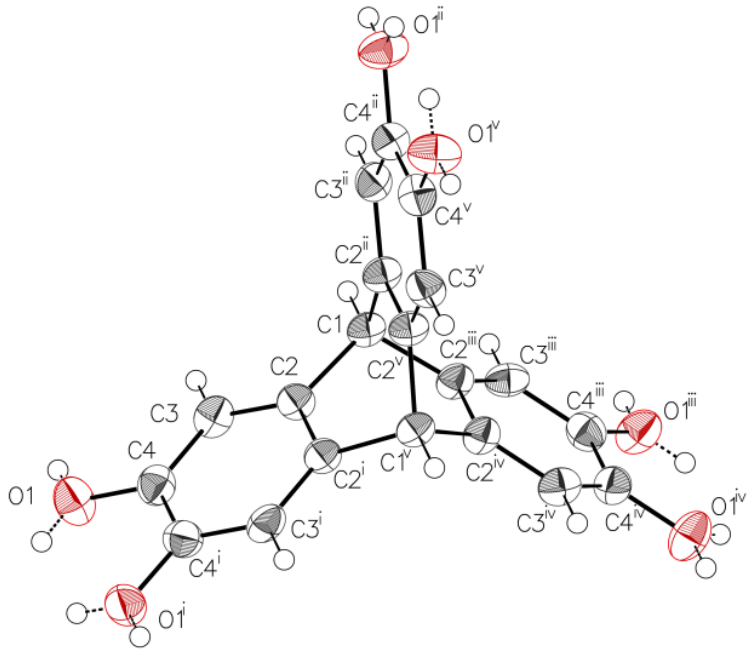

Figure S19. Thermal atomic displacement ellipsoid plot of the structure of crystals of triptycene(triscatechol) **4** grown from Me-THF. The ellipsoids of non-hydrogen atoms are drawn at the 50% probability level, and hydrogen atoms are represented by a sphere of arbitrary size. Symmetry cdes: (i): x, y, 3/2-z; (ii): 1+y-x, 1-x, z; (iii): 1-y, x-y, z; (iv): 1-y, x-y, 3/2-z; (v): 1+y-x, 1-x, 3/2-z. The hydroxyl hydrogen atoms are statistically disordered over two positions with 0.5 occupancy.

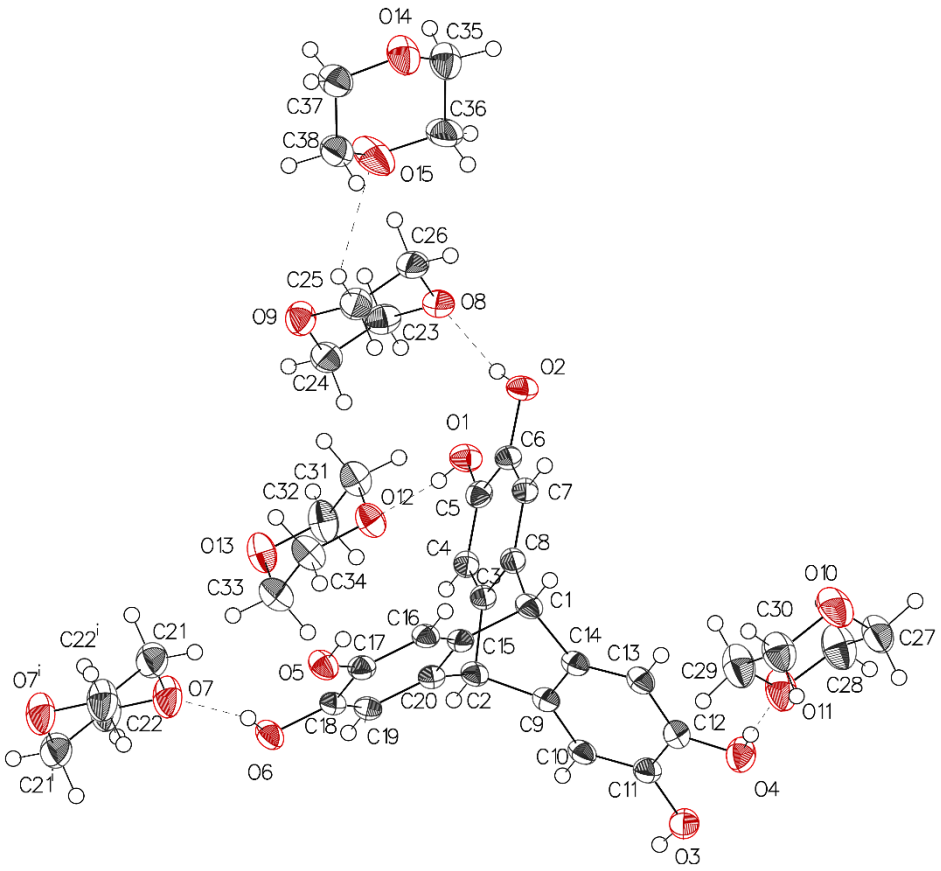

Figure S20. Thermal atomic displacement ellipsoid plot of the structure of crystals of triptycene(triscatechol) **4** grown from dioxane/hexane. The ellipsoids of non-hydrogen atoms are drawn at the 50% probability level, and hydrogen atoms are represented by a sphere of arbitrary size. Only one part of the disordered molecules of dioxane is shown. Symmetry code: (i): -x, 1-y, 2-z.